To the Graduate Council:

I am submitting herewith a dissertation written by Lillian Ruth Frazier entitled "Molecular Hydrogen Adsorbed on MgO (100) Surfaces: A Thermodynamic Study." I have examined the final electronic copy of this dissertation for form and content and recommend that it be accepted in partial fulfillment of the requirements for the degree of Doctor of Philosophy, with a major in Chemistry .

John Z. Larese
John Z. Larese: Major Professor

We have read this dissertation
and recommend its acceptance:

Robert J. Hinde

Michael J. Sepaniak

Paul Crilly

Accepted for the Council:

Carolyn R. Hodges
Vice Provost and
Dean of the Graduate School

(Original signatures are on file with official student records)

Molecular Hydrogen Adsorbed on MgO (100) Surfaces: A Thermodynamic Study

Dissertation presented to complete

the requirements for the

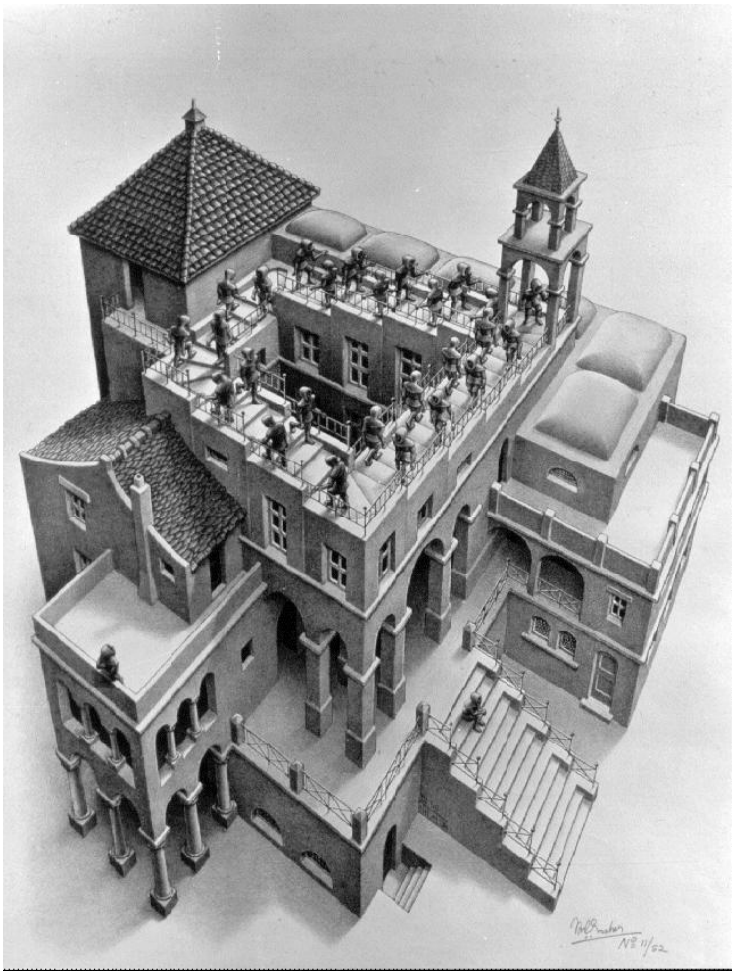
Doctor of Philosophy Degree

University of Tennessee, Knoxville

Lillian R. Frazier

December 2008

Dedication

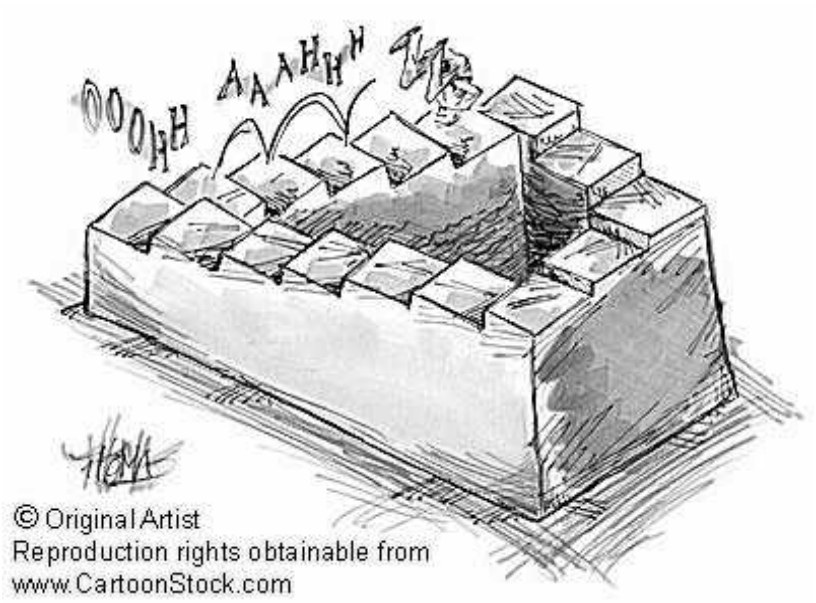


M. C. Escher: Ascending and Descending (1960)

M.C. Escher's drawings have intrigued me for years. They are heavily laden in mathematics, and he uses line shapes which cleverly appear to make the impossible, possible. I wrote to the M.C. Escher foundation and requested permission to use his images throughout my dissertation. They granted my request as long as I included the following: "All M.C. Escher works © 2008 The M.C. Escher Company - the Netherlands. All rights reserved. Used by permission. www.mcescher.com".

I have chosen "Ascending and Descending" for this section as it sums up my view on experimental research. Research is a never-ending grind. You keep working and working. Sometimes it seems as you are getting nowhere and are simply going around in circles. Yet, still you keep at it: climbing your way to some sort of solution. When you think you have finally reached the top, you find there is still further to travel, still more to do, still more that needs to be discovered.

As a graduate student, it is somewhat disheartening that you only have a short time to work on these projects. Often, you cannot get to the end of a project during your tenure, and you must pass the torch, filled with all of the knowledge you have gained and all of the results of your effort, to the next research oriented graduate student to carry on for you. You must trust that they will treat your project with the love and care it so deserves. You will have to trust that they will keep climbing even though sometimes it feels like they will be falling down that never-ending staircase instead of climbing up it.



This dissertation is dedicated to those that have provided me with the support I needed to continue climbing, when I was sure I was falling down those stairs.

My parents: I am where I am in my life largely due to my upbringing. My parents consistently emphasized the importance of education as I was growing up. Without their encouragement, I would most likely never have started climbing the stairs in the first place. I suppose they are also somewhat responsible for the strong will and tenacity which are engrained in my personality, which have given me the ability to keep climbing.

My husband: listens tirelessly to my endless complaints. He was kind enough to commiserate with me, when I felt like I was banging my head against the wall and was so frustrated and depressed that I felt like quitting, and to encourage me to

complete my dissertation for reasons other than improving my ability to become his "sugar mama" and get him a really nice bass boat some day. His love and support have been invaluable. Keep climbing.

My sister: who has just given birth to her 4th child. She has allowed me to become the "cool aunt" to my nieces and nephews (Avery, Lindsey, Ian, and baby Nathan), during a time when I certainly was not in a position to have any children of my own. She always reminds me of my talents. Keep climbing.

My thesis advisor: Dr. John Z. Larese, who has taught me so much about so much. Though, we have had our ups and downs, he has continued to believe in me and my abilities. I also have to dedicate this to Mrs. Larese, who kept Dr. Larese from killing me or throwing me out of the group during the downs. Keep climbing.

The Members and dogs of the Tennessee Valley Golden Retriever Rescue (TVGRR): for giving me a diversion and the ability to work toward finding lost or unwanted dogs new, permanent, loving, adoptive homes. It has been good for my heart! TVGRR's constant questions about when I would finally finish has kept me climbing.

My in-laws, are under the misconception that I am really smart. I keep telling them, I just work really hard. The relatives of the in-laws who insist that it is not

possible to get a Ph.D. without first getting a master's degree, who I will enjoy a bit too much proving them wrong. Keep climbing.

All the dogs that have come into and gone out of my life: my own dogs (Bodhi, Scooby, Baloo, Rocky, Micky, Linus, Danny, Nathan, Piper, and Buddy); my foster dogs; and my foundling dogs, who have spent time in my home and eaten some of my dry wall. They have done a pretty good job at making sure that I don't sleep in too late in the morning. I substituted my alarm clock for those of the four legged variety about four years ago. The snooze button; however, does not work. They listened to me complain when nobody else was around. They are always ready for a hug and a reassuring kiss to let me know that they love me. Keep climbing.

My high school chemistry teachers, Bruce Nance and Eldon Hopkins, opened my eyes to the world of chemistry in such a wonderful way and believed in me asking once if I was going to be their first Ph.D. chemist. Keep Climbing.

My Soccer team provided me such a nice outlet to gear my occasional stress and frustration towards. You have been great Friends and I appreciate your support without asking too often, "Aren't you done yet?" Once they finally realized I didn't really work with dogs for a living. Keep Climbing.

My friends and relatives have supported me by showing faith in me and my ability to succeed. Keep climbing.

I have done a lot of climbing, a lot of circling, and a lot of falling down during my time at the University of Tennessee. Mostly, I have learned that no matter what the obstacles, you have to keep climbing.

"To have peace with this peculiar life; to accept what we do not understand; to wait calmly for what awaits us, you have to be wiser than I am"

- M. C. Escher

"I am the master of my fate; I am the captain of my soul"

- William Ernest Henley

What is important is not what happens to us, but how we respond to what happens to us.

- John Paul Sartre

In between goals, is a thing called life that has to be lived and enjoyed.

- Sid Caesar

Do what you want to do… But want to do what you are doing. Be what you want to be… But want to be what you are.

- Unknown

God grant me the serenity to accept the things I cannot change, the courage to change the things I can, and the wisdom to know the difference

- Celtic Prayer

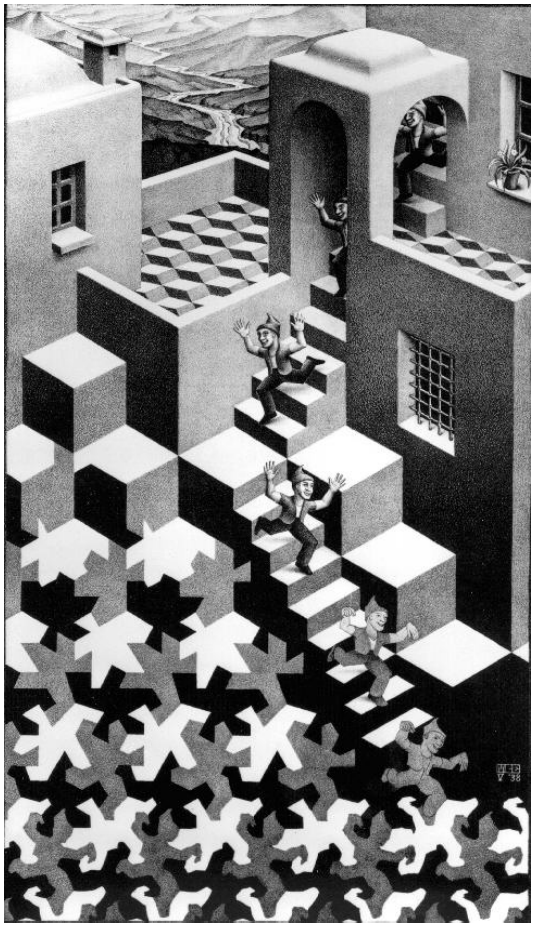
Only those who attempt the absurd can achieve the impossible. I think it's in the basement…Let me go upstairs and check.

- M. C. Escher

Keep Climbing

- Lillian R. Frazier

Acknowledgments



M. C. Escher: Cycle (1938)

I would like to thank the past and present members of the Larese Group, especially: Tom Arnold, Sami Chanaa, Richard Cook, Ben Estes, Michael Felty, David Fernandez-Cañoto, and George Thomas, for all of their help and support over the years. I wish luck to those who remain: Andi Barbour, Paige Landry, Hangning Chen, Andrew Hicks, Allyn Milojevich, and DeborahPenchoff. Stay strong, and keep your eye on the ball, this too shall pass. Good luck fixing all of your own stuff. It is a wonderful learning opportunity that you should not miss out on.

I would also like to thank the great staff in the chemistry department: Computer Guru – Bill Gurley, for bringing my hard drive back from the dead; Electronic Genius – Gary Wynn, for helping me with so many projects which I could not have completed without his assistance, and his ability to help me put the proverbial square peg in the round hole; Machinist Magician– Tim Free, for carefully making so many different items for my research and not complaining too much about them always being rush jobs, also for sharing a few of his tricks with me; Glass Shop Great – Arthur Pratt – for fixing all those quarts tubes I have such a talent for breaking.

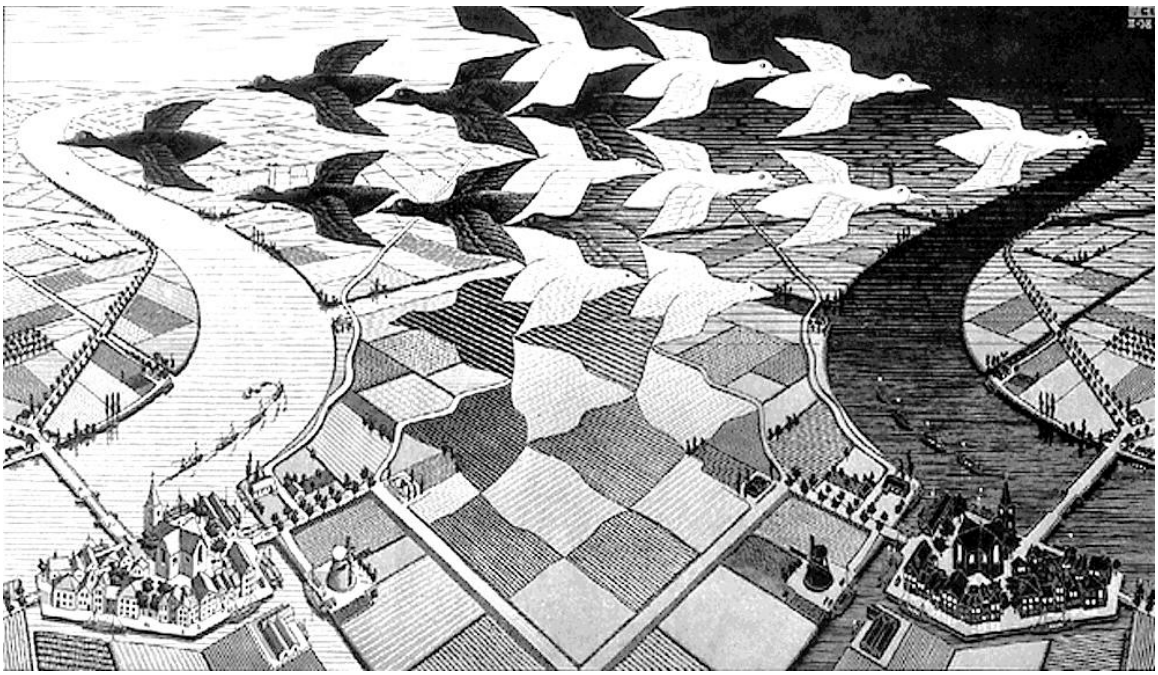
I would like to thank Dr. John Z. Larese for teaching me so much about the way things work, and having enough confidence in my abilities to not freak out when I did things like rip apart the glove box recirculation manifold system. My technical and engineering talents grew under his tutelage. I must also mention the intellectual

discussions which often spiraled off course, but which always made me think. Okay, I know. It is a Dr. of Philosophy Degree!

I must also acknowledge the money people. The research performed herein was made possible by support from the National Science Foundation under grant DMR-0412231, The University of Tennessee, and the US Department of Energy, BES, Materials Chemistry Division under contract DE-AC05-000R22725. Funding also came from Dr. Larese's UT start up funds. Supplementary travel funding for some of my travel was received from the University of Tennessee Chemical Physics Program.

Additional thanks to the M.C. Escher foundation who agreed to let me use his images to infuse a bit of my own personality into this dissertation. I believe there is an Escher drawing which is able to represent almost any concept I wish to discuss.
All M.C. Escher works © 2008 The M.C. Escher Company - the Netherlands. All rights reserved. Used by permission. www.mcescher.com.

Abstract



M. C. Escher: Day and Night (1938)

The thermodynamics of molecular hydrogen adsorbed on MgO (100) surfaces has been examined using high resolution volumetric adsorption isotherm techniques. These studies were undertaken using highly perfect, narrow size distributed MgO nanocubes with essentially single (100) facet exposure and extremely high chemical purity. A narrowly spaced (in temperature) series of isotherms were performed between the temperatures of ~7K and the triple point (13.8 K) using H_2 and D_2 gas.

A minimum of five, and in some cases seven, discrete adsorption steps are clearly observed in each isotherm trace. Analysis of these data indicate that the monolayer film forms a two dimensional phase that is much more compressed than what is observed in the most compact plane of the bulk hcp crystal. This is most likely due to a strong molecule – substrate interaction. As the film thickness increases and the distance between the substrate and adsorbing molecules increases, the molecule-molecule interactions begin to dictate the behavior of the layer growth. The system shows many characteristics of complete wetting behavior.

Using standard thermodynamic analysis, the isosteric heat of adsorption, two-dimensional compressibility, heat of adsorption, and differential (relative to the bulk values) enthalpy and entropy of each layer is determined. Phase boundaries including potential locations of critical points (that may be associated with phase changes) were also identified and used to generate the most complete phase diagram for the H_2-MgO system to date.

Additional interesting adsorption behavior is uncovered upon examination of the numerical derivative of these adsorption traces; a series of intralayer features appear. There is at least one substep feature that is found between each major adlayer vertical risers. These features are identified (in the text)as 2f, 3f, 4f, and 5f. These features are also located in the aforementioned phase diagram. Future work is needed to identify the microscopic process(es) responsible for their appearance.

Table of Contents



M. C. Escher: Waterfall (1961)

CHAPTER 1 **1**

INTRODUCTION **1**

CHAPTER 2 **13**

BACKGROUND **13**

2.1 – SOLID STATE **14**

2.1.1 – CRYSTAL SYSTEMS AND THE BRAVAIS LATTICE 14

2.1.2 – MILLER INDICES AND THE RECIPROCAL LATTICE 24

2.2 – ADSORPTION: STUDY OF PHASE BOUNDARY INTERACTIONS **27**

2.3 – TYPES OF ADSORPTION **29**

2.3.1 – MOLECULE – SURFACE INTERACTIONS 31

2.3.1.1 – The Attractive Force 33

2.3.1.2 – The Repulsive Force 33

2.3.1.3 – The Lennard – Jones Potential 34

2.3.2 – PHYSISORPTION 36

2.3.3 – CHEMISORPTION 37

2.4 – DEVELOPMENT OF ADSORPTION SCIENCE: A HISTORY. **37**

2.5 – TYPES OF ISOTHERMS **43**

2.5.1 – LANGMUIR ISOTHERM 45

2.5.2 – BRUNAUER, EMMET, AND TELLER(BET) ISOTHERM 48

2.5.3 – FHH ISOTHERM 50

2.6 – SURFACE DEFECTS 51

2.6.1 – EDGE EFFECTS 51

2.6.2 – MONATOMIC STEPS 55

2.7 – COMMENSURABILITY 55

2.7.1 – SURFACE ADSORPTION SITES 57

2.8 - WETTING 57

2.8.1 – CONTACT ANGLE 61

2.8.2 – DETERMINATION OF WETTING FROM ISOTHERMAL DATA. 61

2.8.2.1 – Incomplete Wetting Behavior 63

2.8.2.2 – Non-Wetting Behavior 63

2.8.2.3 – Complete Wetting Behavior 65

CHAPTER 3 66

MATERIALS 66

3.1 – METAL OXIDES 67

3.1.1 – SAMPLE PREPARATION 67

3.2 – MAGNESIUM OXIDE 68

3.2.1 – CHARACTERISTICS 70

3.2.1.1 – Sample Quality 70

3.2.1.2 – Sample Size and Structure 70

3.2.1.3 – Defects 73

3.2.2 – METHANE (CH_4) ADSORPTION STUDIES ON MGO (1 0 0) 73

CHAPTER 4 81

EXPERIMENTAL SET-UP 81

4.1 – THE ISOTHERM STATION 82

4.1.1 – CALIBRATION OF THE VOLUME 84

4.2 – COMPUTER CONTROL 87

4.3 – THE SAMPLE 91

4.3.1 – SAMPLE CONFINEMENT 91

4.3.2 – COOLING THE SAMPLE 95

4.4 – TEMPERATURE CONTROL 98

CHAPTER 5 103

ISOTHERMAL ANALYSIS 103

5.1 – CALCULATION OF THE NUMBER OF MOLES ADSORBED 104

5.1.1 – THERMAL TRANSPIRATION CORRECTION 109

5.2 – SURFACE AREA 112

5.2.1 – AREA PER MOLECULE 115

5.3 – CLAUSIUS-CLAPEYRON ANALYSIS 115

5.4 – TWO-DIMENSIONAL COMPRESSIBILITY 118

5.5 – ISOSTERIC HEAT OF ADSORPTION 119

5.6 – CRITICAL TEMPERATURE DETERMINATION 120

5.7 – PHASE DIAGRAM 121

CHAPTER 6 123

H_2 ADSORPTION ON MGO (1 0 0) 123

6.1 – SURFACE AREA CALCULATION OF MGO SAMPLE 124

6.2 – HYDROGEN ISOTHERMS – MONOLAYER CALCULATIONS 124

6.3 – HYDROGEN ISOTHERM – MULTIPLE LAYERS 130

6.4 – ANALYSIS OF THE INDIVIDUAL ADLAYERS 133

6.4.1 – DERIVATIVE 133

6.4.2 – ISOSTERIC HEAT OF ADSORPTION 136

6.4.3 – CLAUSIUS CLAYPERYON 138

6.4.4 – 2 DIMENSIONAL COMPRESSIBILITY (K_{2D}) 145

6.4.5 – DETERMINATION OF POTENTIAL PHASE TRANSITIONS 145

6.5 – DENSITY OF THE LAYERS 150

6.6 – THE PHASE DIAGRAM 156

6.7 – DEUTERIUM 156

6.8 – FUTURE WORK **162**

CHAPTER 7 **166**

CONCLUSIONS **166**

BIBLIOGRAPHY **170**

APPENDIX A **176**

SUPPLEMENTAL MATERIAL **176**

VITA **195**

List of Tables



M. C. Escher: Still Life and Street (1937)

TABLE 1.1– PROPERTIES OF BULK MOLECULAR HYDROGEN 8

TABLE 1.2 – PROPERTIES OF BULK D_2 11

TABLE 2.1 - THE SEVEN CRYSTAL SYSTEMS DIVIDED INTO FOURTEEN BRAVAIS LATTICES 16

TABLE 2.2 – INTERACTION ENERGIES AND RESIDENCE TIMES DETERMINING ADSORPTION TYPE (ADAMSON AND GAST 1997) 30

TABLE 2.3 – THE ADVANCEMENTS OF ADSORPTION EXPERIMENTATION THROUGHOUT HISTORY (DABROWSKI 2001) 38

TABLE 2.4 – THE ADVANCEMENTS OF ADSORPTION THEORY THROUGHOUT HISTORY 41

TABLE 6.1- CLAUSIUS CLAPYERON CURVE FITS 141

TABLE 6.2 - VALUES DERIVED FROM THE CLAUSIUS CLAPYERON DATA 142

TABLE 6.3 – LAYER DENSITY 155

TABLE 6.4 – CRITICAL POINTS INDICATING POTENTIAL PHASE CHANGES 159

TABLE 6.5 – CRITICAL POINTS INDICATING POTENTIAL PHASE CHANGES 160

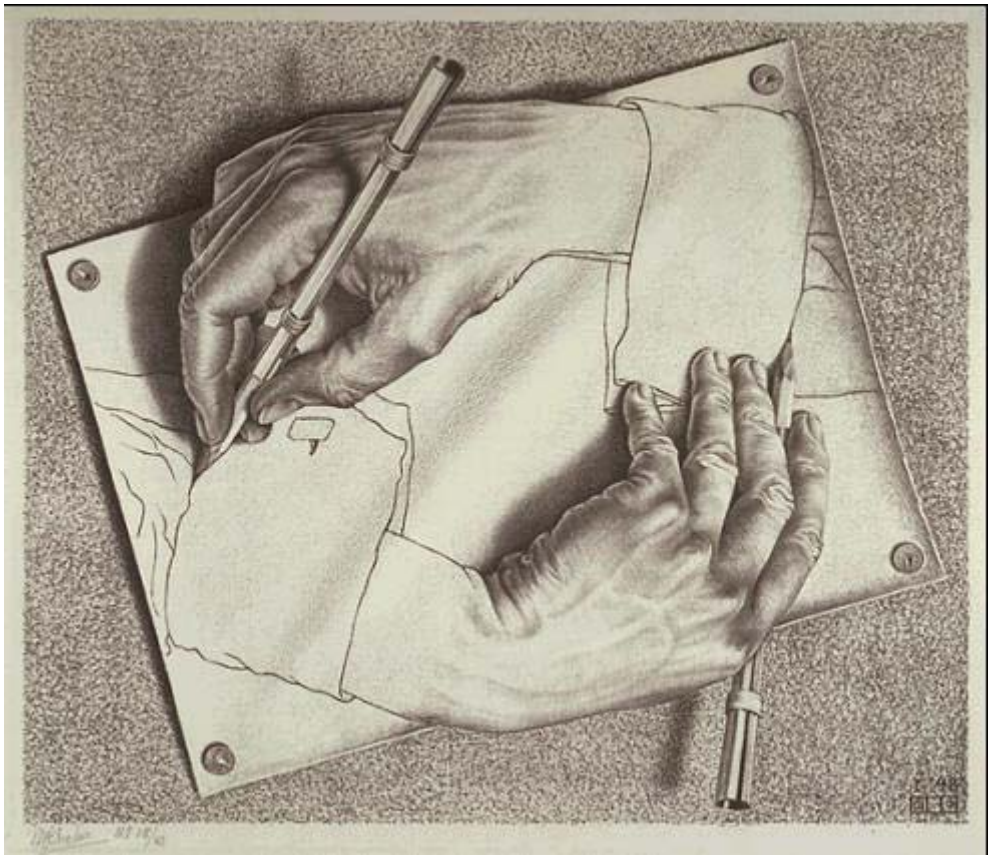
TABLE 6.6 – CLAUSIUS CLAPEYRON CURVE FITS FOR D_2 ON MGO 164

TABLE 6.7 – CLAUSIUS CLAPEYRON RESULTS FOR D_2 ON MGO 165

TABLE A.1 – SAMPLE SURFACE AREAS AND FIGURE NUMBERS 177

TABLE A.2 – MONOLAYER COVERAGE BASED ON POINT B METHOD 193

List of Figures



M. C. Escher: Drawing Hands (1948)

FIGURE 1.1– COVER OF HYDROGEN CONTRACTORS MEETING REPORT MAY 16-19, 2006 _____3

FIGURE 1.2 – MA ISOTHERMS (MA, KINGSBURY ET AL. 1988; MA 1989)_____4

FIGURE 1.3– MA PHASE DIAGRAM (MA, KINGSBURY ET AL. 1988) _____5

FIGURE 1.4 – HELIUM ATOM SCATTERING RESULTS (TOENNIES AND TRAEGER 2007)_____7

FIGURE 1.5 – J.Z. LARESE PRELIMINARY DIFFRACTION STRUCTURE RESULTS_____10

FIGURE 2.1 – THE 14 BRAVAIS LATTICES GROUPED INTO THE 7 CRYSTAL SYSTEMS (OMAR 1975) _____15

FIGURE 2.2 – TWO-DIMENSIONAL BRAVAIS LATTICES. (MIHALY AND MARTIN 1996) _____17

FIGURE 2.3 – SOME CHOICES OF PRIMITIVE UNIT CELLS AND THE CONVENTIONAL UNIT CELL FOR A CENTERED RECTANGULAR LATTICE (MIHALY AND MARTIN 1996) _____19

FIGURE 2.4 - M.C. ESCHER: EIGHT HEADS BASIC BLOCK IS THE BASIS WHICH IS ADDED TO EACH LATTICE POINT TO FORM THE OVERALL PICTURE. THE PRIMITIVE CELL IS SHOWN IN THE DOTTED SQUARE BOX. THERE IS ONE BASIS ON EACH LATTICE POINT._____20

FIGURE 2.5 – M.C. ESCHER: EIGHT HEADS - GENERATED BY TRANSLATING THE BASIS SET TO EACH OF THE LATTICE POINTS VIA A LINEAR COMBINATION OF THE LATTICE VECTORS $\vec{a}$ AND $\vec{b}$ _____21

FIGURE 2.6 – PLANE FILLING MOTIF SHOWN IN THE HEXAGONAL LATTICE _____22

FIGURE 2.7 – M.C. ESCHER: REGULAR DIVISION OF THE PLANE _____23

FIGURE 2.8 – EXAMPLES OF LATTICE PLANES IN REAL SPACE SHOWN ON A $1\times1\times1$ CUBE WITH CORRESPONDING MILLER INDICES SHOWN (KITTEL 1996)_____26

FIGURE 2.9– TWO DIMENSIONAL LATTICE PLANES (ALBERTY AND SILBEY 1955) _____28

FIGURE 2.10– INTERACTION BETWEEN ATOMS AND MOLECULES CONSISTS OF ATTRACTION DOMINATED AT LONG DISTANCES AND REPULSION DOMINATED AT SHORT DISTANCES (ATKINS AND PAULA 1978) 32

FIGURE 2.11 – CHEMISORPTION VS PHYSISORPTION (MCQUARRIE AND SIMON 1997) 35

FIGURE 2.12- FIVE TYPES OF ISOTHERMS AS DEFINED BY BRUNAUER (BRUNAUER 1943) 44

FIGURE 2.13 - THE IUPAC CURRENTLY DEFINES SIX TYPES OF ADSORPTION ISOTHERMS 46

FIGURE 2.14 - TYPES OF SURFACE DEFECTS (MCQUARRIE AND SIMON 1997) 52

FIGURE 2.15– SIMPLIFIED VIEW OF MOLECULAR STACKING 53

FIGURE 2.16 – SIMPLIFIED VIEW OF LAYER BY LAYER GROWTH (THOMY, DUVAL ET AL. 1981) 54

FIGURE 2.17– POSSIBLE ADSORPTION SITES OF A SIMPLE SALT LIKE STRUCTURE. 58

FIGURE 2.18– ADSORPTION SITES AVAILABLE FOR A HEXAGONAL LATTICE 59

FIGURE 2.19- EXAMPLES OF HIGH SYMMETRY COMMENSURATE STRUCTURES ON THE SURFACE OF A SIMPLE CUBIC SUBSTRATE 60

FIGURE 2.20 - DEPICTION OF CONTACT ANGLE CALCULATION 62

FIGURE 2.21- ADDITIONAL ISOTHERM TYPES ASSOCIATED WITH NON WETTING BEHAVIOR (ADAMSON AND GAST 1997) 64

FIGURE 3.1 – PATENTED DEVICE USED IN PREPARATION AND COLLECTION OF METAL OXIDES (KUNNMANN AND LARESE 2001) 69

FIGURE 3.2 - ESR AND AAS RESULTS IN THE COMPARISON OF COMMERCIAL MGO AND THAT PRODUCED IN THE LARESE GROUP 71

FIGURE 3.3– SEM IMAGES OF MGO (100). MGO HAS A SIMPLE CUBIC STRUCTURE AND EXHIBITS SINGLE FACET EXPOSURE OF THE (100) FACE 72

FIGURE 3.4 – TEM IMAGE OF MGO (100) CUBE WITH GRAPHICAL REPRESENTATION OF THE SIMPLE CUBIC ROCK SALT STRUCTURE OF THE MGO (100) CUBE 74

FIGURE 3.5 – UNIT CELL OF THE 100 SURFACE OF MGO IS MARKED BY THE SOLID LINE. THE UNIT CELL CONTAINS EXACTLY ONE MAGNESIUM ATOM AND ONE OXYGEN ATOM. IT IS A SQUARE LATTICE WITH A = 2.98 Å YIELDING A PRIMITIVE UNIT CELL AREA OF 8.88 Å^2. 75

FIGURE 3.6 - OXYGEN VACANCY 76

FIGURE 3.7 – MGO CUBE SHOWING LEDGES AND MONATOMIC STEPS. IT SHOULD BE NOTED THAT EACH SURFACE IS A (100) CRYSTAL FACE 77

FIGURE 3.8 - METHANE SITS ABOVE NEXT NEAREST NEIGHBOR MAGNESIUM ATOMS. THIS GIVES A UNIT CELL OF C(2X2) STRUCTURE WITH LATTICE CONSTANT A = 2.97 Å WITH TWO METHANE MOLECULES PER UNIT CELL. THIS IS EQUIVALENT TO A $\sqrt{2}\times\sqrt{2}$ R 45° STRUCTURE WITH LATTICE CONSTANT A = 4.211 Å WITH ONE METHANE MOLECULE PER UNIT CELL. THE RESULTANT OCCUPIED AN AREA PER MOLECULE OF METHANE IS 17.76 Å^2 PER MOLECULE 79

FIGURE 3.9 – TYPICAL METHANE (CH4) ADSORPTION ISOTHERM ON MGO (100) (LARESE 1998). A GOOD QUALITY MGO SAMPLE SHOW A MINIMUM OF 5 AND AS MANY AS 7 LAYERING TRANSITIONS OF RELATIVELY EVEN HEIGHT VISIBLE BY INSPECTION. 80

FIGURE 4.1 - TYPICAL "ISOTHERM STATION" 83

FIGURE 4.2 – WATER FILLED BULB – FOR VOLUME CALIBRATION 86

FIGURE 4.3 - LABVIEW™ ISOIMAC HIGH RESOLUTION ADSORPTION ISOTHERM STARTUP SCREEN 88

FIGURE 4.4 – FLOW CHART OF ISOTHERM PROCESS 92

FIGURE 4.5 – QUARTZ SAMPLE TUBE 93

FIGURE 4.6 – SAMPLE CELL RING ASSEMBLY 94

FIGURE 4.7 – CRYOSTAT STICK FOR NEUTRON SCATTERING EXPERIMENTS AND LOW TEMPERATURE ISOTHERMAL STUDY (KOEHLER AND LARESE 2000) 96

FIGURE 4.8 – CRYOSTAT 97

FIGURE 4.9 – SAMPLE CELL RING ASSEMBLY MOUNTED TO CRYOSTAT 99

FIGURE 4.10 – ORANGE CRYOSTAT 100

FIGURE 4.11 – DIAGRAMOF ORANGE CROYSTAT 101

FIGURE 5.1 - THERMAL TRANSPIRATION CORRECTION LIES DIRECTLY ON THE SAME LINE AS WITHOUT THE CORRECTION. 111

FIGURE 5.2 – METHANE ISOTHERM RUN AT 77.94K SHOWS GOOD SAMPLE QUALITY WITH MORE THAN 5 ADSORPTION STEPS VISIBLE BY INSPECTION WHICH ARE RELATIVELY EVEN IN HEIGHT. 113

FIGURE 5.3 – POINT B METHOD SHOWN TO DETERMINE MONOLAYER CAPACITY OF THE METHANE ISOTHERM SHOWN IN FIGURE 5.1 114

FIGURE 6.1 – TYPICAL HYDROGEN ISOTHERM 125

FIGURE 6.2 – LOW COVERAGE C2X2 STRUCTURE OF MOLECULAR HYDROGEN ADSORBED ON THE MGO (100) SURFACE HAS A LATTICE CONSTANT A = 5.96 Å CORRESPONDING TO AN AREA PER MOLECULE OF 17.76 $Å^2$. (LARESE, FRAZIER ET AL. 2006) 127

FIGURE 6.3 – HIGH COVERAGE HEXAGONAL STRUCTURE ADSORBED ON THE MGO (100) SURFACE HAS A LATTICE CONSTANT A = 3.46 Å CORRESPONDING TO AN AREA PER MOLECULE OF 10.37 $Å^2$ 128

FIGURE 6.4 – THE MONOLAYER OF ISOTHERM SHOWN IN FIGURE 6.1 129

FIGURE 6.5 – COLLECTION OF ISOTHERMS IS SHOWN FOR A RANGE OF TEMPERATURES 131

FIGURE 6.6 – CLOSE UP OF STEPS 1 THROUGH 3 OF SERIES OF ISOTHERMS 132

FIGURE 6.7 – ISOTHERM AND ITS DERIVATIVE. 134

FIGURE 6.8 – SERIES OF DERIVATIVES SHOWING CONSISTENCY OF THE MAIN PEAKS AND INTERLAYER FEATURES 135

FIGURE 6.9 – ISOSTERIC HEAT OF ADSORPTION FOR T = 9.7 K 137

FIGURE 6.10 – ISOSTERIC HEAT WITH MORE ISOSTERIC POINTS CHOSEN RESULTING IN A GREATER NUMBER OF PEAKS IN THE MONOLAYER 139

FIGURE 6.11 – CLAUSIUS CLAPYERON PLOT OVER ENTIRE TEMPERATURE RANGE. CIRCLES SHOW POTENTIAL BREAKS IN LINEARITY WHICH MIGHT BE ASSOCIATED WITH PHASE TRANSITIONS. 140

FIGURE 6.12 – SMOOTH FIT OF THE LAYER 2 DATA INDICATES 3 DISTINCT REGIONS OF VARYING LINEARITY. THE CRITICAL POINT AS SUGGESTED BY MA IS SHOWN FOR COMPARISON. 144

FIGURE 6.13 – TWO-DIMENSIONAL COMPRESSIBILITY FOR THE SECOND ADSORPTION LAYER. 146

FIGURE 6.14 – TWO-DIMENSIONAL COMPRESSIBILITY PEAKS FOR THE 3RD ADLAYER 147

FIGURE 6.15 – TWO-DIMENSIONAL COMPRESSIBILITY FOR THE FOURTH ADLAYER 148

FIGURE 6.16 – SHOWS THE LOCATIONS ASSOCIATED WITH THE BEGINNING (GREEN), CENTER (YELLOW), AND END (RED) OF THE DERIVATIVE PEAKS. THESE CORRESPOND TO THE DIAMOND, SQUARE, AND TRIANGLE MARKED INDEPENDENTLY TO SHOW THE BEGINNING, INFLECTION POINT AND END OF THE RISER ON THE ISOTHERMAL DATA. THE WIDTH OF THE FEATURE IS TAKEN TO BE THE DISTANCE IN PRESSURE BETWEEN THE GREEN AND RED LINES. 149

FIGURE 6.17 – WIDTHS FOR CRITICAL POINT DETERMINATION, THREE DIVISIONS 151

FIGURE 6.18 - WIDTHS FOR CRITICAL POINT DETERMINATION, FOUR DIVISIONS 152

FIGURE 6.19 – ISOTHERM NORMALIZED BY MONOLAYER COVERAGE TO DETERMINE DENSITY OF LAYERS 153

FIGURE 6.20 – PHASE DIAGRAM FOR THE H2 – MGO(100) SYSTEM 157

FIGURE 6.21 – PHASE DIAGRAM FOR FOUR DIVISIONS 158

FIGURE 6.22 – DEUTERIUM ISOTHERM ALONG WITH THE NUMERICAL DERIVATIVE. CONFIRMATION OF INTERLAYER FEATURES CAN BE CLEARLY SEEN IN THE DERIVATIVE. 161

FIGURE 6.23 – CLAUSIUS – CLAPEYRON PLOT FOR DEUTERIUM ON MGO (100) 163

FIGURE A.1 – METHANE ISOTHERM SAMPLE 606IB 178

FIGURE A.2 – MONOLAYER 606IB 179

FIGURE A.3 – METHANE ISOTHERM SAMPLE 606IC 180

FIGURE A.4 –MONOLAYER 606IC 181

FIGURE A.5 – METHANE ISOTHERM SAMPLE 606IE 182

FIGURE A.6 – MONOLAYER 606IE 183

FIGURE A.7 – METHANE ISOTHERM SAMPLE 606IF 184

FIGURE A.8 – MONOLAYER 606IF 185

FIGURE A.9 – METHANE ISOTHERM SAMPLE 606CB 186

FIGURE A.10 – MONOLAYER 606CB 187

FIGURE A.11 – METHANE ISOTHERM SAMPLE 707A 188

FIGURE A.12 – MONOLAYER 707A 189

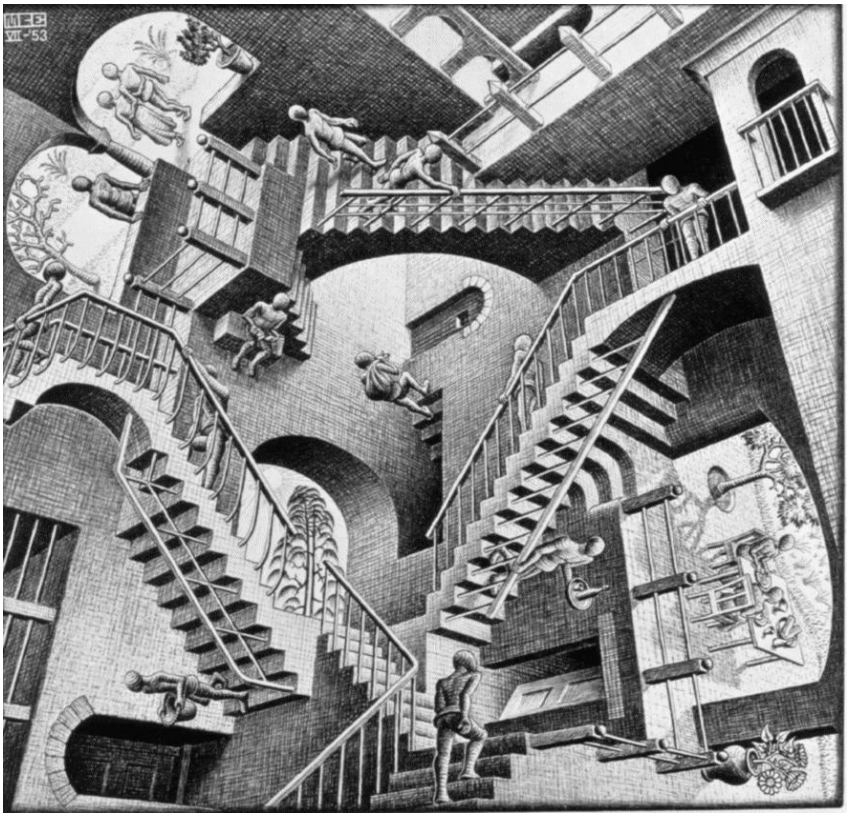
FIGURE A.13 – METHANE ISOTHERM SAMPLE 1107A 190

FIGURE A.14 – MONOLAYER 1107A 191

FIGURE A.15 – METHANE ISOTHERM ON SAMPLE 707AB 192

Chapter 1

Introduction



M. C. Escher: Relativity (1953)

This dissertation focuses on two current "hot topics" in science: nano-materials and hydrogen. Since the beginning of the hydrogen economy initiative, millions of dollars have been spent towards the search of a suitable storage medium. This initiative has aided growth in nano-materials research to find a material capable of meeting the Freedom CAR hydrogen storage system targets. A material capable of achieving 4.5 wt% hydrogen was targeted by 2005 with increases to 6.0% by 2010, and 9.0% by 2015 (USDOE 2003).

This research will examine the aptitude of magnesium oxide as an effective hydrogen storage medium. A report on this system was presented by Dr. John Z. Larese at the DOE Hydrogen Contractors Meeting in 2006. An image of the inelastic neutron scattering results was exhibited on the cover of the corresponding report as shown in figure 1.1 (USDOE 2006).

There has been some previous examination of this system. In Part, this work revisits that performed by Jian Ma who worked at the University of Washington, Seattle with Oscar Vilches. The dissertation work of Dr. Ma focused on the thermodynamic investigation of the H_2 - MgO (100) system. Isothermal analysis led to the discovery of an interlayer feature between the second and third adlayers of the system (Ma 1989). Figure 1.2 shows examples of their isothermal results and Figure 1.3 gives their resulting phase diagram for the H_2-MgO system (Ma, Kingsbury et al. 1988).

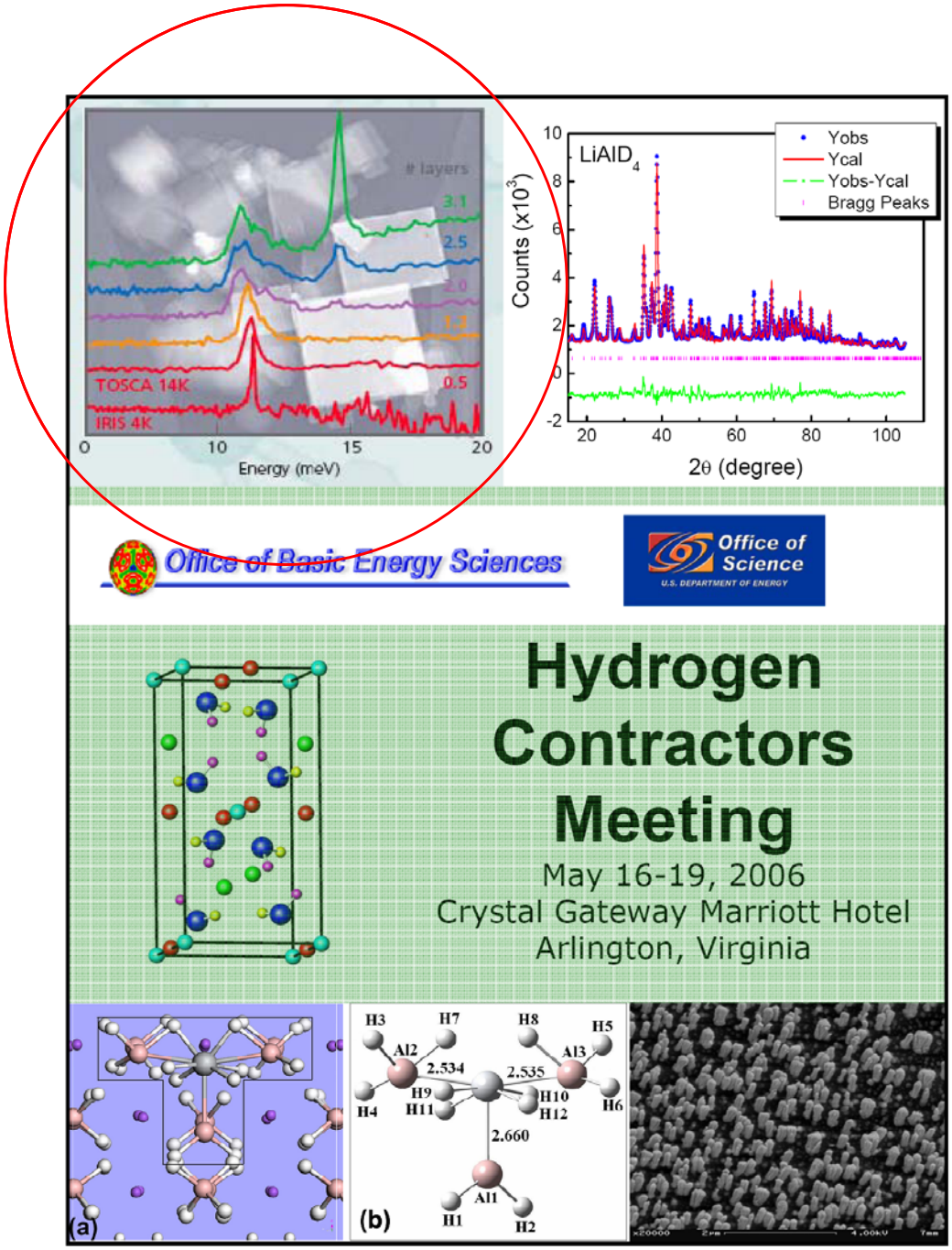


Figure 1.1– Cover of Hydrogen Contractors meeting report May 16-19, 2006 (USDOE 2006).

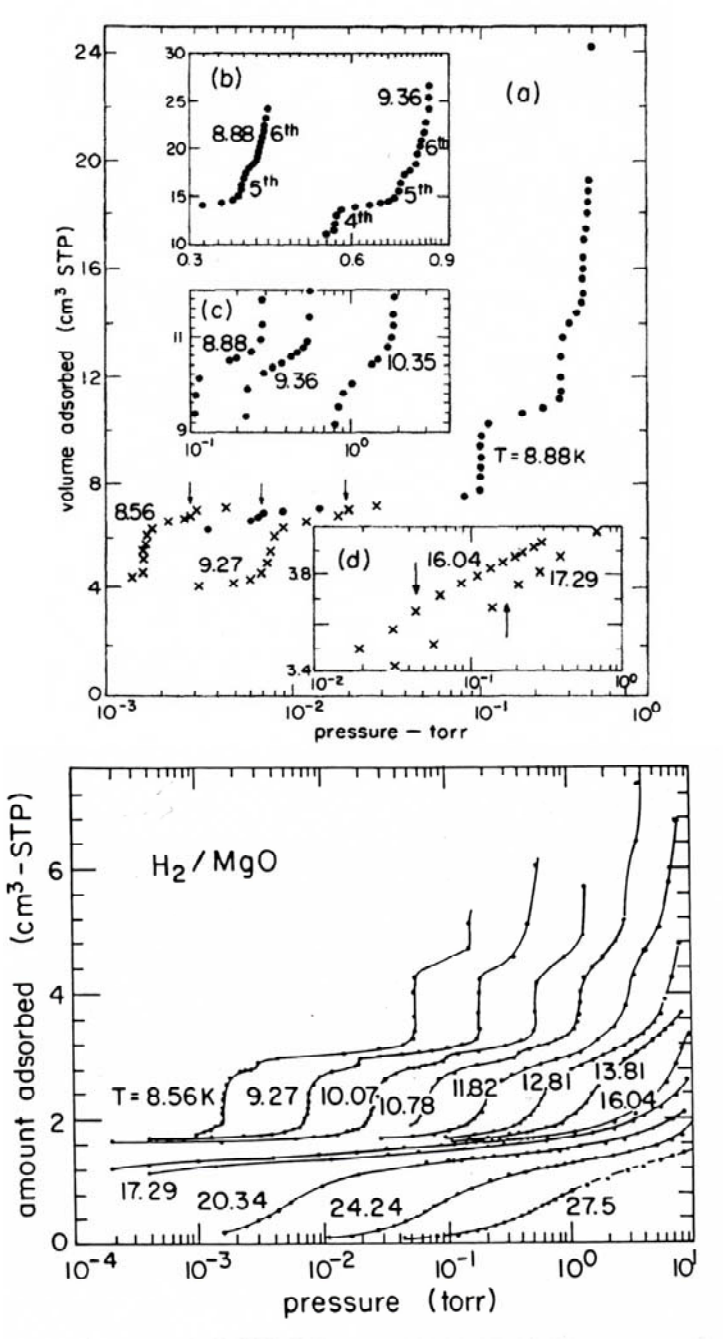


Figure 1.2 – Ma isotherms (Ma, Kingsbury et al. 1988; Ma 1989)

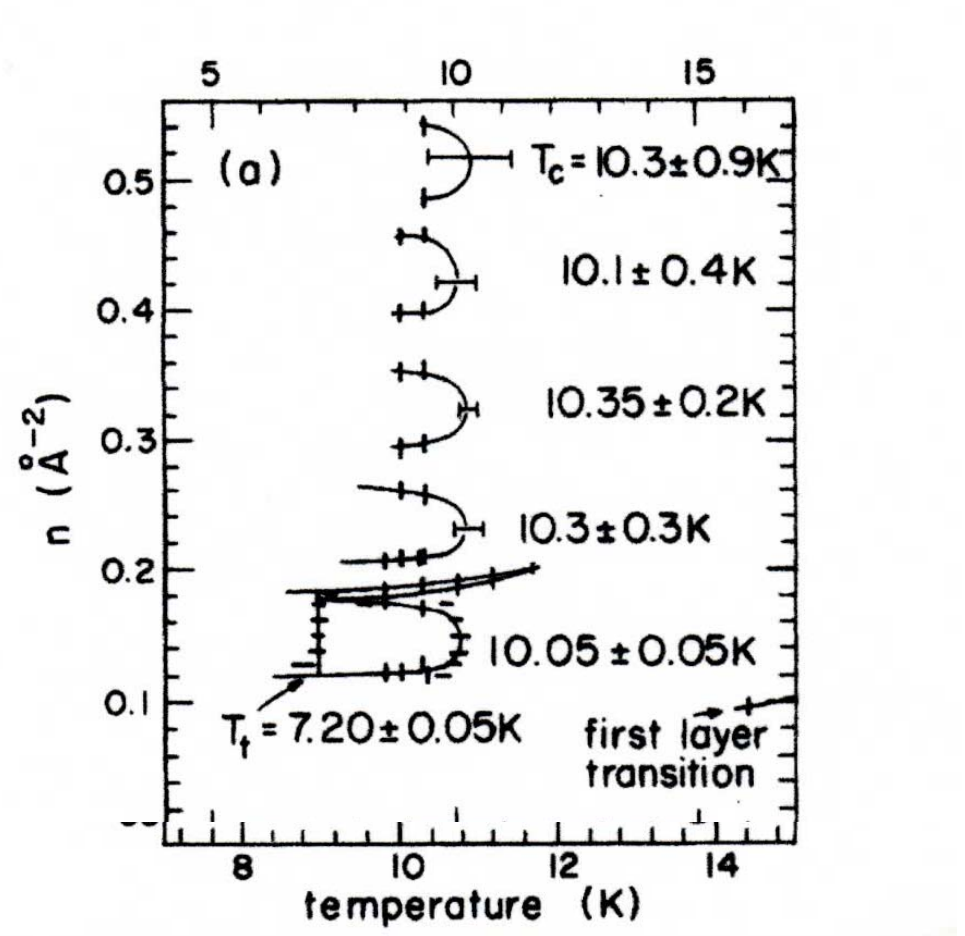


Figure 1.3– Ma Phase Diagram (Ma, Kingsbury et al. 1988)

Previous neutron scattering investigations of Lauter, Degenhardt, and Halsey suggest a low coverage commensurate c(2x2) structure followed by a series of c(2x4), c(2x6) commensurate structures (Degenhardt, Lauter et al. 1987). Helium atom scattering has also been used to study this fascinating system results have been published in (Skofronick, Toennies et al. 2003)and (Toennies and Traeger 2007). They claim to confirm the c(2x4) and c(2x6) intermediate structures. Their results are shown in figure 1.4

In this dissertation, using MgO material of a quality superior to that analyzed earlier, a close examination of the phase diagram is performed by performing a number of adsorption isotherms at temperatures ranging from approximately 7K through the triple point of bulk H_2 of ~13.8K. The properties of bulk Hydrogen are given in Table1.1. Results will be compared to those of Ma and Vilches.

A series of neutron scattering experiments were also performed on this system. Dr. John Z. Larese has analyzed the diffraction results and has proposed low-coverage, island-like growth of a c(2x2) structure and a hexagonal close packed structure at high coverage, with a potential intermediate 2 by compression. He suggests a devils staircase series of p(2x?) intermediate commensurate structures; however, more work will be needed prior to confirming these structures. The preliminary diffraction results along with inelastic neutron scattering results have been published in (Larese, Frazier et al. 2006). A more comprehensive manuscript has

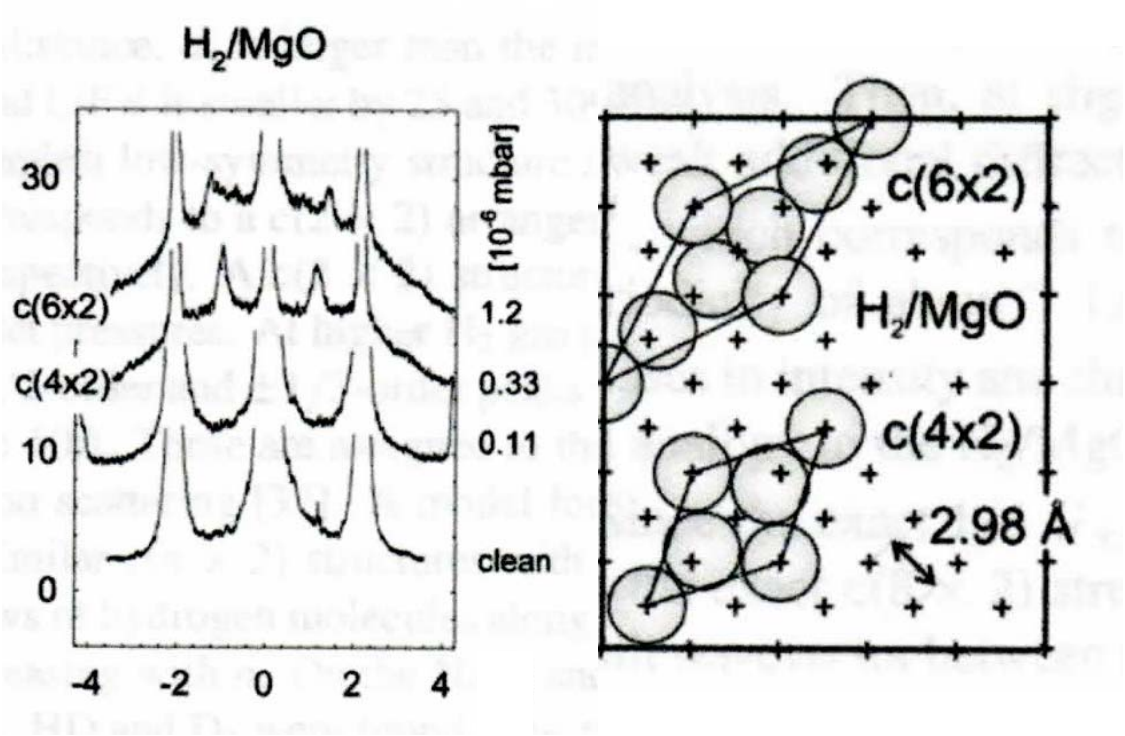


Figure 1.4 – Helium Atom Scattering Results (Toennies and Traeger 2007)

Table 1.1– properties of bulk molecular hydrogen

molecular weight	2.0159
Boiling Point	20.384K (MSDS)
Freezing Point	14K(Bates 2002)
Critical Temperature	32.98K (MSDS)
Critical Pressure	12.80 atm (MSDS)
Critical Density	0.0310 kg/dm^3 (MSDS)
Triple Point Temperature	13.83K (MSDS)
Triple Point Pressure	0.0695 atm (MSDS)
Crystal Structure @ T < 4K	fcc (Bates 2002)
Crystal Structure @ T > 4K	hcp, (Bates 2002) a = 3.789 Å (Silvera 1980)
2D - APM (hcp)	12.43 Å^2/molecule
Heat of Fusion	117.2 J/mol (Souers, Briggs et al. 1977)
Heat of Vaporization	919.5 J/mol (Souers, Briggs et al. 1977)
Heat of Sublimation	1036.7 J/mol (Souers, Briggs et al. 1977)

been written and is in the submittal process. The high and low coverage diffraction results are shown in Figure 1.5. This work was also featured in the 2006 ISIS Highlight. All diffraction work was performed using deuterium (D_2) instead of hydrogen as the adsorbate; therefore, a comparison will also be made between the hydrogen and deuterium isothermal results. Important properties of Deuterium are given in Table 1.2.

This dissertation is divided into six additional chapters and one appendix as follows:

- Chapter 2 will focus on the background material necessary for understanding the concepts of adsorption studies. This will include discussion of the types of adsorption and adsorption isotherms. Additionally, some basic solid state physics will be presented as it relates to surface structure determination. The adsorption characteristics of commensurability and wetting will also be covered.
- Chapter 3 will introduce the reader to magnesium oxide. Magnesium oxide is the substrate used for all studies presented in the main part of this thesis. It's production method and morphology will be discussed as well as some previous experimental results which will be utilized in the characterization of this system.

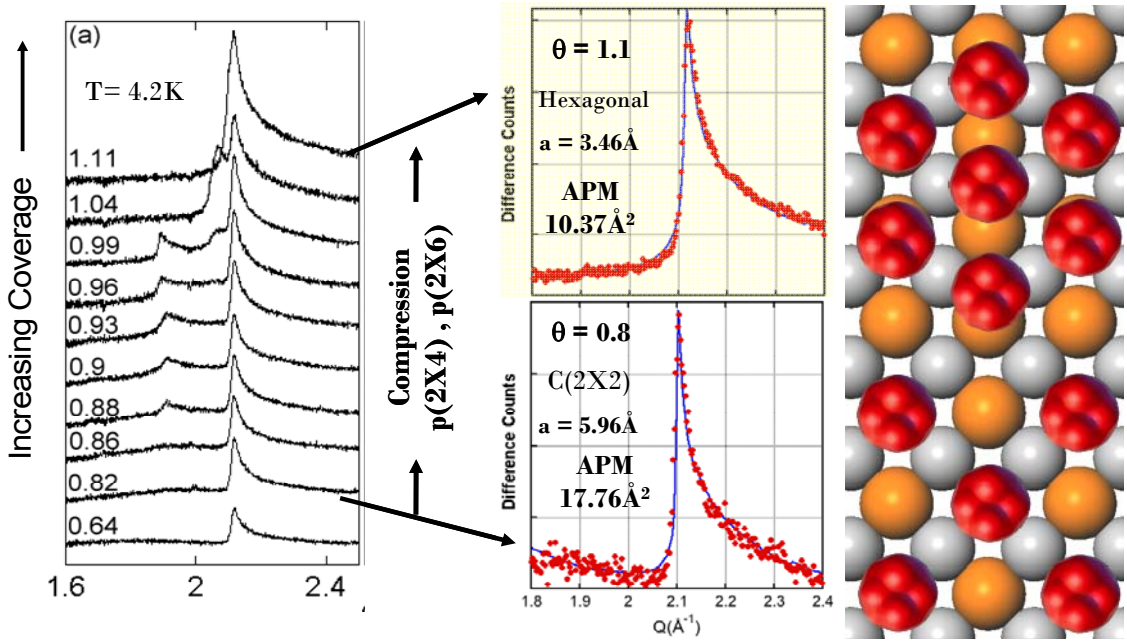


Figure 1.5 – J.Z. Larese preliminary diffraction structure results

(Larese, Frazier et al. 2006)

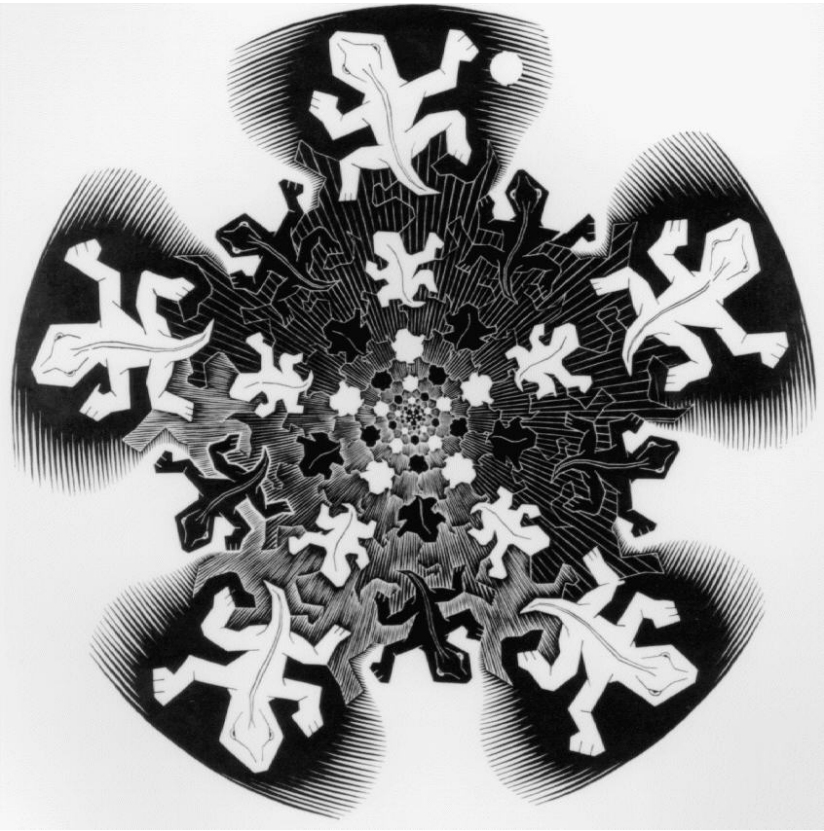
Table 1.2 – properties of bulk D_2

Molecular Weight	4.032
Boiling Point	23.654K (MSDS)
Freezing Point	18.55K (MSDS)
Critical Temperature	38.34K (MSDS)
Critical Pressure	16.43 atm (MSDS)
Critical Density	0.0668 kg/dm^3 (MSDS)
Triple Point Temperature	18.72K (MSDS)
Triple Point Pressure	0.169 atm (MSDS)
Crystal Structure @ T > 4K	a = 3.605 Å (Silvera 1980)
2D – APM (hcp)	11.25 Å^2/molecule
Heat of Fusion	196.6 J/mol (Souers, Briggs et al. 1977)
Heat of Vaporization	1280.7 J/mol (Souers, Briggs et al. 1977)
Heat of Sublimation	1477.3 J/mol (Souers, Briggs et al. 1977)
$\ln(p_0) = A + \frac{B}{T} + CT + DT^2$	A=14.00711 torr, B=-1.612823x10^2 C=-4.861678x10^{-2}, D= 10.56887x10^{-4} (Souers, Briggs et al. 1977)
$\ln(p_0) = A + \frac{B}{T} + B'\ln(T)$	A=4.908319 torr, B=-136.1893, B'=2.463629 (Souers, Briggs et al. 1977)

- Chapter 4 explains the set-up used for all isothermal experiments performed within this dissertation.
- Chapter 5 will include the analysis and theory utilized to get the results given in the following chapters.
- Chapter 6 reveals all thermodynamic results for the H2 adsorption on the MgO (1 0 0) surfaces.
- Chapter 7 wraps everything up and reiterates all conclusions which can be drawn from this set of studies.
- Appendix A will solidify the results given in this dissertation by including supporting data not explicitly shown in the body of the text.

Chapter 2

Background



M.C. Escher: Development II (1939)

2.1 – Solid State

2.1.1 – Crystal Systems and the Bravais Lattice

One element of great interest in nanomaterials and of adsorbed systems is their structure in the solid state. According to Kittel, all crystal structures can be described by the infinite repetition of identical structural units called the unit cell (Kittel 1996). The unit cell must be chosen such that it can fill all space via a series of translation vectors of the form shown in equation(2.1),

$$\vec{T} = a_n \vec{a} + b_n \vec{b} + c_n \vec{c}\,, \tag{2.1}$$

where a_n, b_n, and c_n are integers; and $\vec{a}$, $\vec{b}$, and $\vec{c}$ are crystal-axis vectors. In the two-dimensional case, equation (2.1) simplifies to equation(2.2).

$$\vec{T} = a_n \vec{a} + b_n \vec{b} \tag{2.2}$$

There are seven three-dimensional crystal systems and 14 Bravias lattices which are of interest in the study of materials. These structures are shown in figure 2.1 (Omar 1975) their characteristics are given in Table 2.1 (Omar 1975). In the case of an adsorbed layer, we focus on the two-dimensional Bravais lattices shown in figure 2.2. In either case, what is of interest is the unit cell and how the atoms or molecules in the system fill this unit cell.

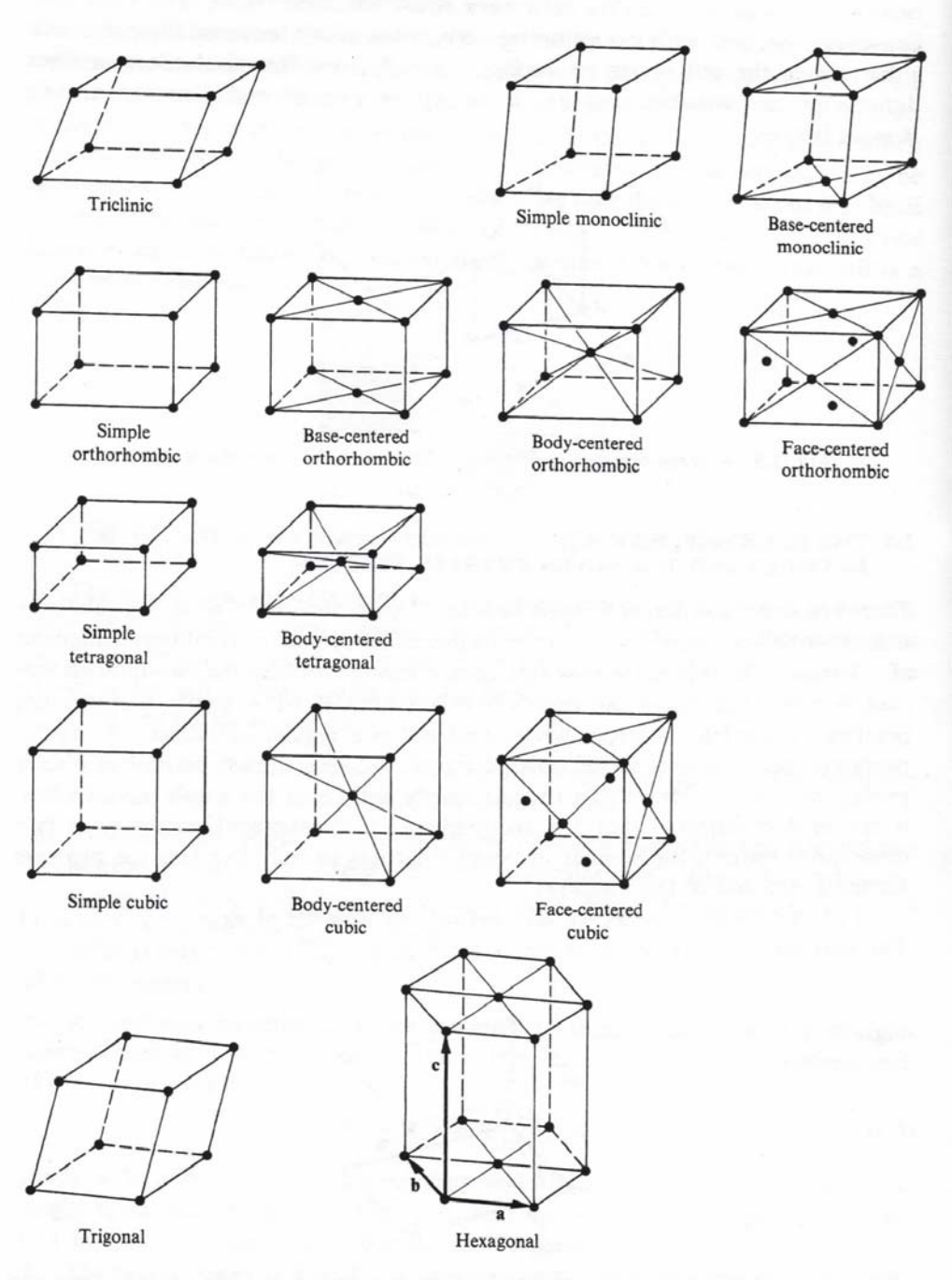


Figure 2.1 – The 14 Bravais lattices grouped into the 7 crystal systems (Omar 1975)

Table 2.1 - The Seven Crystal Systems Divided into Fourteen Bravais Lattices (Omar 1975)

System	Bravias Lattice	Unit Cell Characteristics	Characteristic Symmetry elements
Triclinic	Simple	$a \neq b \neq c$ $\alpha \neq \beta \neq \gamma \neq 90^\circ$	None
Monoclinic	Simple Base Centered	$a \neq b \neq c$ $\alpha = \beta = 90^\circ \neq \gamma$	One 2-fold rotation axis
Orthorhombic	Simple Base-centered Body-centered Face-centered	$a \neq b \neq c$ $\alpha = \beta = \gamma = 90^\circ$	Three mutually orthogonal 2-fold rotation axes
Tetragonal	Simple Body-centered	$a = b \neq c$ $\alpha = \beta = \gamma = 90^\circ$	One 4-fold rotation axis
Cubic	Simple Body-centered Face-Centered	$a = b = c$ $\alpha = \beta = \gamma = 90^\circ$	Four 3-fold rotation axes (along cube diagonal)
Trigonal (rombohedral)	Simple	$a = b = c$ $\alpha = \beta = \gamma \neq 90^\circ$	One 3-fold rotation axis
Hexagonal	Simple	$a = b \neq c$ $\alpha = \beta = 90^\circ$ $\gamma = 120^\circ$	One 3-fold rotation axis

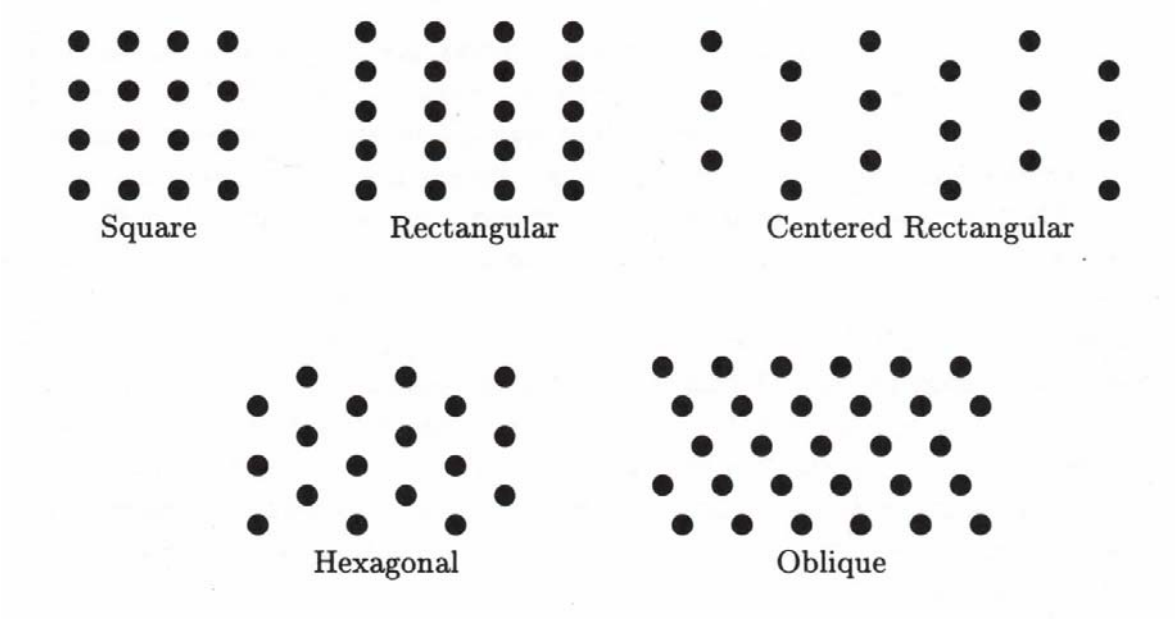


Figure 2.2 – Two-Dimensional Bravais Lattices. (Mihaly and Martin 1996)

The unit cell is anchored to a lattice system whose points are defined by equation(2.1) or (2.2). There is a basis of atoms or elements associated with each lattice point (Kittel 1996). A primitive unit cell is a minimum volume cell, drawn such that there is only one basis set of elements bound by the cell. A conventional unit cell may consist of more than one of these basis sets of elements (Mihaly and Martin 1996). Often, multiple sets of these base elements may need to be included before a proper repeat unit can be defined. Examples of these types of choices are given in figure 2.3.

The use of repeat units which people might be more familiar with is seen in M.C. Escher's tessellation art. For example figure 2.4 shows the basis centered on the lattice point as part of a square lattice. MC Escher's Eight Heads tessellation shown in figure 2.5 is generated by translating the basis to the other lattice points via the lattice vectors shown. Similarly, figure 2.6 shows the hexagonal unit cell and accompanying lattice utilized to generate M.C. Escher's "regular division of the plane" shown in figure 2.7. This is an example of a case where the basis does not just consist of one of each element, but rather of three of each element is combined to make up the overall basis.

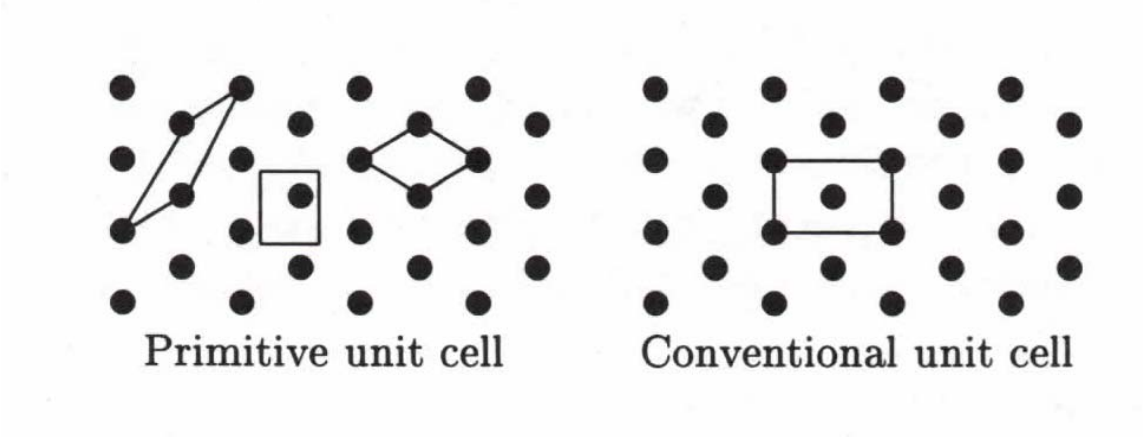


Figure 2.3 – Some choices of primitive unit cells and the conventional unit cell for a centered rectangular lattice (Mihaly and Martin 1996)

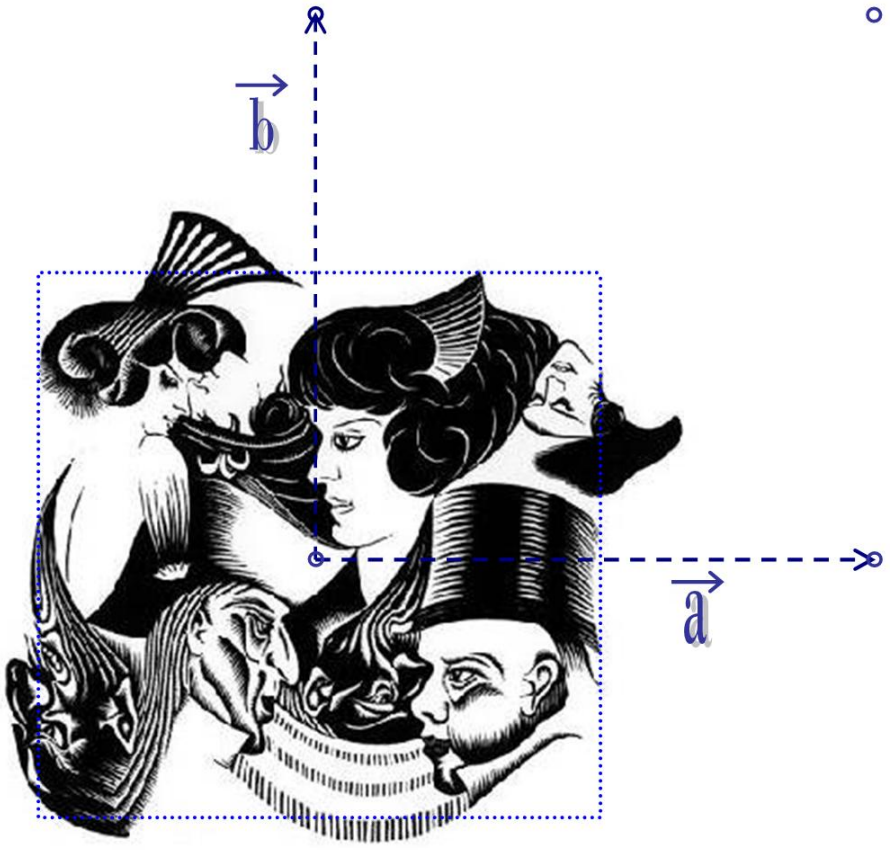


Figure 2.4 - M.C. Escher: Eight Heads Basic Block is the basis which is added to each lattice point to form the overall picture. The primitive cell is shown in the dotted square box. There is one basis on each lattice point.



Figure 2.5 – M.C. Escher: Eight Heads - generated by translating the basis set to each of the lattice points via a linear combination of the lattice vectors $\vec{a}$ and $\vec{b}$

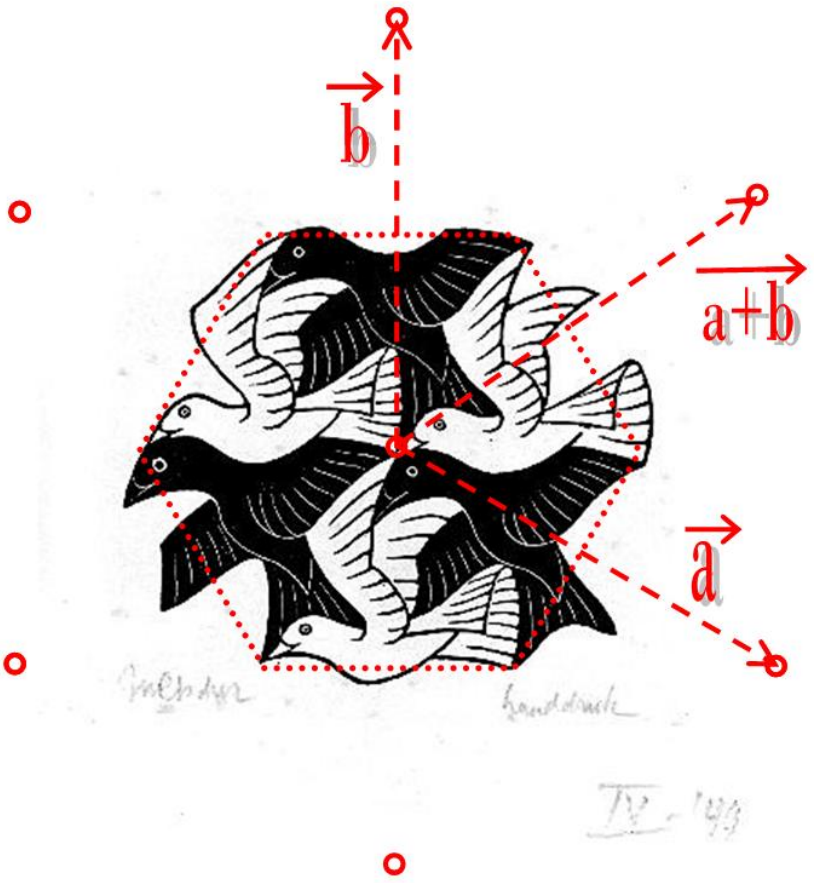


Figure 2.6 – plane filling motif shown in the hexagonal lattice

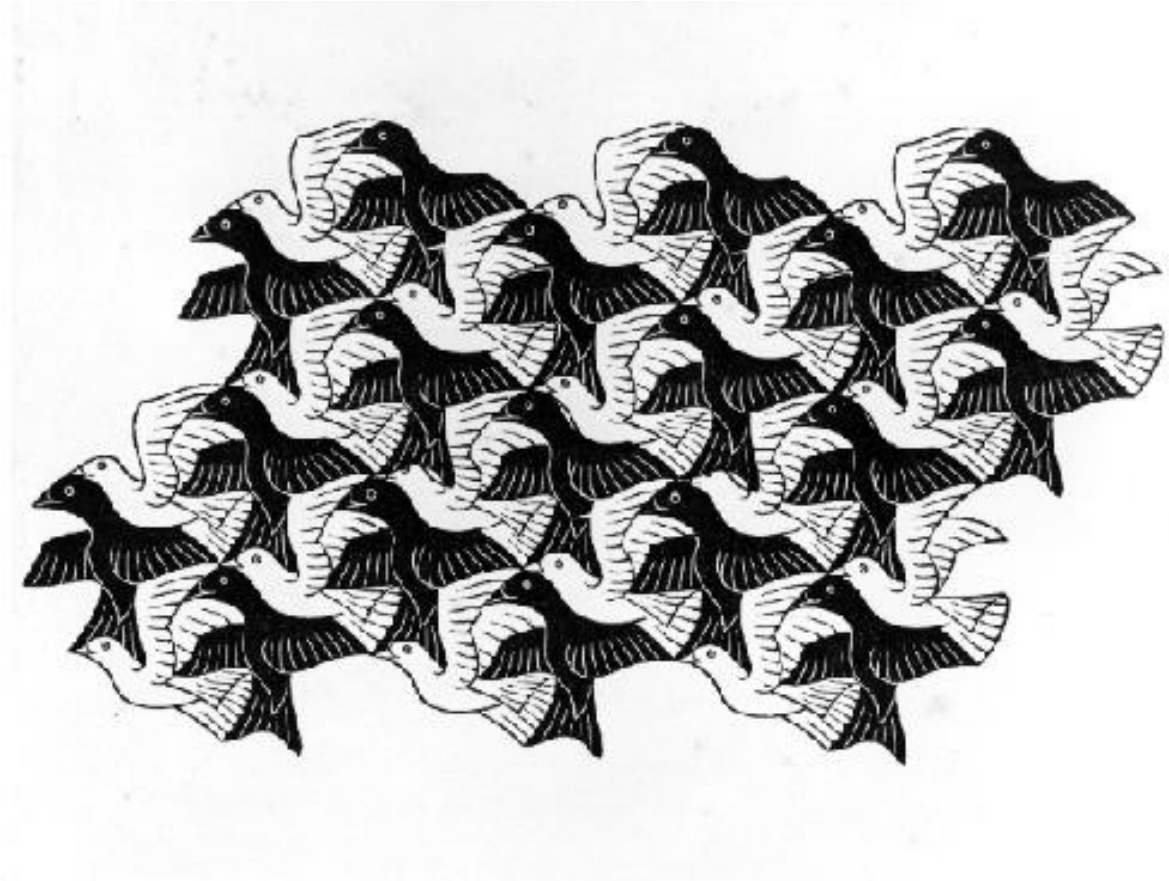


Figure 2.7 – M.C. Escher: Regular division of the plane

2.1.2– Miller Indices and the Reciprocal Lattice

Lattice planes are defined by a vector from the origin of the lattice to point (a, b, c) or (a, b) in the two-dimensional system, where a, b, and c are the points of intersection between the crystal plane and the lattice. This plane is, therefore, perpendicular to the vector, r given in equation(2.3) (Kittel 1996).

$$\vec{r} = a\vec{a} + b\vec{b} + c\vec{c} \tag{2.3}$$

These lattice planes are identified by their Miller indices. Ashcroft and Merman define the miller indices of a lattice plane as the coordinates of the shortest reciprocal lattice vector that is perpendicular to the plane as given in equation(2.4) (Ashcroft and Mermin 1976).

$$\vec{k} = h\vec{a}' + k\vec{b}' + l\vec{c}' \tag{2.4}$$

Here $\vec{a}'$, $\vec{b}'$, and $\vec{c}'$ are the reciprocal lattice vectors as defined in equations (2.5), (2.6) , and (2.7) respectively. The reciprocal lattice vectors are the reciprocal or k-space, equivalent of the crystal axis vectors. The reciprocal lattice is important to the discussion of diffraction.

$$\vec{a}' = 2\pi \frac{\vec{b} \times \vec{c}}{\vec{a} \bullet \left(\vec{b} \times \vec{c}\right)} \tag{2.5}$$

$$\vec{b}' = 2\pi \frac{\vec{c} \times \vec{a}}{\vec{a} \bullet \left(\vec{b} \times \vec{c} \right)} \tag{2.6}$$

$$\vec{c}' = 2\pi \frac{\vec{a} \times \vec{b}}{\vec{a} \bullet \left(\vec{b} \times \vec{c} \right)} \tag{2.7}$$

The lattice plane is then referred to as the (h k l) plane. To calculate h, k, and l, we start by looking at the intersection of the plane in real space (a,b,c). The reciprocal of the points is then taken $\left(\frac{1}{a},\frac{1}{b},\frac{1}{c}\right)$. The lowest common denominator, n, of a, b, and c is then multiplied through to insure that h, k, and l will be whole numbers as given in equation 2.8 (Omar 1975; Burns 1985). It should be noted that h, k, and l are the intersection points of the plane in reciprocal space. It should also be noted that if the intercept is in the negative direction from the given lattice origin, this is noted by adding a bar above the given indices.

$$(h,k,l) = \left(\frac{n}{a},\frac{n}{b},\frac{n}{c}\right) \tag{2.8}$$

Some examples of lattice planes are shown in figure 2.8.

In the two-dimensional case (which is pertinent to describing the adsorbate structure on surfaces) only the first two miller indices are necessary to define the plane. The third indice is zero as there is no height associated with a two dimensional lattice. Therefore we simply deal with the (h,k) plane. Some planes through an

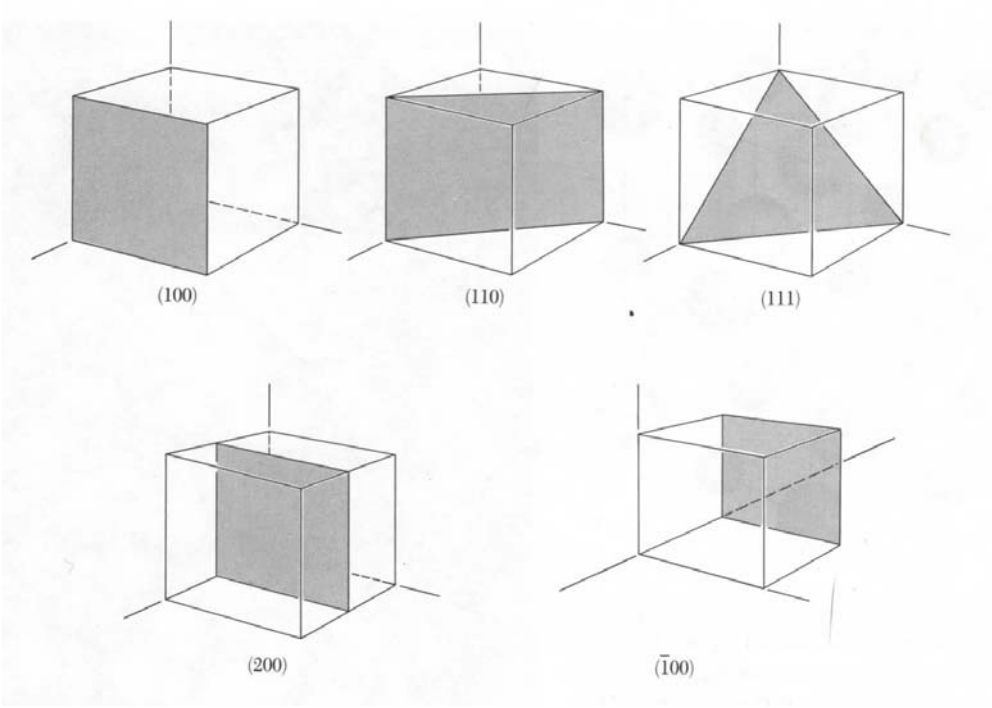


Figure 2.8 – Examples of lattice planes in real space shown on a $1\times1\times1$ cube with corresponding miller indices shown (Kittel 1996)

oblique lattice are shown in figure 2.9 (Alberty and Silbey 1955). Additionally, to discuss positions within the two dimensional lattice, we must only consider lattice vectors $\vec{a}$ and $\vec{b}$. Again the movement in two dimensions is illustrated nicely by M.C. Escher as shown previously in Figures 2.4 through 2.7.

2.2– Adsorption: Study of Phase Boundary Interactions

Many important chemical processes occur at the boundary between two phases. The liquid – liquid, solid – liquid, liquid – gas, and solid – gas boundaries are all worth investigating. Dabrowski defines adsorption as "the change in concentration of a given substance at the interface as compared with the neighboring phases" (Dabrowski 2001). Merriam-Webster recognized the word adsorption in 1882 with the following definition: "the adhesion in an extremely thin layer of molecules (as of gases, solutes, or liquids) to the surfaces of solid bodies or liquids with which they are in contact" (Merriam-Webster).

There are two main components which must be defined in an adsorptive system: the adsorbate and the adsorbent. The adsorbent is the substrate upon which the adsorbate forms a thin film layer. In this dissertation, the adsorbate is the MgO (100) surface, and the adsorbent is molecular hydrogen in the gas phase.

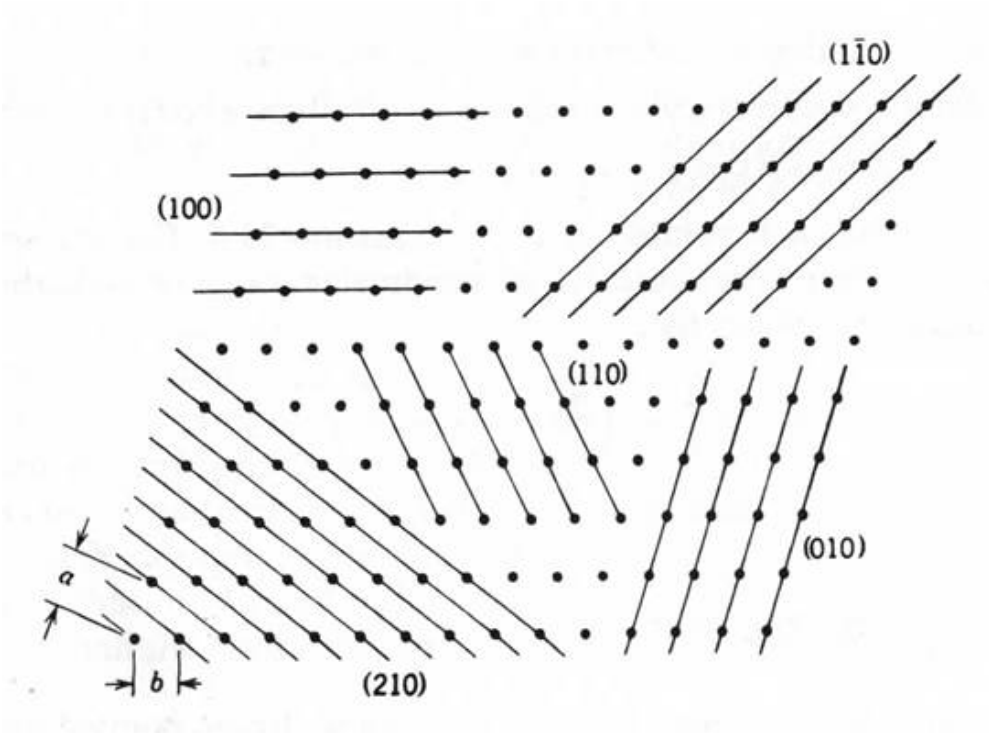


Figure 2.9– two dimensional lattice planes (Alberty and Silbey 1955)

The entire system has two boundaries. First is the boundary between the solid surface and the adsorbed film. Second, is the boundary between the adsorbed film and the bulk. The adsorbed film is often referred to as the interfacial layer. In this dissertation, it is also often referred to as the adlayer. These boundaries give rise to two separate interactions whose balance defines the adsorption. The relative strength of the molecule-substrate (adsorbate-adsorbent) and the molecule-molecule (adsorbate-adsorbate) interactions dictates what occurs in the interfacial film.

2.3 – Types of Adsorption

There are two major classifications of adsorption: Chemisorption and Physisorption. There are three factors which are important in the determination of adsorption type: electron transfer, heat of adsorption, and residence time. These are summarized in Table 2.2.

If an electron is transferred between the adsorbate and the adsorbent, the system is said to be chemisorbed. If no electron transfer occurs, the system falls into the classification of physisorption. The act of electron transfer results in a definite difference in the heat of adsorption of the system.

Therefore, the two classes may be distinguished based on the magnitude of the interaction energy between the surface and the adsorbate. To distinguish between the

Table 2.2 – Interaction energies and residence times determining adsorption type (Adamson and Gast 1997)

Type of Adsorption	Electron Transfer	Heat of Adsorption (J/mol)	Residence Time (seconds)
Physisorption	NO	6 – 40	10^{-12} – 10^{-7}
Chemisorption	YES	80 - 400	10^{2} - 10^{17}

two major types of adsorption an estimation of the molecule-substrate interaction must be determined. If the adsorption energy is on the order of a chemical bond, it is referred to as a chemisorbed system, if it is smaller, then it is considered to be a physisorbed system.

The other consideration in determining the type of adsorption involves the amount of time that the molecule is in contact with the surface. This is referred to as the residence time. In a physisorbed system, molecules are continuously adsorbing onto and desorbing from the surface and the ultimate time actually spent sitting on the surface is extremely small. This is in sharp contrast to a chemisorbed system, where molecules actually become attached to the surface by means of a chemical bond.

2.3.1 – Molecule – Surface Interactions

The interaction of molecules may be divided into an attractive force and a repulsive force which combine to generate an overall potential energy curve representative of the total molecular interactions of the given system. These interactions are depicted in Figure 2.10 (Atkins and Paula 1978).

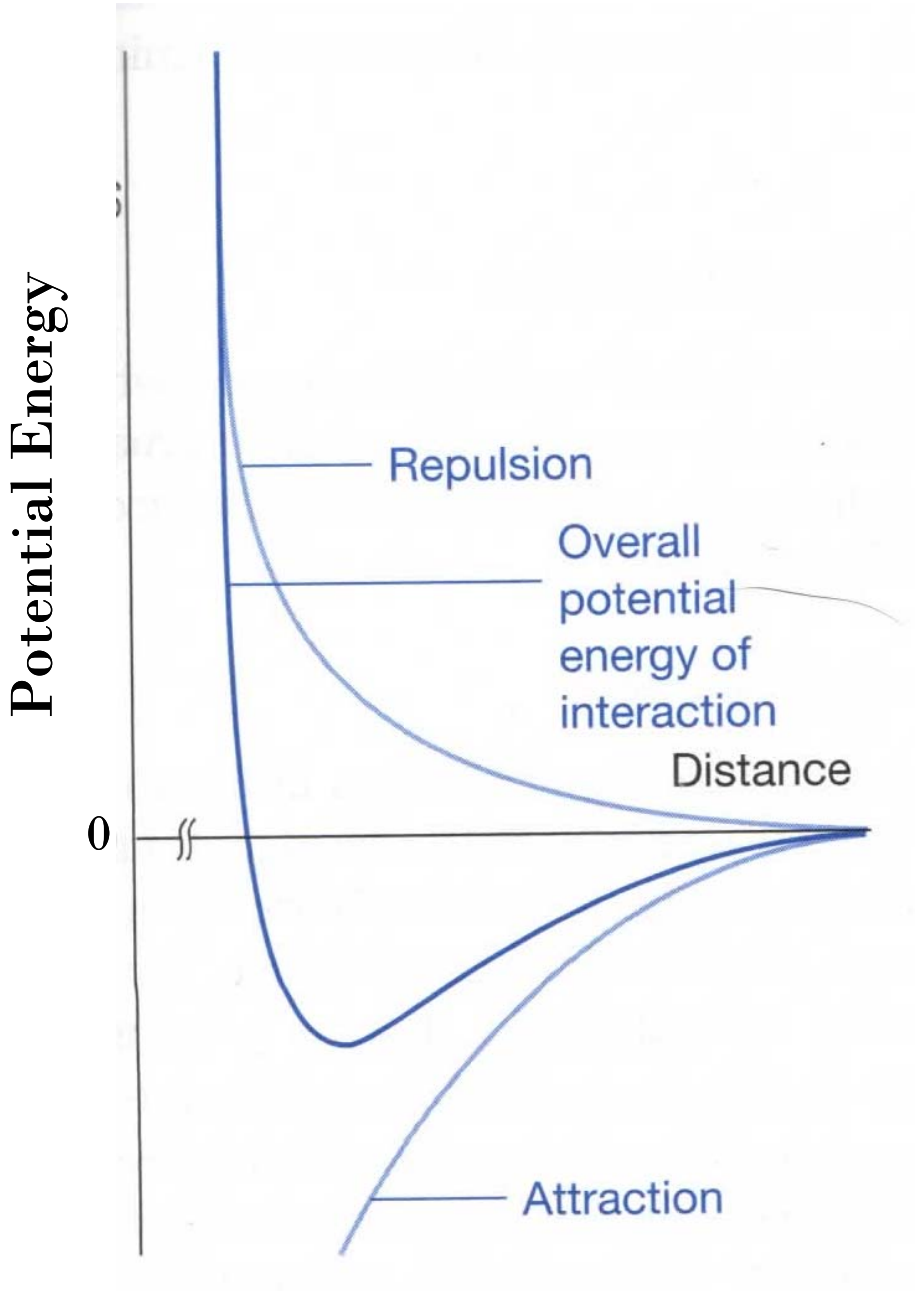


Figure 2.10– Interaction between atoms and molecules consists of attraction dominated at long distances and repulsion dominated at short distances (Atkins and Paula 1978)

2.3.1.1 – The Attractive Force

According to Adamson and Gast, below the critical temperature, gasses tend to adsorb as a result of van der Waals interactions with the surface (Adamson and Gast 1997). Rosenberg suggests that in addition to the van der Waals interactions, described as the one attractive mechanism which is always available. There is always some motion between the electrons and the positively charged nucleus resulting in variations in the shape of the electron cloud. This change results in an induced electric dipole moment. The van der Waals force is said to be responsible for the continuous interaction between the fluctuating dipoles (Rosenberg 1975). In addition to the van der Waals interactions which are present in all systems, one must take into account other forces including other potential binding forces between the two molecules including: ionic bonding (involving the actual transfer of an electron resulting in ion formation), covalent bonding, hydrogen bonding and metallic binding (all of which involve the sharing of electrons between the molecules) (Rosenberg 1975).

2.3.1.2– The Repulsive Force

There is also a repulsive force which arises as the molecules get very close to each other resulting in an overlap of the electron clouds of the two species. There is a repulsion between the like charges. This repulsive force between the electron clouds

counters the attractive forces. The repulsive force grows in intensity as the distance between the species is decreased (Rosenberg 1975). This repulsive force is commonly associated with the Pauli exclusion principal prohibiting the overlap of full electron orbitals (Atkins and Paula 1978).

2.3.1.3– The Lennard – Jones Potential

Commonly, the Lennard-Jones potential, given in equation (2.9), is utilized to model these interactions.

$$U(r) = 4\varepsilon\left(\left[\frac{\sigma}{r}\right]^{12} - \left[\frac{\sigma}{r}\right]^{6}\right) \tag{2.9}$$

The first term is the repulsive term, and the second term is the attractive term. ε is the potential well depth, σ is the crossover point where the potential changes from positive to negative, and r is the distance between the interacting molecules. The well depth is utilized to determine the energy of adsorption. Figure 2.11 shows overall potential curves for chemisorbed and physisorbed systems. Additional attractive forces present in the chemisorbed system result in a deeper potential well and a smaller equilibrium distance between the species (Lennard-Jones 1931).

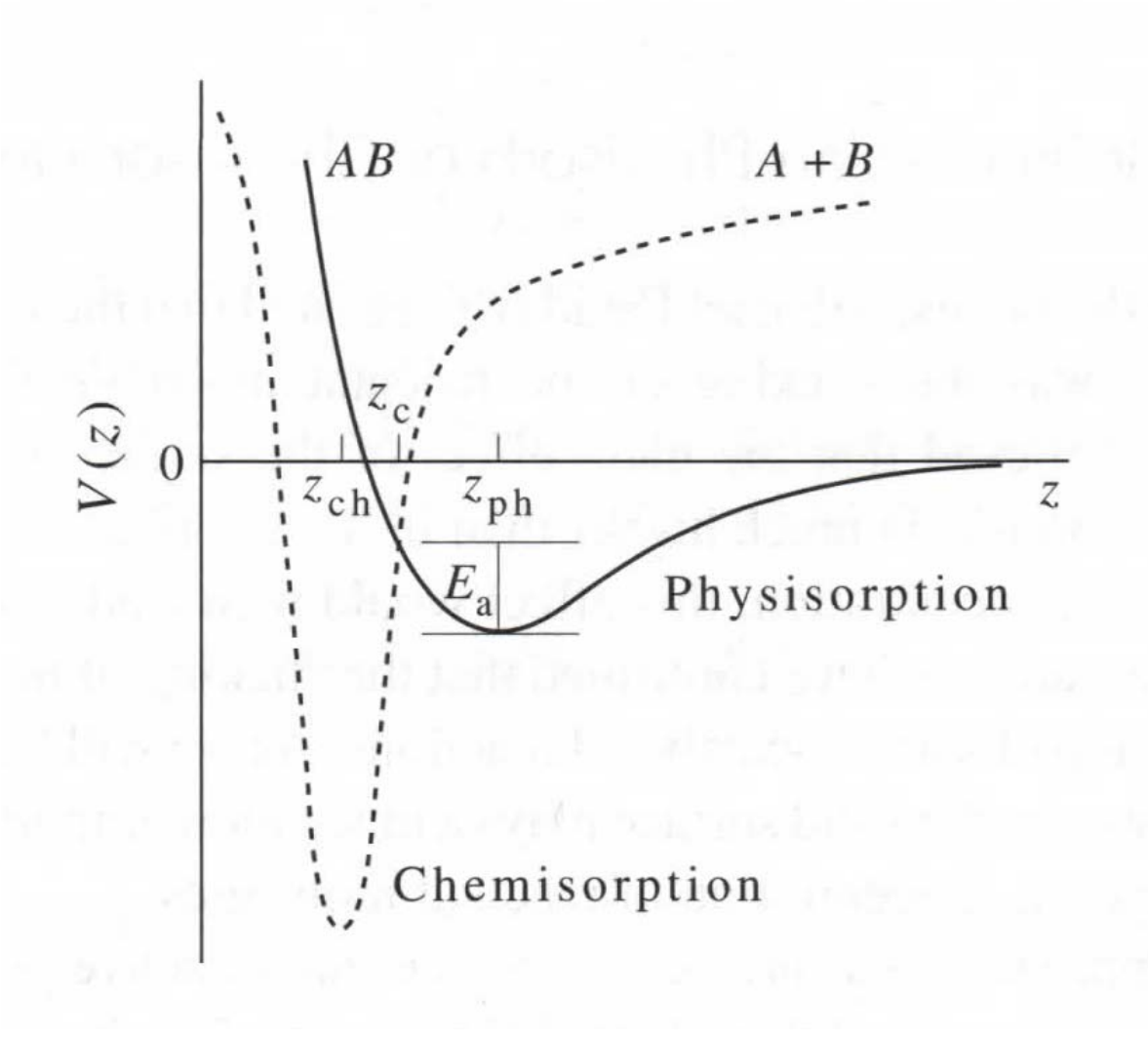


Figure 2.11 – Chemisorption vs Physisorption (McQuarrie and Simon 1997)

2.3.2 – Physisorption

The system discussed in this dissertation is classified as a physisorbed system. No transfer of electrons occurs between the adsorbate and adsorbent. The only attractive force involved in physisorption is the van der Waals interactions. As a result, physisorption mainly occurs at temperatures below the critical temperature of the adsorbate molecule (Adamson and Gast 1997). Physisorbed systems are generally completely reversible. When the adsorbed layer desorbs, the surface remains unscathed by the previous interaction. The act of physisorption is exothermic indicating that the final state of the adsorbed system is lower in energy than that of the bulk system (Samorjai 1994). Desorption is accomplished by simply heating the system a reasonable amount above the critical point of the system.

In a physisorbed system, the adsorbate molecules are continuously adsorbing and desorbing from the surface as evidenced by their short residence times. Equilibrium is reached when the rate of adsorption is equal to the rate of desorption. It is sometimes difficult to conceptualize this type of system. Molecules do not simply hit the surface and stick, they are continuously moving, rearranging, and pushing each other aside to make room for more molecules on the surface. Additionally, in a multilayer system, there is continuous movement between the layers. It is easier to understand the system by thinking in terms of dynamic equilibrium. When the

system is in equilibrium, there is no observable overall difference in the layers with time (Thomy, Duval et al. 1981).

2.3.3– Chemisorption

Chemisorption occurs when a chemical bond, classified by transfer of at least one electron, forms between the adsorbate and the adsorbent. Chemisorbed systems are often irreversible. Chemisorption is possible at any temperature at which the involved chemical reaction is capable of taking place. Often, this occurs at temperatures above the triple point of the adsorbate system. As a result analysis of a chemisorbed system focuses on for the formation of at most one adlayer on the surface as typical techniques used to analyze additional over-layers are no longer relevant (Adamson and Gast 1997). Any catalytic system would be referred to as a chemisorbed system. An effective catalytic system allows for the breaking and reforming of bonds to occur at the surface, allowing a separate chemical reaction to occur resulting in the removal of all species from the surface.

2.4 – Development of Adsorption Science: A History.

Dabrowski gives a history of experimental advancements of adsorption which is reiterated in Table 2.3 (Dabrowski 2001). Debrowski's history of theoretical advancements in adsorption science is reproduced in Table 2.4 (Dabrowski 2001).

Table 2.3 – The advancements of adsorption experimentation throughout history (Dabrowski 2001)

Date	Explorer	Significance
3750 BC	Egyptians and Sumerians	Use of charcoal for reduction of copper, zinc and tin ores for manufacture of bronze
1550 BC	Egyptians	Application of charcoal for medicinal purposes to adsorb odorous vapors from putrefactive wounds and from intestine
460 BC	Hippocrates and Pliny	First recorded application of charcoal filters for purification of drinking water
157 AD	Claudius Galen	Introduced the use of carbons of both vegetable and animal origin to treat a wide range of complaints
1773 1777	Scheele Fontana	Reported some experiments of the uptake of gases by charcoal and clays derived from various sources
1786, 1788	Lowitz	Used charcoal for de-colorization of tartaric acid solutions as result of organic impurities uptake
1793	Kehl	Discussed helpfulness of charcoal for removal of odors from gangrenous ulcer and applied carbons of animal origin for removal of colors from sugar
1974		Charcoal was used in the sugar industry in England as a de-colorization agent of sugar syrups

Table 2.3 – continued

Date	Explorer	Significance
1814	De Saussure	Started systematic studies of adsorption of various gases by porous substances as sea-foam, cork, charcoal, and asbestos. He discovered the exothermic character of adsorption processes
1881	Kayser	Introduced terms "adsorption", "isotherm" or "isotherm curve"; he also developed some theoretical concepts that became basic to monomolecular adsorption theory
1879, 1883	Chapuis	Made the first calorimetric measuremens of heat generation during wetting of various carbon by liquids
1901	Von Ostreyko	Set the basis for commercial development of activated carbons through processes that involve the incorporation of metallic chlorides with carbonaceous materials before carbonization and mild oxidation of charred materials with carbon dioxide or steam at increased temperatures
1903	Tswett	Discovered the phenomenon of selective adsorption, during separation of chlorophyll and other plant pigments by means of silica materials. He introduced the term: "column solid-liquid adsorption chromatography". This discovery was not only the beginning of a new analytical technique, but also the origin of a new field of surface science.
1904	Dewar	Found selective adsorption of oxygen from its mixture with nitrogen, during air uptake by charcoal

Table 2.3 – continued

Date	Explorer	Significance
1909	McBain	Proposed the term "absorption" to determine a much slower uptake of hydrogen by carbon than adsorption. He also proposed the term "sorption" for both adsorption and absorption
1911		The NORIT factory in Amsterdam was founded, now one of the most advanced international manufactures of active carbons
1911		A wood distillation plant was built in Hajnówka (East Poland), initially manufacturing active carbons solely from wood materials. World War I introduced the problem of protecting humans' respiratory tracts from toxic warfare agents.
1915	Zelinsky	Professor of Moscow University was the first to suggest and apply the use of active carbons as the adsorption medium in gas mask.
1941	Martin and Synge	Introduced to laboratory practice the solid-liquid partition chromatography, both in column and planar form
1956	Barrer and Breck	Invented the method of Zeolite synthesis. In this year, the North American Linde Company started production of synthetic zeolites at a commercial scale

Table 2.4 – The advancements of adsorption theory throughout history (Dabrowski 2001)

Date	Name	Significance
1888	Bemmelen Boedocker Freundlich	The so-called Freundlich empirical equation was firstly proposed by van Bemmelen. It is known in literature as Freundlich equation, because Freundlich assigned great importance to it and popularized its use
1911	Zsigmondy	Discovered the phenomenon of capillary condensation. This phenomenon is described by the Kelvin equation for cylindrical pores, with the pore width in the range 2 – 20 nm
1914	Eucken – Polanyi potential theory of adsorption	The basic concept of this theory includes the adsorption potential and the characteristic adsorption curve, which are independent on the temperature
1918	Langmuir	Derived for the first time a clear conceptof monolayer adsorption, formed on energetically homogeneous solid surfaces (kinetic studies). The statement proposed by Langmuir applied to chemisorpton and with some restrictions, to plysisorption. The Langmuir studies of gas adsorption by surfaces led to the formulation of a general treatment of reaction kinetics on surfaces. Langmuir realized that surface catalysis is usually preceded by chemisorption and he interpreted the kinetics of surface reaction in terms of his monolayer equation.
1932	Langmuir awarded the Nobel Prize	In 1932, Langmuir was awarded the Nobel Prize in chemistry for his discoveries and researches in the realm of surface chemistry

Table 2.4 – continued

Date	*Name*	**Significance**
1938	BET	The milestone towards development of adsorption science was the multilayer isotherm equation proposed by Brunauer, Emmett and Teller in 1938. This theory was preceded by two significant papers by Brunauer and Emmet in 1935 and 1937 who for the first time, were successful in determining – by means of isotherm adsorption of six different gasses – the surface area of an iron synthetic ammonia catalyst. They also introduced the point B method.
1940	BDDT	Brunauer, Deming, Deming and Teller proposed a four-adjustable parameter equation, where the forces of capillary condensation were taken into account. This equation as the complex, was rarely used in literature
1946	Dubinin - Radushekevich	Proposed the theory of the volume filling of micropores (TVFM) This approach is based on the potential theory of adsorption introduced by Eucken and Polanyi.

These tables end somewhat prematurely in that Debrowski seemingly ignores the past five decades of advancements. Certainly Thomy and Duval belong on the list for their examination of the adsorption of rare gasses on the surface of a crystalline exfoliated graphite material (Thomy, Duval et al. 1981). Their excellent review of associated two-dimensional phase transitions and their interpretation of layering behavior associated with stepwise growth in the isotherm have certainly influenced the manner in which current physisorbed systems are studied. Additionally, one would certainly expect the development of X-ray and neutron scattering facilities, instruments, and analysis techniques, would make the list of experimental improvements.

2.5 – Types of Isotherms

Originally there were considered to be five basic types of adsorption isotherms which are depicted in Figure 2.12 (Brunauer 1943). The Type I isotherm is representative of the Langmuir type adsorption isotherm. The Langmuir isotherm explains adsorption limited to one monolayer. This isotherm type is explained in more detail in section 2.5.1 (Adamson and Gast 1997). Type II is generally seen in the case of physisorbed systems. The BET model is primarily used to explain this type of adsorption phenomena and is explained in more detail in section 2.5.2.

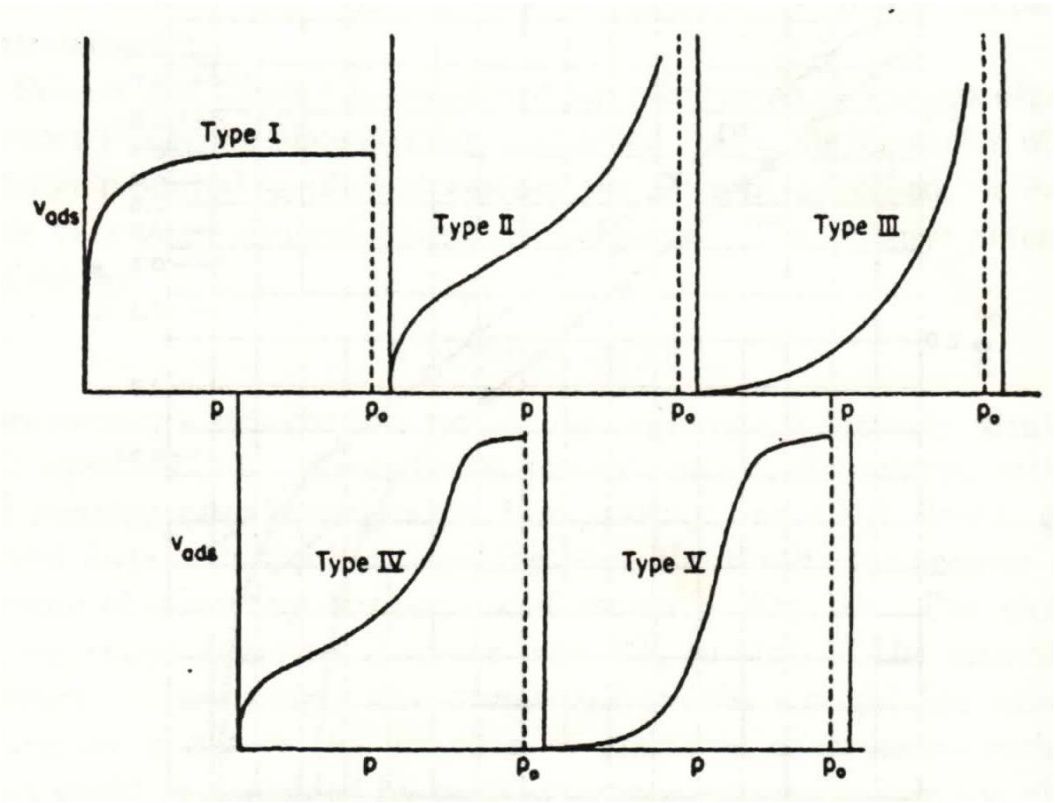


Figure 2.12- Five types of isotherms as defined by Brunauer (Brunauer 1943)

Type III is very rare. It generally occurs for situations in which the molecule-molecule interaction is much greater than the molecule-substrate interaction. In this case the heat of adsorption is less than or equal to the heat of liquefaction (Adamson and Gast 1997).

Types IV and V are seen most often in porous systems and reflect capillary condensation. These isotherm types often exhibit hysteresis. The hysteresis is shown in figure 2.13. Figure 2.13 also includes the now accepted Type VI isotherm which is seen in multilayer adsorption. This is the type of adsorption which is seen in the studies discussed in this dissertation.

2.5.1 – Langmuir Isotherm

A full derivation of the Langmuir isotherm is given in adamson and gast (Adamson and Gast 1997) which essentially reiterates that given by Langmuir (Langmuir 1918). A synopsis of this derivation is given here. The Langmuir isotherm is rooted in the assumption that there are a fixed number of adsorption sites, S. S_1 refers to the number of occupied sites, leaving the number of unoccupied spots to be described by S_0 as described in equation (2.10).

$$S_0 = S - S_1 \tag{2.10}$$

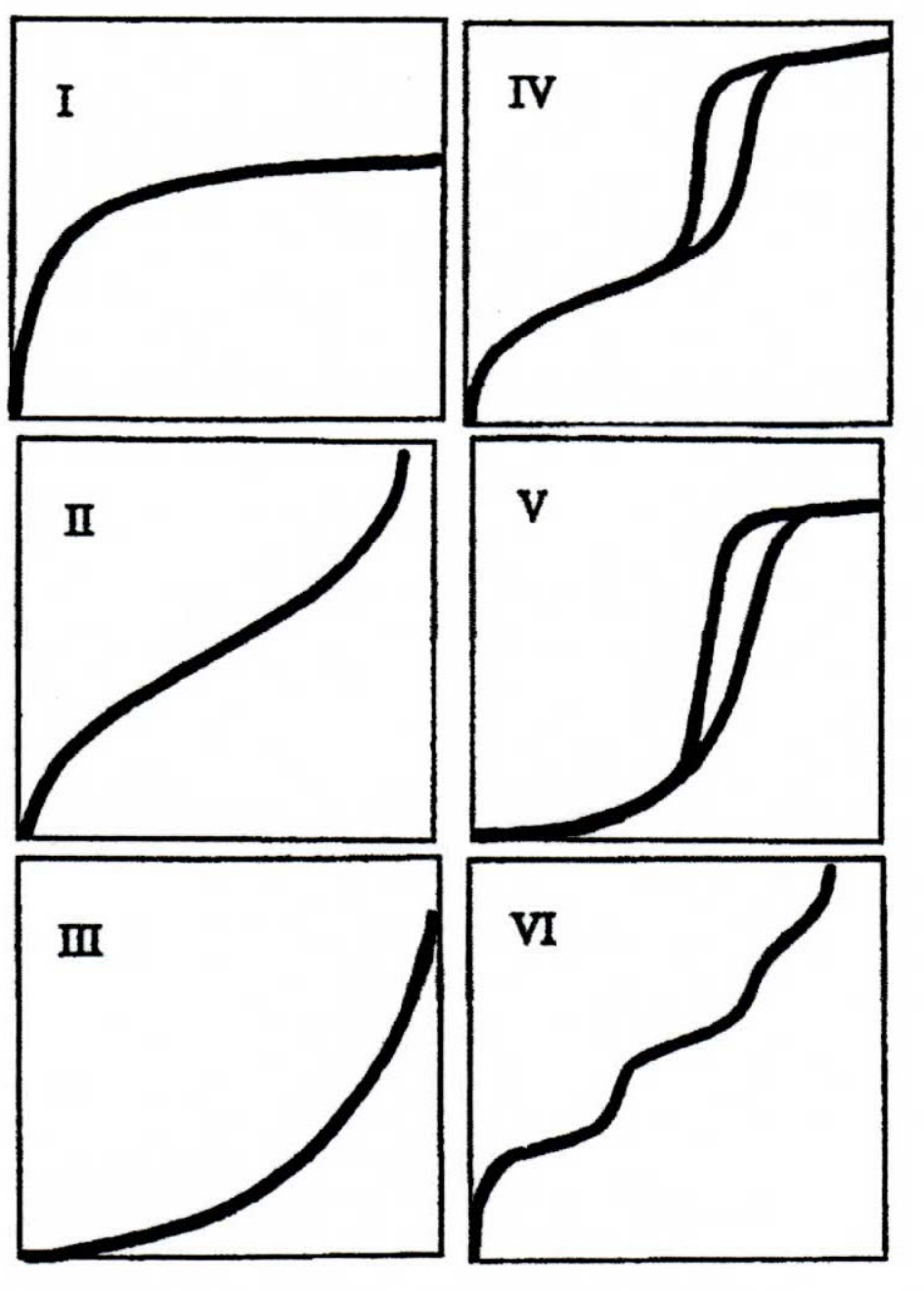


Figure 2.13 - The IUPAC currently defines six types of adsorption isotherms (Donohue and Aranovich 1998)

The rate of evaporation is proportional to the number of occupied spots and equals $k_1 S_1$ the rate of condensation is proportional to the number of unoccupied spots and the pressure P in the system and is given to be $k_2 S_0 P$. At equilibrium equation (2.11) holds.

$$k_1 S_1 = k_2 S_0 P = k_2 P\left(S - S_1\right) \tag{2.11}$$

The fraction of the surface that is covered, θ, is equal to S_1/S. If we define b as the ratio of the rate constants as shown in equation (2.12), θ, can be rewritten as shown in equation (2.13).

$$b = \frac{k_2}{k_1} \tag{2.12}$$

$$\theta = \frac{bP}{1+bP} \tag{2.13}$$

θ may also be written in terms of the number of moles adsorbed, n and the number of moles per gram adsorbed at the monolayer n_m. θ is therefore defined as given in equation (2.14).

$$\theta = \frac{n}{n_m} \tag{2.14}$$

Substitution into equation (2.13) results in equation (2.15).

$$n = \frac{n_m bP}{1 + bP} \tag{2.15}$$

Rearrangement of equation (2.15) results in linear equation (2.16), with slope $1/n_m$ and intercept $1/bn_m$.

$$\frac{P}{n} = \frac{1}{bn_m} + \frac{P}{n_m} \tag{2.16}$$

If the area of an adsorption site, σ^0 , can be estimated then the surface area of the substrate, Σ , can be calculated according to equation , where N_A is Avogadro's number.

$$\Sigma = n_m N_A \sigma^0 \tag{2.17}$$

One major draw back of the Langmuir isotherm is its inability to model behavior beyond the monolayer, $\theta = 1$.

2.5.2 – Brunauer, Emmet, and Teller(BET) Isotherm

Recognizing the shortcomings of the Langmuir isotherm, Brunauer, Emmet, and Teller, proposed an alternative method for dealing with the adsorption of gasses on solid surfaces. The BET isotherm improves upon the Langmuir isotherm in that it removes the limit imposed by the Langmuir isotherm that adsorption is limited to coverage of a single monolayer. It extends its application to include multilayer

adsorption. The properties of the monolayer are assumed to also hold for the additional adlayers.

This isotherm type assumes that the heat of adsorption, Q_{ads}, for all layers above the monolayer should be equivalent to Q_v, the heat of condensation of the liquid adsorbate. Adamson and Gast provide a synopsis of the details regarding the derivation of the BET isotherm first explained by Brunauer, Emmet, and Teller (Brunauer, Emmett et al. 1938). A brief explanation of the results of that derivation is given here. The equilibrium condition is defined such that each layer is said to reach a steady state value in relation to the layer beneath it. This steady state approximation is depicted by equation (2.18).

$$a_i P S_{i-1} = b_i S_i e^{-\left(Q_v / RT\right)} \tag{2.18}$$

The BET equation takes the form given in (2.19).

$$\frac{n}{n_m} = \frac{cx}{(1-x)\left[1+(c-1)x\right]} \tag{2.19}$$

Where c is given by equation (2.20) and x is defined by equation(2.21).

$$c = e^{(Q_1 - Q_v)/RT} \tag{2.20}$$

$$x = \frac{P}{P_0} \tag{2.21}$$

Equation (2.19) can be written in a linear form according to equation(2.22).

$$\frac{x}{n(1-x)} = \frac{1}{cn_m} + \frac{(c-1)x}{cn_m} \tag{2.22}$$

The BET equation is capable of adequately describing a physisorbed system at intermediate coverages ($0.8 < \theta < 2.0$). This analysis still falls short in the explanation of the multilayer isotherm (Adamson and Gast 1997).

2.5.3 – FHH isotherm

The BET isotherm does not effectively approximate the adsorption behavior at high coverage. The FHH isotherm was first derived separately by Frenkel (Frenkel 1946) and Halsey (Halsey 1948) and Hill (Hill 1949). A complete description of the theories involved in the derivation of this isotherm can be found in those publications. Adamson and Gast does a good job of summarizing their assumptions and conclusions (Adamson and Gast 1997). The FHH explanation suggests that at high coverage, the behavior of the adlayer has properties similar to that of the bulk system. It is assumed that the molar entropy of these upper adlayers is the same as that of the bulk. The FHH equation is given by equation(2.23).

$$\ln\left(\frac{p}{p_0}\right) = \frac{k}{\theta^s} \tag{2.23}$$

Here, k is a constant specific for the given gas-solid system, and s is an empirical parameter associated with the dispersion forces r^{-6} term. The FHH equation is

seemingly valid for adlayers three and above, but has major shortcomings at low coverages (Adamson and Gast 1997).

2.6 – Surface Defects

Figure 2.14 shows the typical types of surface defects which may be present in the material. Defects such as these tend to increase edge effects which are seen in the isotherms.

2.6.1 – Edge Effects

Figure 2.15 is a simplified view of edge effects. If one uses a sterric model of spherical atoms as an example, then imagine stacking billiard balls to create crystals by which they can quite readily understand crystal growth. As you begin stacking the balls on top of the first layer, it is impossible to fit as many balls in the second layer as are present in the first. Similarly, the third layer contains fewer balls than the second, the fourth less than the third, and so on. We will use this simple model to further illustrate some surface properties. Figure 2.16 utilizes this simple model to show layer growth for a simple Methane isotherm.

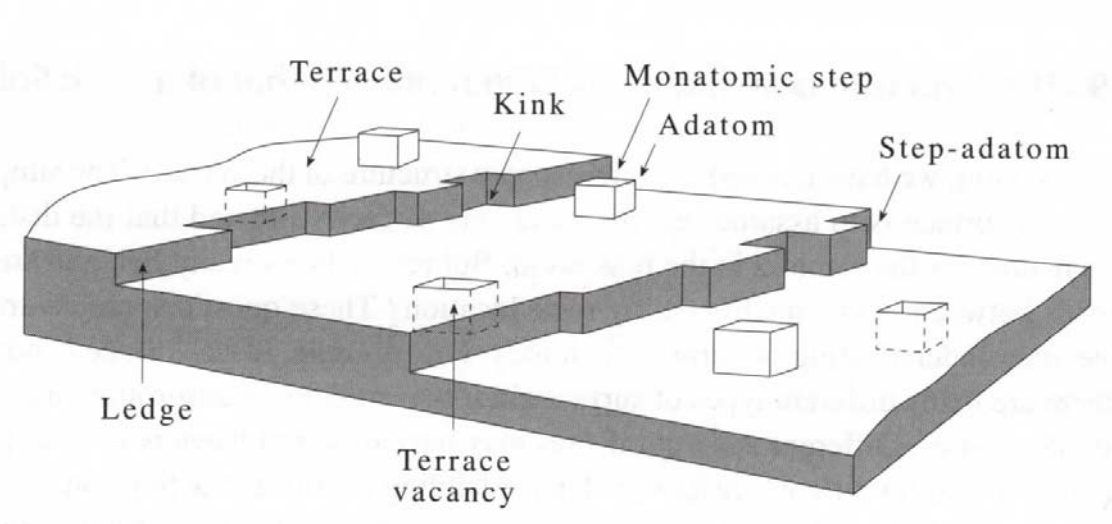


Figure 2.14 - Types of surface defects (McQuarrie and Simon 1997)

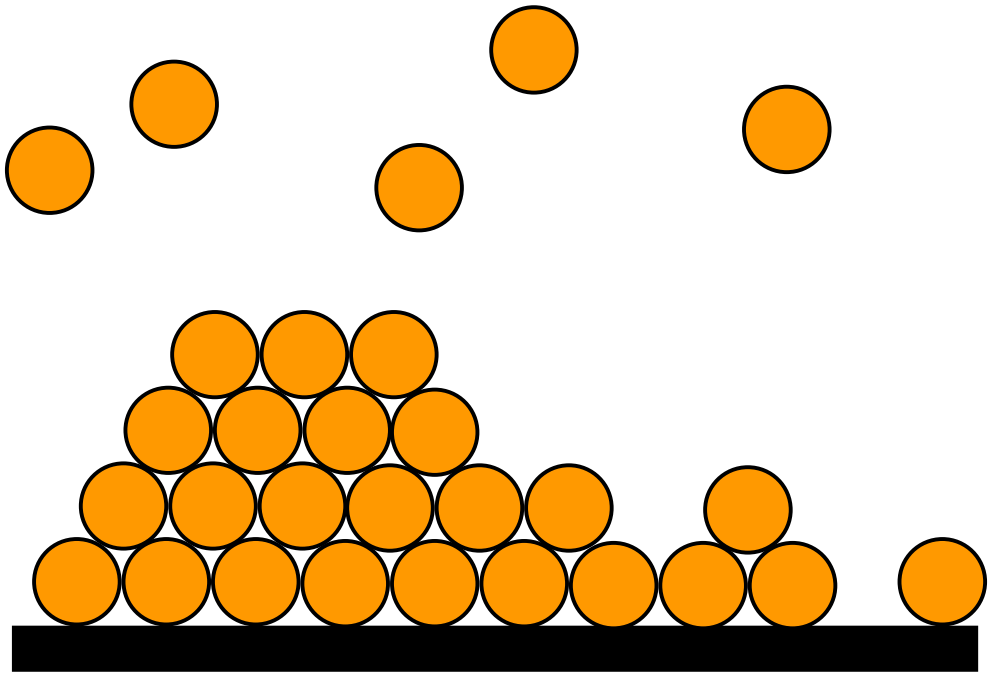


Figure 2.15– Simplified view of molecular stacking

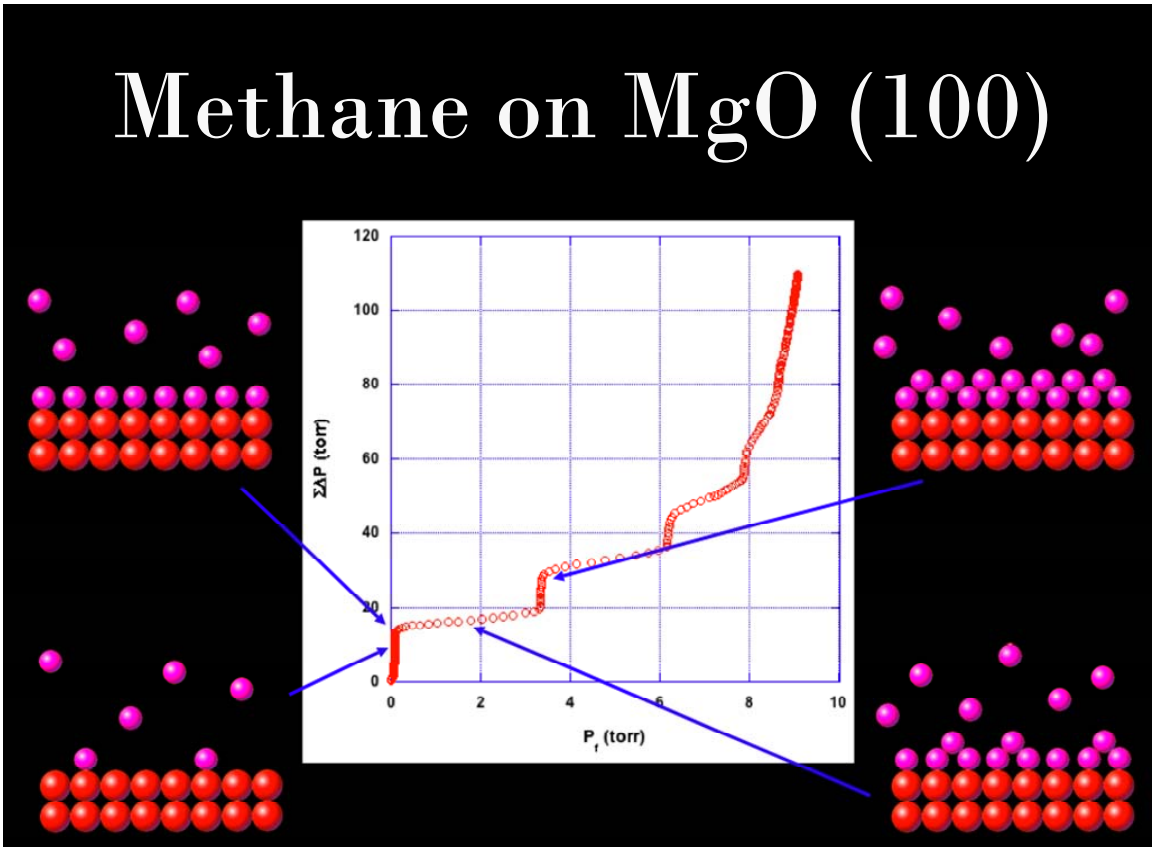


Figure 2.16 – simplified view of layer by layer growth (Thomy, Duval et al. 1981)

2.6.2– Monatomic Steps

This result is exactly what happens when molecules adsorb (stack themselves) onto the surface of a substrate. This effect is evidenced by a slight decrease in step height with increasing coverage. The surface defects, such as the monatomic steps shown in figure 2.14, serve to increase the area available for monolayer coverage, while they are often too small for bi-layer or tri-layer formation. This effect results in a disproportionately high first adlayer step in relation to the higher adsorption steps in the isotherms.

2.7 – Commensurability

An adlayer is considered to be commensurate with the under-layer structure if there is a one-to-one correlation between the layers. This means that the molecules in the adlayer arrange themselves on the under-layer in a regular pattern. There exists a single vector which can be applied to identical positions in the unit cells of the under-layer which connects to the unit cell of the over-layer (Samorjai 1994). There is interest as to the over-layer structure being commensurate with the substrate, as well as the layers themselves being commensurate with one another.

The structure of the adsorbed monolayer is in general affected by the structure of the substrate. Strong substrate-molecule interactions are responsible for the ultimate fill pattern of the monolayer. As further adlayers form on the surface they are influenced by both molecule-molecule interactions as well as molecule-substrate interactions. The further away from the surface the molecule gets the smaller the substrate-molecule interaction becomes, and the more likely it becomes for the adlayer structure to approach bulk like behavior.

The closer the monolayer structure is to the bulk structure, the more likely the adlayers further from the surface will fit into that structure. This similarity manifests itself in more adlayer steps being visible in the adsorption isotherms. If the surface induced film structure differs greatly from the bulk, adsorption isotherms tend to exhibit fewer (if any) discrete stepwise increases. Because the molecule-substrate interaction decreases significantly with distance, the behavior of adlayers beyond the second layer is dominated by molecule-molecule interactions (due to distance from the surface and the shielding effect of the lower adlayers) perfect matches between the adsorbed film and the substrate are the exception not the rule, there will usually not be more than two to three adlayers visible prior to reaching the saturated vapor pressure of the system.

2.7.1 – Surface Adsorption Sites

There are generally three types of sites of high symmetry available for adsorption on solid, crystalline surfces: A-top, the bridge or saddle point, and the interstitial or hollow site (Steele 1974; Steele 1996). These sites are depicted in figure 2.17 for a simple salt-like structure, square lattice. Figure 2.18 shows these sites for a hexagonal lattice. If the monolayer is commensurate with the surface, the unit cell of the adlayer will most likely fall into a direct correlation with one of these sites in the unit cell of the substrate (correspondence could be one-to-one, i.e. 1x1, or two-to-one (2x1), or two-to-two (2x2), etc.). Examples of some commensurate structures are shown in Figure 2.19.

2.8- Wetting

Wetting is a term often used to denote how the growth of an adlayer film on the surface takes place. There are three general types of wetting phenomena: complete wetting, in-complete wetting, and non-wetting. Wetting like many adsorption properties is rooted in the competition between the molecule-surface interactions and the molecule-molecule interactions (Dash 1975). The classification is related to the determination of the contact angle that the molecular film makes with the surface. There are several excellent references on the subject of surface wetting by

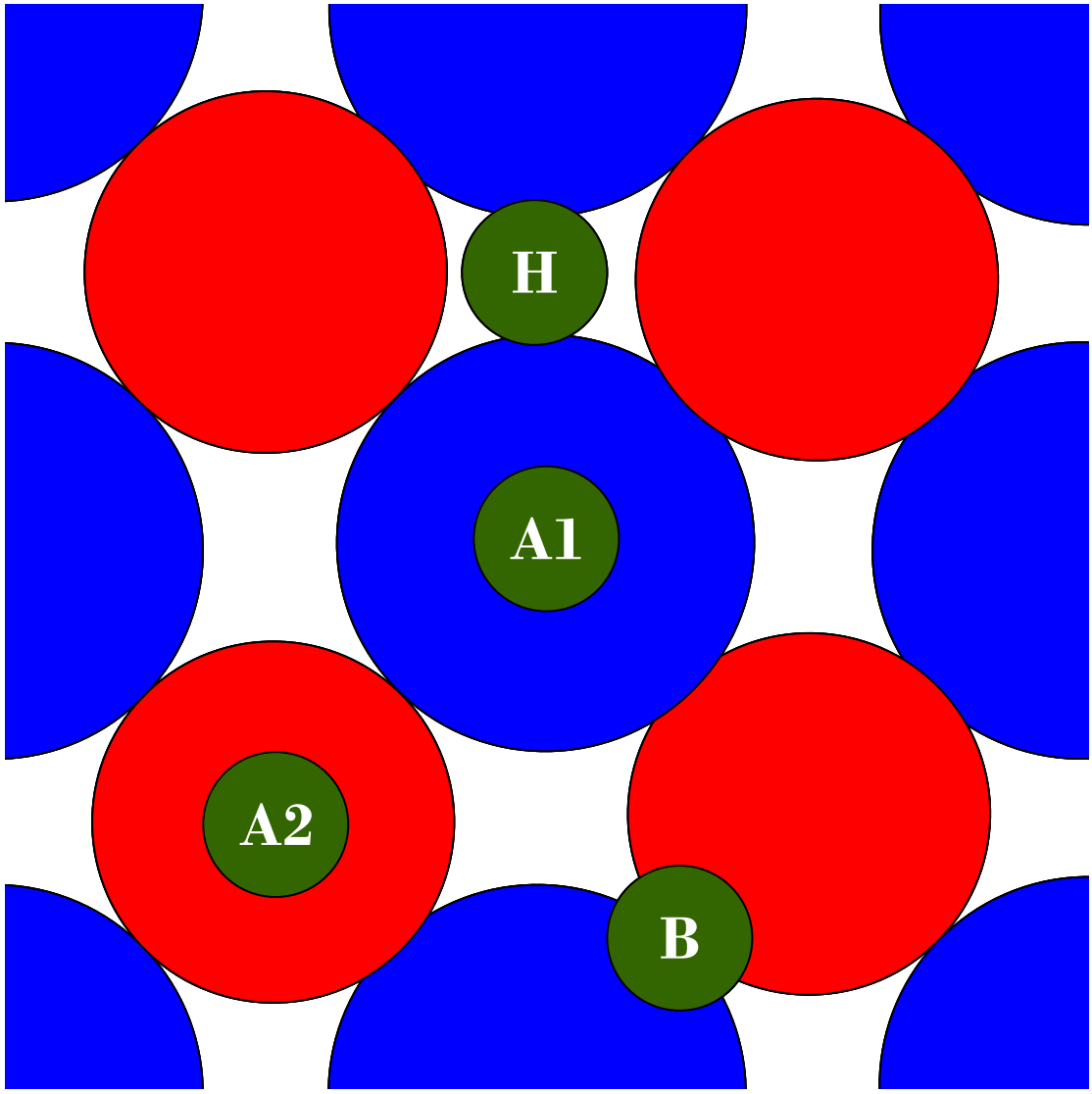


Figure 2.17– Possible adsorption sites of a simple salt like structure.

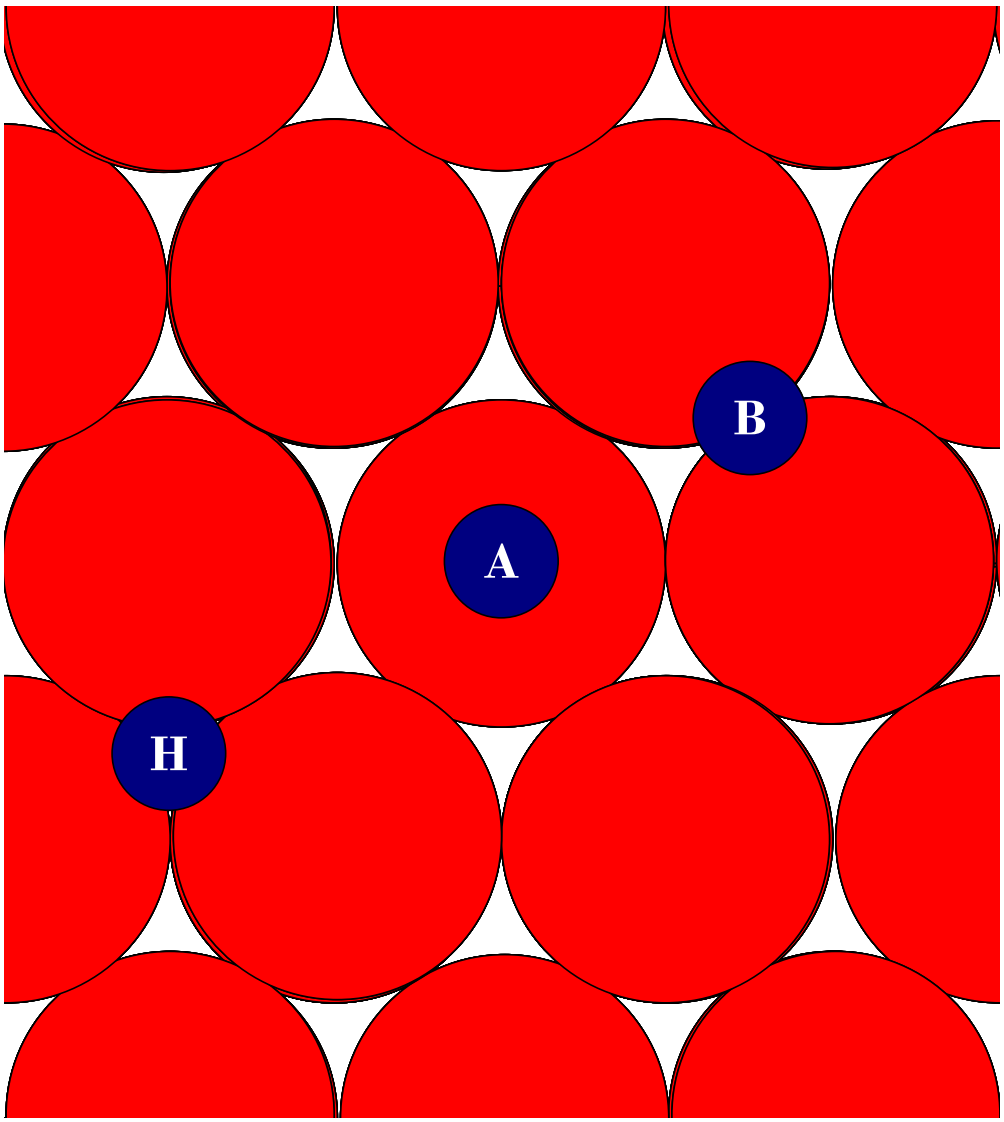


Figure 2.18– Adsorption sites available for a hexagonal lattice

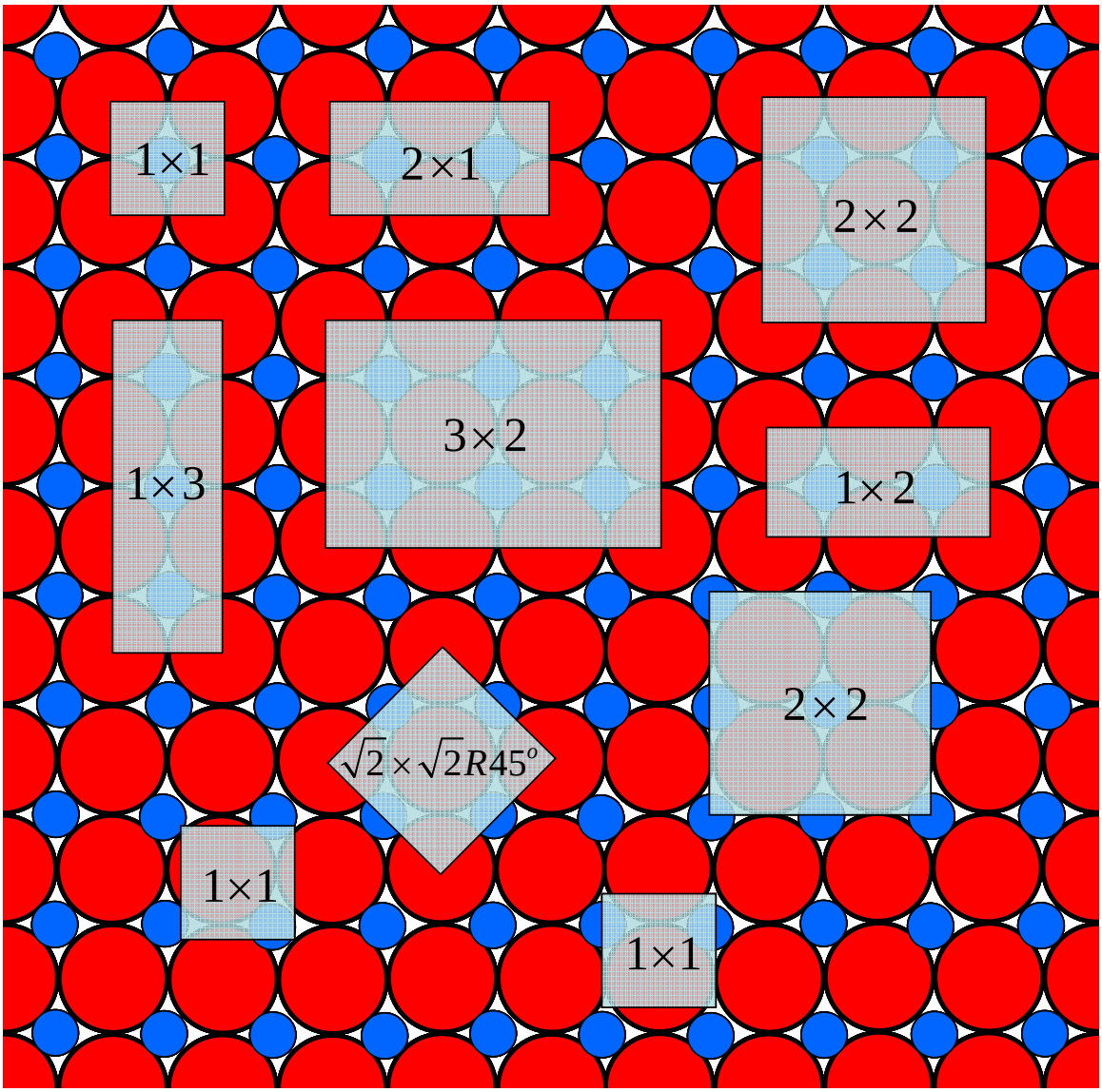


Figure 2.19- examples of high symmetry commensurate structures on the surface of a simple cubic substrate

authors such as M. Schick (Schick 1990), D. Beysens (Beysens 1988), S. Dietrich (Detrich 1988), G. Dash (Dash 1977), and Thomey and Duval (Thomy and Duval 1994).

2.8.1 – Contact angle

The manner in which a drop of liquid interacts with a surface is described by the contact angle. Figure 2.20 shows an illustration depicting the contact angle that a drop of adsorbate makes when adsorbed on the surface. If the droplet beads up completely, like a drop of mercury, it is said to be non-wetting this would be equivalent to a contact angle of 180°. In contrast if the liquid spreads out completely, it would have a contact angle of 0° (the complete wetting case). In between these extremes lies incomplete wetting for contact angles $0° < \theta < 180°$. Adamson and Gast actually suggest that incomplete wetting could begin to occur for systems with contact angles greater than 90° (Adamson and Gast 1997).

2.8.2 – Determination of wetting from isothermal data.

The wetting behavior of adsorbed films can be obtained by monitoring the manner in which volumetric isotherms behave as the saturated vapor pressure, p_o, is approached.

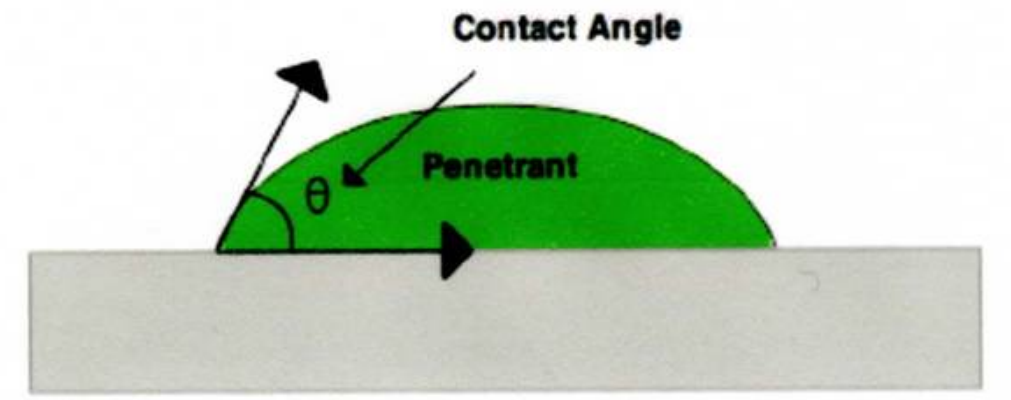


Figure 2.20 - depiction of contact angle calculation

2.8.2.1 – Incomplete Wetting Behavior

It is not surprising that in-complete wetting is the most common type as it covers such a wide range of contact angles and often reflects the fact that the surface directed structure is incompatible with the bulk structure (Stranski and Krastanow 1937; Dash and Pandit 1981). Molecule-surface interactions are quickly overcome by molecule-molecule interactions as the film thickness increases. This could result, for example, in a small number of adsorption steps being recorded prior to the system forming the bulk at the SVP. Incomplete wetting results in a finite film thickness. Isotherm types I, IV, avd V are representative of incomplete wetting systems. These were shown previously in Figure 2.13.

2.8.2.2 – Non-Wetting Behavior

A non-wetting system has little to no substrate-molecule interaction (Volmer and Webber 1926; Dash 1975). As the p_o is reached a sharp discontinuity is seen in the isotherm. There is not considered to be any layering occurring in this situation. As more adsorbate molecules are added to the system, only bulk like droplets are present on the surface. Two additional types of isotherms are suggested to exhibit the non-wetting system. Adamson and Gast reveal two additional isotherm types which we will call types VII and VIII shown in figure 2.21 which are representative of non-wetting behavior (Adamson and Gast 1997).

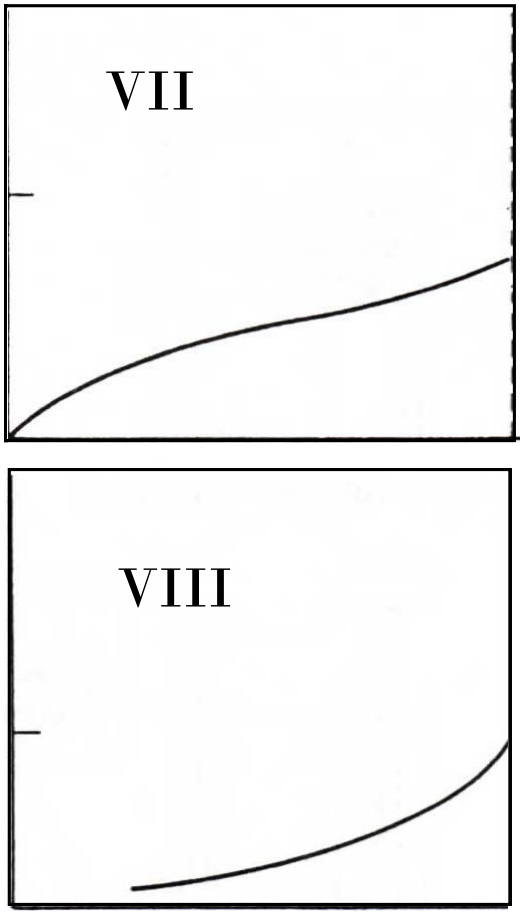


Figure 2.21- Additional isotherm types associated with non wetting behavior (Adamson and Gast 1997)

2.8.2.3– Complete Wetting Behavior

For the alternate extreme of complete-wetting to occur requires the surface directed structure to closely approximate that of the bulk solid. Therefore, when the molecule-molecule interactions begin to dominate the system, the adlayers are content to adsorb on the surface as it imitates the bulk (Frank and Merwe 1979; Dash and Pandit 1981). In this case, layer growth asymptotically approaches the SVP. Generally only small spherical molecules and rare gasses exhibit complete wetting behavior. Isotherm Types II, III, and VI as shown previously in figure potentially show complete wetting behavior.

Chapter 3

Materials



M. C. Escher: Order and Chaos (1950)

3.1 – Metal Oxides

3.1.1 – Sample Preparation

Metal Oxide Powders used in this study were prepared in-house using a patented method developed by Walter Kunnmann and John Z. Larese US Patent Number 6,179,897 (Kunnmann and Larese 2001). Typically a stream of Argon gas is directed into a vertically aligned Pyrex™ sample collection chimney capped with metal end pieces gravity sealed with rubber gaskets. The top cap is fitted with baffles to reduce loss of the fine powder product with the outlet gas. This cap is attached via a KF™ flanged hose leading to an active fume hood which helps direct the gas flow through the chamber and finally into an exhaust system. In order to purge the air from the synthetic chamber, ultra high purity Argon gas is passed through the system for several hours in until the air in the chamber is considered to be sufficiently replaced by Argon gas resulting in a low humidity inert atmosphere for reaction. All gas flows are computer controlled using AREA flow regulation for inlet stream valves.

The metal is placed inside a graphite crucible with additional graphite pieces filling up the remainder of the volume. The metals are then heated inductively using a Lepel™ RF Generator. Upon vaporization of the metal, Oxygen is introduced using a halo shaped ring delivery system equipped with small holes which serve to direct the flow

into the vapor rising from the crucible. The reaction is allowed to proceed until the resultant reaction fire dies out. During the reaction, the metal oxide product is collected on the walls of the reaction chamber. Figure 3.1 shows this apparatus in use for metal oxide preparation. As soon as the collection chamber cools sufficiently to be touched by human hands, it is disassembled and the metal oxide powder is collected and stored in vials under argon and placed in argon filled desiccators.

3.2 – Magnesium Oxide

Magnesium Oxide (MgO) is the substrate utilized as the adsorbent in the studies discussed in this dissertation. Magnesium Oxide is produced, utilizing high purity (99.9%) magnesium ingot ordered from the Alfa Asear Corporation, via the above technique. The reaction takes place according to the following reaction mechanism:

$$xMg(s) + yC(s) \rightleftharpoons Mg_xC_y(s) \tag{3.1}$$

$$Mg_xC_y(s) \longrightarrow xMg(g) + yC(s) \tag{3.2}$$

$$Mg(g) + \underset{excess}{O_2(g)} \longrightarrow MgO(s) \tag{3.3}$$



Figure 3.1 – Patented device used in preparation and collection of metal oxides (Kunnmann and Larese 2001)

3.2.1 – Characteristics

3.2.1.1 – Sample Quality

A comparison study between our MgO and that available commercially from Aldrich was performed. In addition to electron microscopy (SEM and TEM), Electron Spin Resonance (ESR) and Atomic Adsorption Spectroscopy (AAS) methods were used. The ESR comparison is shown in Figure 3.2. The results clearly show that MgO produced following the Kunnmann-Larese method is of high purity, with manganese ions present as the main impurity. In contrast, to the commercially available MgO whose impurities include: Cobalt, Chromium, Iron, and Manganese ions. AAS evaluation has shown the levels of manganese to be present on the order of ~5ppm.

3.2.1.2 – Sample Size and Structure

The MgO we produced for this study has an average particle size on the order of 200nm, and exhibits single facet exposure of the (1 0 0) face. For exploring the 2D to 3D behavior, particles of this size are desired to minimize edge effects. The simple cubic rock salt structure of MgO makes it an ideal metal oxide for study. SEM images (taken with a Hitachi S-4700) of this MgO are shown in Figure 3.3. A TEM image

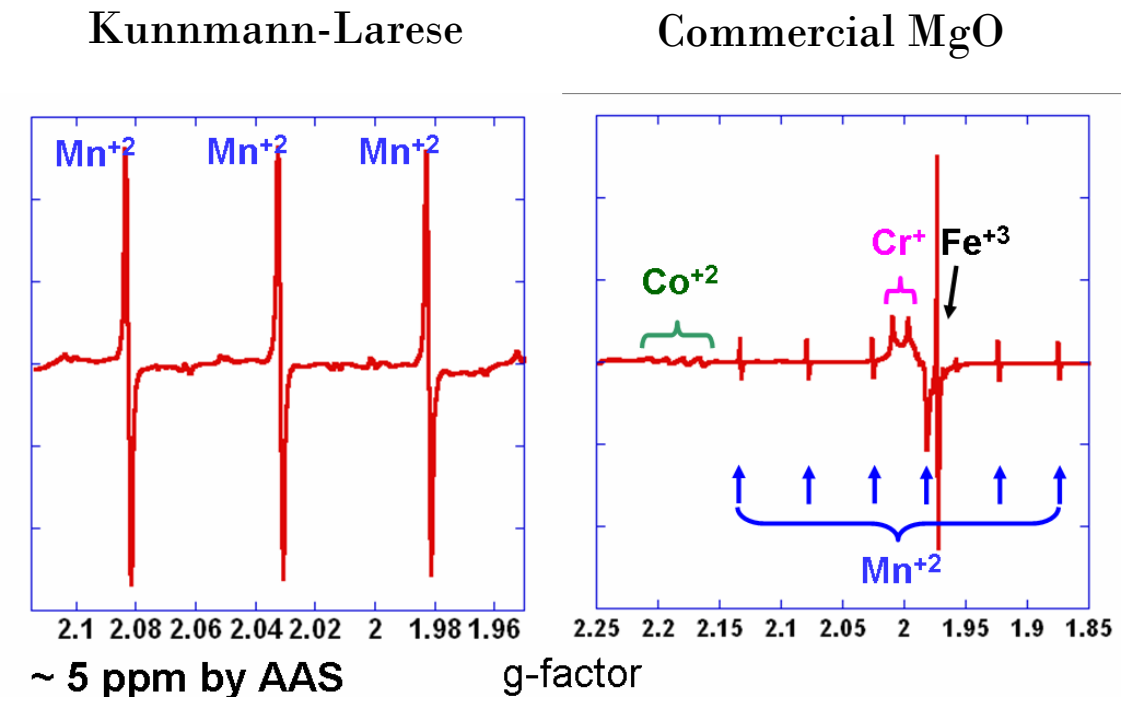


Figure 3.2 - ESR and AAS results in the comparison of commercial MgO and that produced in the Larese Group

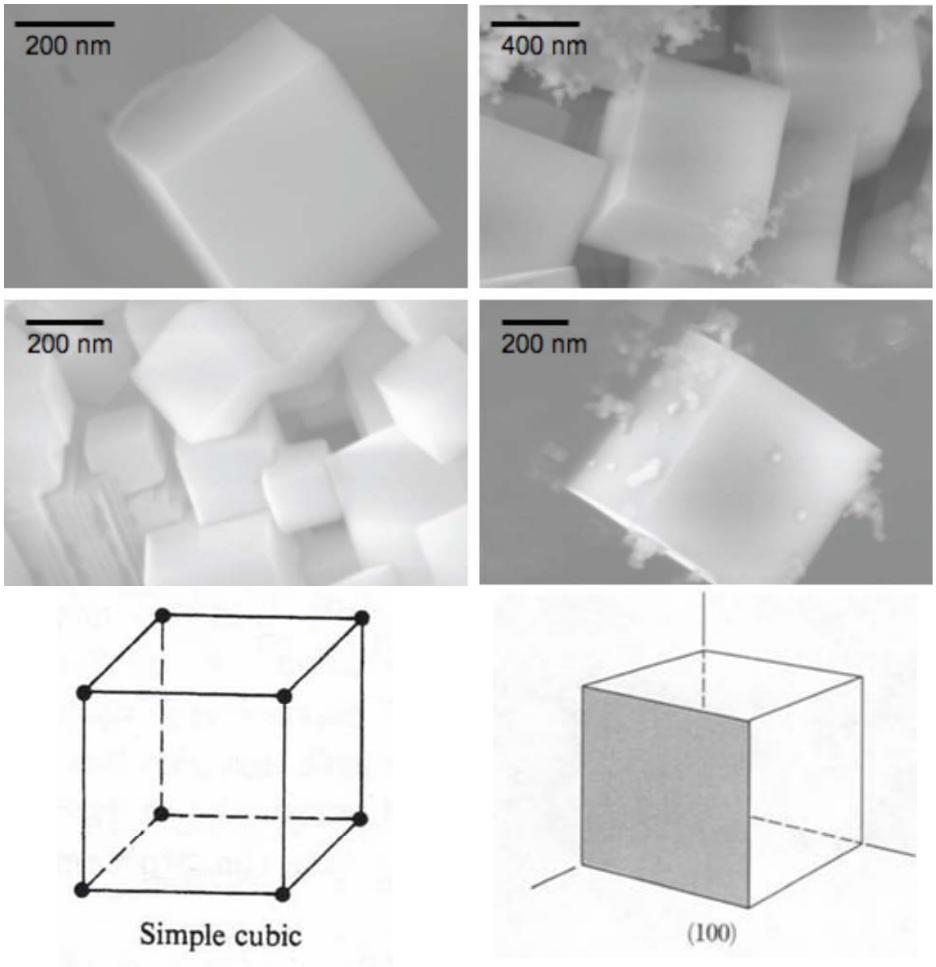


Figure 3.3– SEM images of MgO (100). MgO has a simple cubic structure and exhibits single facet exposure of the (100) face

(taken on a Hitachi HD-2000 model STEM) and a graphical representation of the MgO cube are shown in Figure 3.4. The unit cell of the ionic crystal is shown in Figure 3.5. The unit cell consists of exactly one magnesium atom and one oxygen atom and has a lattice constant of 2.98Å. The MgO produced has a surface area on the order of 10 m^2/g and exhibits a good surface area to volume ratio.

3.2.1.3 – Defects

The most prominent defects seen in MgO are O^{2-} vacancies. Figure 2.14 describes this as a terrace vacancy. This vacancy is depicted in figure 3.6 . Another common defect results from the hydroscopic nature of the MgO. If the MgO is stored improperly or left open to the atmosphere for too long, it allows water to come into contact with the surface of MgO. The water attacks the low coordination sites of the MgO: the corners and edges of the (100) cubes. This results in the generation of monatomic steps or ledges as described in chapter 2. An example of this defect is seen in the SEM image shown in Figure 3.7.

3.2.2 – Methane (CH_4) adsorption studies on MgO (1 0 0)

Much study has been done regarding the interaction with CH_4 and MgO. In 1985, Coulomb, Madih, Croset and Lauter, determined that CH_4 forms a

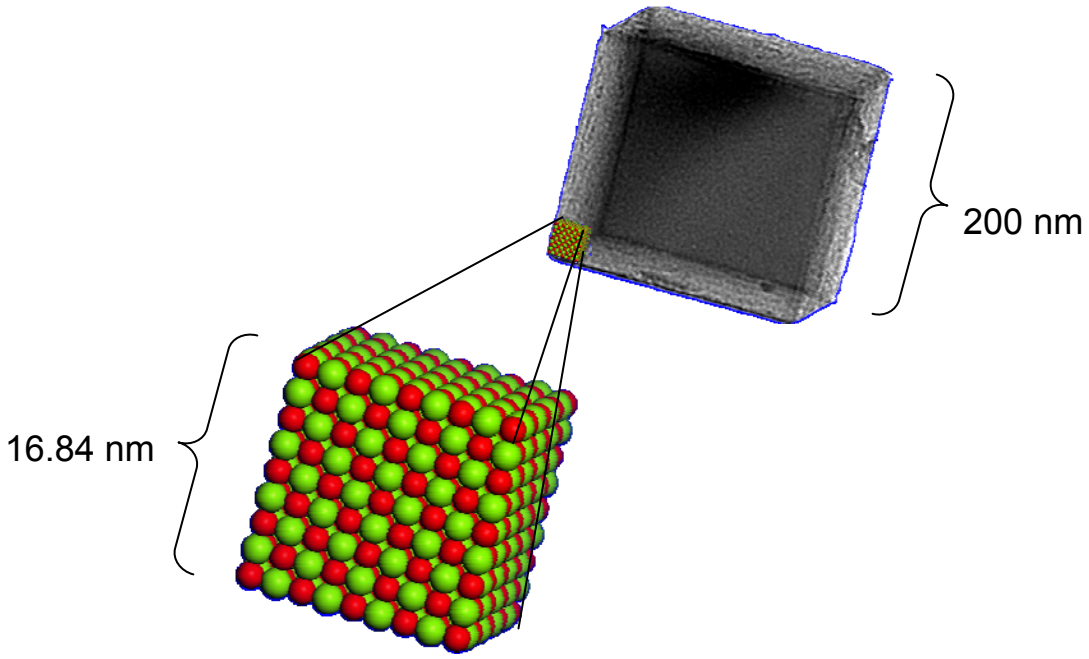


Figure 3.4 – TEM image of MgO (100) cube with graphical representation of the simple cubic rock salt structure of the MgO (100) cube

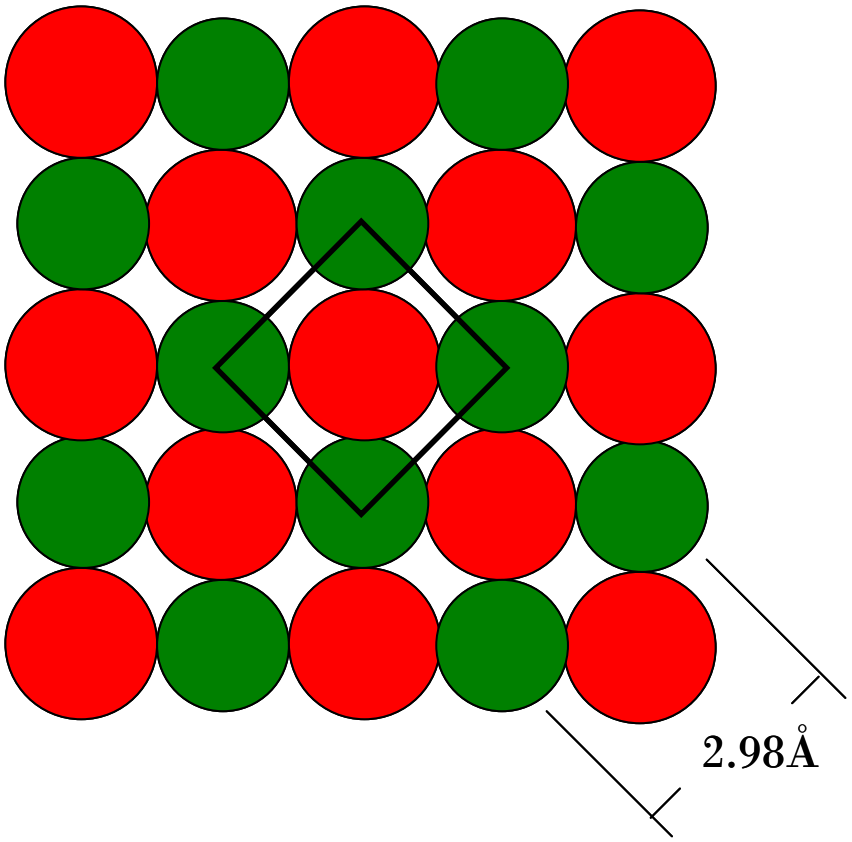


Figure 3.5 – Unit Cell of the 100 surface of MgO is marked by the solid line. The unit cell contains exactly one magnesium atom and one oxygen atom. It is a square lattice with a = 2.98 Å yielding a primitive unit cell area of 8.88 Å^2.

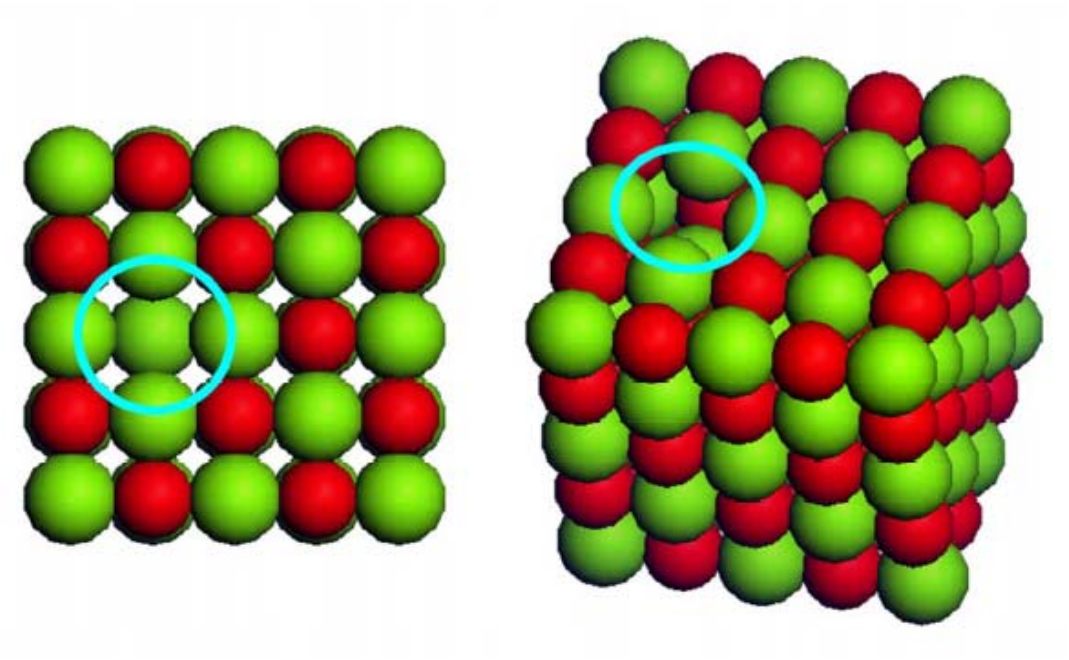


Figure 3.6 - Oxygen vacancy

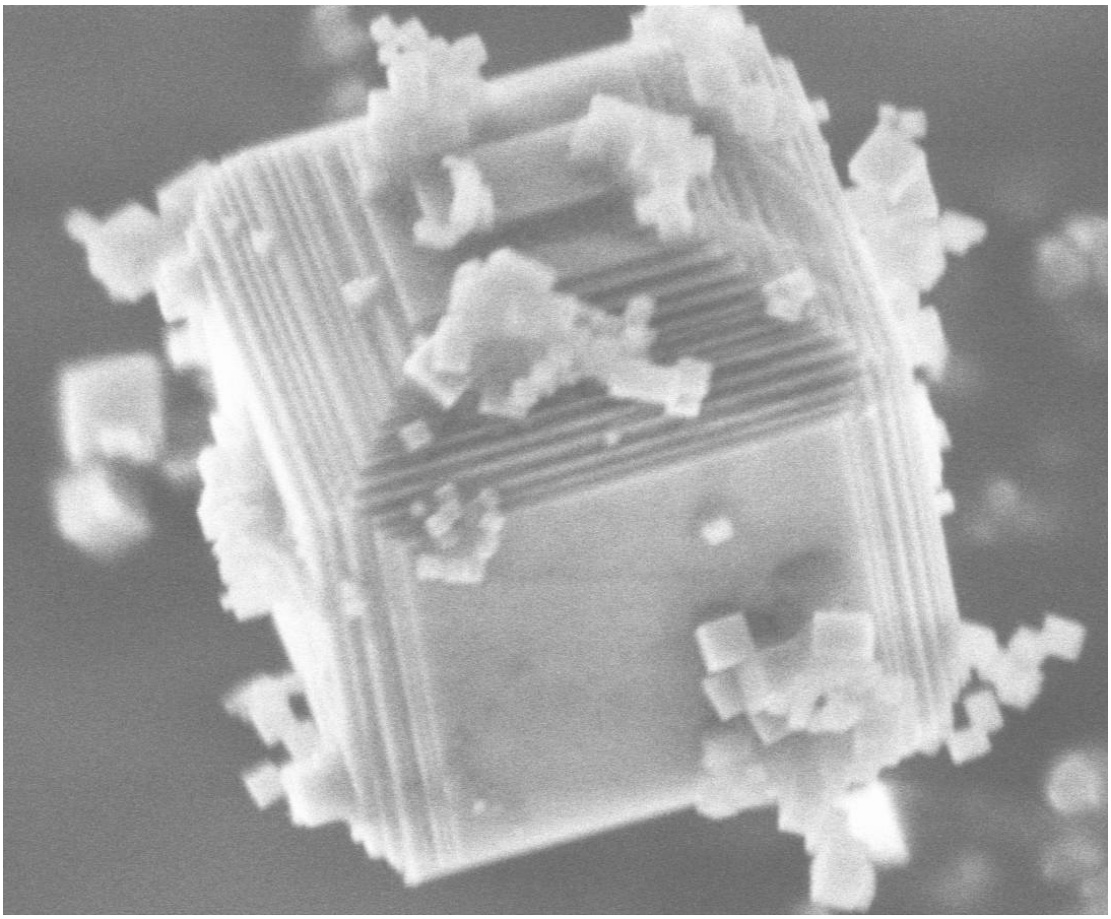


Figure 3.7 – MgO cube showing ledges and monatomic steps. It should be noted that each surface is a (100) crystal face

commensurate c(2x2) square solid structure on the surface of MgO (100) (Coulomb, Madih et al. 1985).Larese and coworkers later confirmed the structure and, using high resolution inelastic neutron scattering (INS) techniques, furthermore discovered that the CH4 sits in the dipod down configuration as opposed to the tripod down. They label the commensurate structure as a $\sqrt{2} \times \sqrt{2}$ R 45° (Larese 1998; Drummond, Sumpter et al. 2006). Figure 3.8 shows that both nomenclatures refer to the exact same structure. A full thermodynamic study of the system has since been performed (Freitag and Larese 2000). A typical CH_4 on MgO (100) isotherm is shown in figure 3.9.

The combination of the methane isotherm along with the knowledge of the surface over layer structure has proved to be a useful benchmark experiment for the thermodynamic studies on MgO (100) performed in the Larese group. The CH_4 isotherm is used as an indicator of sample quality. Furthermore the structure results along with the monolayer capacity are used to determine the exact surface area of a given sample. These calculations are explained in more detail in chapter 5.

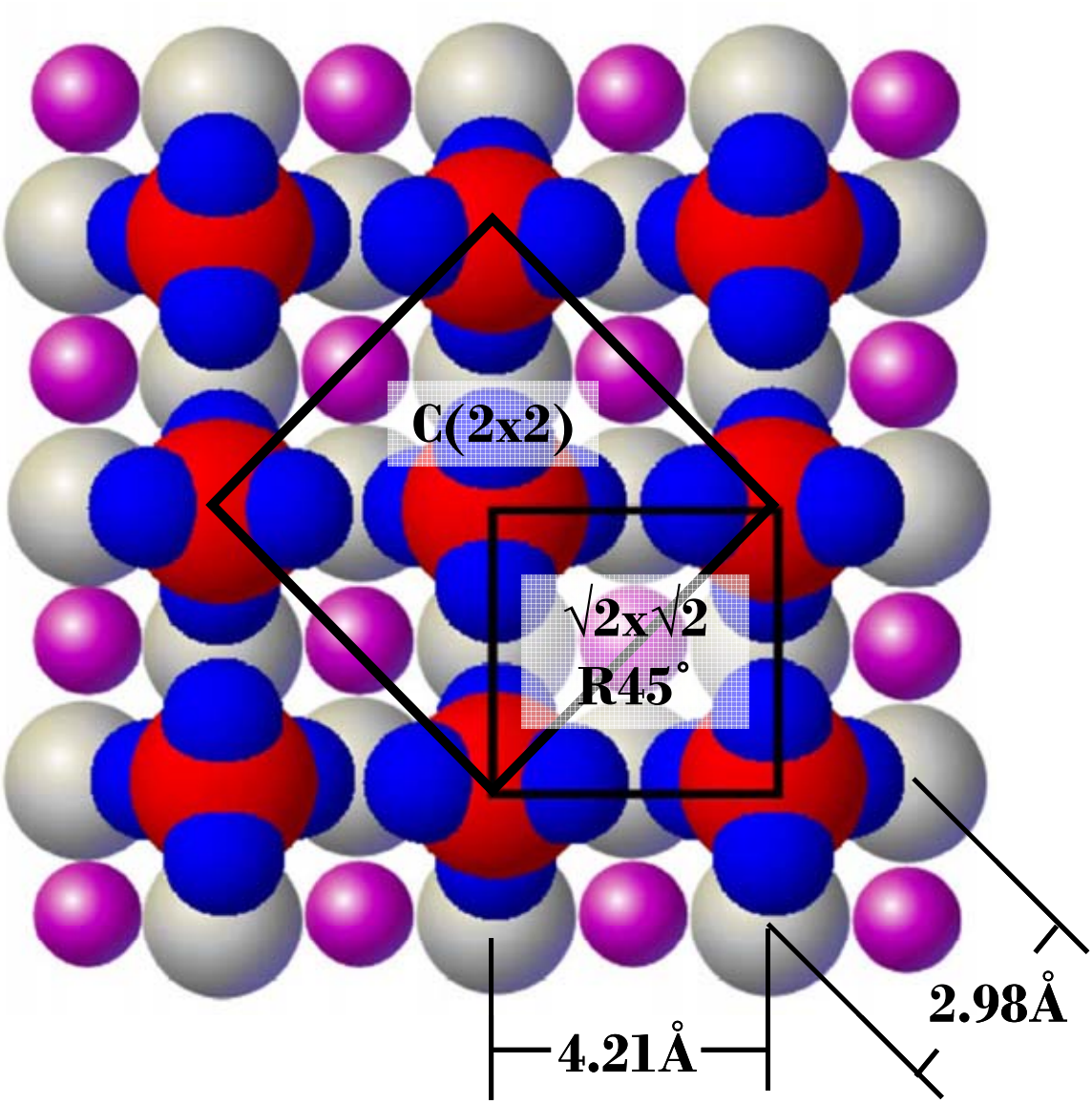


Figure 3.8 - Methane sits above next nearest neighbor magnesium atoms. This gives a unit cell of c(2x2) structure with lattice constant a = 2.97 Å with two methane molecules per unit cell. This is equivalent to a √2×√2 R 45° structure with lattice constant a = 4.211 Å with one methane molecule per unit cell. The resultant occupied an area per molecule of methane is 17.76 Å² per molecule

(Drummond, Sumpter et al. 2006)

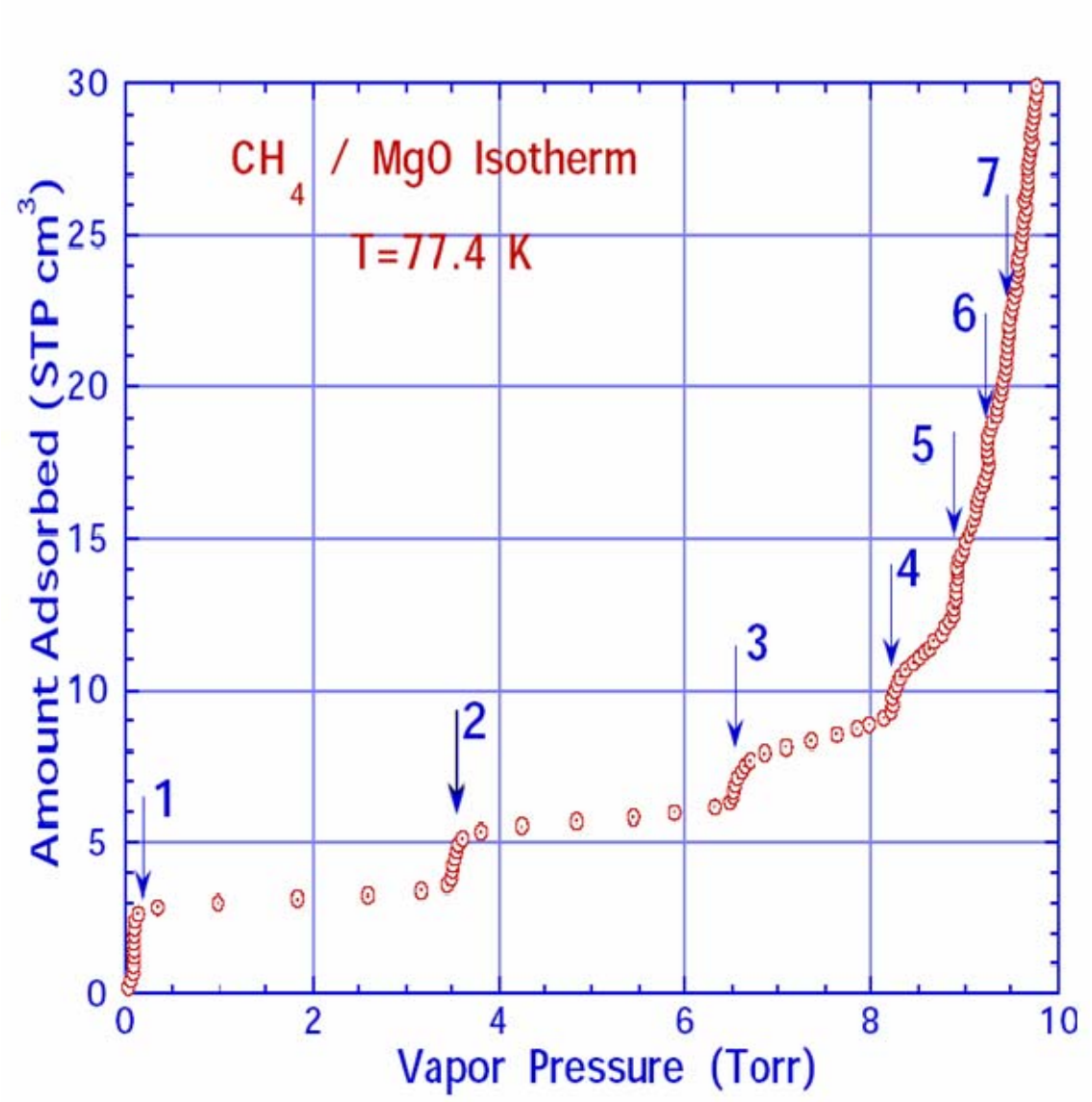
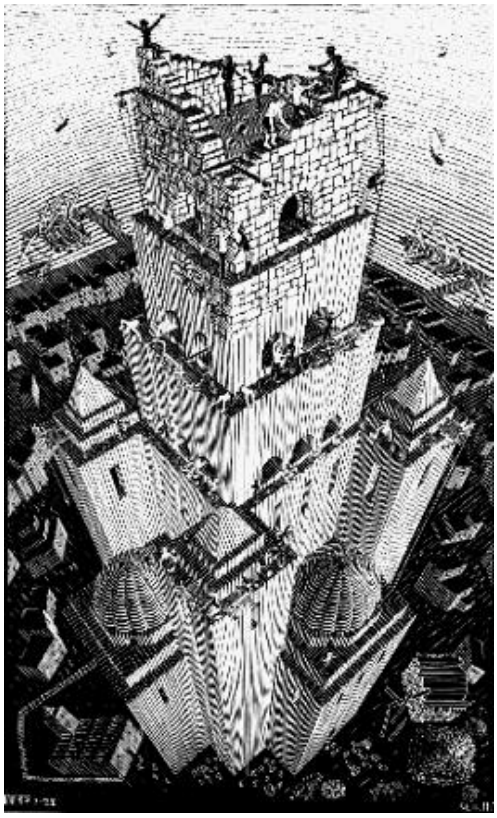


Figure 3.9 – Typical Methane (CH4) adsorption isotherm on MgO (100) (Larese 1998). A good quality MgO sample show a minimum of 5 and as many as 7 layering transitions of relatively even height visible by inspection.

Chapter 4

Experimental Set-up



M,C, Escher: Tower of Babel (1928)

4.1 – The Isotherm Station

High-resolution volumetric adsorption isotherms were performed using self-built, automated gas handling systems in conjunction with either liquid cryogen filled dewars or commercially available low temperature cryostat systems purchased from Advanced Research Systems in Allentown, Pennsylvania. Isotherm systems consist of a stainless steel manifold system with sections bound by a series of four automated valves and a number of manual valves. A typical system is diagramed in Figure 4.1.

These stations consist of three main sections. The first, the gas reservoir, is bound by the gas inlet ports, the bypass valve and Valve 2. The gas reservoir contains the adsorbate gas used in the isotherm. The second section, the dosing volume, consists of two parts: the calibrated volume and the arm volume. The calibrated volume is bound by Valves 2, 3, and 4, the pressure transducers, and the last valve between valve 1 and the rest of the system. The arm volume exists between this same valve and valve 1. The third main section, the dead space volume, consists of the volume contained in the capillary section beyond Valve 1 and that of the sample cell itself.

All valves shown in Figure 4.1 are Swagelok™, B-4HK bellows valves with the exception of the two labeled as metering valves. Valve 1 isolates the sample and dead space volume from the calibrated volume. Valve 2 isolates the gas reservoir from the

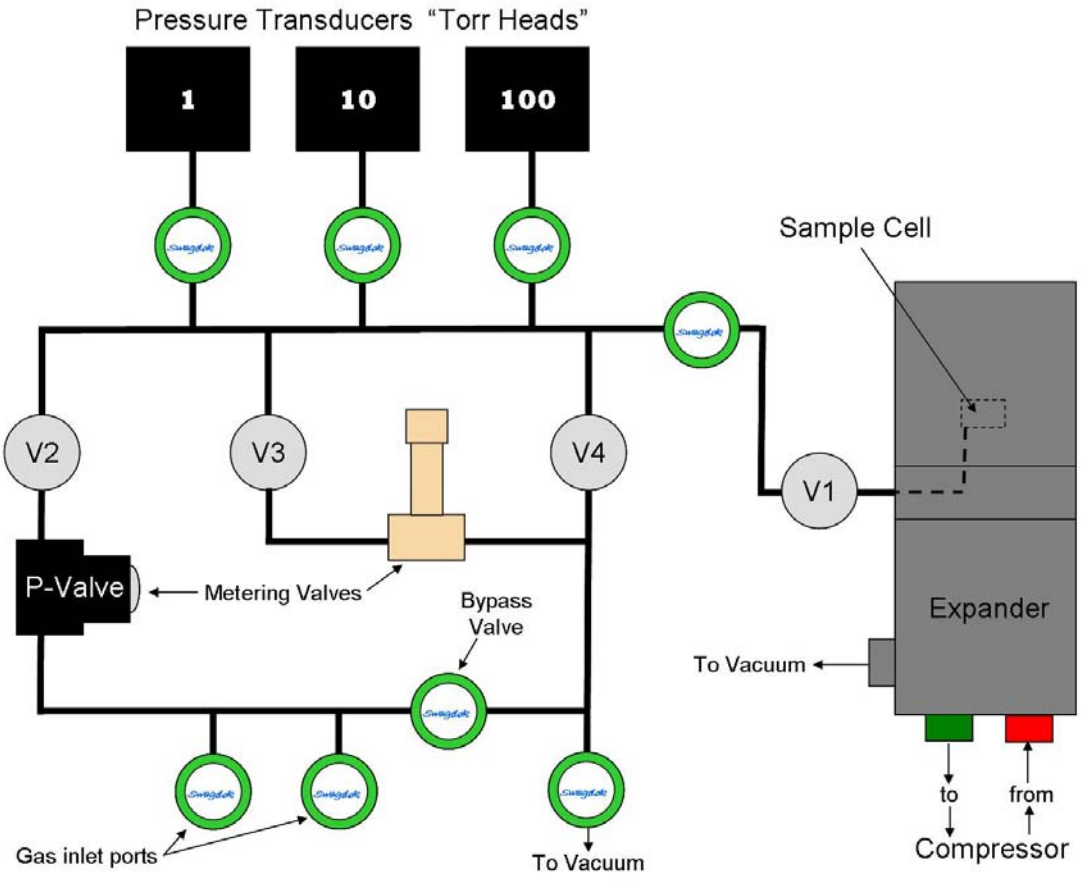


Figure 4.1 - Typical "Isotherm Station"

calibrated volume. Valves 3 and 4 isolate the calibrated volume from the vacuum. Valve 4 allows unhindered evacuation of the calibrated volume. Valve 3 allows for a controlled reduction of the pressure of the calibrated volume as it is isolated from the pumping system by a manually operated Swagelok™ metering valve. The P-Valve, or proportional valve, is a voltage driven metering valve manufactured by MKS instruments. Voltages applied over a range of zero and 24 volts correspond to the valve being nominally closed and fully open. The fully open position allows for a leak rate of ~100 sccm. The opening of Valve 2 then allows for a controlled increase in the pressure of the calibrated volume.

4.1.1 – Calibration of the Volume

Volumes needed for analysis are calculated by first performing multiple helium gas expansions from a known volume into an unknown volume. The Boyle's Law, as expressed in equation(4.1), is then used to analyze the data and calculate the desired volume (Zumdahl 1986).

$$P_1V_1 = P_2V_2 \tag{4.1}$$

Here, P_1 is the initial pressure measured by the system in the known volume, V_1. The gas is expanded into the new total volume V_2 consisting of the known volume and the volume to be calculated. P_2 is the pressure measured by the system after the helium

gas is expanded into the new volume V_2. Therefore the volume of the unknown section is calculated using equation(4.2). The desired volume is then determined from equation(4.3).

$$V_{total} = V_2 = \frac{P_1 V_1}{P_2} \tag{4.2}$$

$$V_{desired} = V_2 - V_1 \tag{4.3}$$

The initial calculation of the volume of the calibrated volume is performed using a bulb previously calibrated by filling it completely with distilled, degassed, water at a known constant temperature. The bulb is considered filled when a hemi-sphere of water is visible at the top ¼ inch tube opening as shown in figure 4.2. The bulb is weighed and the density of water at the measured temperature is then used to calculate the volume of water occupying the volume as shown in equation (4.4).

$$V_{water}(cc) = \frac{\rho_{H_2O@Temperature}\left(g/cc\right)}{mass(g)} \tag{4.4}$$

Then, the actual volume is determined by subtracting away the volume of the hemisphere of water from the total, as indicated in equation (4.5).

$$V_{bulb}(cc) = V_{water}(cc) - \frac{4}{3}\pi r^3(cc) \tag{4.5}$$

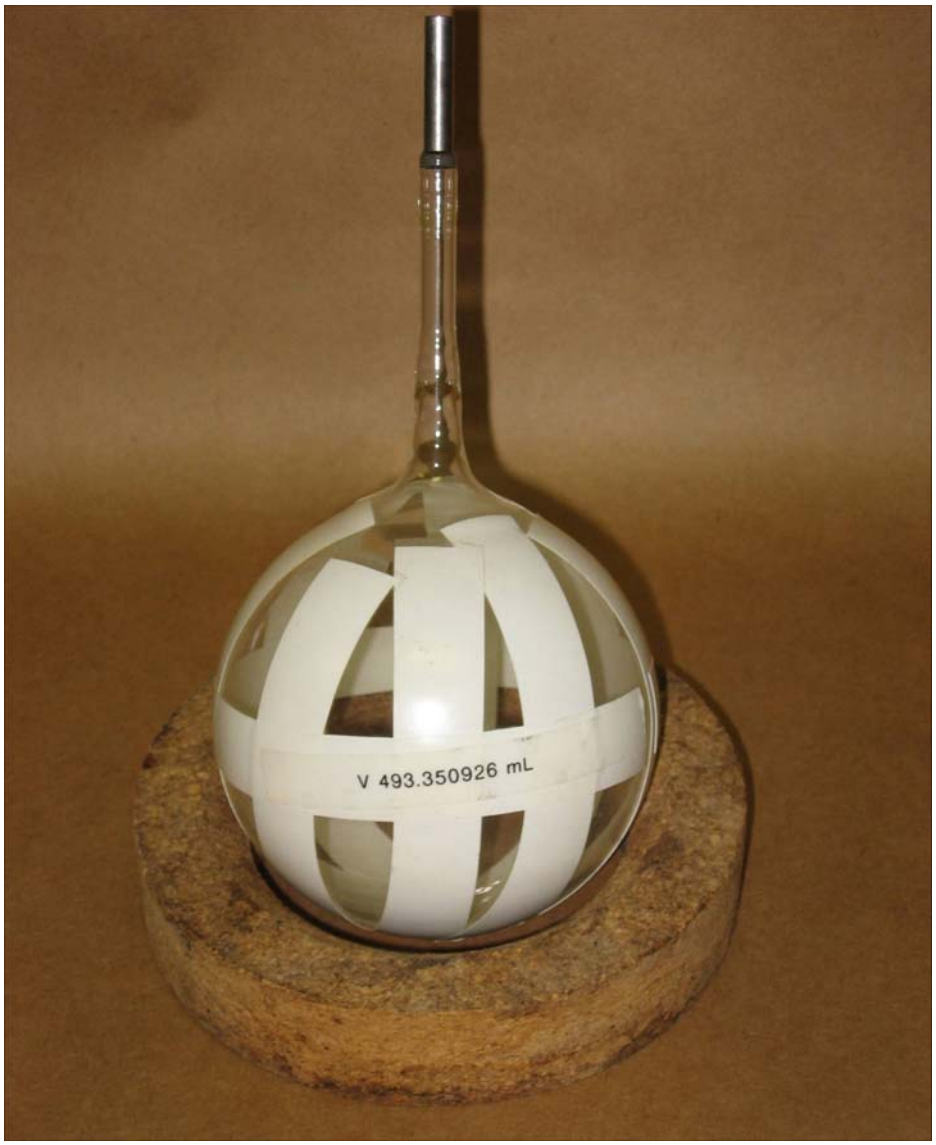


Figure 4.2 – Water filled bulb – for volume calibration

Here, r, is one half of the inside diameter of the ¼ inch tube opening as measured using a digital caliper device. This water filling procedure is repeated multiple times in order to reduce the error of the measurement below 0.1%. Once the calibrated volume of the system is determined, it is then used as the known volume to calibrate the attached arm volume giving rise to a known dosing volume. The dosing volume is then utilized to calculate the dead space volumes of attached samples.

4.2 – Computer Control

Valves 1, 2, 3, 4 and the proportional valve are automated valves controlled via a self-made control box interfaced with a computer running a proprietary Labview™ program (Mursic, Lee et al. 1996). When an "isotherm" is run, the user sets several parameters prior to start of the experiment. These parameters are shown in the white boxes at the bottom of the set up screen for an adsorption isotherm is shown in Figure 4.3.

"P(start)" is the selected pressure of the first dose of gas. This is generally the same as the value selected for the shot size, "Δp", or the amount of overpressure one wants to introduce to the system during each dosing process, or "point". The limit on the accuracy of the dose size, "P tol (%)", is also dictated: dose size is generally restricted to five to fifteen percent of the set point. A choice is also made as to how to

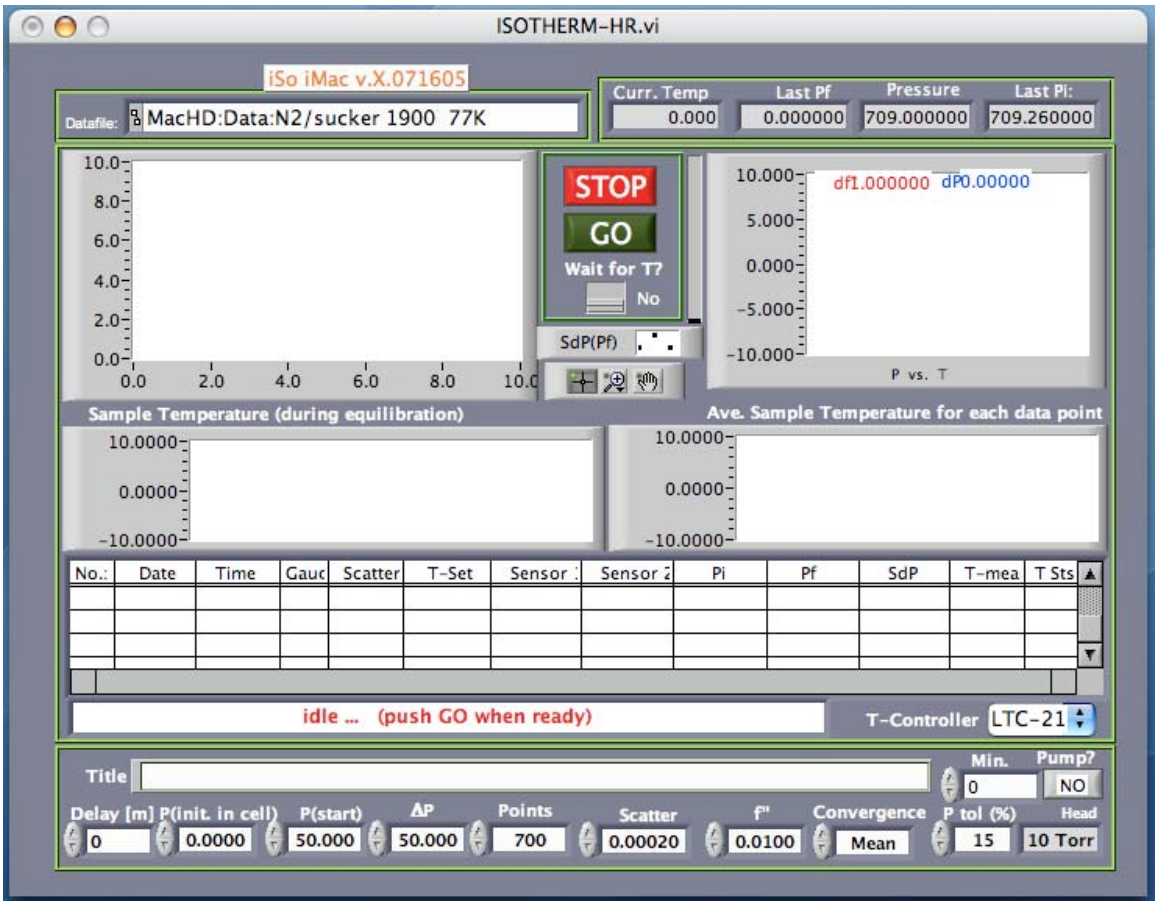


Figure 4.3 - Labview™ Isoimac High Resolution adsorption isotherm startup screen

determine when a point is complete. The two most common "convergence" choices are "time" and "mean". If the time option is chosen, the point is allowed to equilibrate for a given amount of time dictated by the scatter setting in minutes. If the "mean" option is chosen (this is the most common option for experiments performed in this dissertation), the point is allowed to equilibrate until the pressure changes less than the dictated scatter setting between readings approximately one minute apart. The mean scatter setting for experiments such as those performed herein is between 0.00001 and 0.0001 torr. In one minute intervals, the pressure reading is plotted, and the change in pressure between these points is noted in the upper right hand corner of the program screen shown in Figure 4.3 during the equilibration of each point.

The Labview™ Isoimac program operates the isotherm system by controlling the valves in a manner that agrees with all of the input parameters. The program controls the dosing process by first opening valve 2 and reading the pressure. The program keeps valve 2 open until the pressure reaches the tolerance level of the set point. If the pressure exceeds the set point above the set tolerance, the program then opens valve 3 to reduce the pressure slowly until it meets the user specified value. If the pressure in the dosing volume falls below the tolerance of the set point value, valve 2 is opened again to increase the pressure. Once the program has manipulated valves 2 and 3 to effectively reach the appropriate dosing pressure, valves 2 and 3 are

closed; the pressure is read and entered as the input pressure, p_i; and valve 1 is opened allowing the dose of gas access to the adsorbate contained in the sample cell.

The pressure is allowed to equilibrate as explained above; valve 1 is closed; and the final pressure, p_f, is recorded. The change in pressure, "delta p", for the point is calculated as shown in equation (4.6) for the nth equilibration point,

$$\Delta p_n = p_{i_n} - p_{f_n} \tag{4.6}$$

and the sum of these "sum of the delta p", calculated as shown in equation (4.7) for the nth equilibration point,

$$\Sigma\Delta p_n = \sum_{n=1}^{n} \Delta p_n = \Sigma\Delta p_{n-1} + \Delta p_n \tag{4.7}$$

is plotted against the final pressure, p_{f_n}, of the given point by the isoimac program, in the upper left hand corner of the screen, so that the progress and distinguishing features of the isotherm can be monitored while the experiment is running. The program dictates the new p_{i_n} set point by adding the user specified shot size to the p_f reading of the previous point $p_{f_{n-1}}$ as shown in equation (4.8).

$$p_{i_n} = p_{f_{n-1}} + \Delta p \tag{4.8}$$

This addition insures an overpressure in the dosing volume as compared to the sample or dead space volume thus molecules will always move from the high pressure dosing

volume into the low pressure sample volume. This process is repeated until the user stops the isotherm program or until the designated number of points is reached. Generally the isotherm is stopped once the final pressure of the points, p_f, begin to very closely approach the saturated vapor pressure, SVP, of the gas at the temperature of the isotherm. A simplified flow chart showing the operation of the system via the lab view program is shown in Figure 4.4.

4.3 – The Sample

4.3.1 – Sample Confinement

Samples are confined for study in one of three ways: a quartz tube, or an oxygen-free high conductivity (OFHC) copper cell. The quartz tube consists of a narrow quartz tube capped with a Swagelok™ manual valve. This assembly is shown in Figure 4.5.

Most commonly, the sample is confined in an indium sealed oxygen free copper cell mounted onto an aluminum ring via a stainless steel capillary tube. The sample space is capped by a manual Swagelok™ valve. This ring assembly is shown in Figure 4.6.

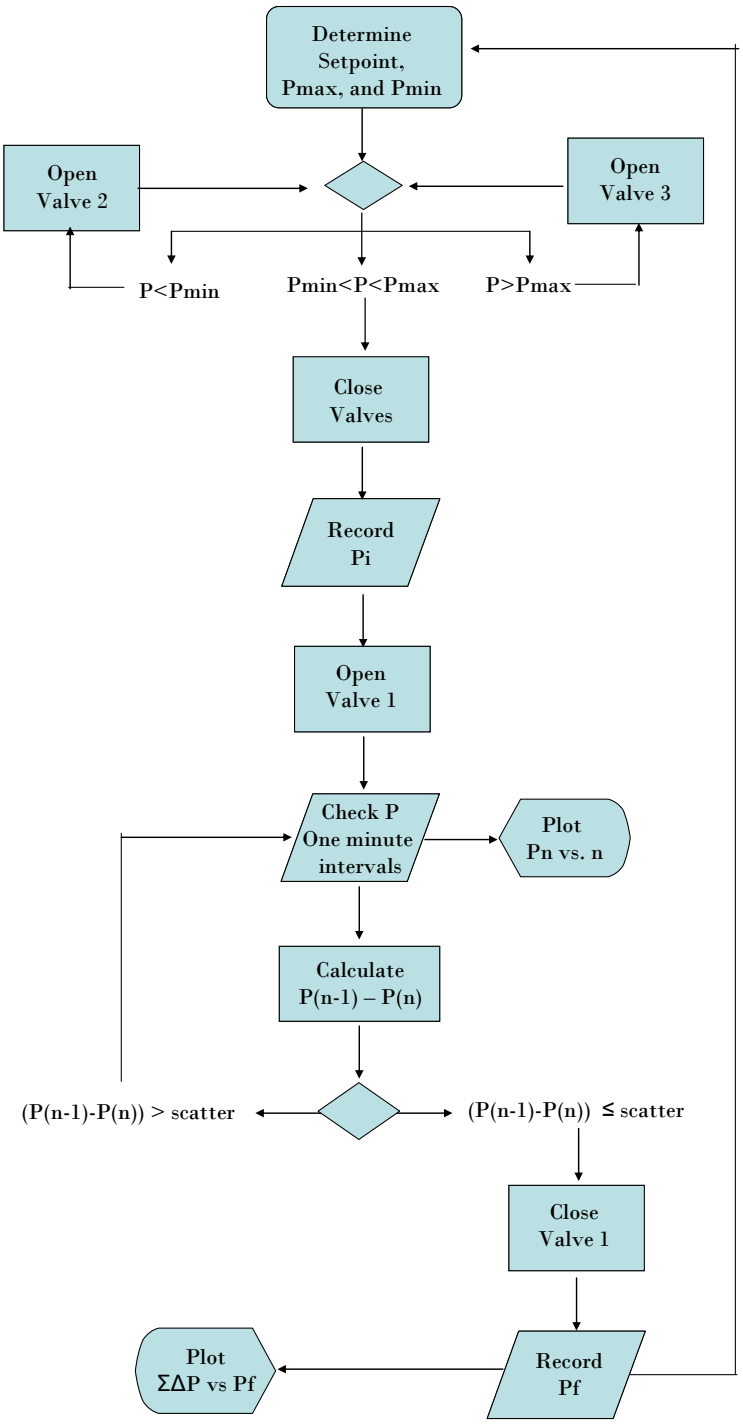


Figure 4.4 – Flow Chart of Isotherm Process



Figure 4.5 – Quartz Sample Tube

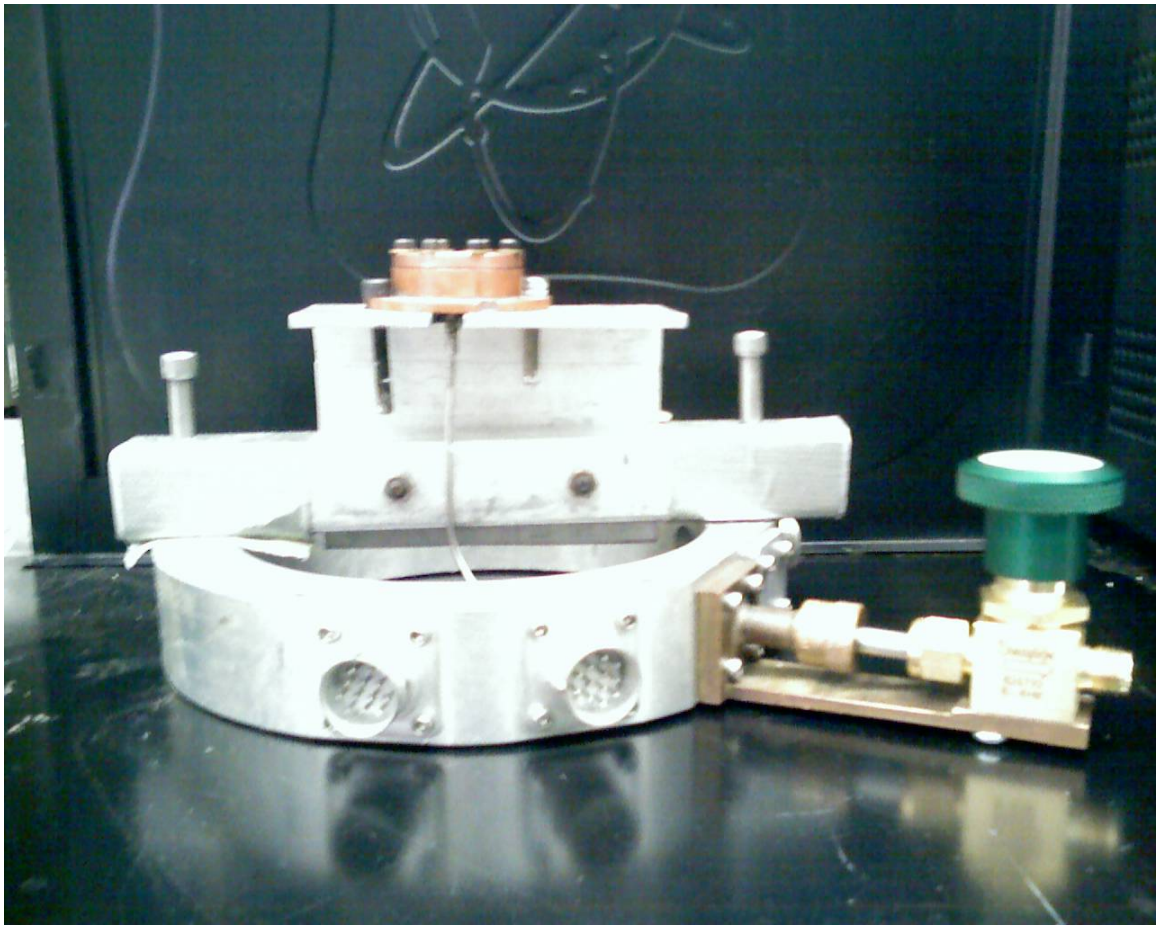


Figure 4.6 – Sample Cell Ring Assembly

Low temperature (< 7K) samples and neutron samples are confined in indium sealed sample cans. The lids are made of oxygen free copper, and the cell is either made of oxygen free copper for most isothermal studies, or aluminum or vanadium for neutron samples. A long capillary (diameter ~ 2mm) with terminus in a through hole in the copper lid and in a manual valve is confined in a vacuum jacketed "stick assembly" such as that shown in Figure 4.7 (Koehler and Larese 2000).

4.3.2 – Cooling the Sample

Sample temperature is controlled in one of three ways. If a sample is being cooled in a quartz tube, the quartz tube is immersed in a Dewar filled with a fluid (e.g. liquid nitrogen, water and ice, acetone and dry ice) that maintains temperature throughout the isotherm. The most common cryogen used here is liquid nitrogen, which maintains the quartz tube sample environment at a temperature of 77.4K. Similarly, an ice water bath could be used to maintain a 273K environment.

Most commonly, cryostats are utilized to control sample environment. Closed System cryostats, manufactured by Advance Research Systems, are used to maintain sample temperature using the Gifford-McMahon refrigeration cycle. The cryostat system is a closed cycle helium refrigerator consisting of two parts: the compressor and the expander. The expander portion of the cryostat is shown in figure 4.8. The two parts are connected via flexible, reinforced, pressurized, stainless steel lines. The



Figure 4.7 – Cryostat Stick for neutron Scattering Experiments and low temperature isothermal study (Koehler and Larese 2000)

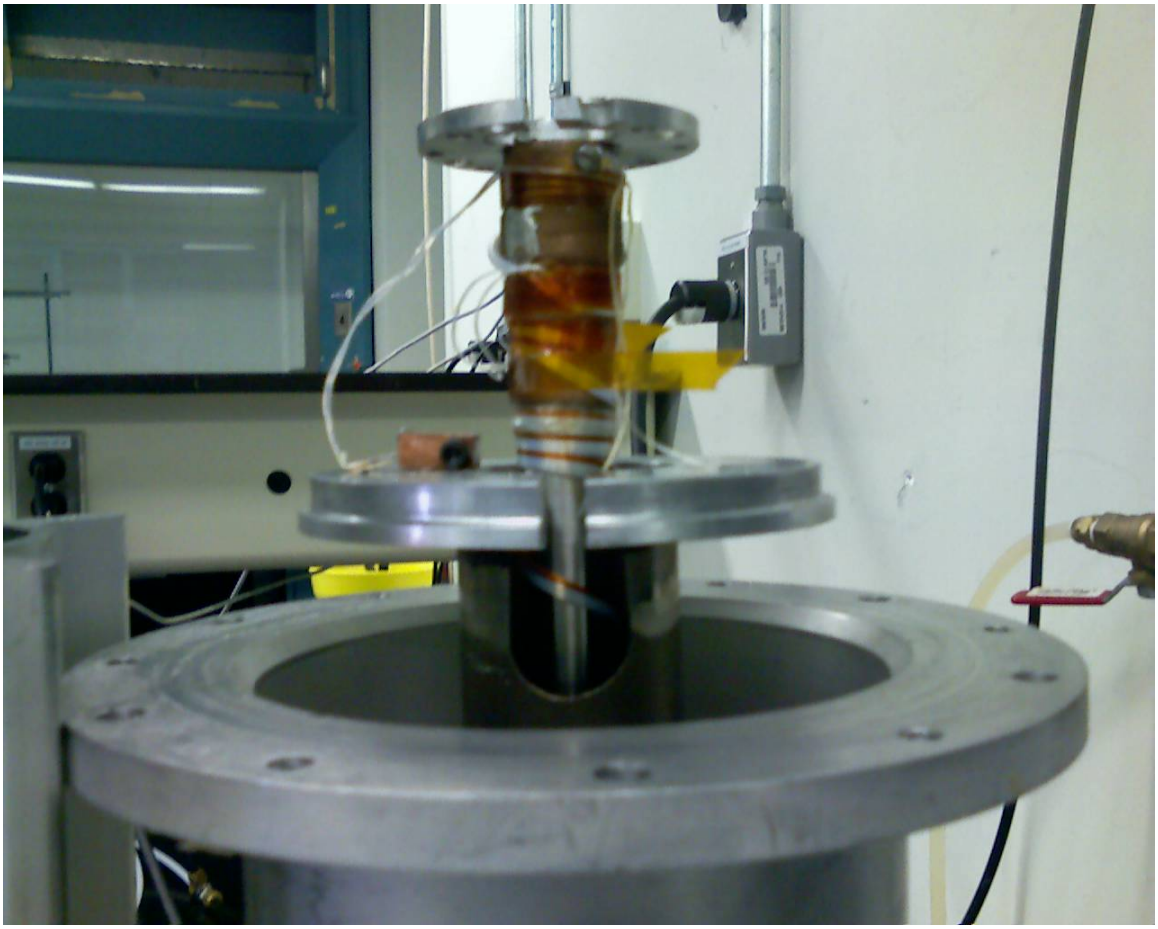


Figure 4.8 – Cryostat

supply side comes out of the compressor and provides high pressure helium to the expander unit. A piston in the unit expands the gas and then the resultant lower pressure gas is returned to the compressor. In the cryostat case, the sample ring shown in Figure 4.6 is mounted to the vacuum jacket and cold finger as shown in Figure 4.9.

Finally, an "Orange Cryostat", manufactured by AS Scientific Product Ltd may be used to establish a low temperature sample environment ($325K \leq T \leq 1.5K$). It is a liquid-helium operated, flow-cryostat system. A picture of the cryostat is shown in figure 4.10, and its schematic is shown in figure 4.11.

The sample space is thermally isolated from the outside temperatures by the liquid helium bath, the liquid nitrogen bath, and the vacuum jacket. Temperature of the cryostat is cooled by adjusting the cold valve and warm valve which maintain the flow of helium into and out of the annular space respectively. This system is most often utilized when very low temperatures are needed. It is routinely used for performing neutron scattering measurements.

4.4 – Temperature Control

The temperature is monitored and controlled using a Neocerra™ LTC-21 Temperature Controller. This device is interfaced to both the computer and the

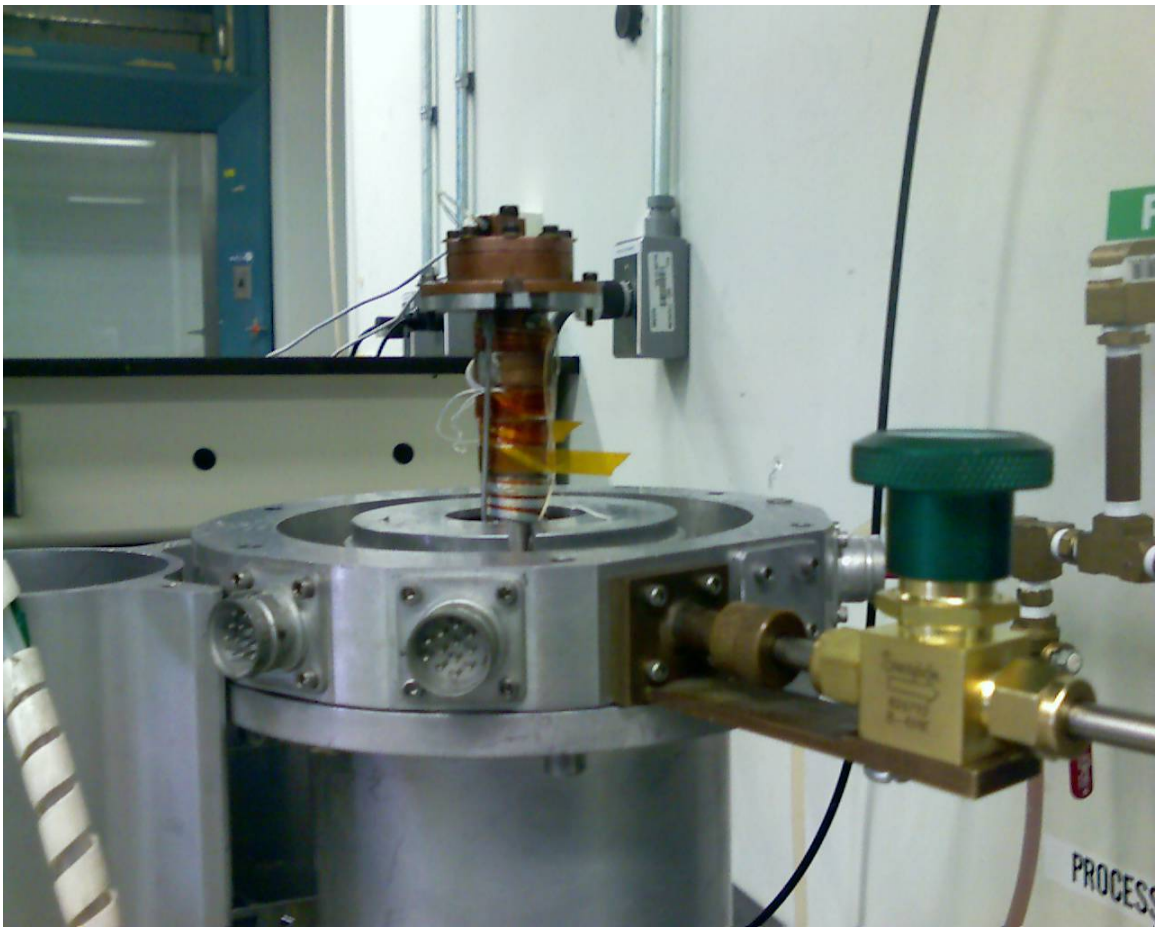


Figure 4.9 – Sample cell ring assembly mounted to cryostat



Figure 4.10 – Orange Cryostat

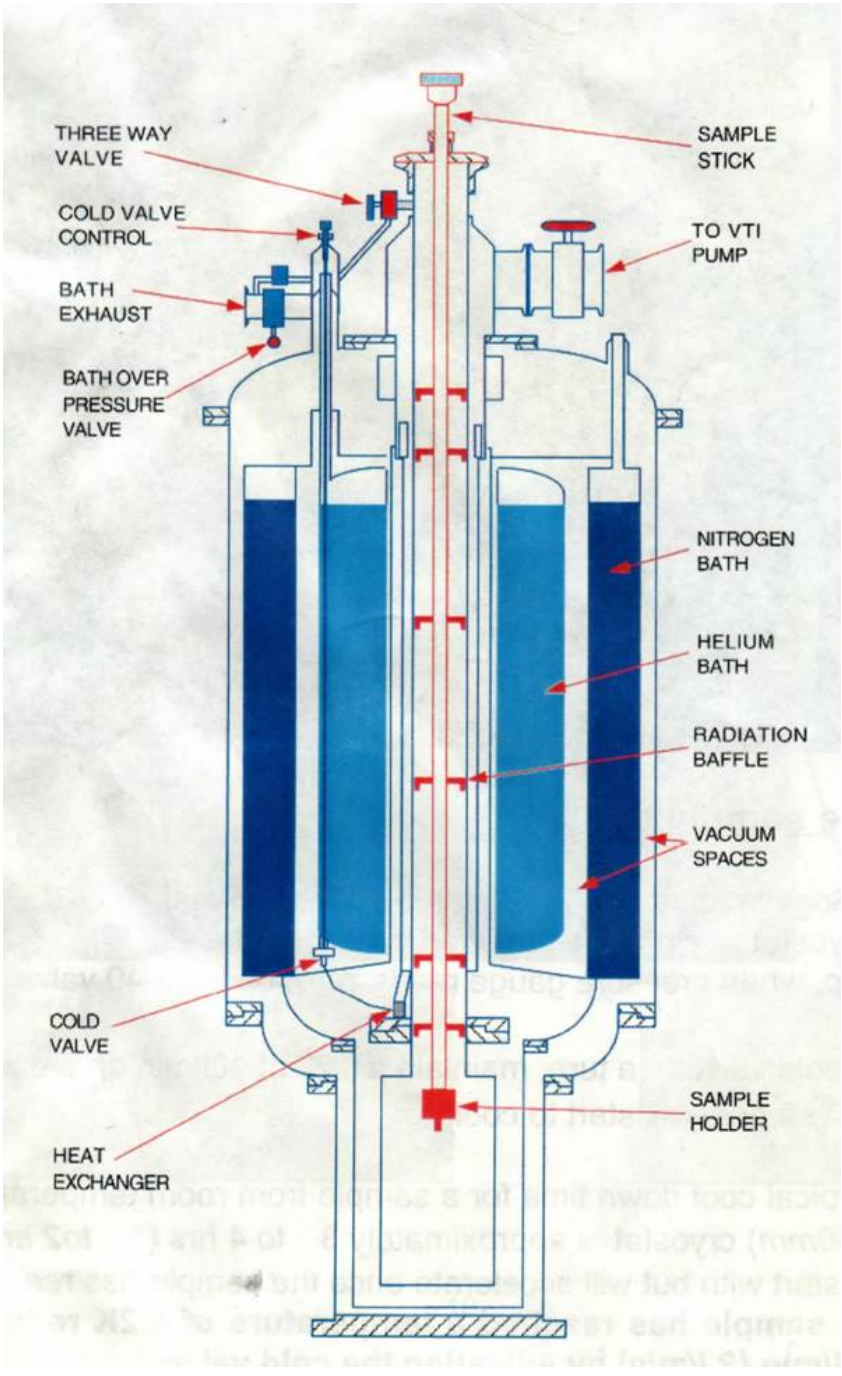


Figure 4.11 – diagramof orange croystat

cryostat. It is able to control the temperature of the cryostat within 5mK of the set point temperature (between ~250K and 4.2K) by controlling the amount of heat supplied by the heater on the cold-head of the cryostat.

Two Lakeshore™-10 Silicon Diode thermometers are connected to the cryostat. One is mounted at the top of the cold finger. This is the control thermometer. The other is mounted in an OFHC copper block mounted to the top of the OFHC copper sample cell. Signals from these thermometers are sent to the computer program and are recorded in the Labview™ program sample file along with the average temperature and standard deviation of the control thermometer. The Neocerra™ LTC-21 is similarly used to maintain the temperature of the sample space of the orange cryostat.

Chapter 5

Isothermal Analysis



M. C. Escher: Portrait of G. A. Escher (1935)

5.1 – Calculation of the Number of Moles Adsorbed

The sample output file from the Labview™ Isomac program contains all data needed to analyze the isotherm. The output file contains 15 columns: dosing point number; date of point completion; time of point completion; torr head size utilized in isotherm experiment; scatter setting for point; set point temperature for isotherm; control sensor temperature at point completion; second sensor temperature reading at point completion; initial dosing pressure, p_i; final equilibrium pressure, p_f; the sum of the delta p, $\Sigma\Delta p_n$; Average temperature of dosing point; standard deviation of the average temperature; the high temperature recorded during the equilibration period; and the low temperature recorded during the equilibration period. The first quantity of interest is the number of moles adsorbed by the sample.

The Δp recorded by the isoimac program is recorded at room temperature and relates to the pressure change in the dosing volume during the equilibration period. This is the maximum number of moles that could be adsorbed by the sample. Utilizing the ideal gas law shown in equation(5.1),

$$pV = nRT \tag{5.1}$$

where: p, is pressure; V, is volume; n, is the number of moles; R, is the ideal gas constant; and T, is the temperature. So, the number of moles introduced to the

adsorbate sample is the same as the number of moles exiting the dosing volume during the nth equilibration period can be calculated using equation (5.2), rearranged as equation (5.3).

$$\Delta p_n V_{dose} = n_{exiting} RT_{roomtemp} \tag{5.2}$$

$$n_{exiting} = \frac{\Delta p_n V_{dose}}{RT_{roomtemp}} \tag{5.3}$$

The number of moles exiting the dosing volume is the maximum number of moles available for adsorption by the sample.

It can be assumed that an adsorbed molecule has no partial pressure and therefore does not contribute to the overall pressure of the system. Thus, the molecules exiting the system that are not adsorbed by the sample should be represented by the final pressure of the dosing point since the dosing volume and dead space volumes must be in equilibrium. Therefore, if we assume that p_{f_n} is an accurate measure of the final pressure of the sample cell, then the number of moles not adsorbed by the sample, but still in the dead space volume can be represented by equation(5.4).

$$n_{samplecell_{notadsorbed}} = \frac{p_f V_{samplecell}}{RT_{isotherm}} \tag{5.4}$$

We take the volume of the sample cell, at the temperature of the isotherm to be equivalent to the volume of the sample cell calculated at room temperature due to the insignificant volume change of the copper cell over the given range in temperature. The difference in the value of the coefficient of thermal expansion for copper varies less than 16.5×10^{-6} between room temperature and zero Kelvin. (Nix and MacNair 1941)

A correction needs to be made to the estimate of the number of moles adsorbed, given in equation(5.4), to correct for those molecules introduced into the sample cell that were not adsorbed by the adsorbate sample. Therefore, the actual number of moles adsorbed by the sample during the nth dosing point is given by equation(5.5).

$$n_{adsorbed} = n_{exiting} - n_{samplespace_{notadsorbed}} \tag{5.5}$$

The correction is not quite as simple as might be suggested in equation(5.5). One cannot calculate an accurate value for equation (5.5) by simply subtracting equation (5.4) from equation (5.3) due to the discrepancy in the temperatures of the two volumes. We must make a correction to determine the equivalent number of room temperature moles we need to subtract from the number room temperature moles entering the sample space. This is done by first determining the effective volume of the sample cell at room temperature. The question becomes: how much volume

would the moles in the sample space occupy at room temperature. One can solve the ideal gas law for R as shown in equation(5.6).

$$R = \frac{pV}{nT} \tag{5.6}$$

Since R is constant for any set of conditions the relationship shown in equation (5.7) can be used to determine values for different sets of conditions.

$$\frac{p_{roomtemp} V_{effective@roomtemp}}{n_{roomtemp} T_{roomtemp}} = \frac{p_{isothermT} V_{isothermT}}{n_{isothermT} T_{isothermT}} \tag{5.7}$$

If the goal is to determine how much volume these isotherm temperature moles occupy at room temperature, n_{iso} is equal to $n_{roomtemp}$. As described earlier, the pressure at room temperature is a good approximation of the pressure in the sample cell, so $p_{roomtemp}$ is equal to p_{iso}. These equivalencies allow equation (5.7) to simplify to equation (5.8):

$$\frac{V_{effective@roomtemp}}{T_{roomtemp}} = \frac{V_{isothermT}}{T_{isothermT}} \tag{5.8}$$

The effective volume occupied by the moles at room temperature is then given by equation(5.9).

$$V_{effective@roomtemp} = \frac{V_{isothermT} T_{roomtemp}}{T_{isothermT}} = \frac{V_{samplespace} T_{roomtemp}}{T_{isothermT}} \tag{5.9}$$

Equation (5.5) is then accurately described by equation (5.10)

$$n_{adsorbed_x} = \frac{\Delta p_x V_{dose}}{RT_{roomtemp}} - \frac{p_{f_x} V_{effective@roomtemp}}{RT_{roomtemp}} \tag{5.10}$$

Substitution of equation (5.9) simplifies the equation describing the number of moles adsorbed during the x^{th} dose to that shown in equation (5.11).

$$n_{adsorbed_x} = \frac{\Delta p_x V_{dose}}{RT_{roomtemp}} - \frac{p_{f_x}}{RT_{roomtemp}} \frac{V_{isothermT} T_{roomtemp}}{T_{isothermT}} = \frac{\Delta p_x V_{dose}}{RT_{roomtemp}} - \frac{P_{f_x} V_{samplespace}}{RT_{isothermT}} \tag{5.11}$$

There is a problem of potential over correction if we calculate the total number adsorbed by summing equation (5.11) over all points, x. One must not subtract the same moles twice from the sample space. Equation (5.11) is only valid for $x = 1$, where the previous p_f is zero, or for the determination of the number of moles adsorbed at any given single point. For every point following $x = 1$ we must use equation (5.12) to determine the number of additional moles adsorbed if one plans on summing the equation over all points, x.

$$n_{adsorbed_x} = \frac{\Delta p_x V_{dose}}{RT_{roomtemp}} - \frac{\left(p_{f_x} - p_{f_{x-1}}\right) V_{samplespace}}{RT_{isothermT}} \tag{5.12}$$

Alternatively, we can look at the sum of the delta p column and calculate an accurate value for the sum of moles adsorbed as given in equation (5.13).

$$\sum_{x=1}^{m} n_{adsorbed_x} = \frac{\sum \Delta p_x \cdot V_{dose}}{RT_{roomtemp}} - \frac{p_{f_x} V_{samplespace}}{RT_{isothermT}} \tag{5.13}$$

Since the moles in the sample space are being subtracted from the sum each time, it is equivalent to calculating the number of moles at a given single point; thus, there is no problem of potential over correction. A good check of calculations is to plot the raw data and the corrected data: the line shapes and relative heights of given features should be identical.

Often, it is useful to report the amount adsorbed as volume per surface area of the given adsorbate at standard temperature and pressure. This quantity is calculated using equation (5.14), where A is the surface area of the given sample.

$$V_{adsorbed}(cc/m^2) = \frac{n_{adsorbed\,(moles)} R_{\left(\frac{cc \cdot torr}{mol \cdot K}\right)} T_{(273.15K)}}{p_{(760torr)} A_{(m^2)}} \tag{5.14}$$

5.1.1 – Thermal Transpiration Correction

The thermal transpiration effect is a resultant of a large temperature difference between the dosing volume and the sample volume which are linked by means of a small capillary. Takaishi and Sensui proposed a pressure correction method to deal with this issue (Takaishi and Sensui 1963). For a dosing volume at T_2, P_2 and a sample volume at T_1, P_1 separated by a thin capillary of diameter d (T measured in Kelvins, P measured in mmHg, and d measured in mm) the relationship between the two volumes is given by equation (5.15).

$$\frac{\left(P_2/P_1\right)-1}{\sqrt{T_2/T_1}-1}=\frac{1}{A^*X^{*2}+B^*X^*+C^*\sqrt{X^*}+1} \tag{5.15}$$

Where X* is given in equation (5.16),

$$X^*=\frac{P_2 d}{\overline{T}} \tag{5.16}$$

and $\overline{T}$ is defined in equation (5.17).

$$\overline{T}=\frac{\left(T_1+T_2\right)}{2} \tag{5.17}$$

Rearranging the equation and solving for P_1 gives the resultant usable equation shown in equation (5.18).

$$P_1=P_2\left[\frac{A^*X^{*2}+B^*X^*+C^*\sqrt{X^*}+1}{\sqrt{\frac{T_2}{T_1}}+A^*X^{*2}+B^*X^*+C^*\sqrt{X^*}}\right] \tag{5.18}$$

Here A*, B* and C* are constants specific to the adsorbate. For Hydrogen, $A^*=1.24\times10^5$, $B^*=8.00\times10^2$, and $C^*=10.6$.

To reevaluate the isothermal data based on the thermal transpiration correction, equation (5.18) is applied to calculate new values for p_i and p_f and the resultant p_i* and p_f* are used to recalculate the number of moles adsorbed using the calculation given previously in equation (5.11). Figure 5.1 shows a comparison of the

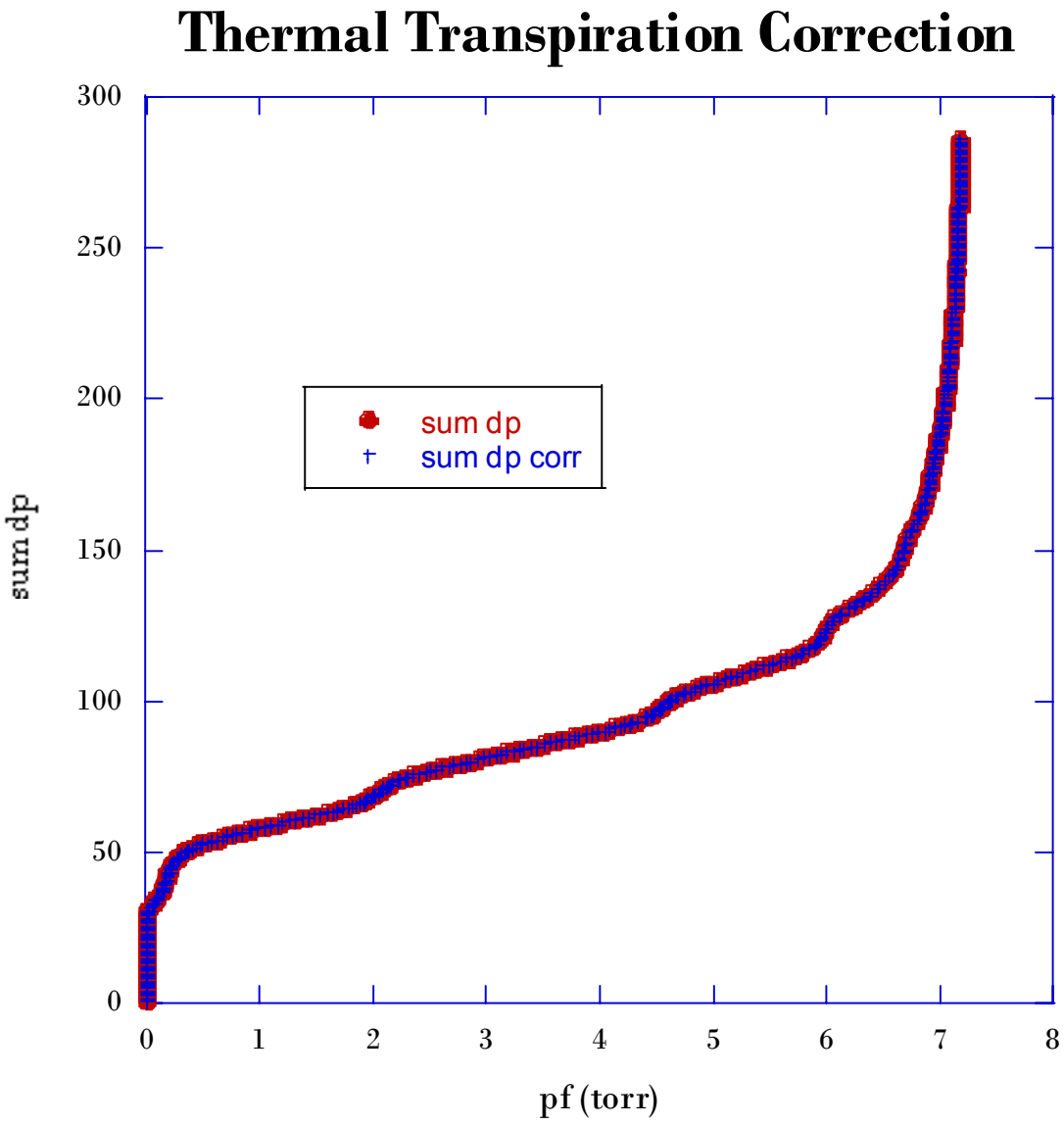


Figure 5.1 - Thermal transpiration correction lies directly on the same line as without the correction.

raw data and the corrected data. It appears that for our set up, that there is little to no change in the overall data due to the thermal transpiration effect.

5.2 – Surface Area

Once the methane isotherm is performed on a given sample, the available surface area of that sample can be calculated. As explained in Chapter 3, CH_4 forms a commensurate monolayer above the surface with a given molecule of CH_4 occupying 17.76 $Å^2$ (Coulomb, Madih et al. 1985; Larese 1998) as previously shown in figure 3.8; therefore, we can assess sample surface area once the number of methane molecules present in the monolayer us ascertained.

The surface area of a given sample is calculated by first determining its monolayer capacity, or the number of moles of adsorbent that form one monolayer of molecules on the available adsorbate surface. For Magnesium Oxide samples, a methane adsorption isotherm at 77K or liquid nitrogen temperatures is run on each sample for this purpose, a typical example is shown in figure 5.2. Emmett and Brunaer's "Point B Method" (Emmett and Brunauer 1937) is used to deduce from the first step of the isotherm the number of moles of gas required to form one monolayer of coverage. This method is shown in Figure 5.3. Since the Methane molecular footprint of 17.76 $Å^2$ on the surface of MgO, the surface area of each sample can be calculated using equation(5.19)

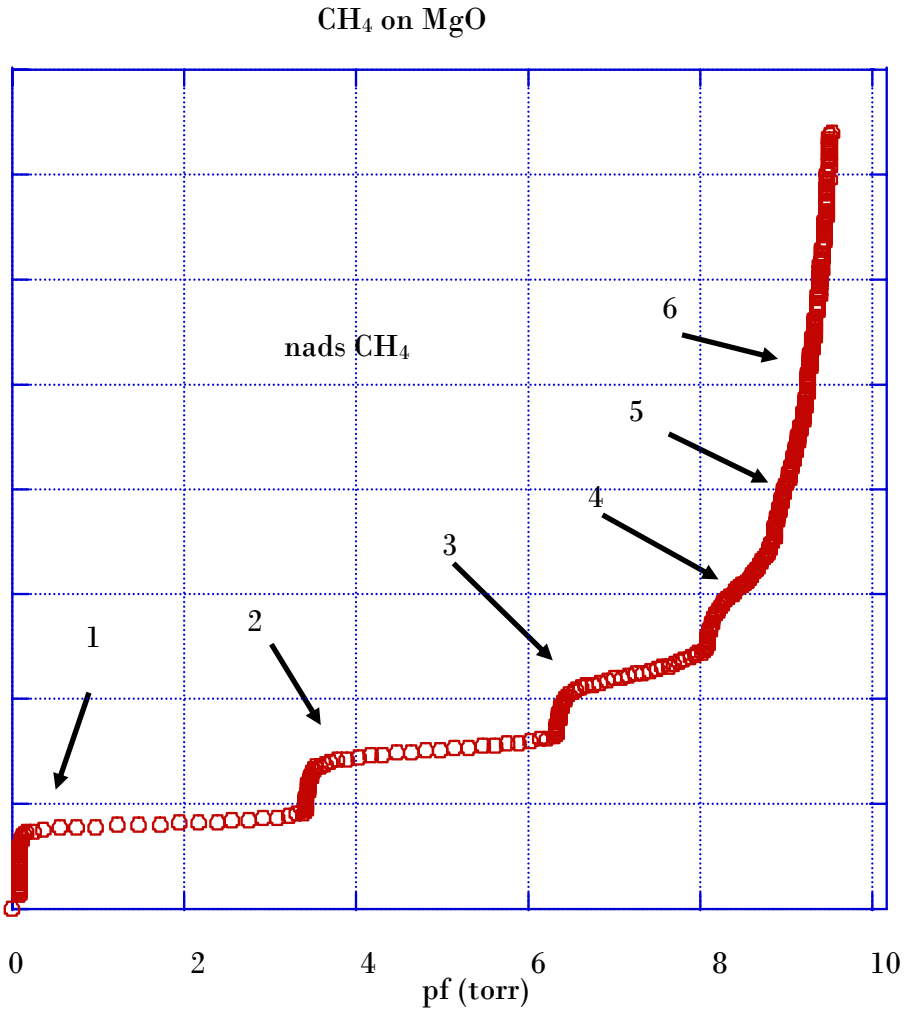


Figure 5.2 – Methane Isotherm run at 77.94K shows good sample quality with more than 5 adsorption steps visible by inspection which are relatively even in height.

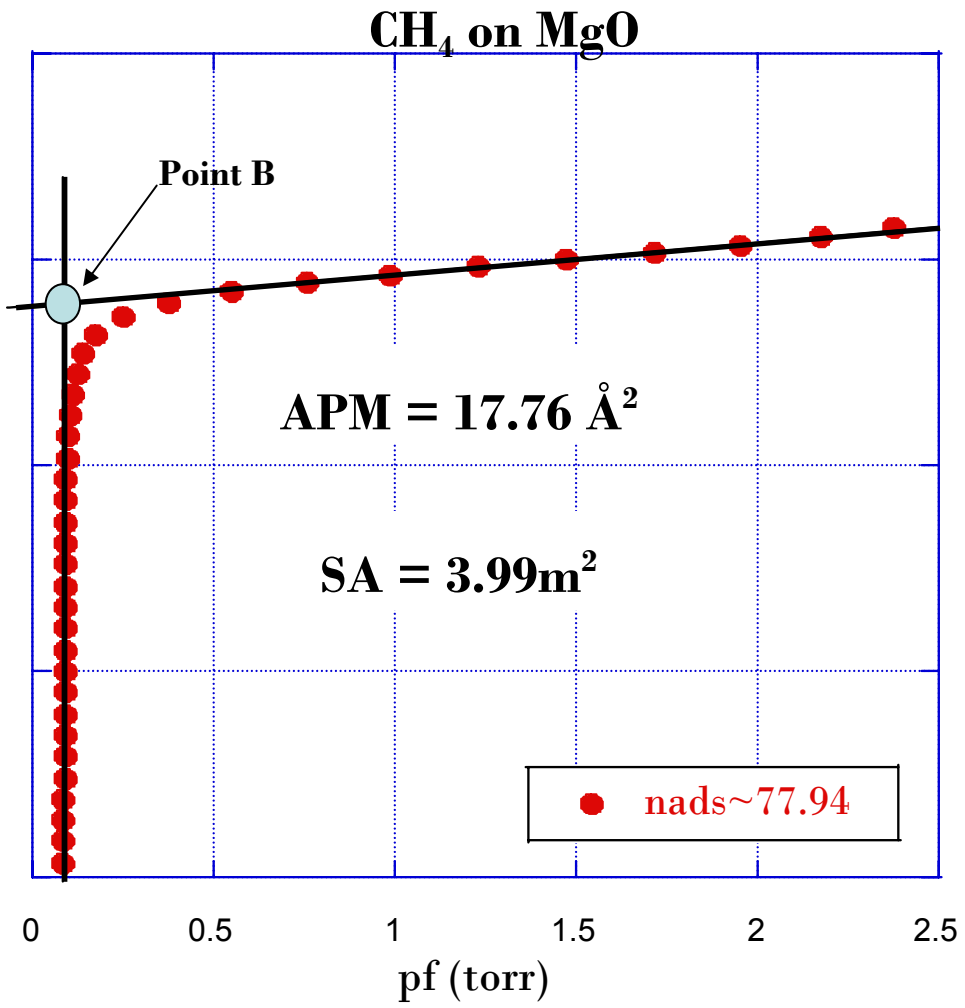


Figure 5.3 – point B method shown to determine monolayer capacity of the Methane isotherm shown in figure 5.1

$$A\left(m^2\right) = \frac{\#moles\left(CH_4\right)}{monolayer} \cdot \frac{6.022\times10^{23} molecules}{mole} \cdot \frac{17.76 \text{Å}^2}{molecule} \cdot \left(\frac{1 meter}{1\times10^{10} \text{Å}}\right)^2 \quad \textbf{(5.19)}$$

Sample quality is also assessed with this methane isotherm. A minimum of five nominally equi-height adsorption steps are usually needed to be observed in order to use the sample in an experiment. It should be noted that the majority of the data presented herein was gathered using the sample of MgO shown in Figures 5.2 and 5.3.

5.2.1 – Area per Molecule

Once the surface area of the sample is known, the area occupied per molecule for any adsorbate gas can be determined. Again, the point B method is used to determine the number of molecules in the monolayer of the experimental system. The area per molecule (APM) of the system is then calculated according to equation(5.20).

$$APM = \frac{SurfaceAreaMgO}{molecules_{monolayer}} \quad (5.20)$$

5.3 – Clausius-Clapeyron Analysis

Each feature on the adsorption isotherm is looked at carefully and independently. To aid in this analysis, the first derivative of the isotherm data is

taken numerically. It is not surprising that stepwise increases in the amount adsorbed result in dramatic changes in the numerical derivative. The peaks in the derivative are used to locate the pressure at the center of the vertical riser of each adsorption step or location of a less dramatic feature. This process is repeated for each set of isothermal data over a series of temperatures. The pressure at which the system achieves its saturated vapor pressure is also noted for each temperature.

The saturated vapor pressure can also serve as an aid (i.e. a separate gas thermometer) to confirm the actual sample temperature in each experiment by comparing the value to a plot of saturated vapor pressure versus temperature. This data is available in the form of Antoine Equations for the given adsorbent system. Antoine Equations for various gasses are available on the NIST WebBook (NIST). The webbook, however, has no information on Hydrogen gas within the temperature range under investigation. There are three SVP versus Temperature (in Kelvin) equations available which were used instead. These are shown in equation (5.21) (Brickwedde and Scott 1948), the solid-gas vapor pressure estimate in equation (5.22) (Souers, Briggs et al. 1977), and the liquid-gas vapor pressure in equation (5.23) (Souers, Briggs et al. 1977).

$$\ln\left(\mathrm{P(torr)}\right) = 4.56488 - \frac{47.2059}{T} + 0.03939\mathrm{T} \qquad (5.21)$$

$$\ln(p(torr)) = 2.678183 - \frac{86.94152}{T} + 2.860678\ln(T) \tag{5.22}$$

$$\ln(p(torr)) = 10.62782 - \frac{102.7498}{T} + 0.0533981T - 0.0001105632T^2 \tag{5.23}$$

The SVP was used to determine the sample Temperature using each of these three equations. The actual sample temperature was then taken to be the average of the three.

Once the peak position is determined and the temperature is established the location of each feature and the SVP is plotted using the form of the Clausius-Clapeyron equation given in (5.24).

$$\ln\left(p_n(torr)\right) = -A_n\frac{1}{T} + B_n \tag{5.24}$$

Here, T is the temperature in Kelvin, p_n is the pressure in torr of the feature, and n refers to the step or feature number. For the saturated vapor pressure $n = \infty$ as it represents the bulk fluid or molecules above an infinitely thick film. A_n and B_n, represent the negative slope and the intercept of a linear fit through the data points for the nth feature, respectively. A derivation of the Clausius-Clapeyron equation is given in (Novakovic, Ninic et al. 1967).

The enthalpy of adsorption can be calculated from these data as shown in equation (5.25); where R, is the ideal gas constant.

$$Q_{ads} = \Delta H_{ads_n} = RA_n \tag{5.25}$$

Once evaluated, these parameters additionally allow for the calculation of the differential enthalpy and differential enthalpy of each adsorbed layer or feature relative to that of the bulk (or SVP) using equations (5.26) and (5.27).

$$\Delta H_n = -R\left(A_n - A_\infty\right) \tag{5.26}$$

$$\Delta S_n = -R\left(B_n - B_\infty\right) \tag{5.27}$$

5.4 – Two-Dimensional Compressibility

The two-dimensional isothermal compressibility is the two dimensional analog of the three dimensional compressibility. The three dimensional compressibility is a measure of the relationship between changes in pressure and changes in volume according to equation (5.28).

$$K_{3D} = -\frac{1}{V}\left(\frac{\partial V}{\partial P}\right) \tag{5.28}$$

When changing from three dimensions to two dimensions, volume becomes the molecular area of the adsorbate, σ. Pressure defined as force per unit area, becomes what is known as the spreading pressure, ϕ, which is defined as the pressure needed to

maintain an adsorbed film. The two dimensional analog is then rewritten as shown in equation (5.29) (Phillips and Larese 1997).

$$K_{2D} = \frac{1}{\sigma}\left(\frac{\partial \sigma}{\partial \phi}\right) \tag{5.29}$$

The two dimensional compressibility can be rewritten to describe the change in spreading pressure of an adsorbed film as a function of chemical potential (Mutaftschiev, 2001). This is the form of the equation, given in equation (5.30), which will be utilized in calculations performed in this dissertation.

$$K_{2D} = \frac{A \cdot p_f}{N_A \cdot k_B \cdot T \cdot N^2}\left(\frac{dN}{dp}\right)_T \tag{5.30}$$

Where, A, is the surface area of the sample; p_f, is the final pressure for a given equilibration point; N_A, is Avogadro's Number; k_B, is Boltzman's constant; T, is the sample temperature of the given isotherm; and N, is the number of moles adsorbed at the completion of a given equilibration point; (dN/dp), is the first derivative of the given isotherm.

5.5 – Isosteric Heat of Adsorption

The isosteric heat of adsorption is defined as the energy required to remove or desorb one adsorbate molecule from the adsorbed surface film and move it into the

bulk. This value is dependent on both coverage and temperature. The isosteric heat is calculated using two isotherms close in temperature according to equation (5.31) or explicitly by taking the difference of the isothermal data as expressed in equation (Dash 1975).

$$Q_{ST} = RT^2 \left(\frac{\partial(\ln(p))}{\partial T} \right) \tag{5.31}$$

$$Q_{ST} = R\overline{T}^2 \left(\frac{\Delta \ln p_f}{\Delta T} \right)_n \tag{5.32}$$

This equation is valid for $0.5K \le \Delta T \le 1.5K$, $\overline{T}$ is the average temperature of the two isotherms. Peaks in the isosteric heat should correspond to the adsorption layers and features in the isothermal data (Freitag and Larese 2000).

5.6 – Critical Temperature Determination

Potential phase changes in the adsorbed molecular film can be identified using the features of the isotherm, by monitoring the variations in the full width at half maximum (FWHM) of the associated peaks in the numerical derivative as a function of temperature. (Larher 1992). Depending on the nature of the phase transformation, there is generally a noticeable change, in the width of these numerical derivative peaks as the phase change takes place. Using a set of isotherms phase

transformation temperature can be determined by plotting the FWHM of the peaks as a function of T. Because the temperature dependence of the compressibility width is usually significantly different on each side of the transition temperature, the data on either side are fit separately. We then use the intersection of the fits to pinpoint the temperature at which potential phase changes may occur.

5.7 – Phase Diagram

Just as phase diagrams exist for three dimensional molecules separated into gas, vapor, and solid phases, two dimensional phase diagrams can be generated for a two dimensional adsorbed film. In addition to detrmining the phases present in the adsorbed layer (solid, liquid, vapor) there is interest in determining the phase of the bulk which is in equilibrium with the adsorbed layer (Dash 1985).

Phase diagrams are intended to delineate the boundaries between different phases of the adsorbed layer. There are four points of interest which must be determined before a complete phase diagram can be assigned. The left, or low temperature, boundary occurs with the first indication of the appearance of the feature. The right, or high temperature, boundary is set by the critical temperature of the feature, calculated as described above. The horizontal boundaries are associated with the onset and completion of the feature. These limits are associated with the boundaries of the peak in the first derivative. The determination of these boundaries

is more clearly discussed in chapter 6, section 6.4.5. The phase diagram is then plotted as a density (molecules/Å^2) vs. Temperature curve where density, ρ, is defined by equation (5.33) for comparison with the phase diagram generated by Jian Ma shown previously in Figure 1.3 (Ma, Kingsbury et al. 1988). Further discussion of the types of phase transitions present in surface films may be found in (Dash and Ruvalds 1980)

$$\rho = \frac{N_{ads}(moles)}{m^2} \bullet \frac{6.022 \times 10^{23}\left(molecules\right)}{mole} \bullet \frac{\left(m\right)^2}{\left(1 \times 10^{10}\, Angstrom\right)^2} \qquad (5.33)$$

Chapter 6

H_2 Adsorption on MgO (1 0 0)



M. C. Escher: Reptiles (1943)

6.1 – Surface area calculation of MgO sample

As discussed in the previous chapters, a methane isotherm is used to determine the surface area of each MgO Sample. The methane isotherm for the following isotherms performed on MgO sample 606Ia was shown in Chapter 5, Figure 5.2. The isotherm confirms good quality of the MgO sample, the surface area was determined to be 3.999m^2 as evidenced in Figure 5.3. This sample weighed 0.5g giving an overall surface area for the sample of ~8m^2/g. The surface areas of the other samples used in this study were determined in the same manner and are tabulated in Appendix A, Table A.1. The surface area of the sample is used to normalize the samples in order to compare results and correlate the behavior for different samples. The methane isotherm for each of the samples is shown in Appendix A.

6.2 – Hydrogen Isotherms – Monolayer Calculations

Ultra High Purity (UHP) grade molecular hydrogen, obtained from Matheson Tri-Gas corporation, was used throughout the experiments discussed herein. A characteristic hydrogen isotherm is shown in figure 6.1. One of the main quantities of interest in the adsorption study is the calculation of the area occupied per molecule of adsorbate.

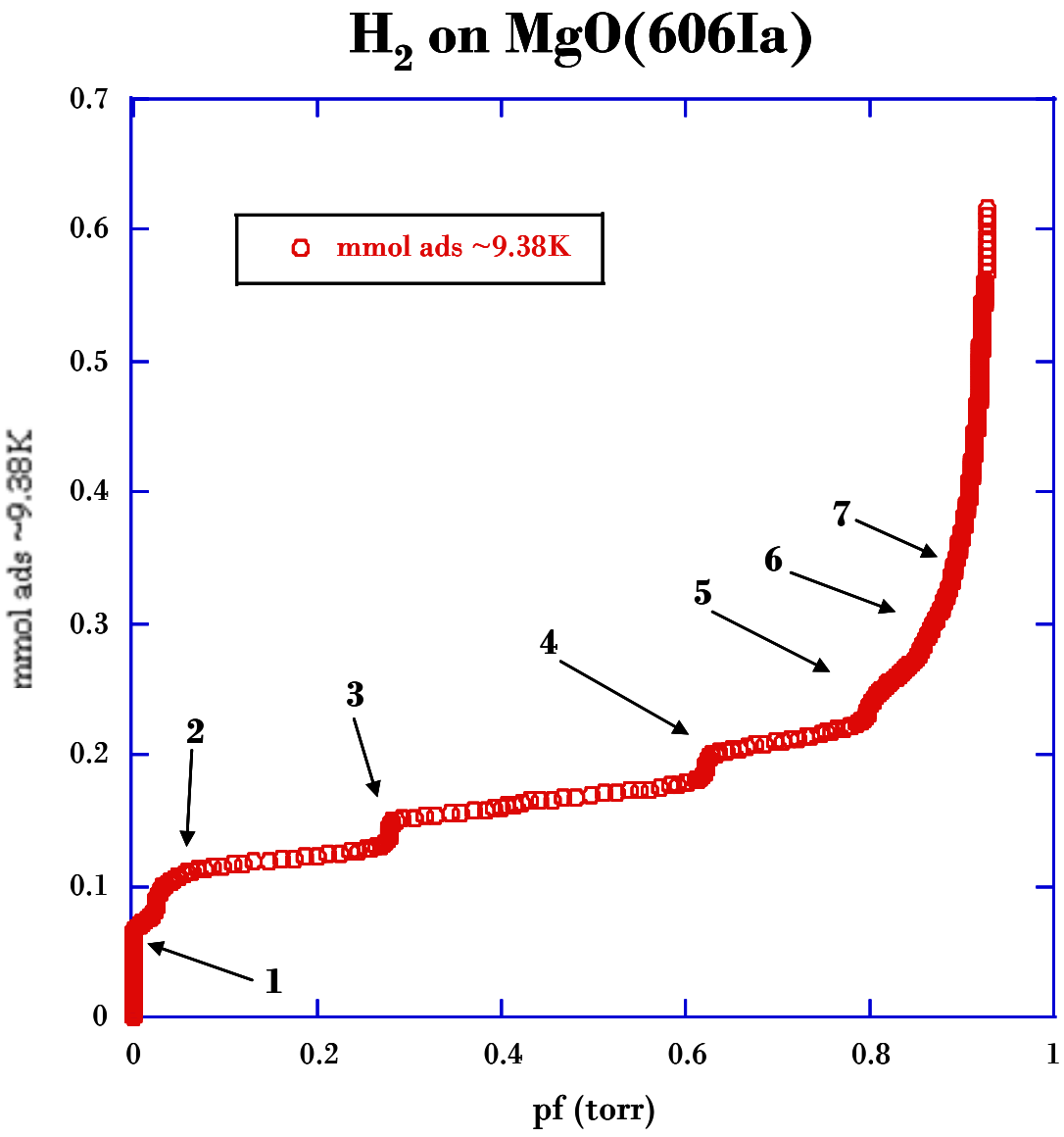


Figure 6.1 – Typical hydrogen isotherm

Earlier structural work by Degenhardt , Lauter and Halsey (Degenhardt, Lauter et al. 1987) described in Chapter 1 postulated that the first layer adsorbs in a series of commensurate configurations depending on the surface coverage. At low coverage ($\theta < 0.8$ monolayer), island-like growth occurs in a c(2x2) commensurate structure as seen in figure 6.2. As more molecules adsorb, the monolayer film compresses until it forms a hexagonal close packed pattern on the surface shown in Figure 6.3. The completion of the hexagonal pattern would correspond with monolayer completion.

The number of moles of hydrogen needed to nominally complete the monolayer is determined using the point B method as shown in Figure 6.4 and summarized for each isotherm in Appendix A, Table A.2. Using these data, the average density of the hydrogen monolayer as calculated by the point B method is 0.0162 ± 0.007 mmol/m^2. This value corresponds to 0.0975 molecules/Å^2. The footprint of a single molecule at monolayer completion is 10.25 Å^2/molecule. This is in excellent agreement with the neutron scattering result of 10.37 Å^2/molecule. It should be noted that this is far denser than the density of bulk solid hydrogen, 12.43 Å^2/molecule. This suggests that the surface is responsible for directing the hydrogen molecules into a configuration that is over 10% denser than it naturally forms in the bulk solid.

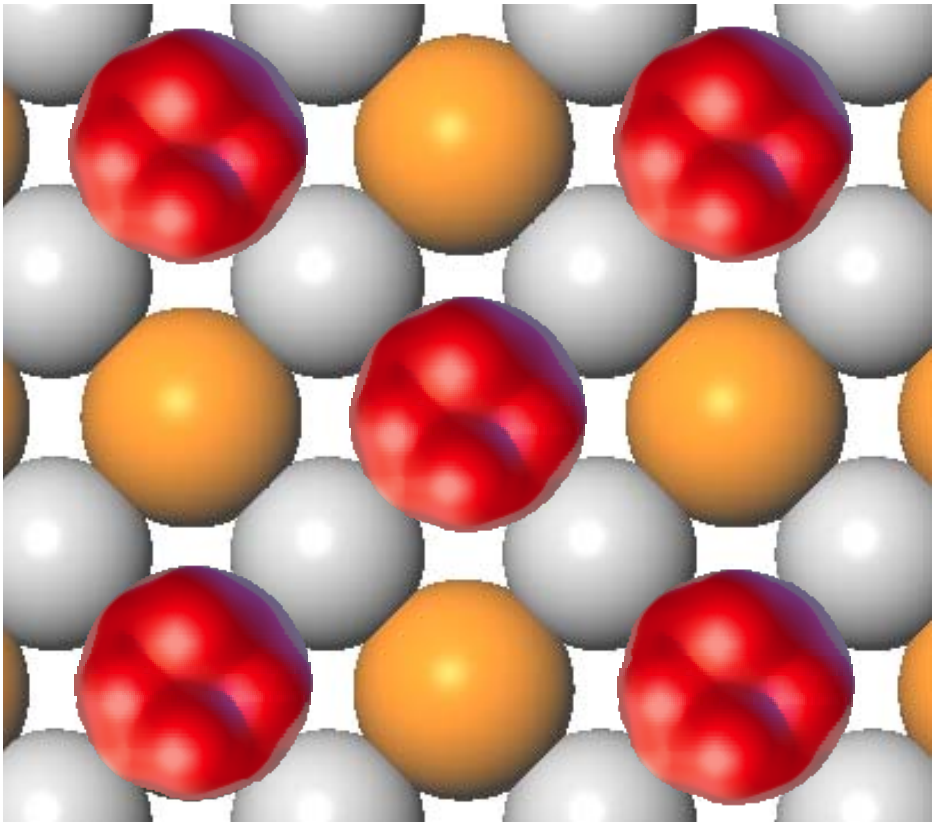


Figure 6.2 – Low coverage c2x2 structure of molecular hydrogen adsorbed on the MgO (100) surface has a lattice constant a = 5.96 Å corresponding to an area per molecule of 17.76 Å^2. (Larese, Frazier et al. 2006)

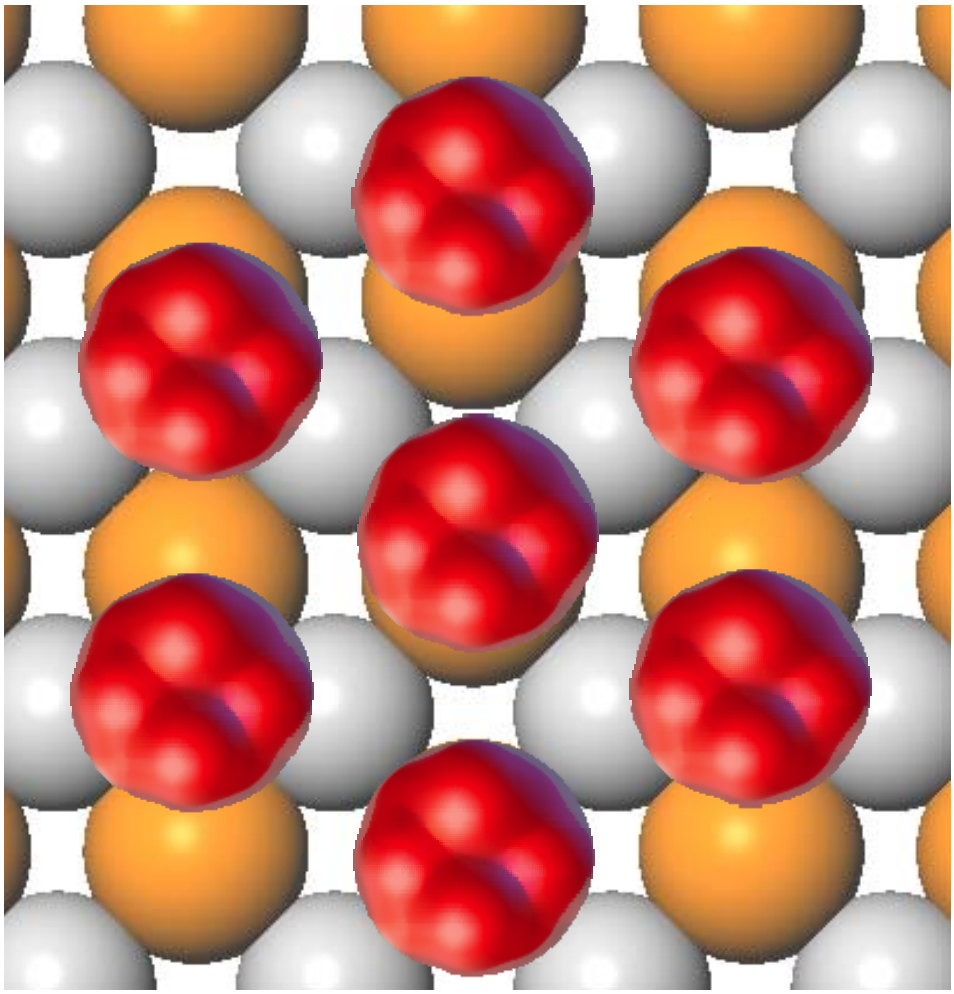


Figure 6.3 – High coverage hexagonal structure adsorbed on the MgO (100) surface has a lattice constant a = 3.46 Å corresponding to an area per molecule of 10.37 Å^2

(Larese, Frazier et al. 2006)

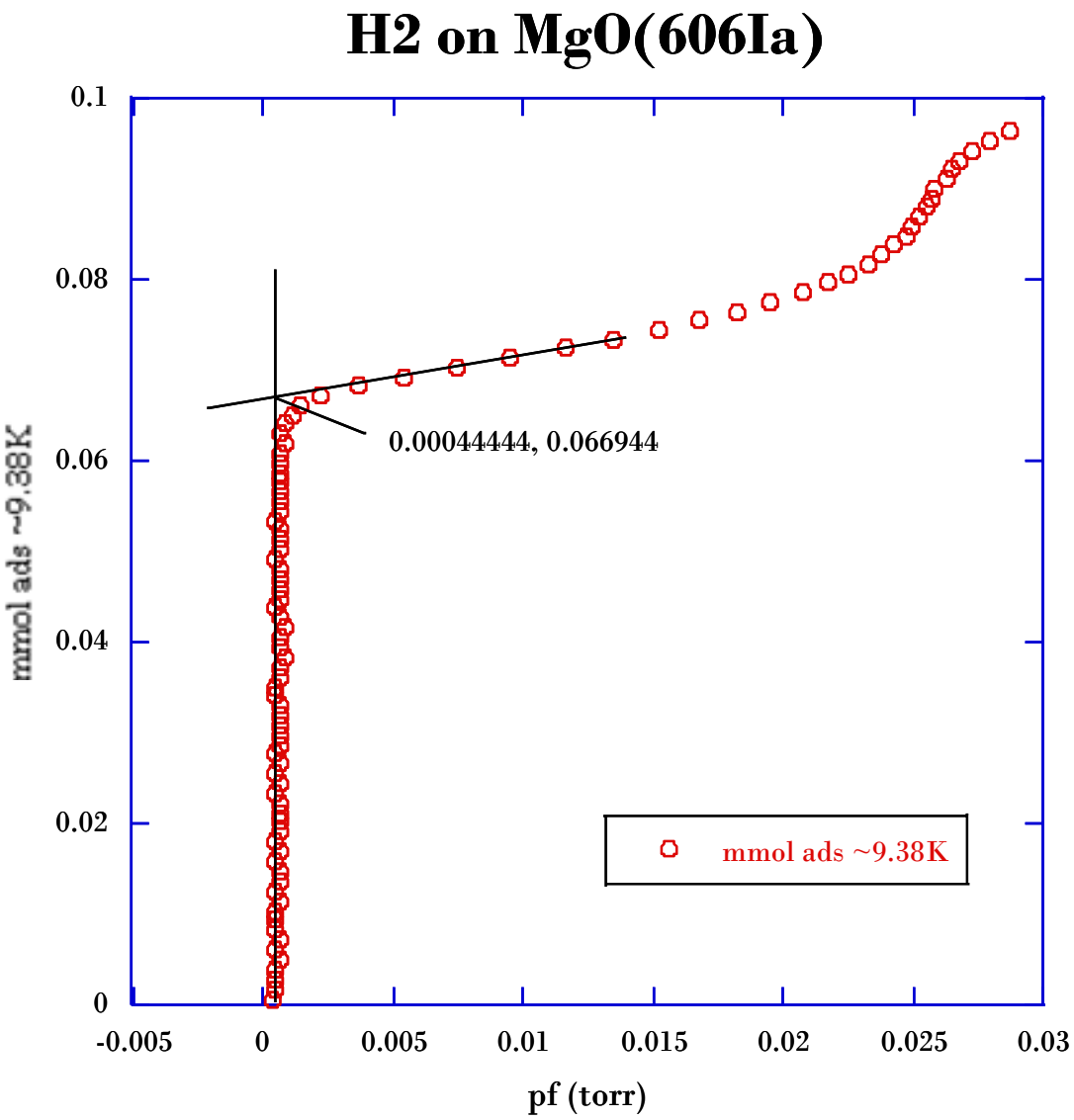


Figure 6.4 – The monolayer of isotherm shown in Figure 6.1

6.3 – Hydrogen Isotherm – Multiple layers

A typical hydrogen isotherm consists of 5 to 7 adsorption steps which are visible by inspection as indicated in Figure 6.1. Isotherms were performed at temperatures ranging from approximately 7K through the bulk triple point of 13.74K. A subset of these isotherms is shown in figure 6.5. One can see that as temperature increases the risers become less vertical, decreasing in height and increasing in breadth. However, it should be noted that the beginning of each adlayer begins at approximately the same coverage. Therefore, although the height of the riser decreases, the overall coverage of the layer remains constant. Also upon closer inspection shown in figure 6.6, it should be noted that the isotherms do not cross with increasing temperature. This figure also shows very consistent monolayer coverage over the entire temperature range.

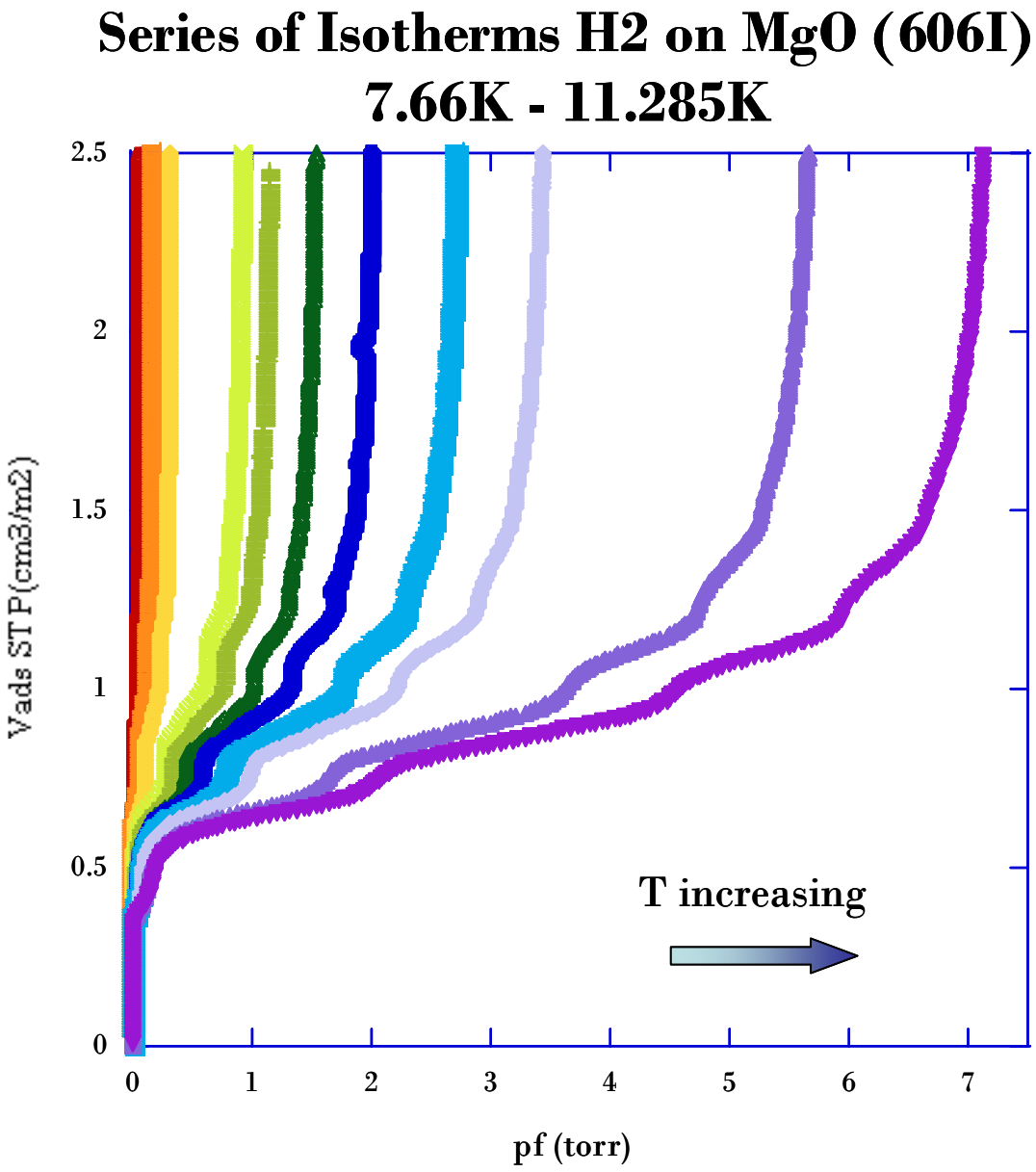


Figure 6.5 – Collection of isotherms is shown for a range of temperatures

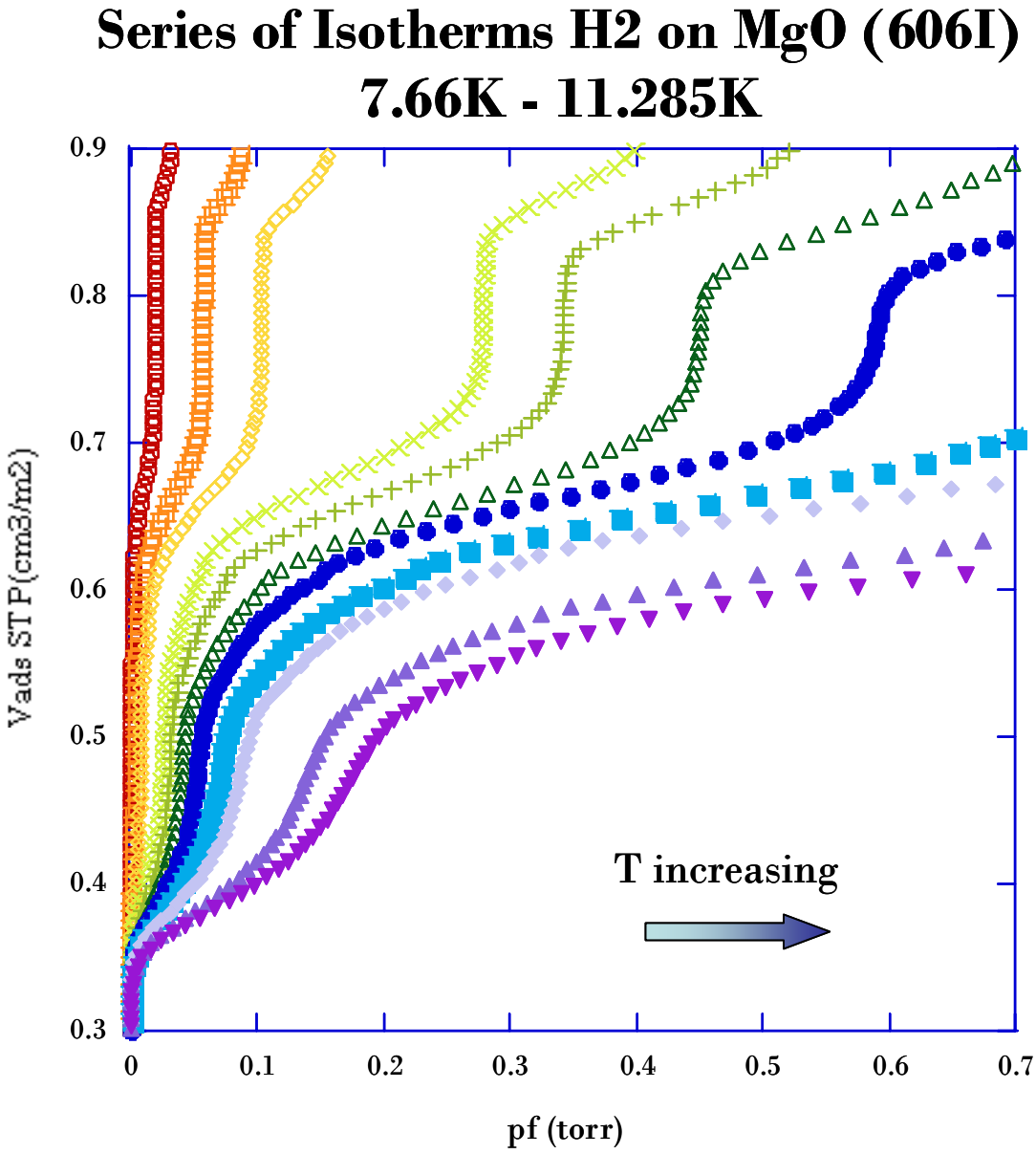


Figure 6.6 – Close up of steps 1 through 3 of series of isotherms

6.4– Analysis of the individual adlayers

6.4.1 – Derivative

The position of the center of the adlayer riser is calculated by inspection of the numerical derivatives of the isothermal data. Figure 6.7 shows the derivative of the isotherm shown in Figure 6.1. In addition to the extremely sharp prominent features in the derivative traces there are some additional features within the individual adlayers are present as evidenced by the additional weaker peaks. These features appear consistently throughout the set of isotherms as shown in figure 6.8. In fact, there may be two weak peaks present in the second layer regime: one in the shoulder of the main peak labeled 2s, and the other is labeled 2f. The feature that appears roughly midway between the prominent derivative peaks associated with layers3, 4, and 5 are labeled 3f, 4f, and 5f respectively. The equilibrium pressure locations of these features are given in Table B.3.

It is necessary to determine the location of the adlayers (center of the peaks in the numerical derivative) in order to calculate the values of the heat of adsorption, and the differential enthalpy and entropy for the layers. The widths of these peaks are also useful in locating the position of potential phase transitions and the boundaries of a phase diagrams.

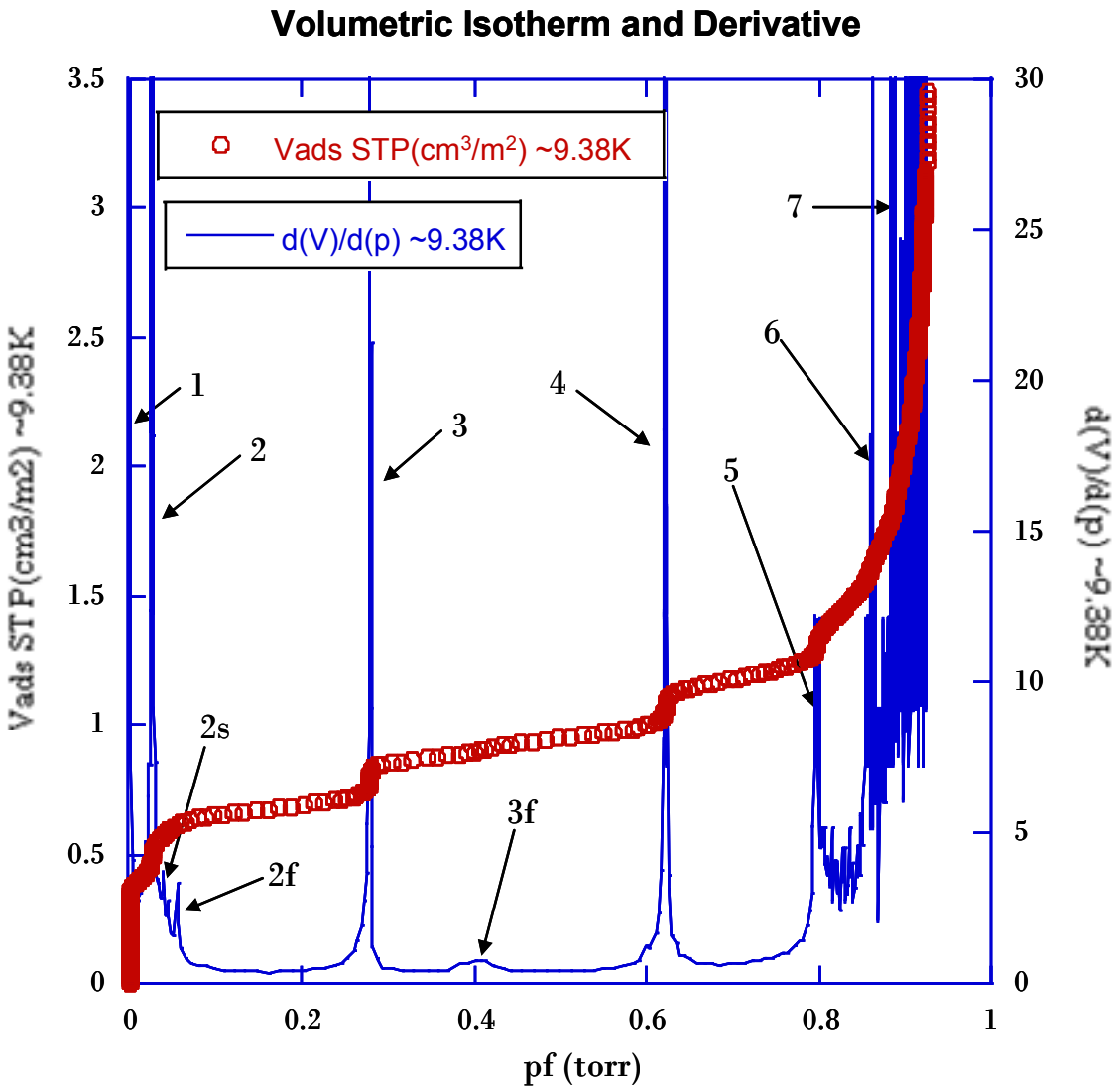


Figure 6.7 – Isotherm and its derivative.

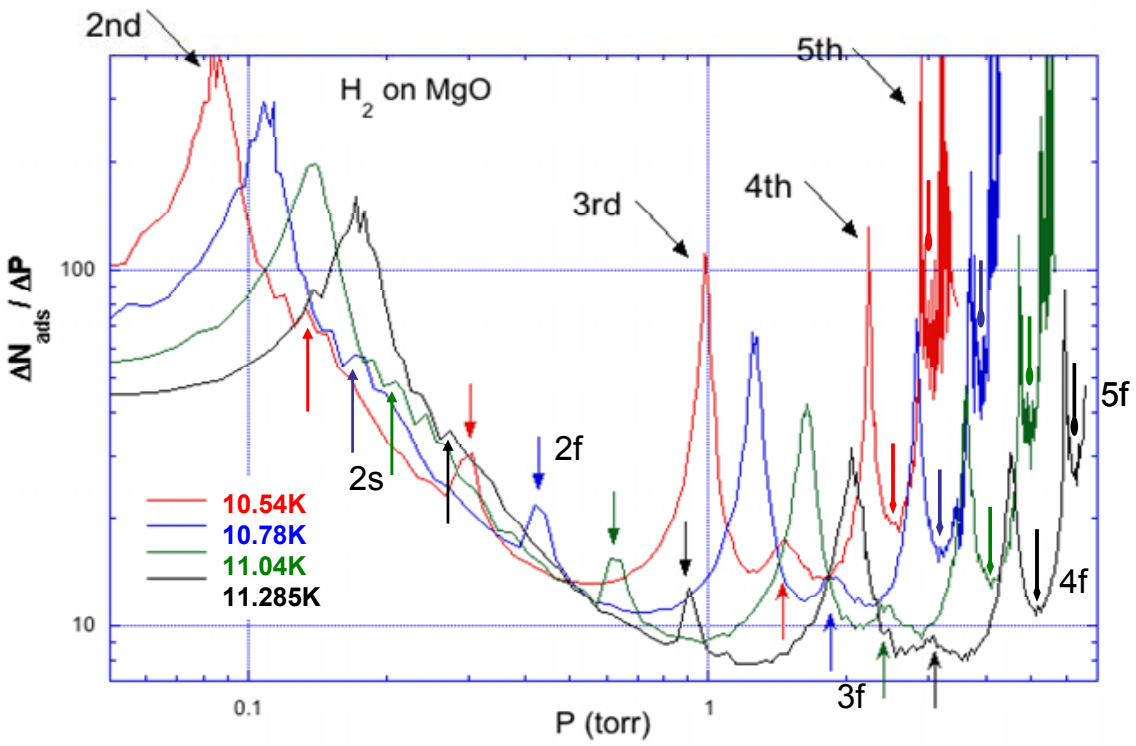


Figure 6.8 – series of derivatives showing consistency of the main peaks and interlayer features

6.4.2 – Isosteric Heat of Adsorption

The isosteric heat of adsorption is an important thermodynamic parameter when examining the layering properties of the adsorbed film. It enables one to determine how the heat of adsorption varies with coverage at a given temperature. Figure 6.9 shows the isosteric heat of adsorption for an average temperature of 9.7K calculated from two isotherms which were separated by 1.24 K. One can clearly see

the adsorption steps. Because the isosteric heat involves taking the numerical derivative of a pair of isotherms it is not surprising to suggest tat the additional peaks that are visible should correspond to the interlayer features with in the 2^{nd} , 3^{rd}, and 4^{th} adlayer.

The multiple peaks present in the first layer could correspond nicely with the series of commensurate structures hypothesized to occur during the completion of the monolayer; however, since the commensurate structures are supposed to build ina devil's staircase sequence, one would expect to see more peaks corresponding to the stepwise commensurate compression of the monolayer. The noise in the isothermal data in the region of the first layer (due to resolution limits at low pressures) makes itt is difficult to explain the exact nature of these peaks. Also depending of the number of isosteric points calculated, one can somewhat alter what that portion of the isosteric heat plot looks like. If one increases the number of calculated isosteric points

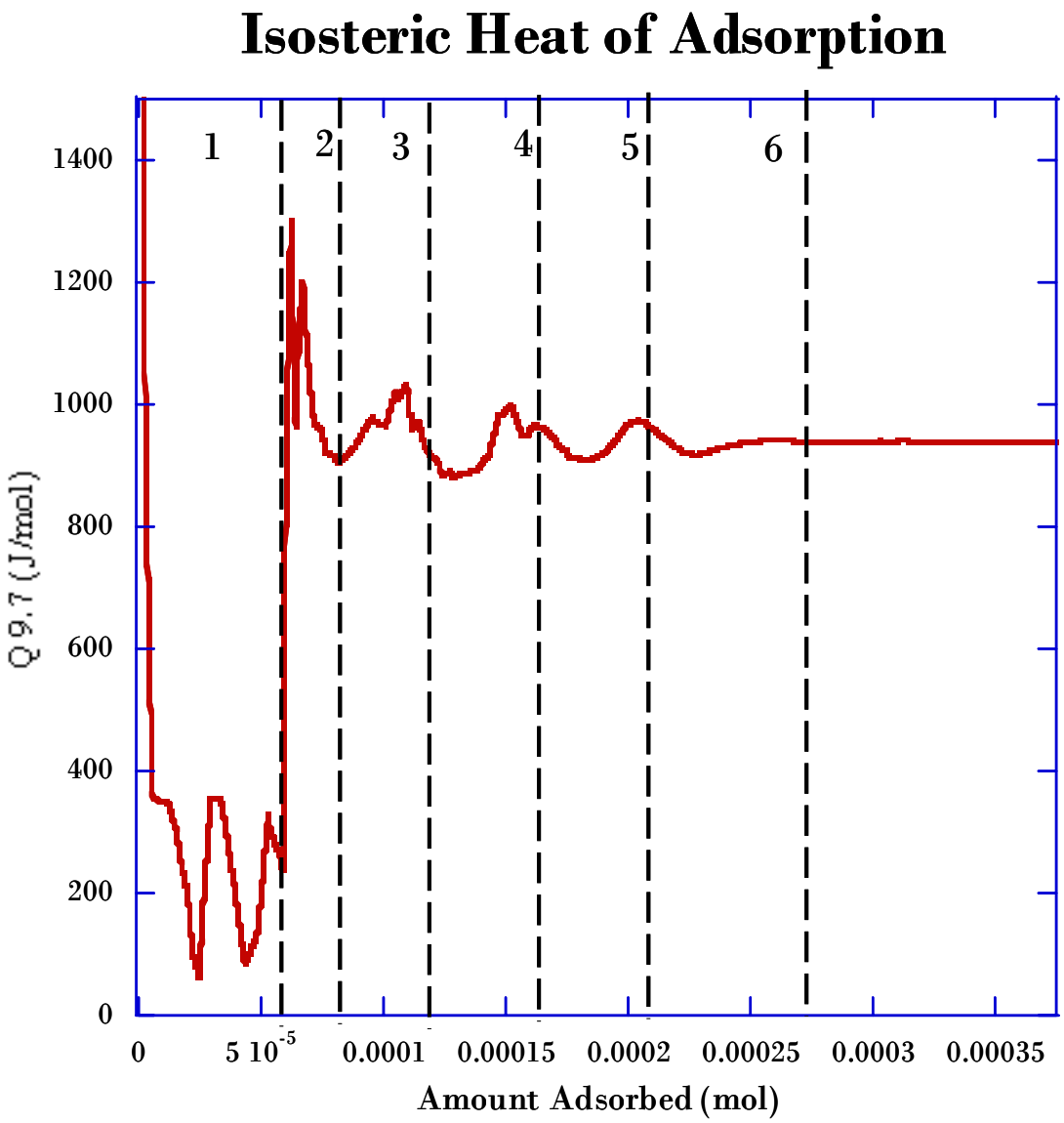


Figure 6.9 – Isosteric heat of adsorption for T = 9.7 K

in this region, the noise in the first adlayer increases dramatically and more peaks become visible as seen in figure 6.10.

The dotted vertical lines, shown in figure 6.9, indicate layer or feature completion. The isosteric heat oscillates and appears to be approaching the heat of vaporization for molecular hydrogen, 919.5 J/mol.

6.4.3– Clausius Clayperyon

Figure 6.11 shows the Clausius Clayperyon plot for the layers and features. The curve fits and error are given in Table 6.1. The corresponding values for the Qads, ΔH, and ΔS are given in Table 6.2.

As the adsorbed film thickens and thesystem pressure approaches the saturated vapor, Q_{ads} usually decreases and, ΔH and ΔS usually approach zero as the layers of the adsorbed film behave more bulk-like. The ΔS values seem to follow this trend rather nicely with the exception of the value for the 2f feature. The Saturated Vapor Pressure Clausius Clapeyron curve is generally the least steep of all such curves. That is not the case here.

There is a sharp decrease in the Qads beyond the second layer. This can be explained by a loss of surface control over the adlayers beyond the second layer. At

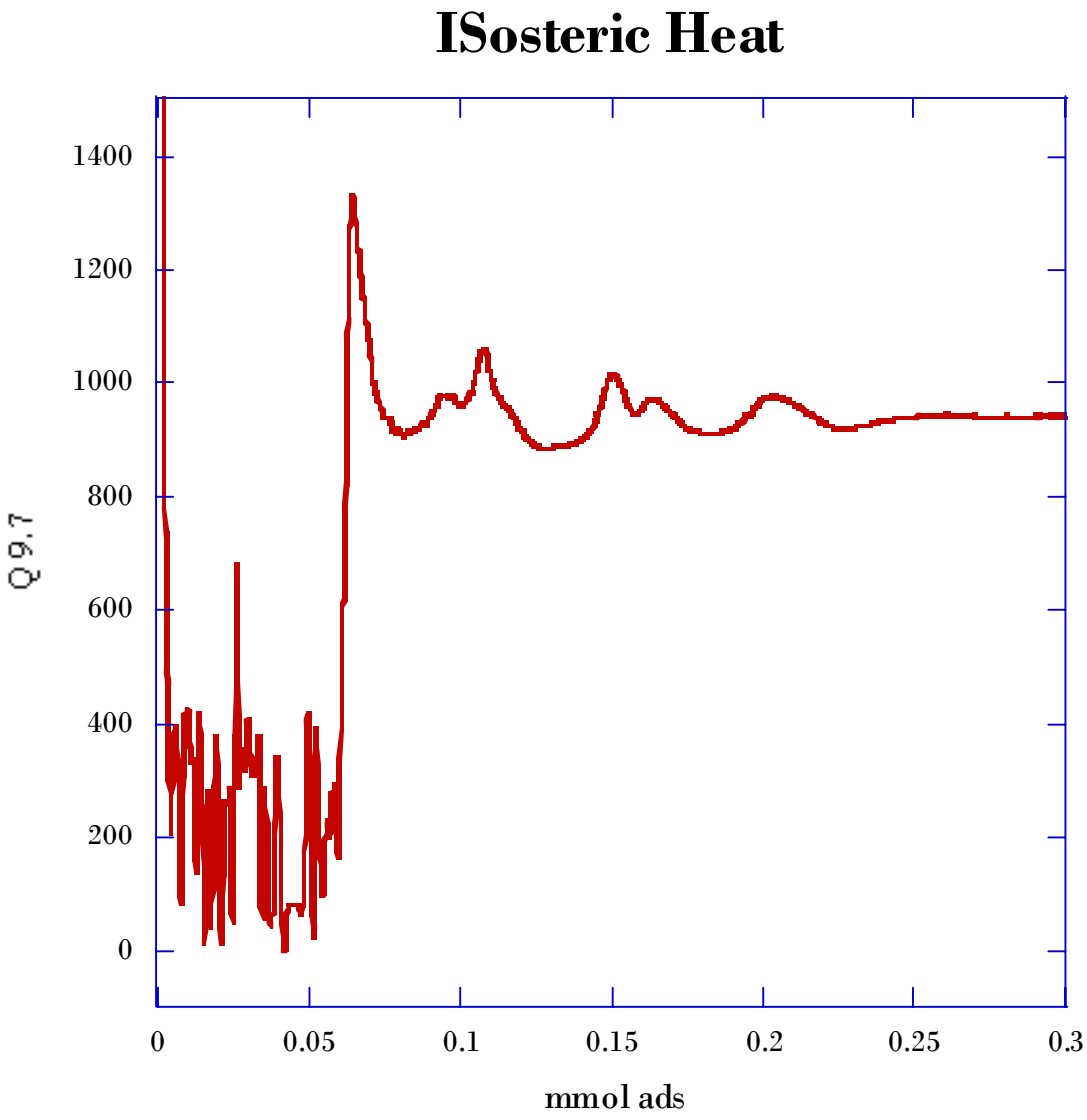


Figure 6.10 – isosteric heat with more isosteric points chosen resulting in a greater number of peaks in the monolayer

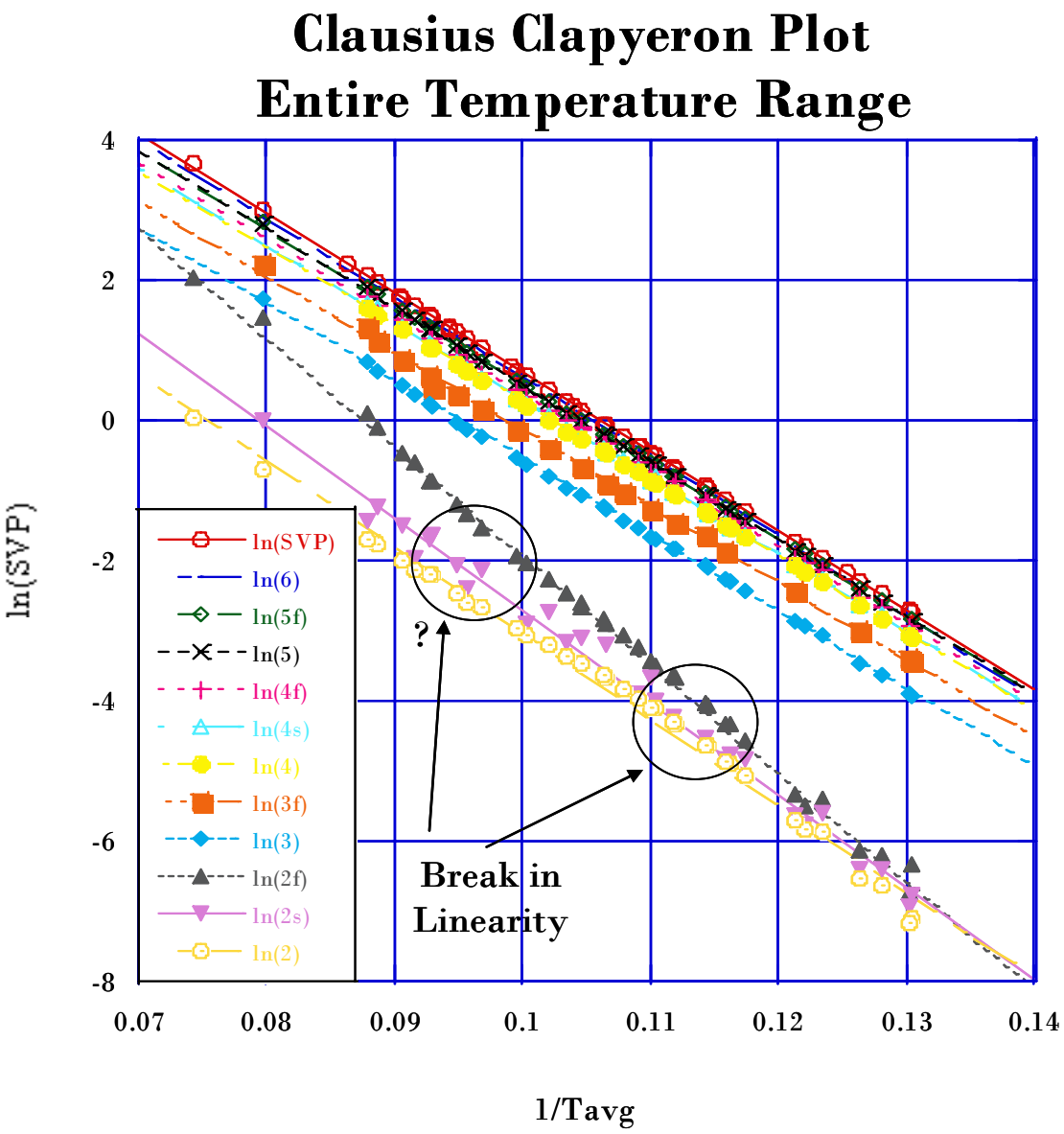


Figure 6.11 – Clausius Clapyeron Plot over entire temperature range. Circles show potential breaks in linearity which might be associated with phase transitions.

Table 6.1- Clausius Clapyeron Curve Fits

Step	A (K)	Error A(K)	B	Error B	R^2 value
2	122.6	1.9248	9.2365	0.20646	0.99571
2s	131.39	2.4511	10.439	0.265	0.99516
2f	154.19	1.1991	13.525	0.12862	0.99894
3	109.55	0.40531	10.412	0.043787	0.99977
3f	109.04	1.0995	10.767	0.11649	0.99898
4	109.41	0.15605	11.193	0.017041	0.99997
4s	109.96	0.34682	11.288	0.037873	0.99984
4f	109.70	0.37327	11.357	0.040775	0.99982
5	110.65	0.24204	11.576	0.025978	0.99992
5f	110.80	0.25597	11.605	0.027473	0.99991
6	112.95	0.28395	11.894	0.029061	0.99992
SVP	113.08	0.22165	11.991	0.023485	0.99992

Table 6.2 - Values derived from the Clausius Clapyeron Data

Layer	Q_{ads} (j/mol)	Error Q_{ads}	ΔH (J/mol)	Error ΔH	ΔS (J/K·mol)	Error ΔS
2	1018.338	16.00344	-79.1525	16.1092	22.9018	1.727649
2s	1092.421	20.37928	-152.236	20.46243	12.9039	2.211936
2f	1281.988	9.969725	-341.083	10.13862	-12.7542	1.051413
3	910.8359	3.369885	29.34962	3.840873	13.1283	0.413119
3f	906.5956	9.141617	33.58993	9.325521	10.1768	0.988024
4	909.6719	1.297453	30.51363	2.253789	6.63484	0.241251
4s	914.2448	2.883579	25.9407	3.422165	5.844981	0.370516
4f	912.0831	3.103497	28.10247	3.609412	5.27129	0.391229
5	919.9817	2.012403	20.20385	2.728726	3.45045	0.291168
5f	921.2289	2.128222	18.9567	2.815228	3.20934	0.300505
6	939.1047	2.360857	1.080864	1.475623	0.80649	0.310659
SVP	940.146	1.842873	-------	-------	-------	--------

which point the molecule-molecule interactions begin to overtake the molecule-substrate interactions. This alone does not explain the deviation from the expected trend. One problem could be caused by attempting to apply the Clausius-Clapeyron equation across potential phase boundaries. Another potential problem causing deviation from the expected behavior could be explained by variations in density between the layers. This suggestion will be investigated further in section 6.5.

It is obvious looking at step 2 that there is a definite break from linearity in the low T (high 1/T) region. This poses somewhat of a problem as the Clausius Clapeyron equation is not necessarily valid across phase boundaries. This discontinuity in the slope could indicate that a phase boundary has been crossed. There is a second potential break in linearity at higher T (low 1/T) as well.

A best fit curve to the second layer data is shown in figure 6.12. The curve indicates two clear breaks in linearity resulting in three potential regions. If we wish to accommodate the critical point calculated by Jian Ma shown in Figure 1.3 (Ma, Kingsbury et al. 1988) which lies near the center of the other two breaks in linearity, we can divide the data into four regions of different linearity. Further evaluation of the isothermal data is required to determine other potential phase boundaries. This analysis is explained in section 6.4.5.

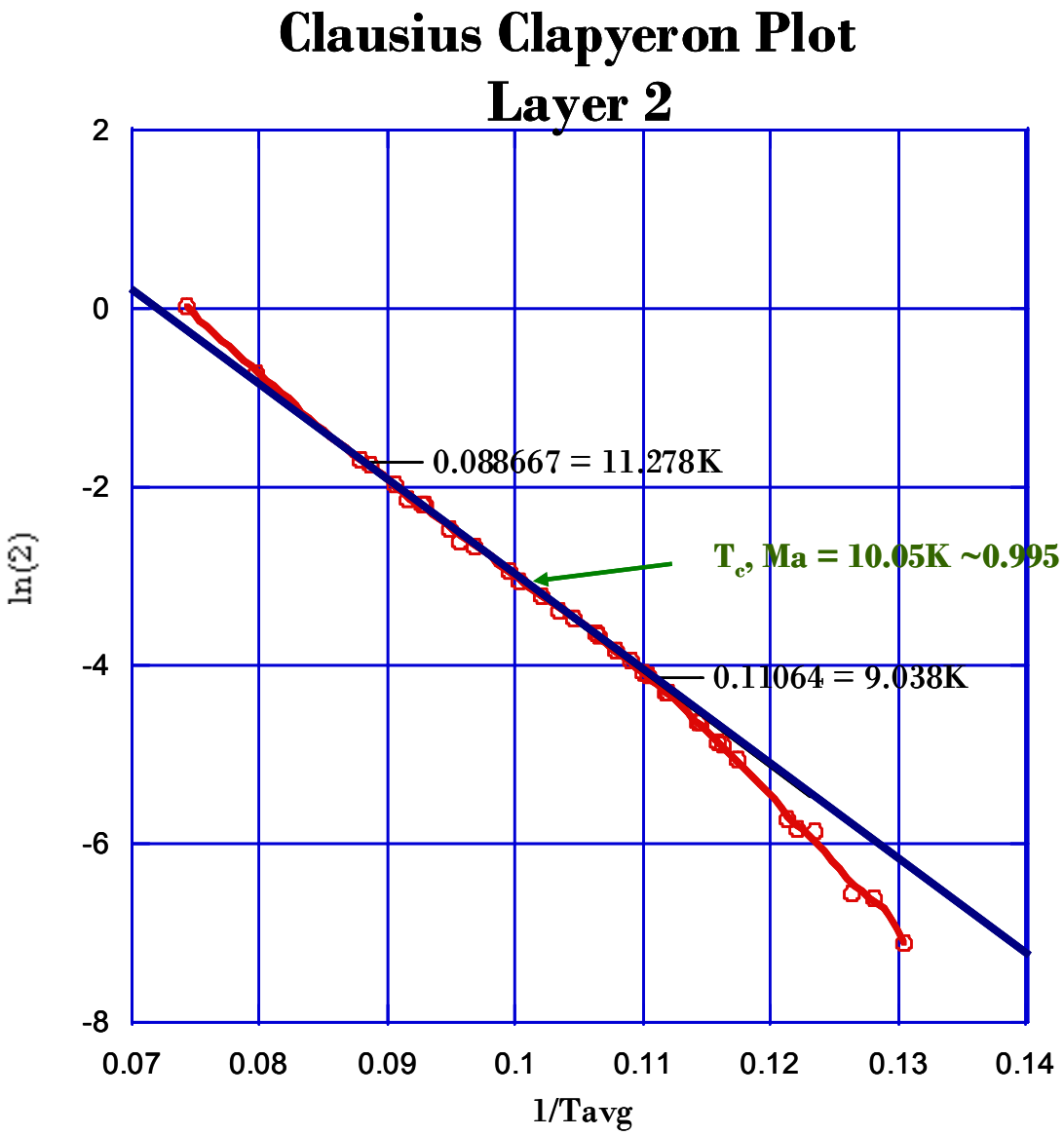


Figure 6.12 – smooth fit of the layer 2 data indicates 3 distinct regions of varying linearity. The critical point as suggested by Ma is shown for comparison.

6.4.4 – 2 Dimensional Compressibility (K_{2D})

The two-dimensional compressibility is calculated using equation 5.24. The isothermal compressibility peaks are discernable for only the second, third and fourth layers and are shown in Figures 6.13, 6.14, and 6.15 respectively. Compressibility features associated with the first layer are difficult to resolve because of the low pressures and poorer relative pressure resolution of the capacitance manometer in this region; hence, the derivative peaks are not well formed. Therefore, the K_{2D} for the first layer is somewhat uncertain. The K_{2D} peaks for layers 5 and above begin to overlap due to their proximity to the saturated vapor pressure. It can easily be seen that for layers where K2D is readily observable that the K2D peaks broaden and decrease in height with increasing temperature. This is associated with the same trends seen in the adsorption risers themselves as seen previously in figure 6.5.

6.4.5 – Determination of Potential Phase Transitions

Ordinarily, the FWHM of the K2D peaks are used to determine the potential locations of possible phase transitions. Here, the width of the features was determined in a two fold fashion as shown in figure 6.16. The base of these derivative peaks were used to mark the beginning and end points for each feature in the phase

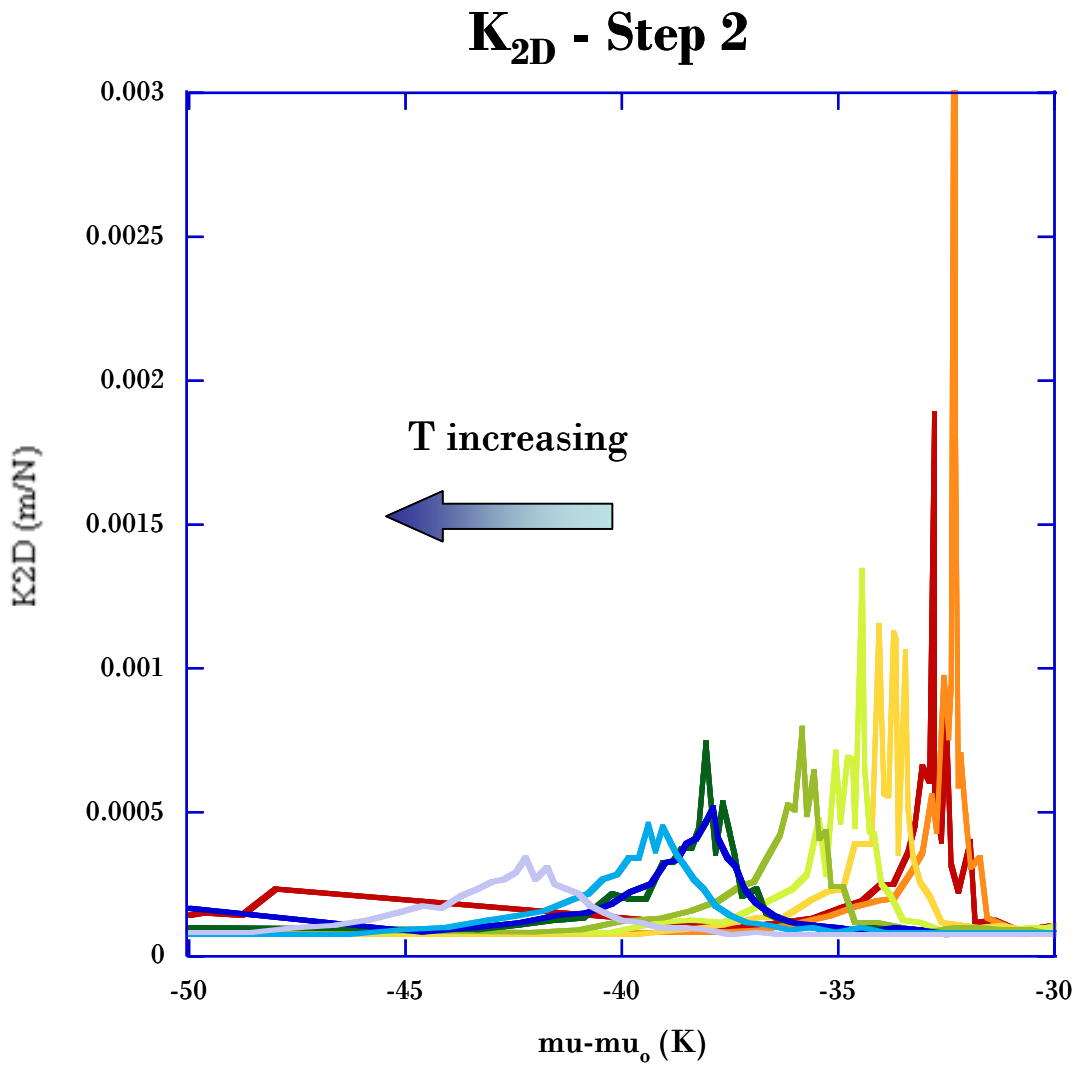


Figure 6.13 – Two-Dimensional Compressibility for the second adsorption layer.

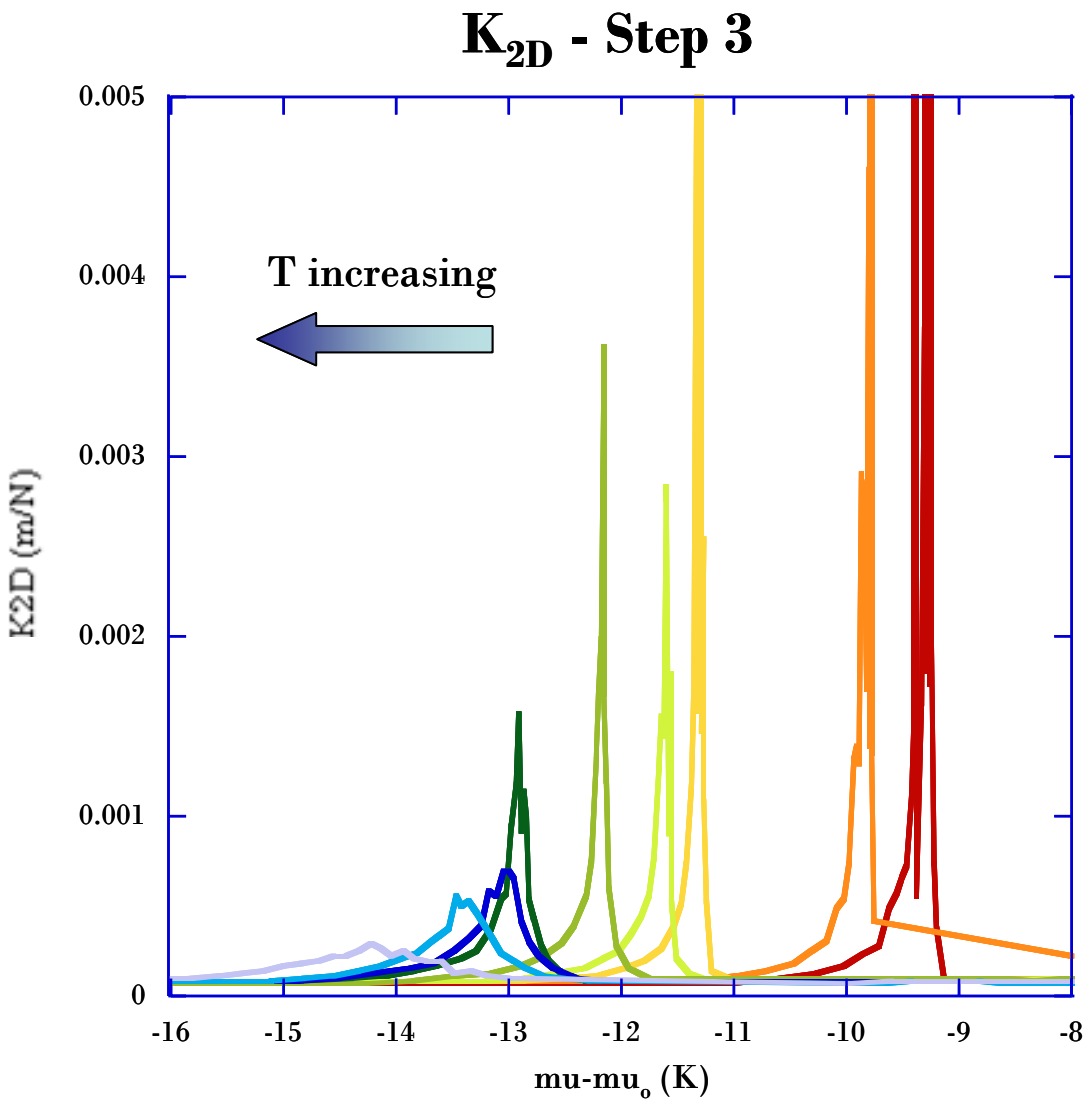


Figure 6.14 – Two-dimensional compressibility peaks for the 3rd adlayer

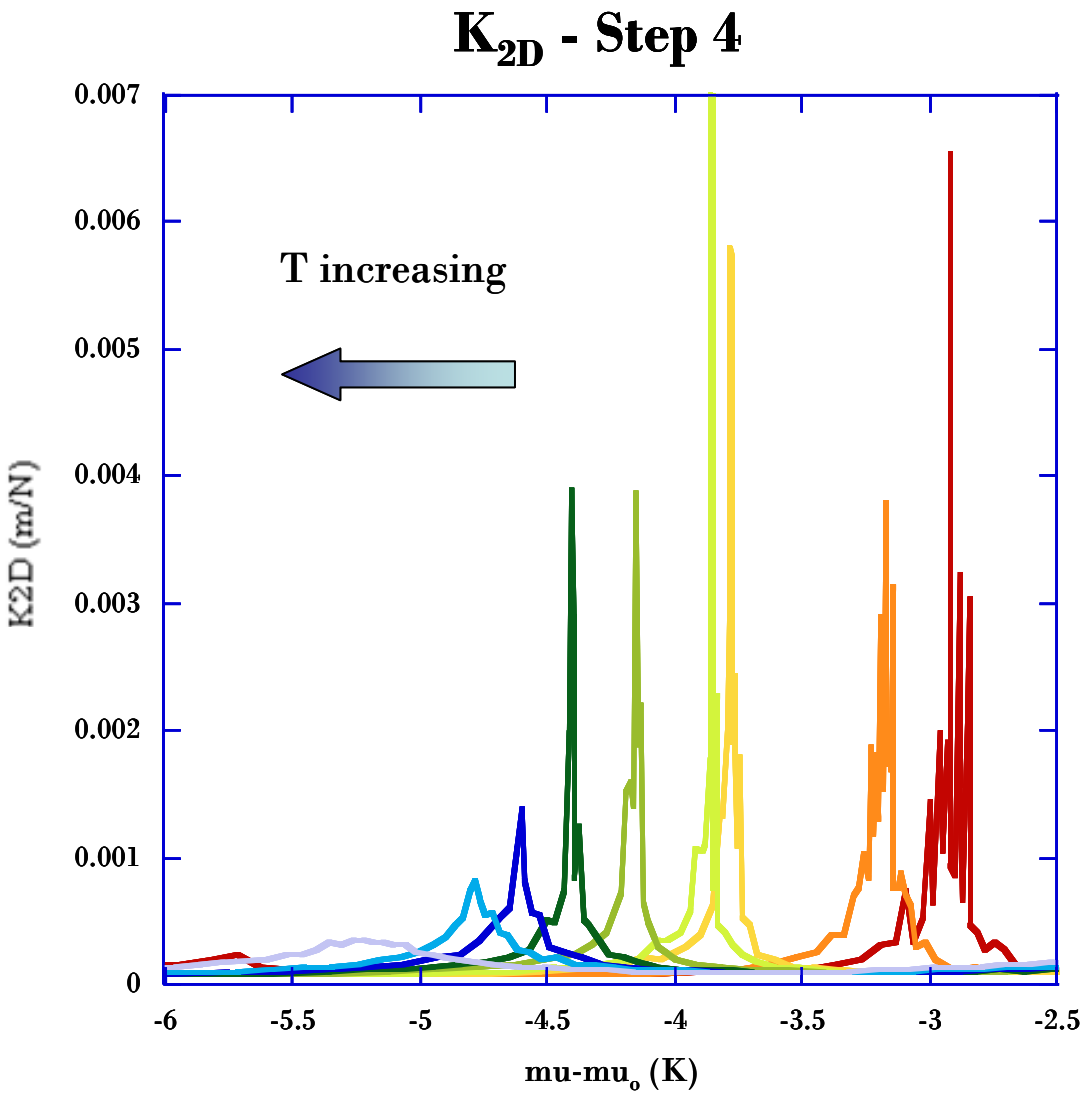


Figure 6.15 – Two-dimensional compressibility for the fourth adlayer

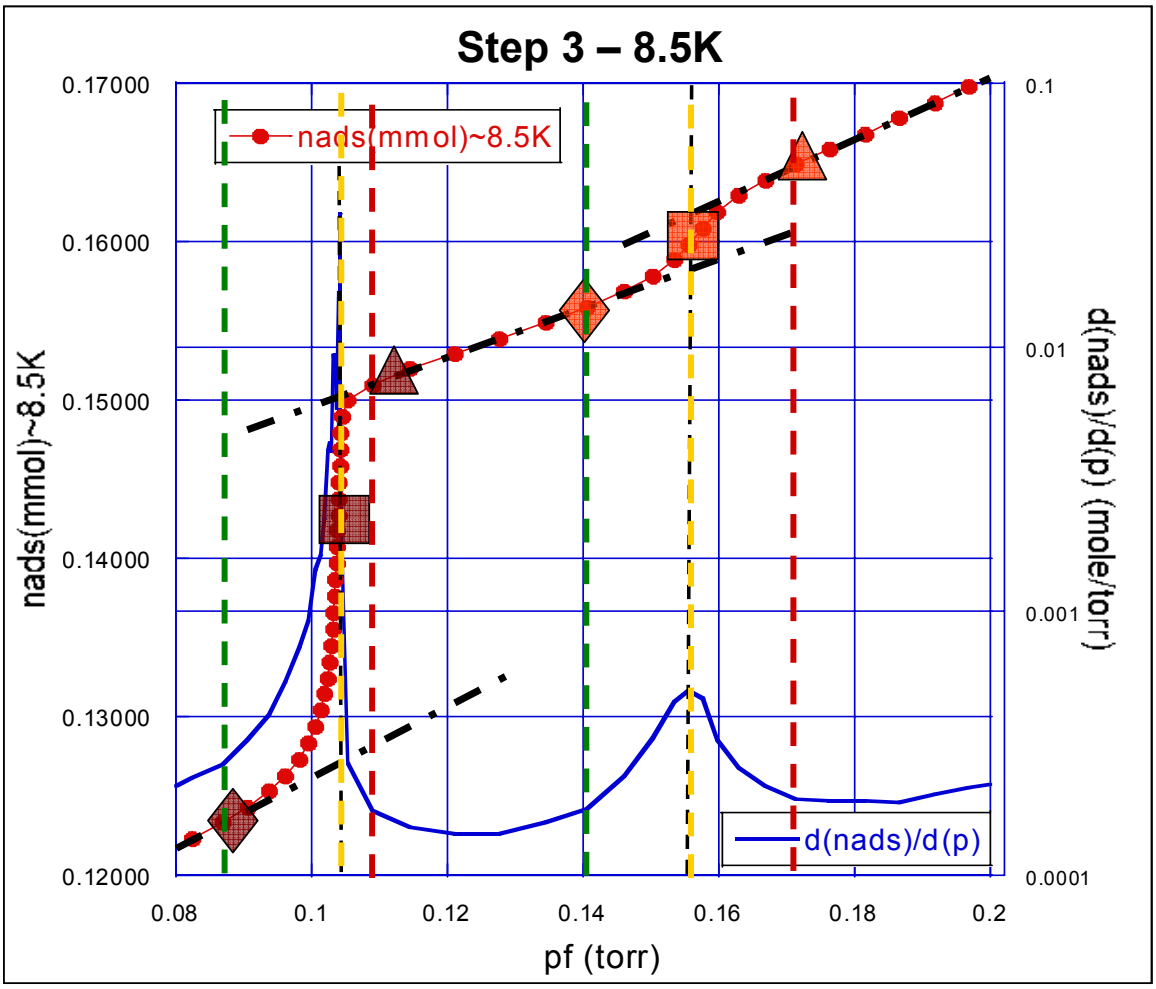


Figure 6.16 – Shows the locations associated with the beginning (green), center (yellow), and end (red) of the derivative peaks. These correspond to the diamond, square, and triangle marked independently to show the beginning, inflection point and end of the riser on the isothermal data. The width of the feature is taken to be the distance in pressure between the green and red lines.

diagram. These endpoints directly correspond to the locations where the isothermal data begins to merge into the vertical riser and merge back into the plateau following each feature as shown in figure 6.16. The full width at the base of the peaks in the first derivative of the isotherms was, therefore, used to represent the width of the feature.

We postulate here that by following the change in slope of the width as a function of temperature, one can identify the location of phase changes. The entire set of data was divided into both 3 sections and 4 sections. These divisions are shown for the third adlayer in figures 6.17 and 6.18 respectively. These divisions do not, however improve the adherence to the expected behavior in Q_{ads} and ΔH.

6.5 – Density of the Layers

We can examine the variations in density of the adlayers in isotherms by normalizing the isotherms by monolayer coverage. This is accomplished by dividing the number of moles adsorbed by the number of moles present at nominal monolayer completion obtained via the point B method. One such isotherm is shown in Figure 6.19. It is obvious by looking at this figure that the density of the upper layers is smaller than that of the monolayer. This is definitely expected due to the fact that

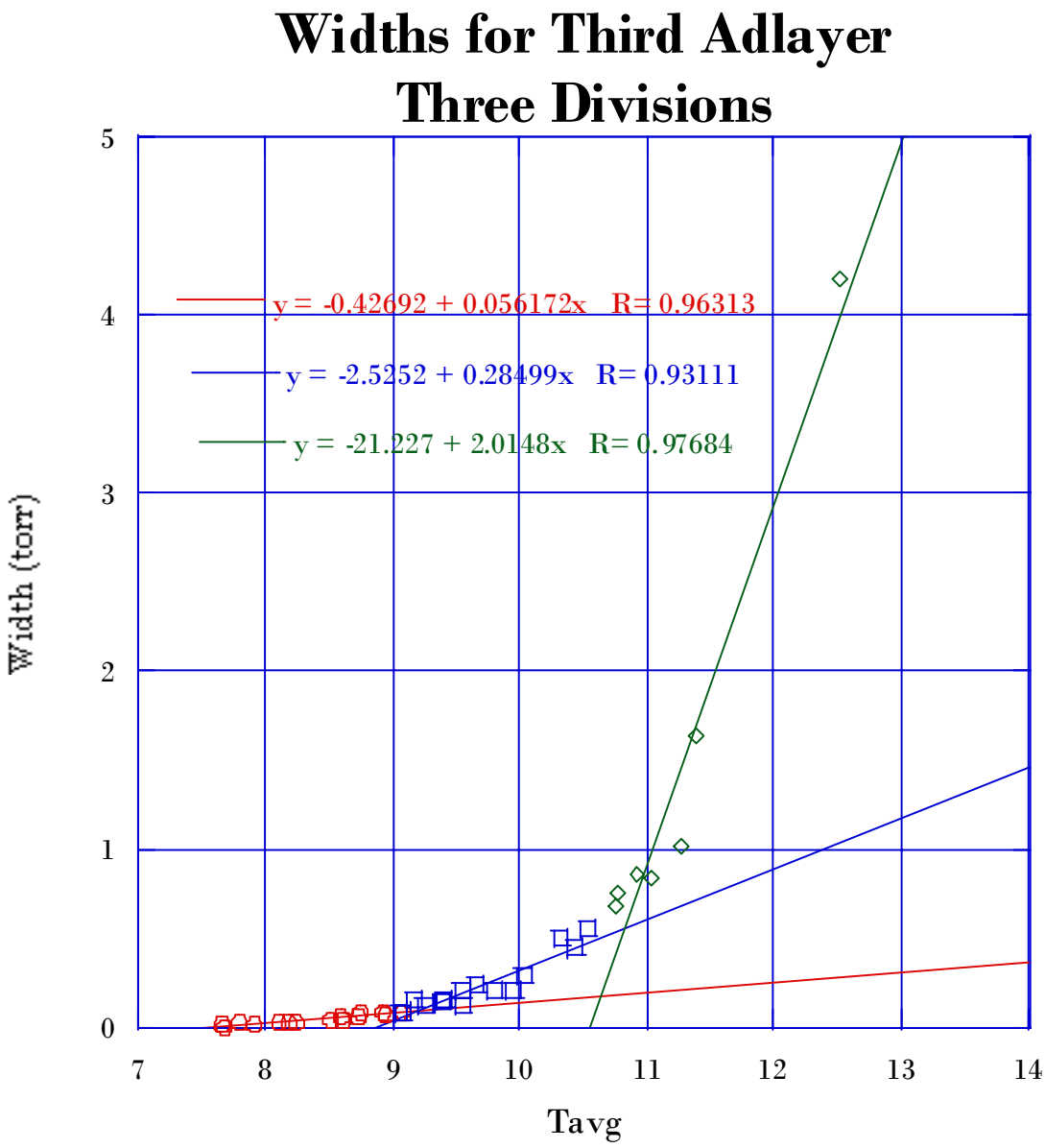


Figure 6.17 – Widths for Critical point Determination, three divisions

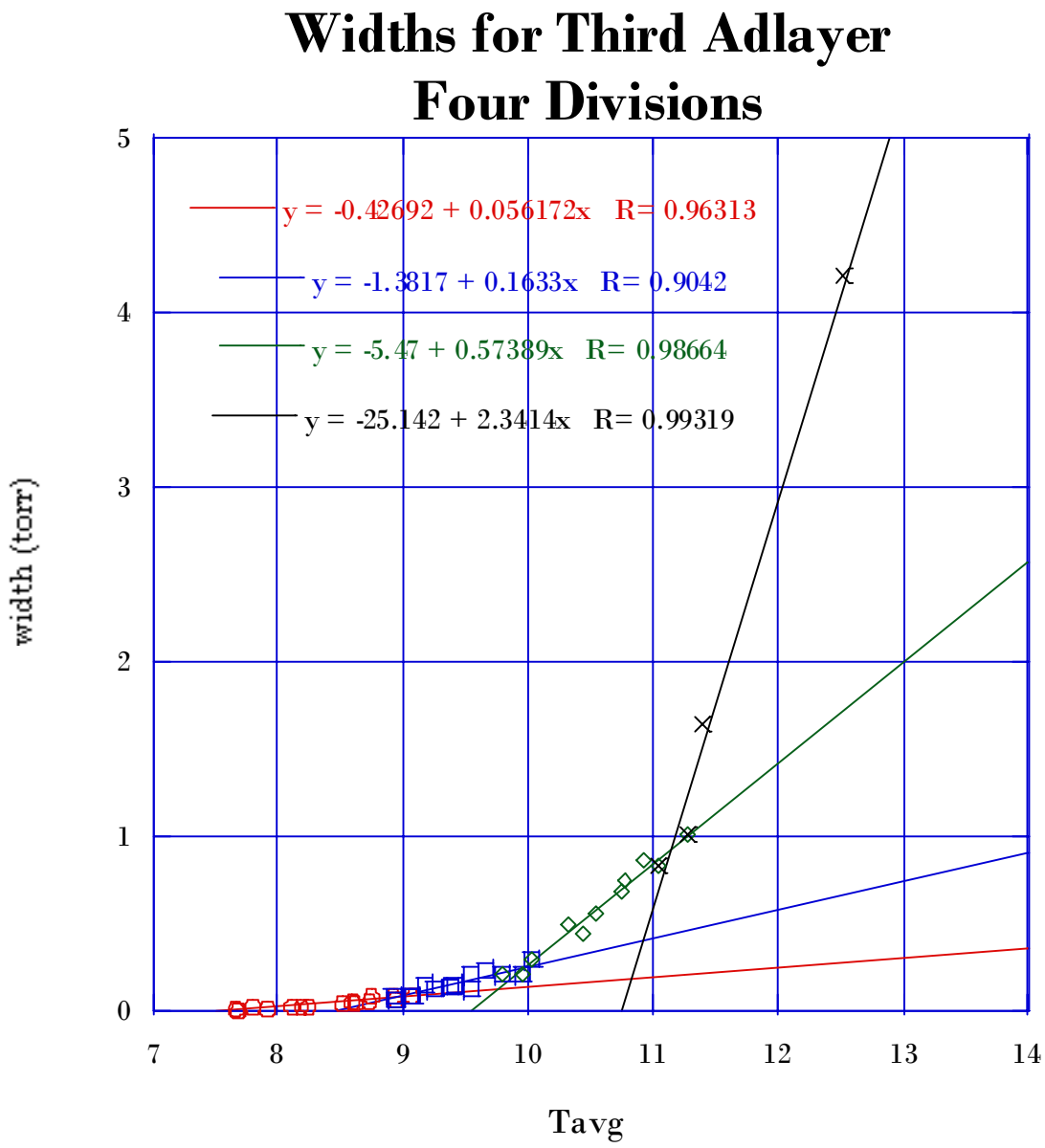


Figure 6.18 - Widths for Critical point Determination, four divisions

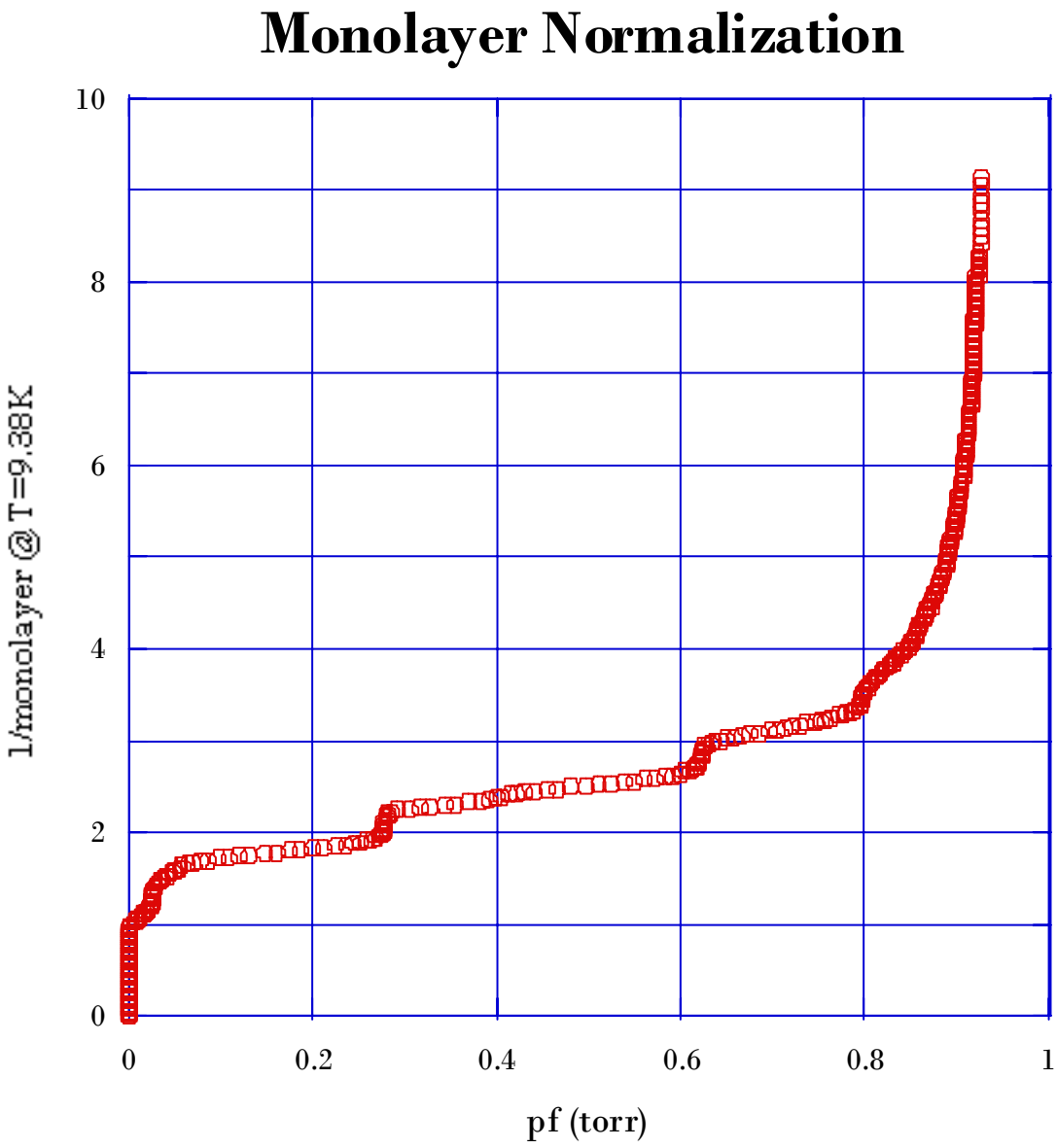


Figure 6.19 – Isotherm normalized by monolayer coverage to determine density of layers

the monolayer density is distinctly above that of bulk hydrogen. It is expected that the density of the layers decreases with increasing distance from the surface as the surface looses control over the adlayer structure.

The density in the layers can be assessed by determining the number of additional moles added to the system for a given layer or feature by subtracting the number of moles at layer completion of the previous step. For this purpose, we will assume that a layer continues to build until the advent of the major vertical riser associated with the starting point of the formation of the following adlayer (the green line marking the start of the major step as shown in Figure 6.16). The average values for the steps are given in Table 6.3. These calculations assume that as in the first layer, the features present between the layers add to the density of the low layer. The overall number of additional moles of the individual layer is taken as the distance between the green lines associated with the initiation of the subsequent adlayers. It can be seen that the density increases as the layer builds. One can see that the density of the adlayers approaches that for the bulk solid, yielding an area per molecule very close to 12.43 $Å^2$/molecule. This is most likely the reason we see such excellent layering behavior in the system.

Table 6.3 – layer density

Layer	mmol ads ($mmol/m^2$)	Additional mmol ads ($mmol/m^2$)	Density of low layer ($molecules/Å^2$)	APM ($Å^2/molecule$)
1end/2start	0.01737367	0.01737367	0.10462425	9.55801381
2	0.02398565	0.00661198	0.03981733	25.114692
2s	0.02552111	0.00814744	0.04906389	20.38159
2f	0.02792635	0.01055268	0.06354825	15.7360747
2end/3start	0.03038938	0.01301571	0.07838062	12.7582565
3	0.03957722	0.00918784	0.05532915	18.0736541
3f	0.04099938	0.01061	0.06389342	15.6510646
3end/4start	0.04352947	0.01314009	0.07912963	12.6374907
4	0.05114336	0.00761389	0.04585082	21.8098604
4s	0.0522274	0.00869793	0.05237892	19.0916494
4f	0.05457749	0.01104802	0.06653118	15.0305468
4end/5start	0.05707239	0.01354292	0.08155546	12.2615951
5	0.06283916	0.00576677	0.03472748	28.7956378
5f	0.06489059	0.0078182	0.04708119	21.2399068
5end/6start	0.0705287	0.01345631	0.0810339	12.3405139

6.6 – The Phase Diagram

The Potential phase diagrams for the system are is shown in Figure 6.20 and 6.21. The critical points are taken from the results of breaking the systems into 3 and 4 sections respectively as shown previously in figures 6.1 and 6.18. The potential critical points are given in table 6.4 and 6.5 respectively. The additional interlayer features seen are a good step into finally unraveling the overall picture of the layering behavior of the H_2 MgO(100) system.

6.7 – Deuterium

As all neutron diffraction work is done using deuterium as opposed to hydrogen, it is important that we examine that system as well. Isotherms were run on a single sample at temperatures ranging from approximately 9.5K to 13.5K. Figure 6.22 shows that interlayer features are once again seen in the isothermal data just as they were in the hydrogen system. Just as in the hydrogen case, the layering transitions were confirmed using the first derivative. As explained earlier, the location of each feature was taken to be the peak in the numerical derivative. For this study focus was limited to the main adsorption steps and the interlayer features 2f – 5f as

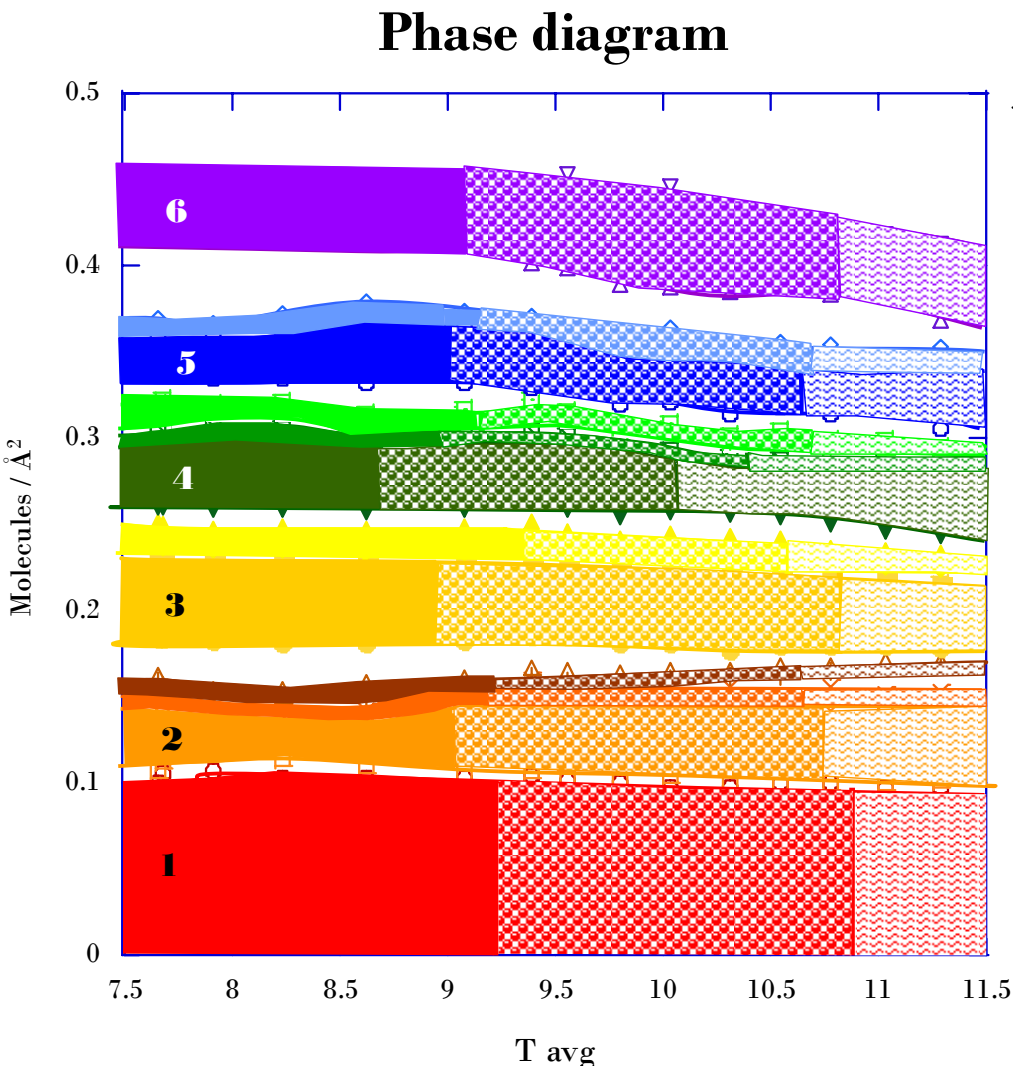


Figure 6.20 – Phase diagram for the H2 – MgO(100) system

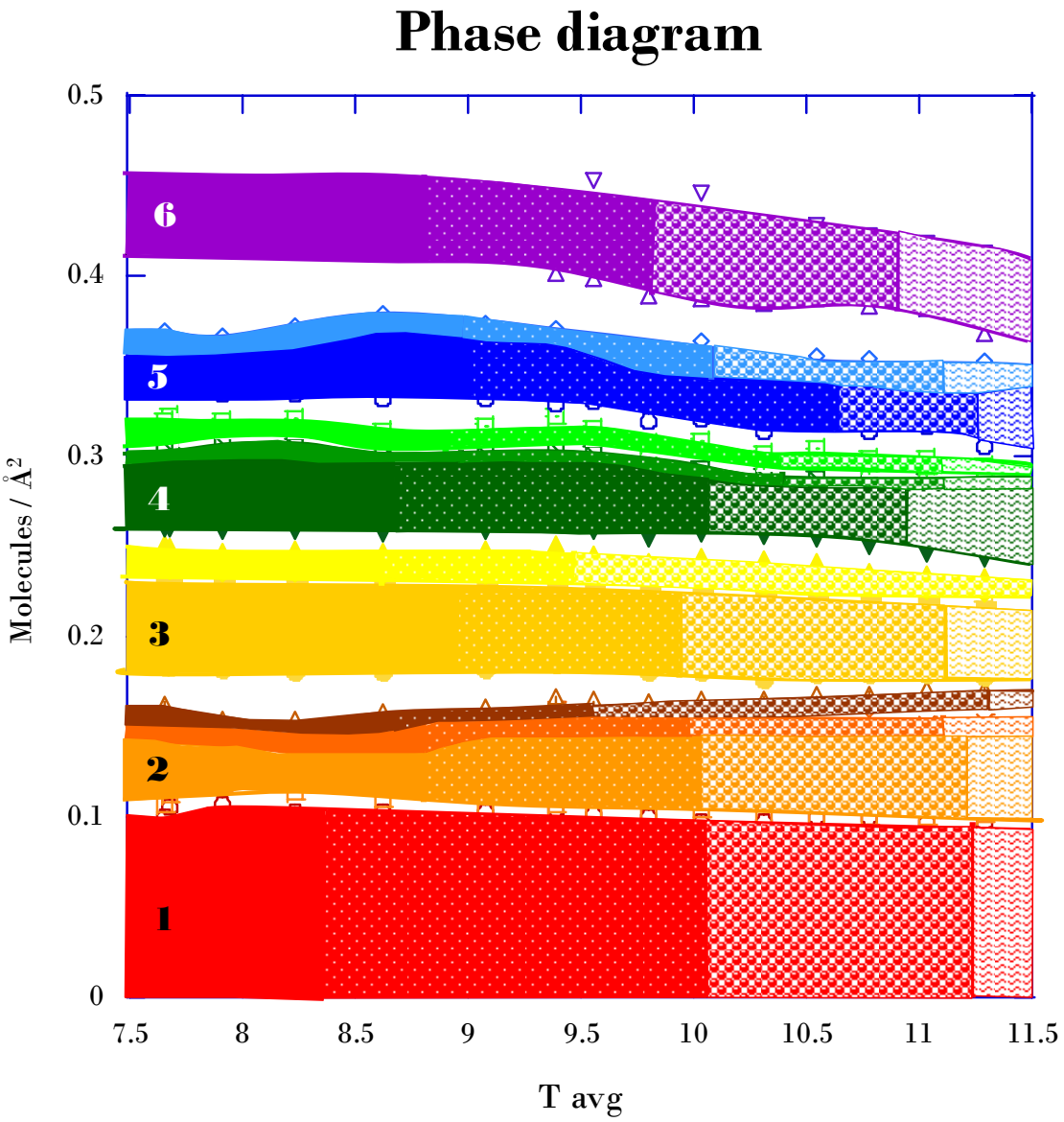


Figure 6.21 – Phase diagram for four divisions

Table 6.4 – Critical Points Indicating Potential Phase Changes

Layer	Tc – a	Tc - b
1	9.21	10.95
2	9.04	10.73
2s	9.31	10.69
2f	9.341	10.657
3	9.17	10.81
3f	9.26	10.61
4	8.52	10.11
4s	8.81	10.42
4f	9.15	10.63
5	8.96	9.34
5f	9.24	10.78
6	9.06	10.72

Table 6.5 – Critical Points Indicating Potential Phase Changes

Layer	Tc – a	Tc - b	Tc – c
1	8.42	10.05	11.33
2	8.85	10.13	12.19
2s	8.82	9.98	11.16
2f	8.64	10.07	11.31
3	8.91	9.96	11.13
3f	8.51	9.48	11.66
4	8.75	10.19	10.85
4s	8.9	10.31	11.11
4f	8.70	10.22	11.27
5	8.94	10.57	11.22
5f	8.91	10.06	11.17
6	8.85	9.79	10.79

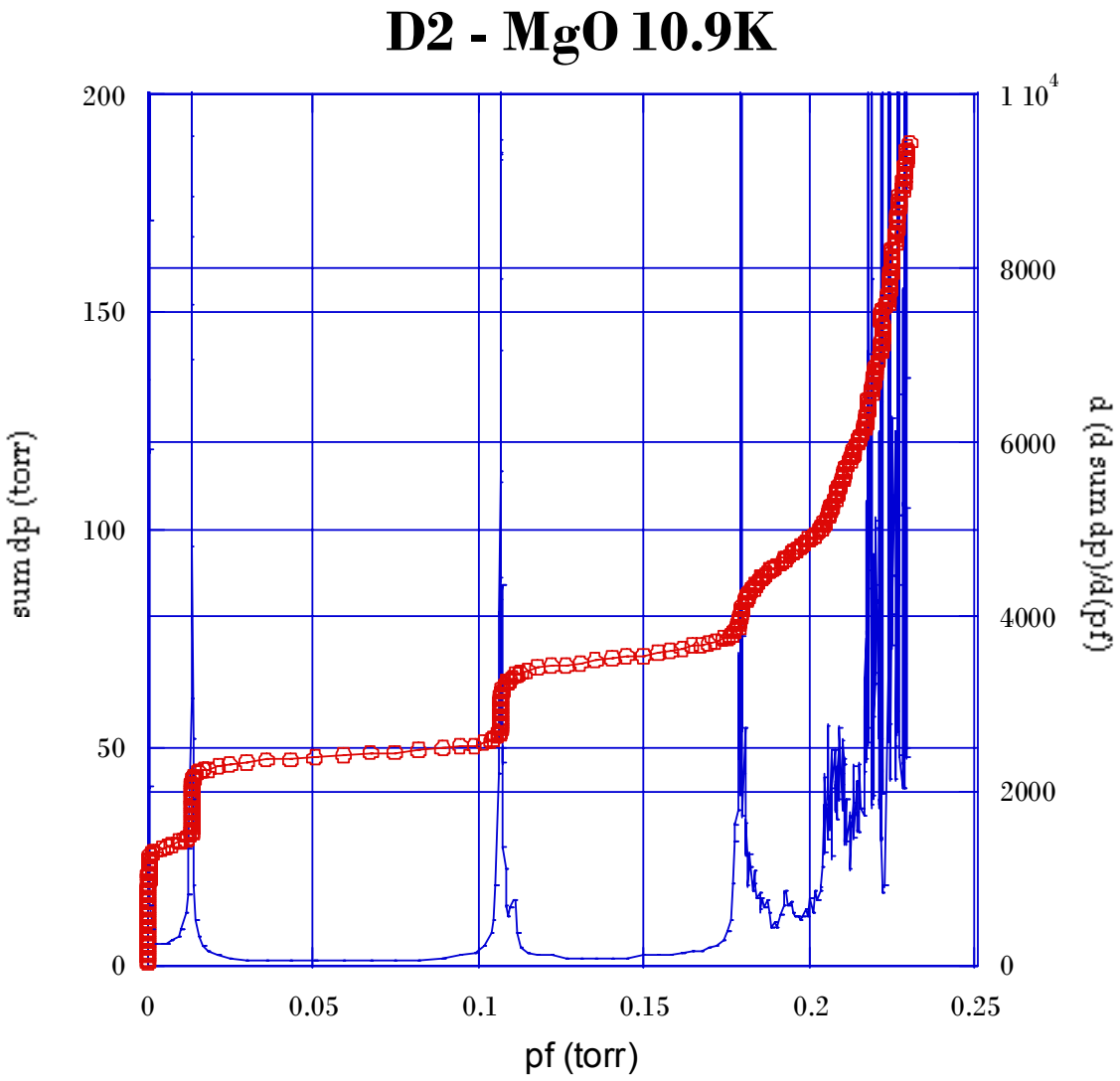


Figure 6.22 – Deuterium isotherm along with the numerical derivative. Confirmation of interlayer features can be clearly seen in the derivative.

described for the hydrogen system. The Clausius-Clapeyron plot is shown in figure 6.23. Table 6.6 gives the linear fits and error for each feature. Table 6.7 gives the resulting values of Q_{ads}, ΔH and ΔS for the system. The overall patterns seen for hydrogen in tables 6.1 and 6.2 seem to be mirrored in the deuterium case as well. However, the overall heat of adsorption for the adlayers seems to be higher for D_2 than for H2. The surface area of the 707Ab sample of MgO was $2.76m^2 \sim 9.2m^2/g$ Deuterium coverage of $4.62x10^{-5}$ moles yields an area per molecule of around 10 $Å^2$. This is again in good agreement with the projected 10.25 $Å^2$ based on the neutron scattering results

6.8 – Future work

The thermodynamic experiments described in the bulk of this dissertation have proven to be extremely challenging. In order to develop a microscopic description of these findings, it is clear that further neutron scattering studies in the multilayer region are necessary. In this way it will be possible to shed some more light on exactly what is happening in the H_2-MgO system in the multilayer regime. Diffraction studies including constant coverage increasing temperature experiments will also elucidate the phase transitions in this very intricate system.

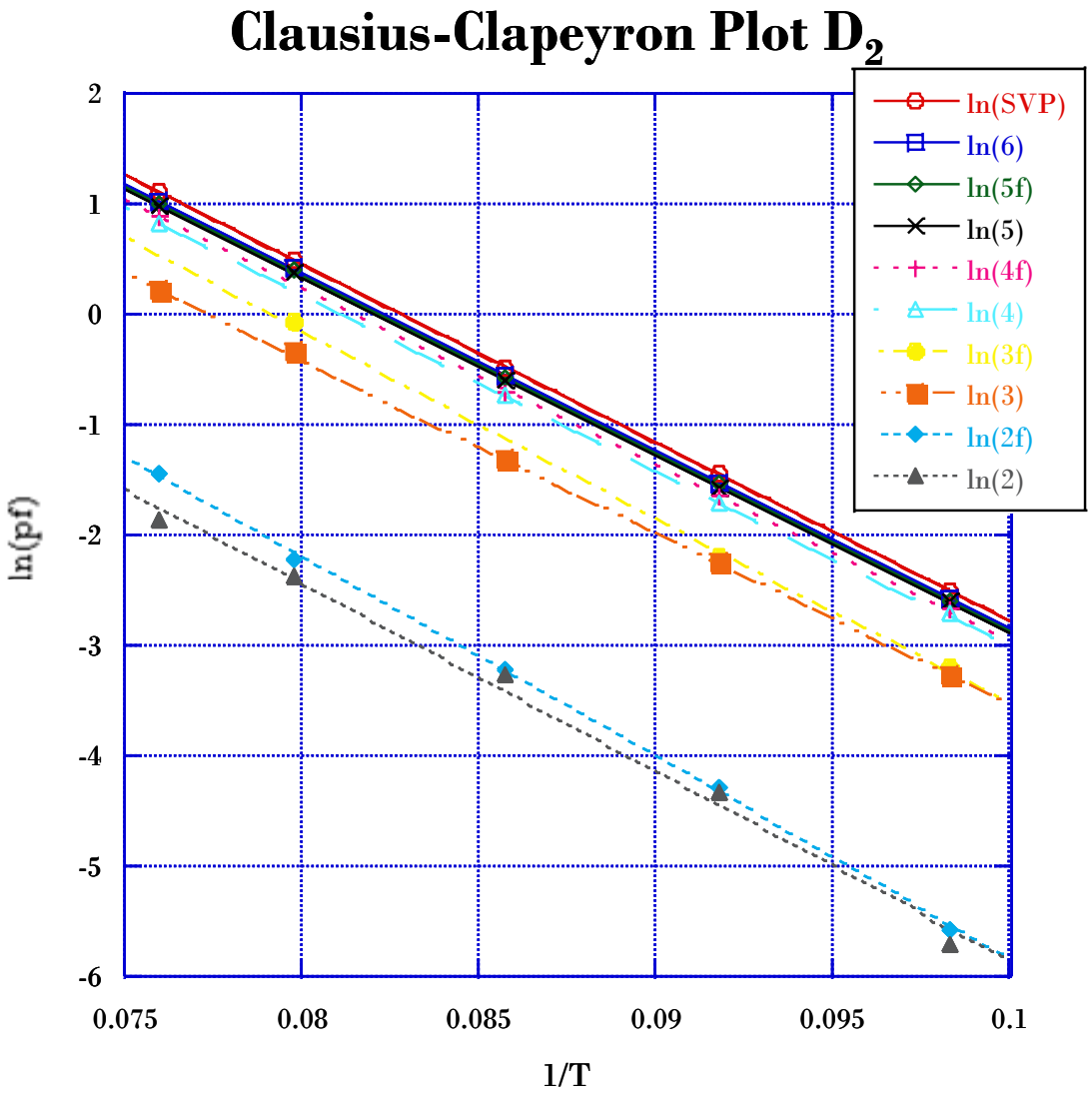


Figure 6.23 – Clausius – Clapeyron plot for Deuterium on MgO (100)

Table 6.6 – Clausius Clapeyron Curve Fits for D_2 on MgO

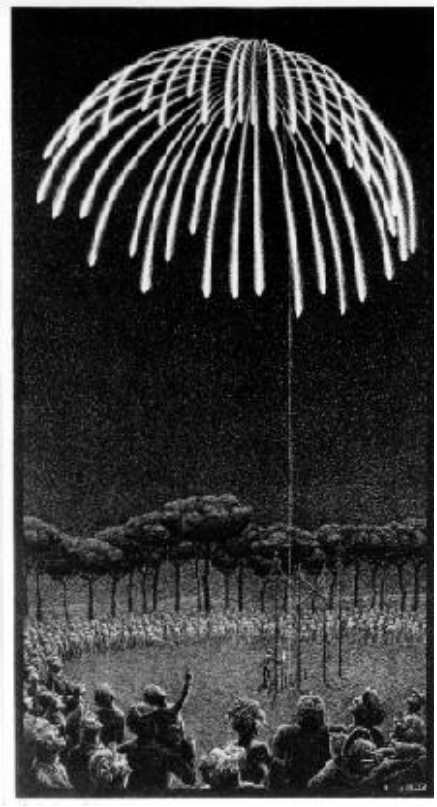
Feature	A (K)	A error (K)	B	B error	R^2
2	170.72	8.5749	11.224	0.74342	0.99624
2f	182.12	2.9528	12.366	0.256	0.99961
3	156.49	0.87771	12.125	0.076095	0.99995
3f	169.04	6.7889	13.388	0.61299	0.99919
4	158.68	1.4889	12.871	0.13154	0.99991
4f	159.7	1.5597	13.016	0.1378	0.9999
5	160.88	0.6635	13.205	0.057523	0.99997
5f	161.03	0.47731	13.24	0.041381	0.99999
6	161.41	0.3465	13.295	161.41	0.99999
svp	161.52	0.21312	13.375	0.018477	1

Table 6.7 – Clausius Clapeyron Results for D_2 on MgO

Feature	Qads (J/mol)	Q_{ads} error (J/mol)	ΔH (J/mol)	ΔH error (J/mol)	ΔS J/molK	ΔS error J/molK
2	1419.424	71.29463	-76.492	71.31665	17.88415	6.182955
2f	1514.208	24.55058	-171.276	24.61445	8.389169	2.134008
3	1301.111	7.297579	41.82117	7.509626	10.39293	0.651064
3f	1405.456	56.44522	-62.5239	56.47303	-0.10809	5.098922
4	1319.319	12.37922	23.61275	12.5054	4.190427	1.104405
4f	1327.8	12.96788	15.13211	13.08838	2.984848	1.15597
5	1337.611	5.516565	5.321183	5.794161	1.413438	0.502333
5f	1338.858	3.968518	4.074031	4.346142	1.122436	0.376795
6	1342.018	2.880919	0.914578	3.382234	0.665147	1342.018
SVP	1342.932	1.771952				

Chapter 7

Conclusions



M. C. Escher: Fireworks (1933)

The adsorption of molecular hydrogen onto MgO (100) surfaces system is incredibly complicated. The adsorption occurs in a layer by layer fashion all the way into the bulk saturated vapor pressure. Based on this growth pattern it is believed that molecular hydrogen appears to completely wet the MgO (100) surface.

There are a minimum of 5 vertical steps visible in the isothermal data corresponding to adlayer formation. Upon further inspection of the first derivative of the isotherms, additional peaks become visible which seem to indicate additional interlayer features. There appear to be interlayer features present between all of the adlayers distinguishable in the derivative. These features are further confirmed by the isosteric heat plots.

The exact nature of these features is unknown. Features which may be associated with the first layer potentially correspond to the compression of the monolayer from a c(2x2) structure existing at low coverage to the hcp structure which seems to exist at monolayer completion. The density of this hcp structure of the monolayer is compressed in relation to the bulk solid hcp structure. This compression is the result of the surface-molecule interactions outweighing the molecule-molecule interactions allowing the surface to direct the adlayer into a formation that deviates by nearly 10% from the bulk. One potential force associated with this large molecule-surface interaction could be associated with an approximation of magnesium hydride.

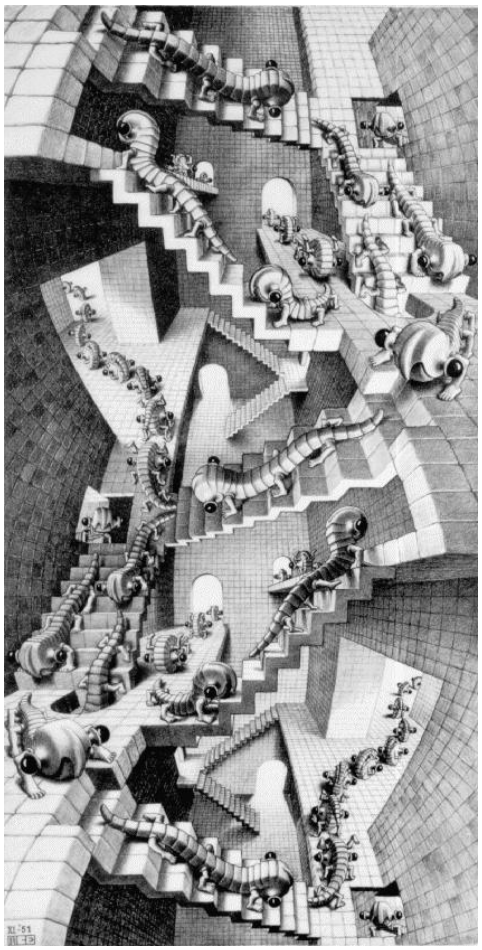
Theoretical work performed by Dr. R.J. Hinde of the University of Tennessee suggest a much higher interaction potential between the Mg^{+2} than the O^{-2} ions in the surface of the MgO substrate. The hydrogen molecules tend to associate themselves with the magnesium ions. The approximation the formation of MgH_2 could account for the strong interaction potential. There is no suggestion that the H_2 dissociates upon adsorption nor is there suggestion of electron transfer.

It is conceivably possible that the features seen in the higher adlayers also correspond to a compression of the adlayer. Beyond the second layer, the molecule-molecule interactions begin to outweigh the surface-molecule interactions due to increased distance from the surface as well as a shielding effect from the first two adlayers. Layers 3 and above tend to have heats of adsorption on the order of that of the bulk saturated vapor pressure. The density of these upper layers more closely approximates that of the bulk solid. This similarity of the structure of that of the bulk allows many layers to form on the surface far beyond the reaches of the surface-molecule interaction. The fact that these layers tend toward a configuration similar to that seen in the bulk enables the complete wetting behavior seen in the isotherms.

A more complete phase diagram for the H_2 – MgO (100) system was developed through this study. The potential critical points were determined by focusing on changes in the linearity of the peak width as a function of temperature. The horizontal boundaries were taken from the initiation and completion points of each

feature. These points are associated with the beginning and the end of the associated peaks in the derivative. Additional neutron scattering investigations need to be performed. Multilayer diffraction is needed to determine the structure of the higher adlayers. In conjunction, a temperature profile needs to be performed to determine the exact location of the phase changes in the system.

Bibliography



M. C. Escher: House of Stairs (1951)

Adamson, A. W. and A. P. Gast (1997). Physical Chemistry of Surfaces. New York, John Wiley & Sons, Inc.

Alberty, R. A. and R. J. Silbey (1955). Physical Chemistry. New York, John Wiley & Sons, Inc.

Ashcroft, N. W. and N. D. Mermin (1976). Solid State Physics. Fort Worth, Saunders College Publishing, Harcourt Brace College Publishers.

Atkins, P. and J. d. Paula (1978). Physical Chemistry. New York, W. H. Freeman and Company**:** 1140.

Bates, S. C. (2002). Compilation of the Engineering Properties of Solid Hydroen. Glastonbury, Thoughtventions Unlimited LLC.

Beysens, D. (1988). Study of Wetting and Adsorption Phenomena at Fluid and Fluid Mixture Interfaces. Les Houches: Liquids at Interfaces. J. Charvolin, J. F. Joanny and J. Zinn-Justin. Amsterdam, Les Houches. **10:** 502-546.

Brickwedde and Scott (1948). Journal of Research of the National Bureau of Standards **41**(5).

Brunauer, S. (1943). The Adsorption of Gases and Vapors. London, Oxford University Press.

Brunauer, S., P. H. Emmett, et al. (1938). "Adsorption of Gases in Multimolecular Layers." J. Am. Chem. Soc. **60**(2): 309-319.

Burns, G. (1985). Solid State Physics. Orlando, Academic Press, Inc. Harcourt Brace Jovanovich.

Coulomb, J. P., K. Madih, et al. (1985). "Evidence of a Square Two-Dimensional Solid of Methane Physisorbed on the (100) Surface of Magnesium Oxide." Phyical Review Letters **54**(14).

Dabrowski, A. (2001). "Adsorption - from theory to practice." Advances in Colloid and Interface Science **93**(1-3): 135-224.

Dash, G. (1977). "Clustering and Percolation Transitions in Helium and Other Thin Films." Physical Review B **15**(6).

Dash, J. G. (1975). Films on Solid Surfaces. New York, Academic Press.

Dash, J. G. (1985). Between Two and Three Dimensions. Physics Today. **December**.

Dash, J. G. and R. D. Pandit (1981). "Phase Transitions in Heterogeneous Films." Physical Review B **24**(1).

Dash, J. G. and J. Ruvalds, Eds. (1980). Phase Transitions in Surface Films. NATO Advanced Study Institutes Series. New York, Plenum Press.

Degenhardt, D., H. J. Lauter, et al. (1987). "Structures of D2 on MgO Powder." Japaneese Journal of Applied Physics Supplement **26**.

Detrich, S. (1988). Wetting Phenomena. Phase Transitions. **1**.

Donohue, M. D. and G. L. Aranovich (1998). "Classification of Gibbs Adsorption Isotherms." Advances in Colloid and Interface Science **76-77**: 137-152.

Drummond, M. L., B. G. Sumpter, et al. (2006). "Density functional investigation of the adsorption of a methane monolayer on an MgO(100) surface." Physical Review B **73**(19).

Emmett, P. H. and S. Brunauer (1937). "The Use of Low Temperature van der Waals Adsorption Isotherms in Determining the Surface Area of Iron Synthetic Ammonia Catalysts." Journal of the American Chemical Society **59**.

Frank, F. and J. v. d. Merwe (1979). "Misfitting Monolayers." Proceedings of the Royal Society of London **198**.

Freitag, A. and J. Z. Larese (2000). "Layer growth of methane on MgO: An adsorption isotherm study." Physical Review B **62**(12): 8360-8365.

Frenkel, J. (1946). Kinetic Theory of Liquids. Oxford, Clarendon.

Halsey, G. (1948). "Physical Adsorption on Non Uniform Surfaces." Journal of Chemicl Physics **16**.

Hill, T. L. (1949). "Physical Adsorption and the Free Volume Model for Liquids." Journal of Chemical Physics **17**: 590.

Kittel, C. (1996). Introduction to Solid State Physics. New York, John Wiley & Sons, Inc.

Koehler, C. F. and J. Z. Larese (2000). "Cryostat insert with gas loading capabilities for use in neutron diffraction studies." Review of Scientific Instruments **71**(1): 324-325.

Kunnmann, W. and J. Z. Larese (2001). Method for the generation of variable density metal vapors which bypasses the liquidus phase. U. States. **6,179,897**.

Langmuir, I. (1918). "THE ADSORPTION OF GASES ON PLANE SURFACES OF GLASS, MICA AND PLATINUM." J. Am. Chem. Soc. **40**(9): 1361-1403.

Larese, J. Z. (1998). "Neutron scattering studies of the structure and dynamics of methane absorbed on MgO(100) surfaces." Physica B **248**: 297-303.

Larese, J. Z., L. Frazier, et al. (2006). "Direct observation of molecular hydrogen binding to magnesium oxide (100) surfaces." Physica B-Condensed Matter **385**: 144-146.

Larher, Y. (1992). Physics and Chemistry of Materials with Low-Dimensional Structures **16**: 261.

Lennard-Jones, J. E. (1931). "Cohesion." The Proceedings of the Physical Society **43**.

Ma, J. (1989). A Thermodynamic Study of Molecular Hydrogen Adsorbed on Magnesium Oxide. Physics. Seattle, University of Washington. **Ph. D.:** 117.

Ma, J., D. L. Kingsbury, et al. (1988). "Multilayer Adsorption of H2 on MgO Substrates." Physical Review Letters **61**(20).

McQuarrie, D. A. and J. D. Simon (1997). Physical Chemistry: A Molecular Approach. Sausalito, California, University Science Books.

Merriam-Webster. "Dictionary." from www.merriam-webster.com.

Mihaly, L. and M. C. Martin (1996). Solid State Physics: Problems and Solutions. New York, John Wiley & Sons, Inc.

MSDS. "MSDS information for Matheson Gasses." from www.mathesontrigas.com.

Mursic, Z., M. Y. M. Lee, et al. (1996). "Computer-controlled apparatus for performing high-resolution adsorption isotherms." Review of Scientific Instruments **67**(5): 1886-1890.

NIST. "NIST Chemistry Webbook." from http://webbook.nist.gov/chemistry/.

Nix, F. C. and D. MacNair (1941). "The Thermal Expansion of Pure Metals: Copper, Gold, Aluminum, Nickel, and Copper." Physical Review **60**.

Novakovic, M., N. Ninic, et al. (1967). "A Derivation of the Clausius-Clapeyron Equation." Journal of Engineering Physics **13**(1).

Omar, M. A. (1975). Elementary Solid State Physics: Principles and Applications. Reading, Massachusetts, Addison-Wesley Publishing Company.

Phillips, J. M. and J. Z. Larese (1997). "Microscopic structure and transitions in xenon multilayer films." Physical Review B **56**(24): 15938-15946.

Rosenberg, H. M. (1975). The Solid State. Oxford, Oxford University Press.

Samorjai, G. A. (1994). Introduction to Surface Chemistry and Catalysis. New York, John Wiley & Sons.

Schick, M. (1990). Introduction to Wetting Phenomena. Les Houches: Liquids At Interfaces. J. Charvolin, J. F. Joanny and J. Zinn-Justin. Amsterdam, Les Houches. **9:** 419-496.

Silvera, I. F. (1980). "The Solid Molecular Hydrogens in the Condensed Phase: Fundamentals and Static Properties." Reviews of Modern Physics **52**(2).

Skofronick, J. G., J. P. Toennies, et al. (2003). "Helium Atom Scattering Studies of he Structure and Vibrations of H2 Physisorbed on MgO(100) Single Crystals." Physical Review B **67**.

Souers, P. C., C. K. Briggs, et al. (1977). Hydrogen Vapor Pressures from 4 to 30K: A Review, Lawrence Livermore Laboratory, University of California, Livermore.

Steele, W. A. (1974). The Interaction of Solids with Solid Surfaces. The International Encyclopedia of Physical Chemistry and Chemical Physics. New York, Pergamon. **3**.

Steele, W. A. (1996). "Monolayers of Linear Molecules Adsorbed on the Graphite Basal Plane: Structures and Intermolecular Interactions." Langmuir **12**.

Stranski, I. and L. Krastanow (1937). "Zur Theorie der orientierten ausscheidung von ionenkristallen aufeinander." Monatshefte fuer Chemie/ Chemical Monthly **71**(1).

Takaishi, T. and Y. Sensui (1963). "Thermal Transpiration Effect of Hydrogen, Rare Gases, and Methane." Transactions of the Faraday Society **59**.

Thomy, A. and X. Duval (1994). "Stepwise Isotherms and Phase Transitions in Physisorbed Films." Surface Science **299**: 415.

Thomy, A., X. Duval, et al. (1981). "Two-Dimensional Phase Transitions as Displayed by Adsorption Isotherms on Graphite and Other Lamellar Solids." Surface Science Reports **1**.

Toennies, J. P. and F. Traeger (2007). "The Structures and Vibrations of H2 monolayers on NaCl, MgO and LiF: Similarities and Differences." Journal of Physics: Condensed Matter **19**.

USDOE. (2003). "Basic Research Needs for the Hydrogen Economy: Report of the Basic Energy Sciences Workshop on Hydrogen Production, Storage, and Use." from www.er.doe.gov/bes/reports/files/files/NHE_rpt.pdf.

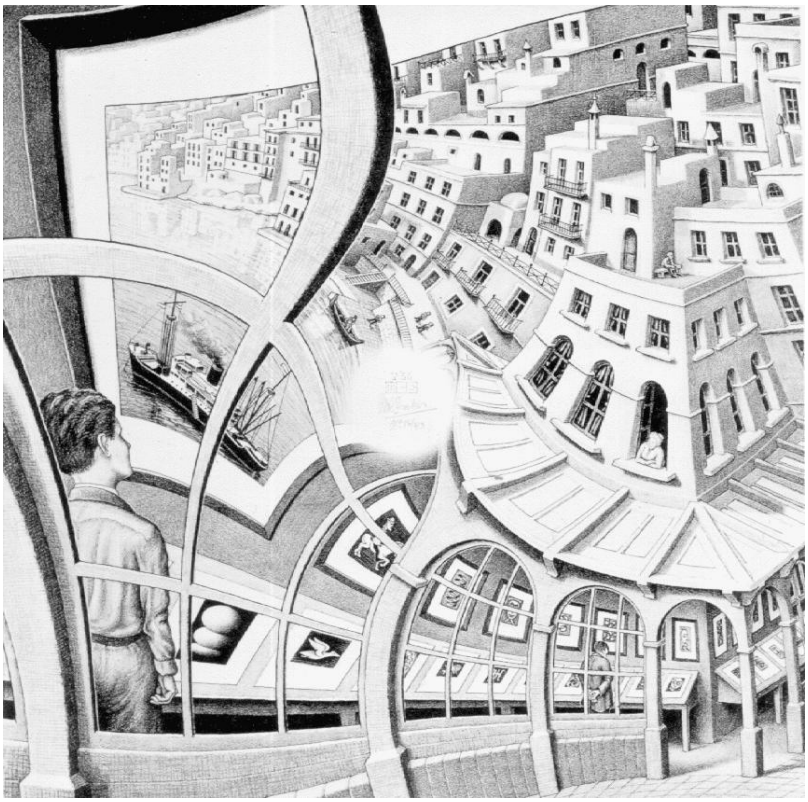
USDOE. (2006). "Hydrogen Contractors Meeting." from www.er.doe.gov/bes/dms/Publications/Contractor_Meetings/Hydrogen_BES-2006.pdf.

Volmer, M. and Z. Webber (1926). "Nucleus Formation in Supersaturated Systems." Zeitschrift fur Physik Chemie **119**.

Zumdahl, S. S. (1986). Chemistry. Lexington, Massachusetts, D.C. Heath and Company.

Appendix A

Supplemental Material



M. C. Escher: Print Gallery (1956)

Table 7.1 – Sample surface areas and figure numbers

Sample	Surface Area (m^2)	CH4 isotherm Figure	Monolayer Figure
606Ia	3.999	5.1	5.2
606Ib	3.8352	A.1	A.2
606Ic	2.6898	A.3	A.4
606Ie	2.3985	A.5	A.6
606If	3.5565	A.7	A.8
606Cb	2.7508	A.9	A.10
707A	3.1719	A.11	A.12
1107A	3.3726	A.13	A.14

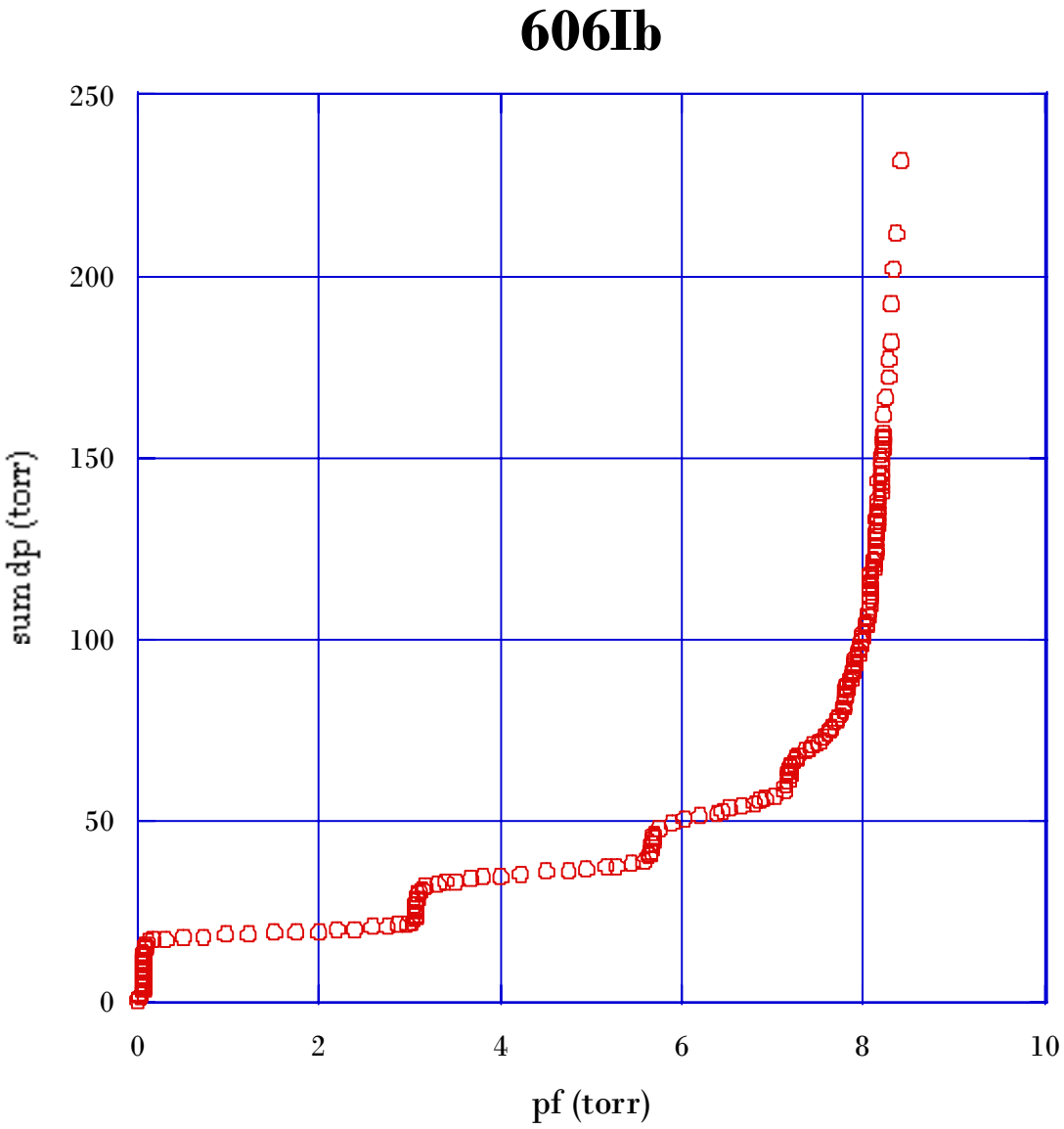


Figure A.1 – Methane isotherm sample 606Ib

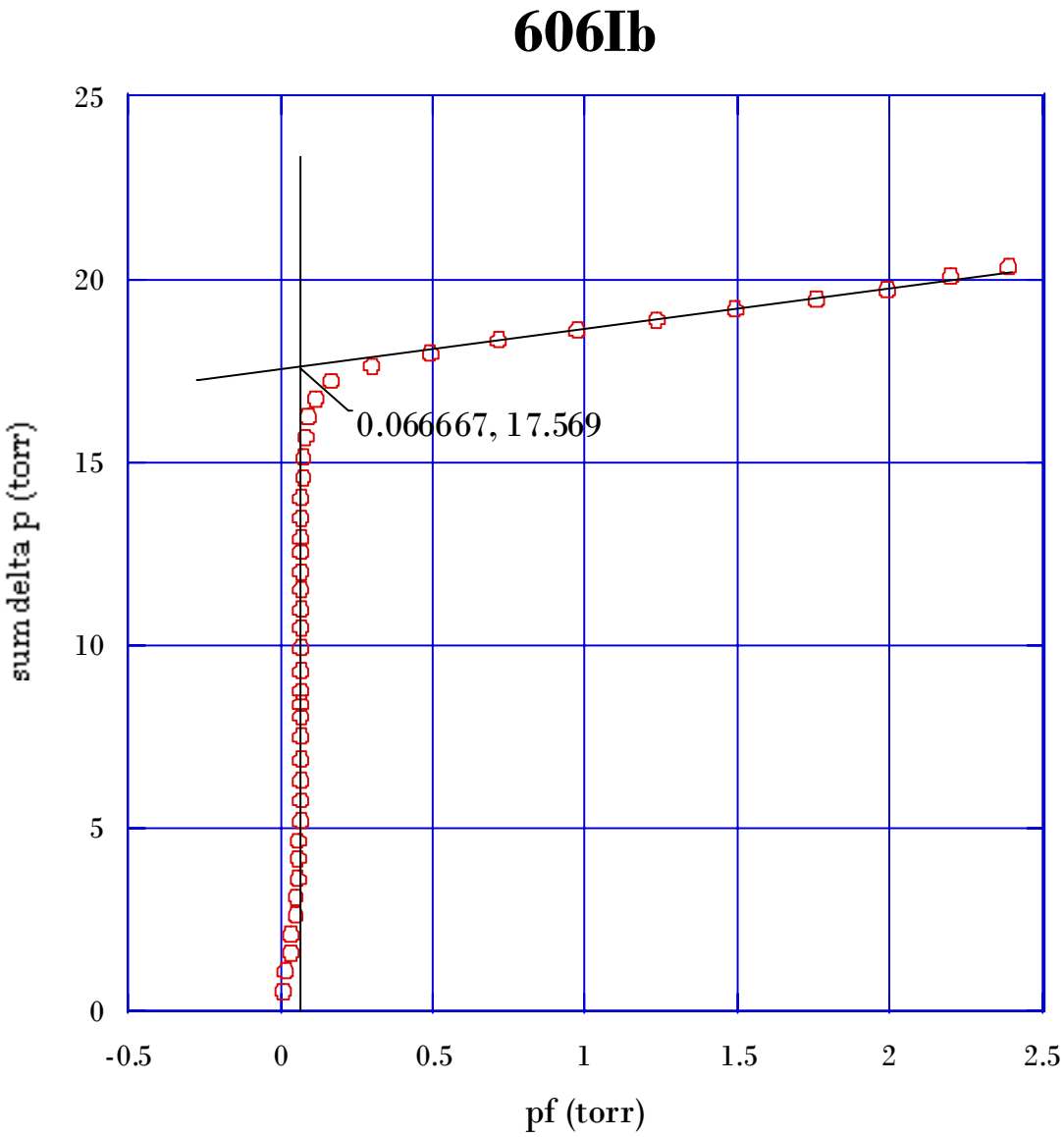


Figure 7.2 – monolayer 606Ib

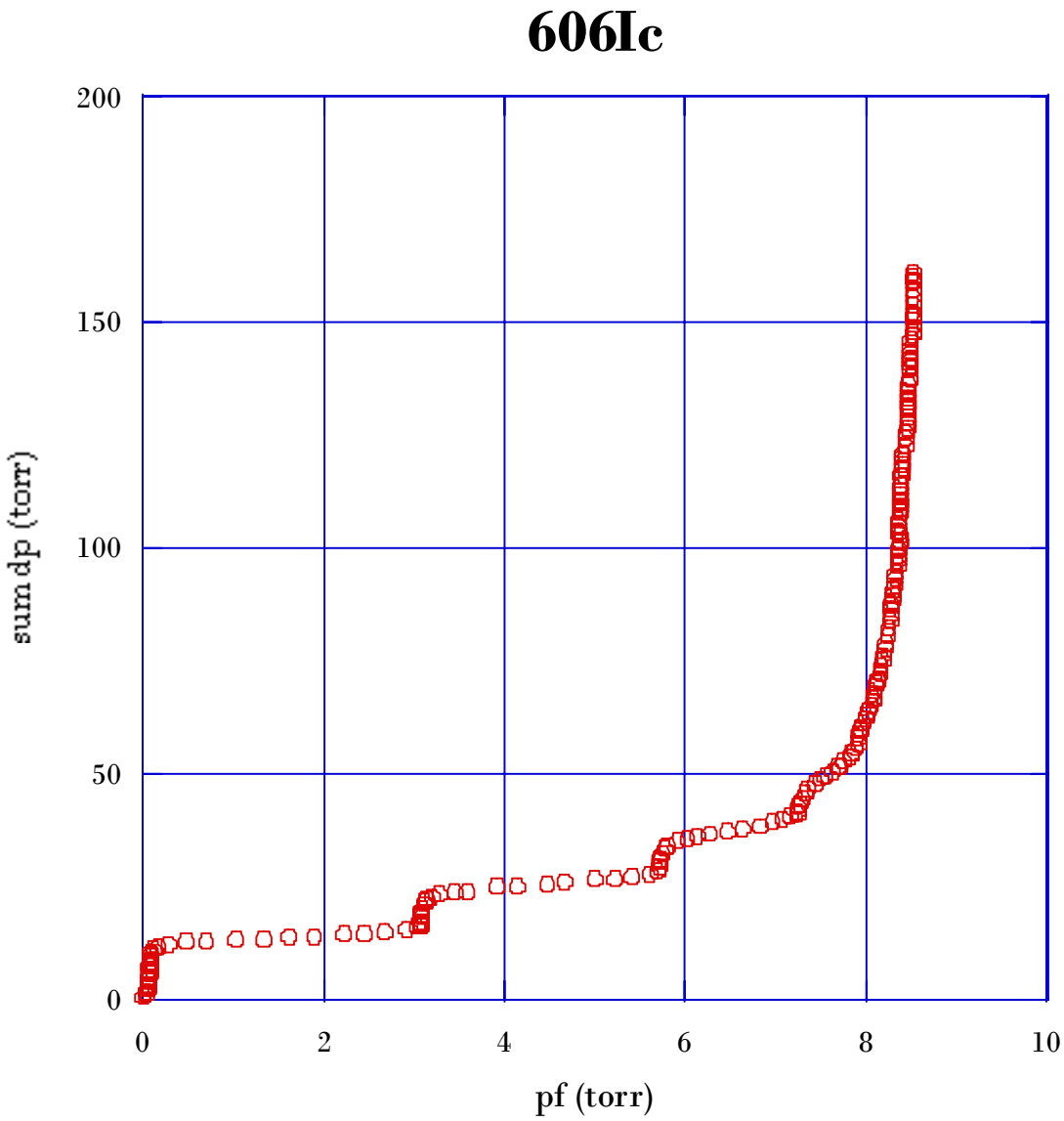


Figure A.3 – Methane Isotherm Sample 606Ic

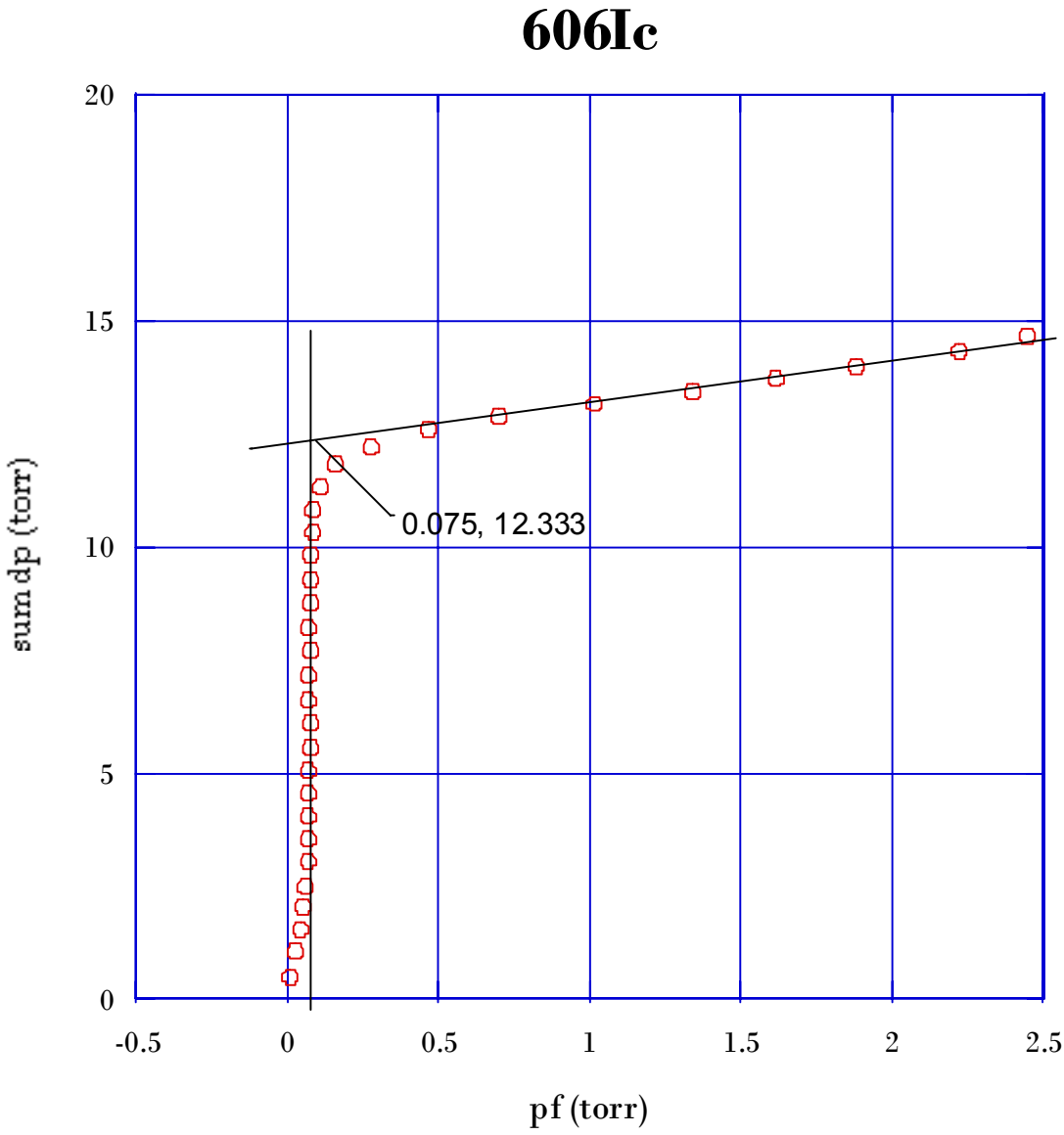


Figure A.4 –monolayer 606Ic

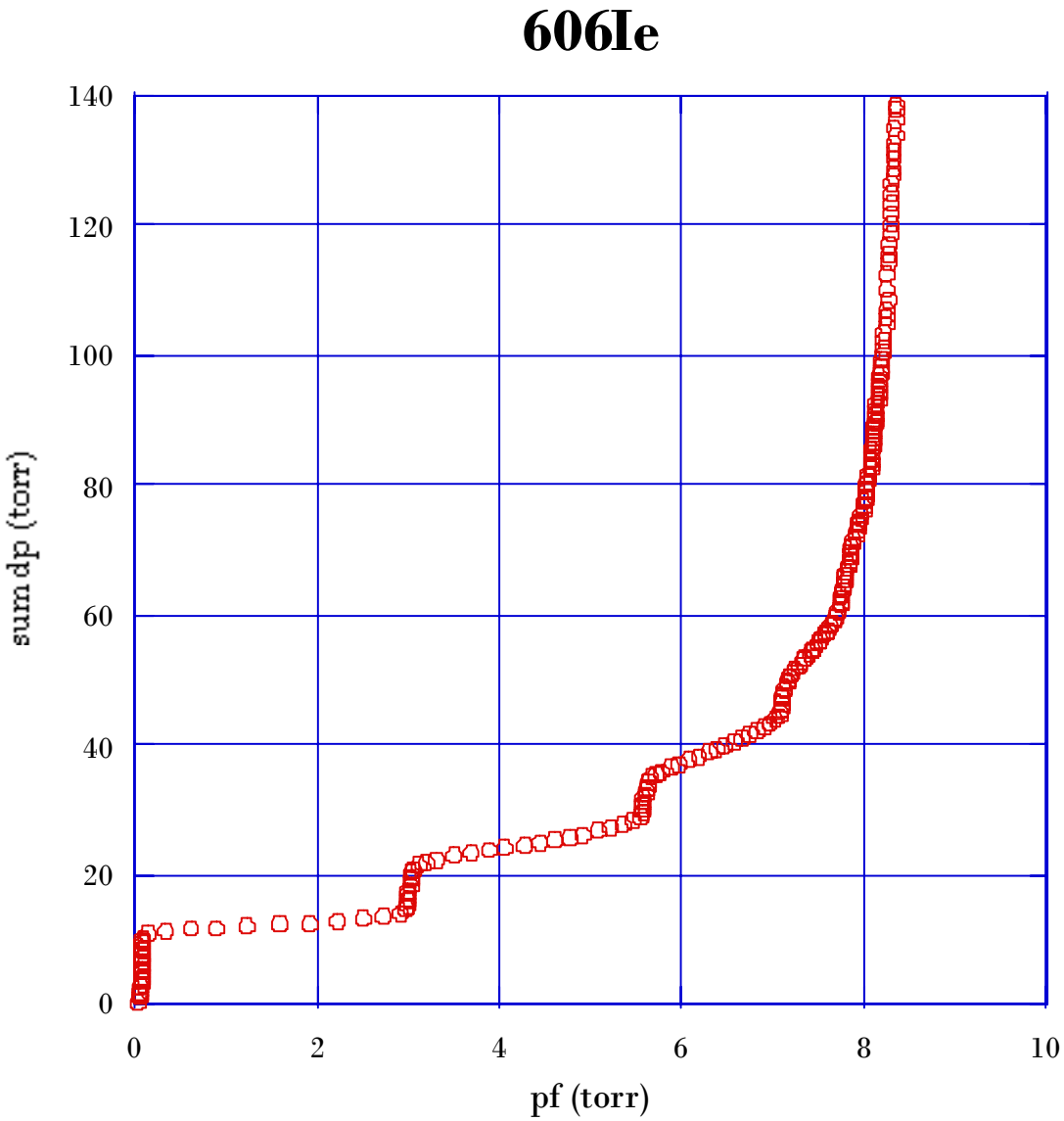


Figure 7.5 – Methane Isotherm Sample 606Ie

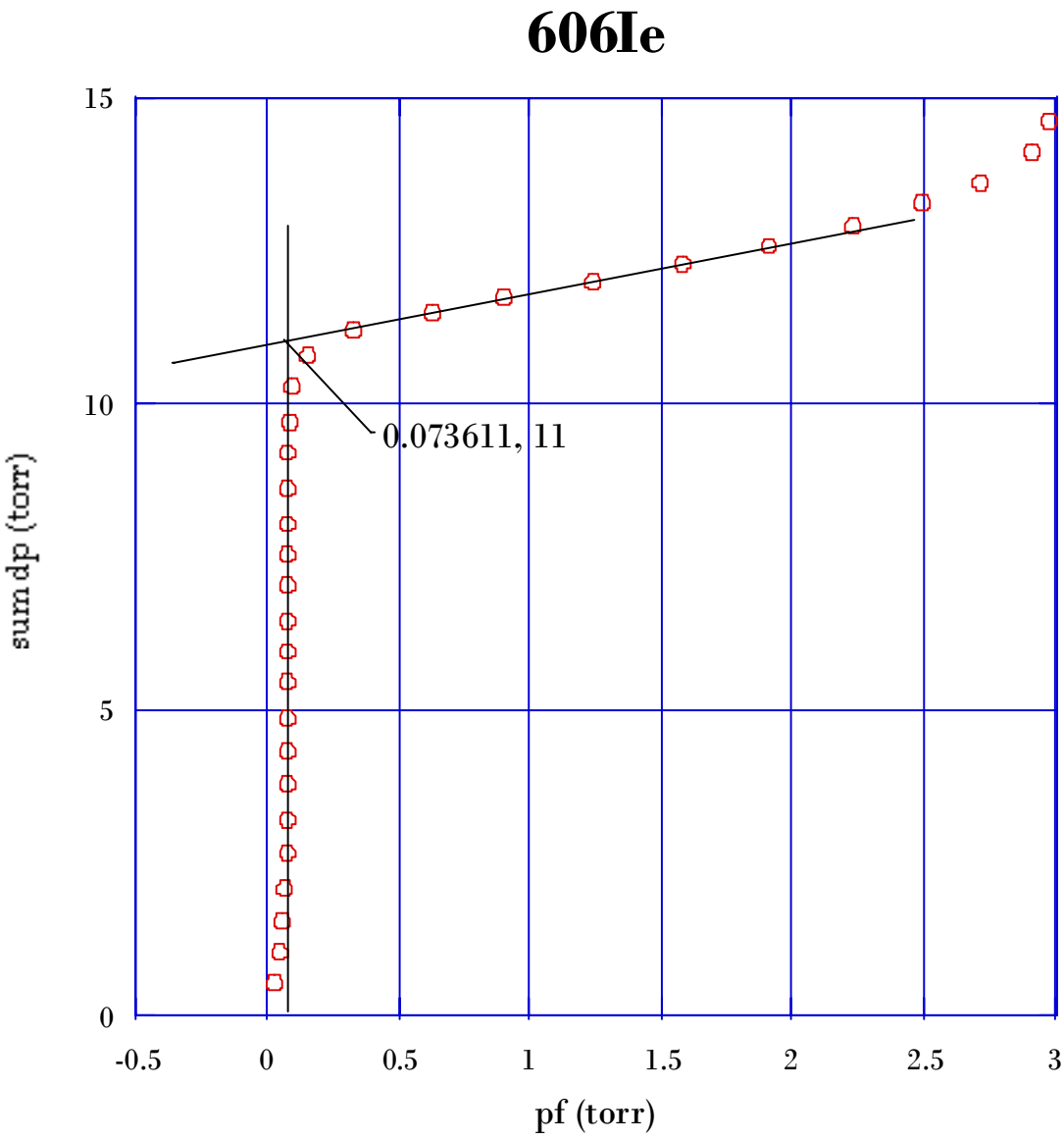


Figure 7.6 – monolayer 606Ie

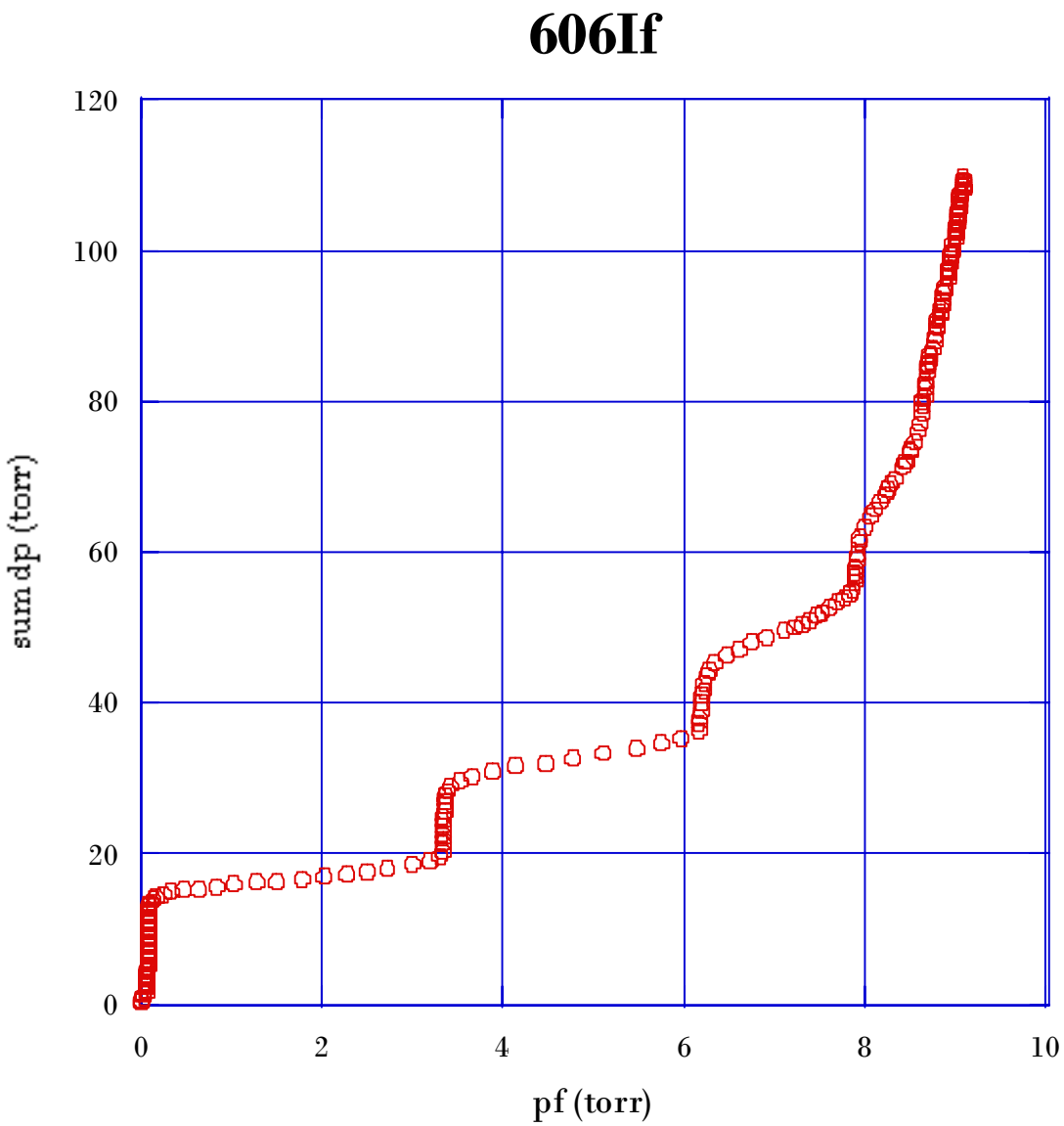


Figure 7.7 – Methane Isotherm Sample 606If

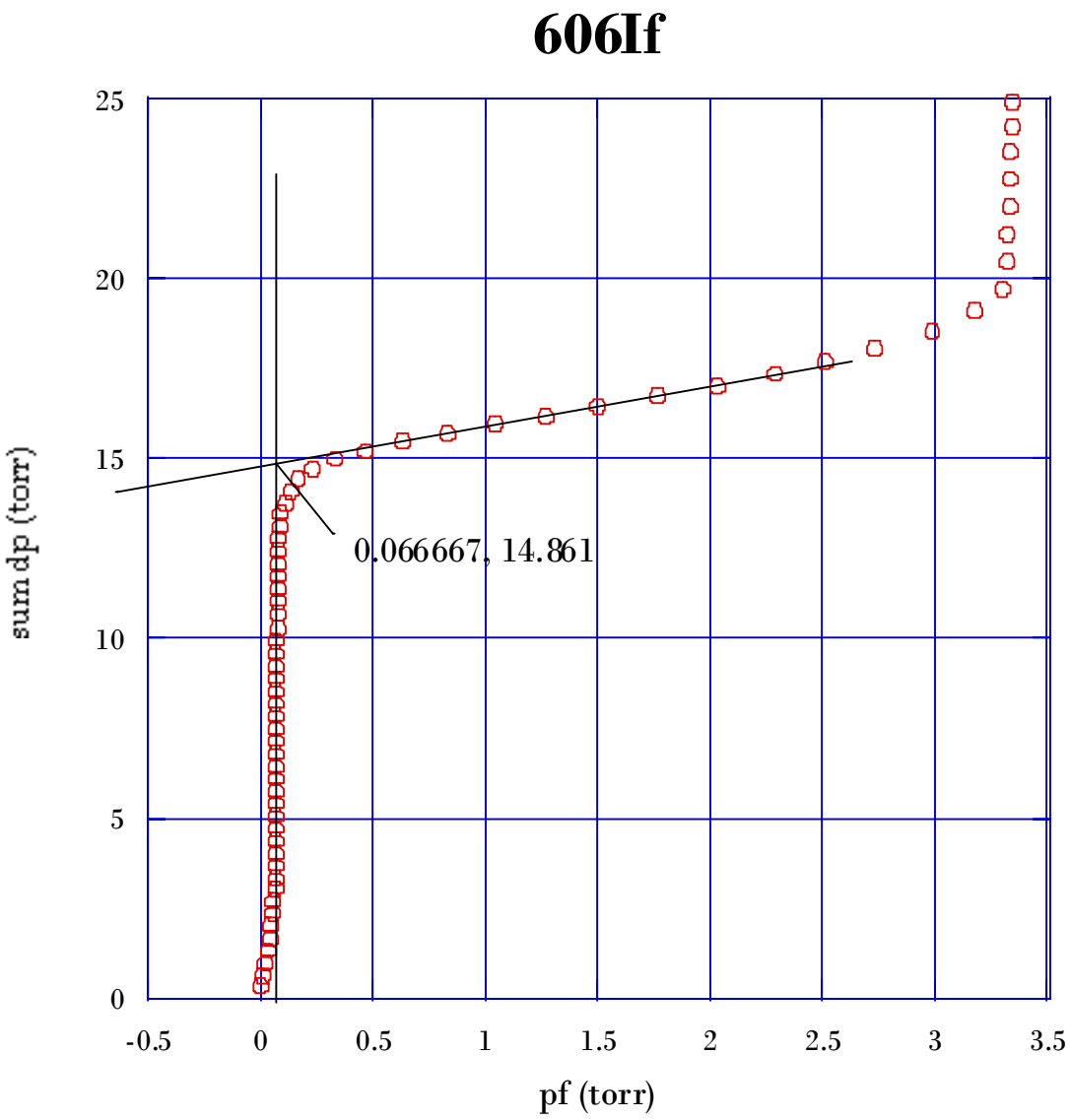


Figure 7.8 – monolayer 606If

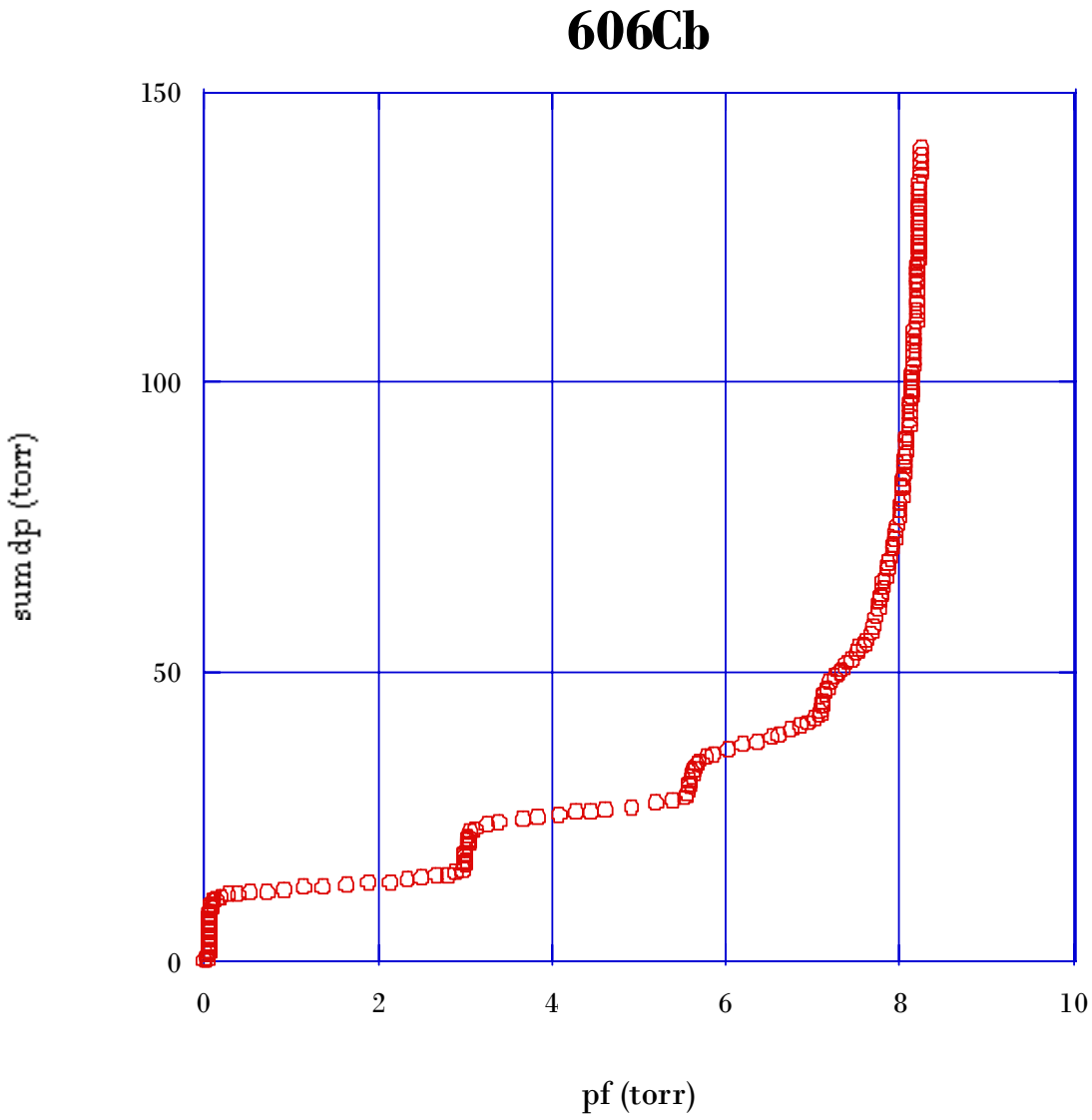


Figure A.9 – Methane Isotherm Sample 606Cb

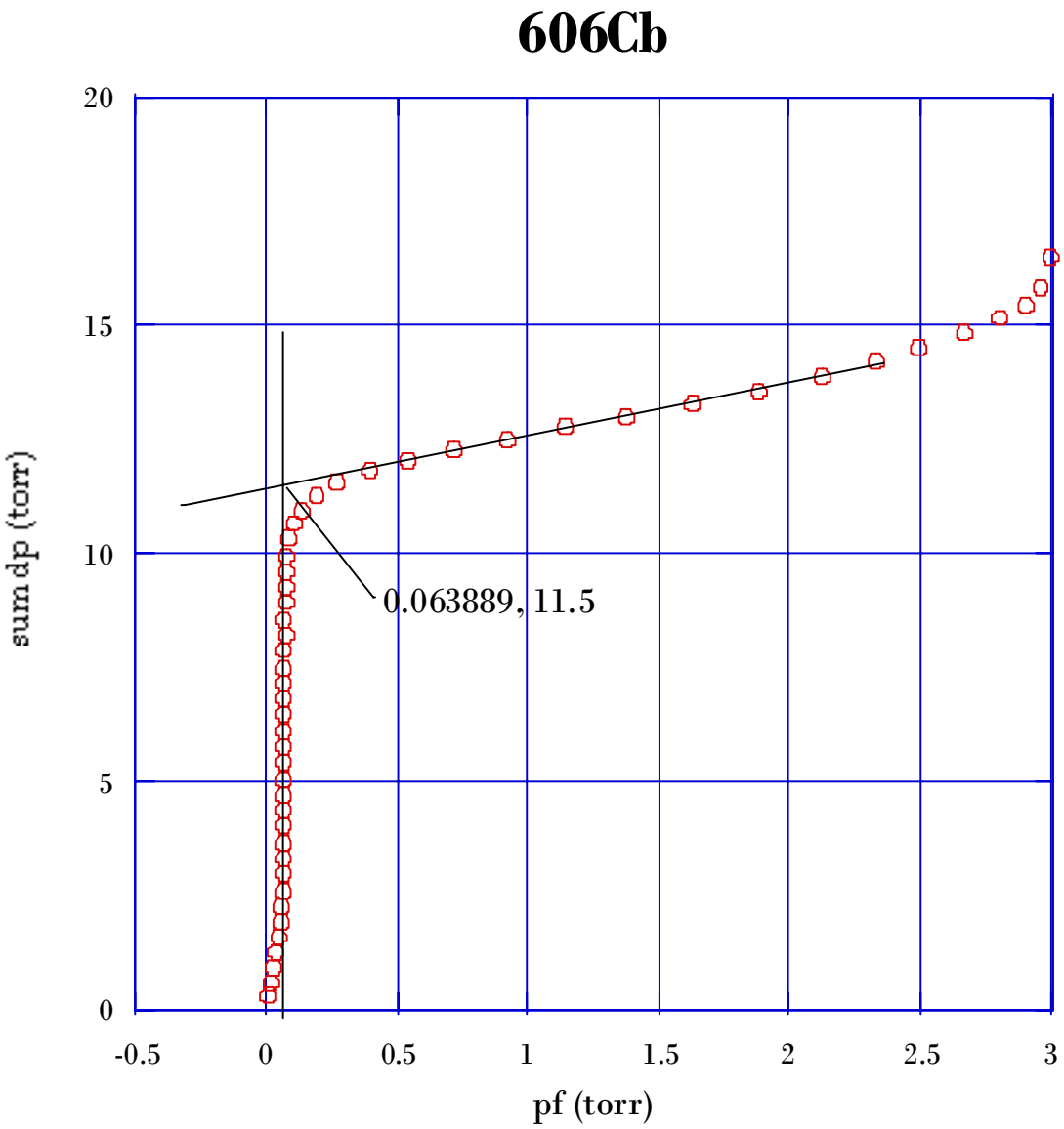


Figure 7.10 – Monolayer 606Cb

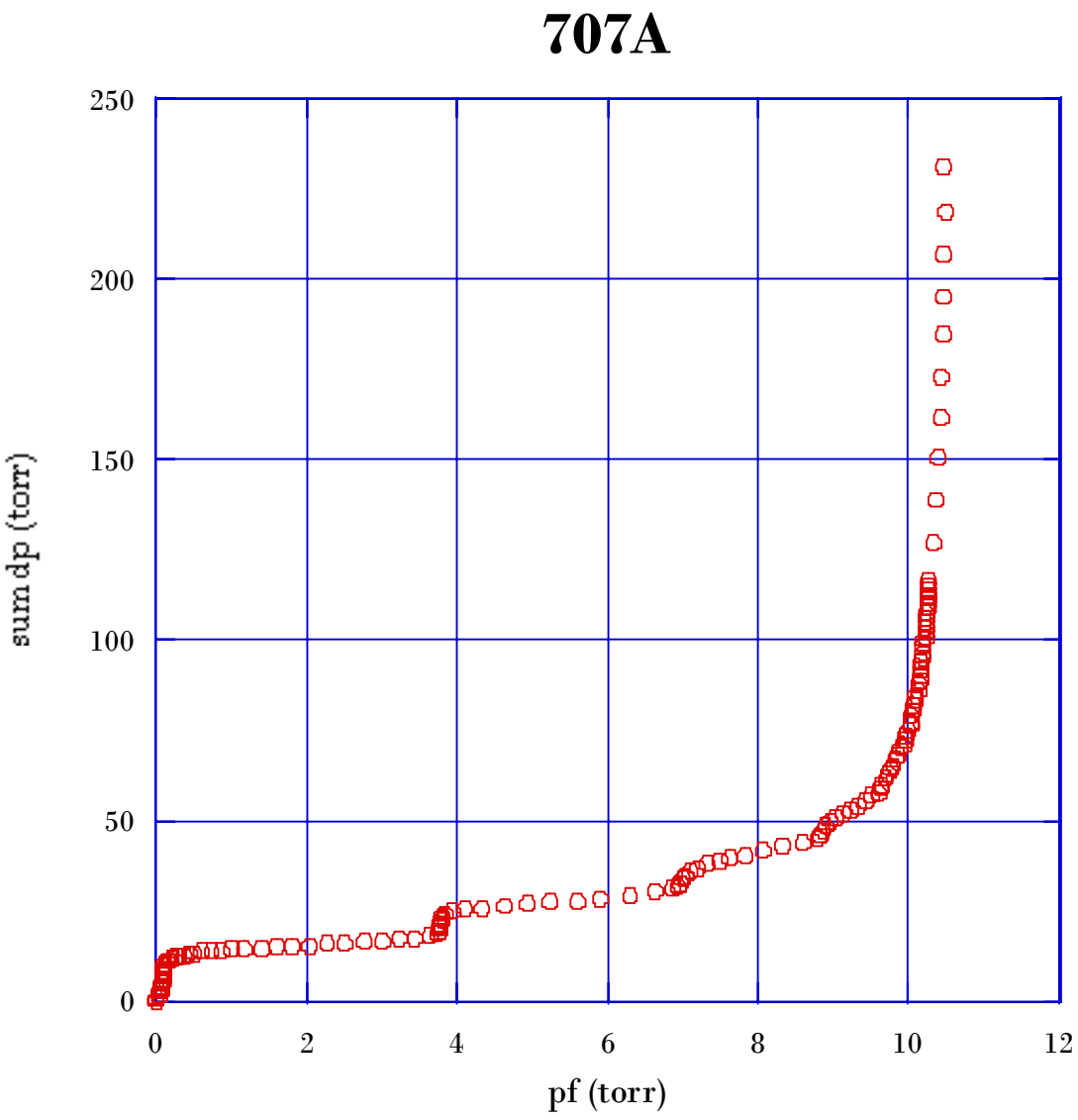


Figure A.11 – Methane Isotherm Sample 707A

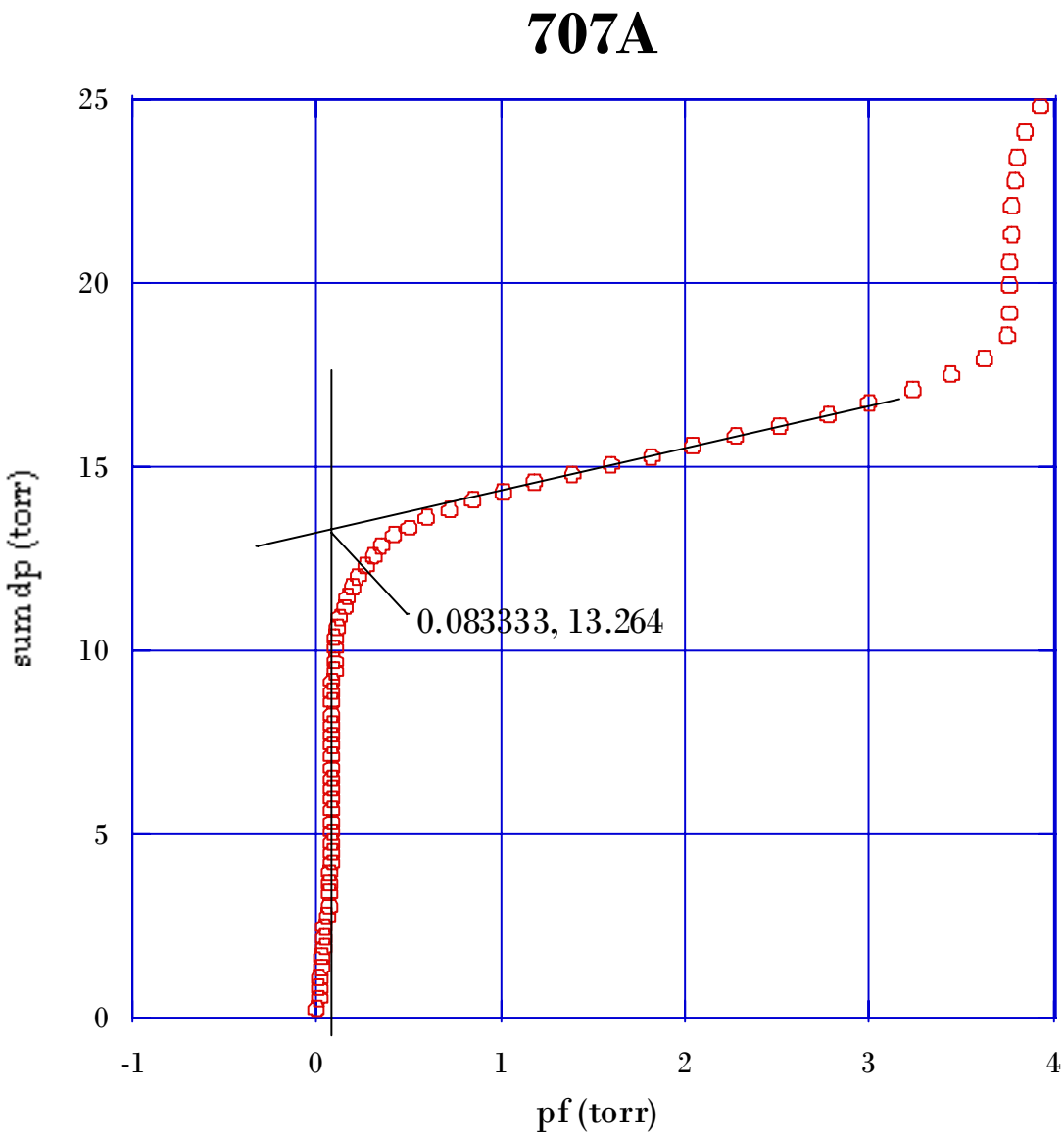


Figure 7.12 – monolayer 707A

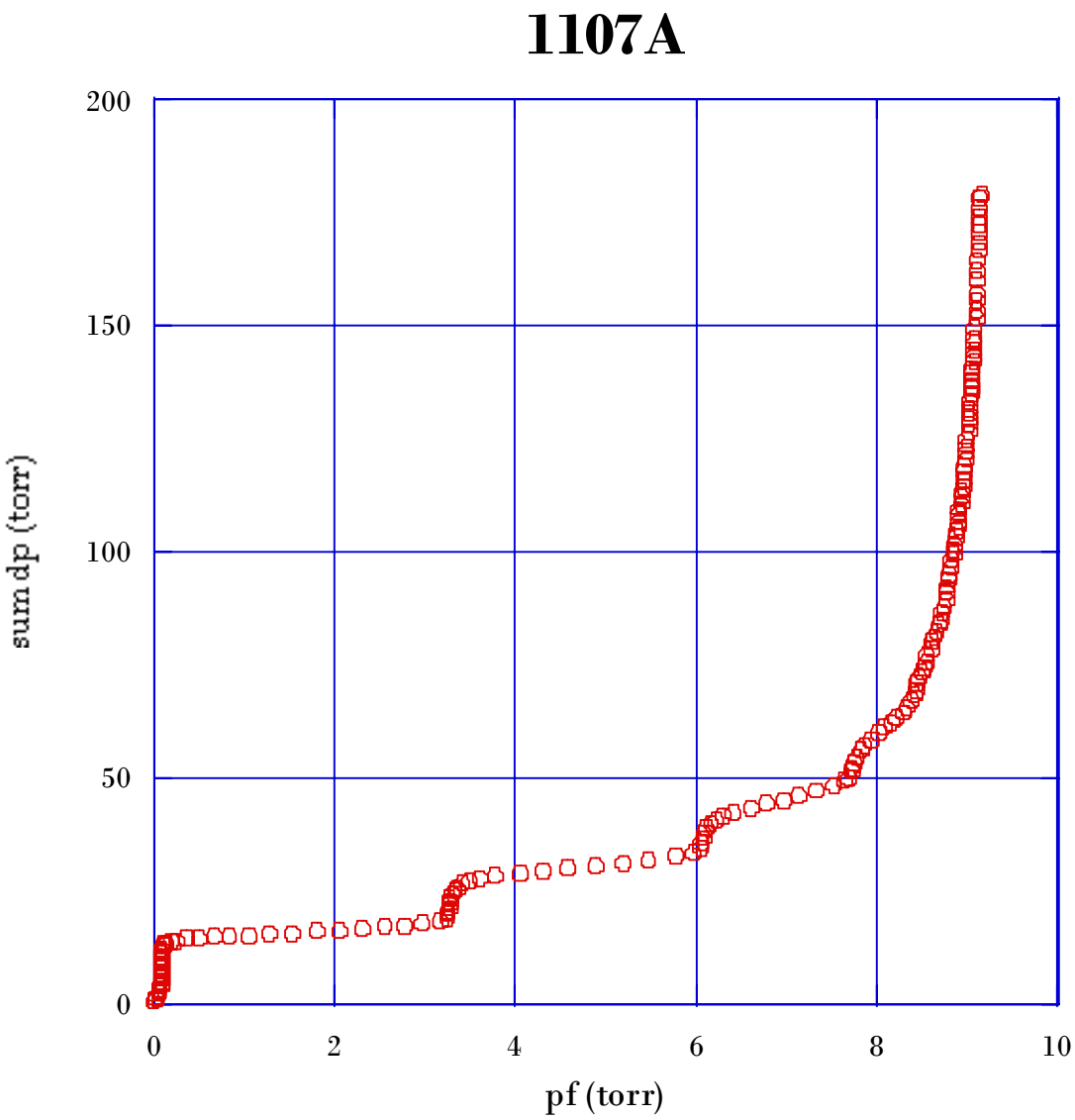


Figure 7.13 – Methane Isotherm Sample 1107A

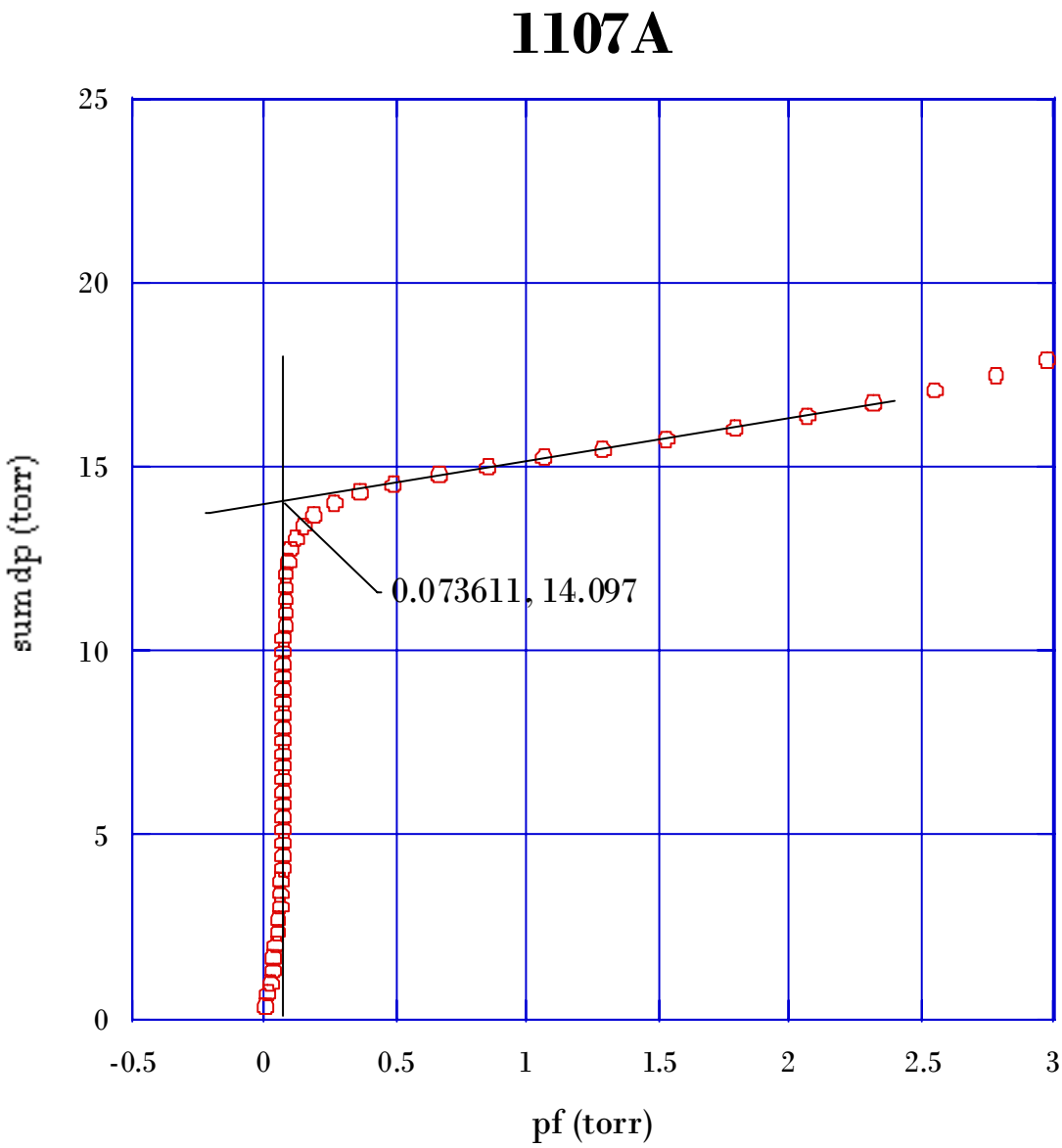


Figure 7.14 – monolayer 1107A

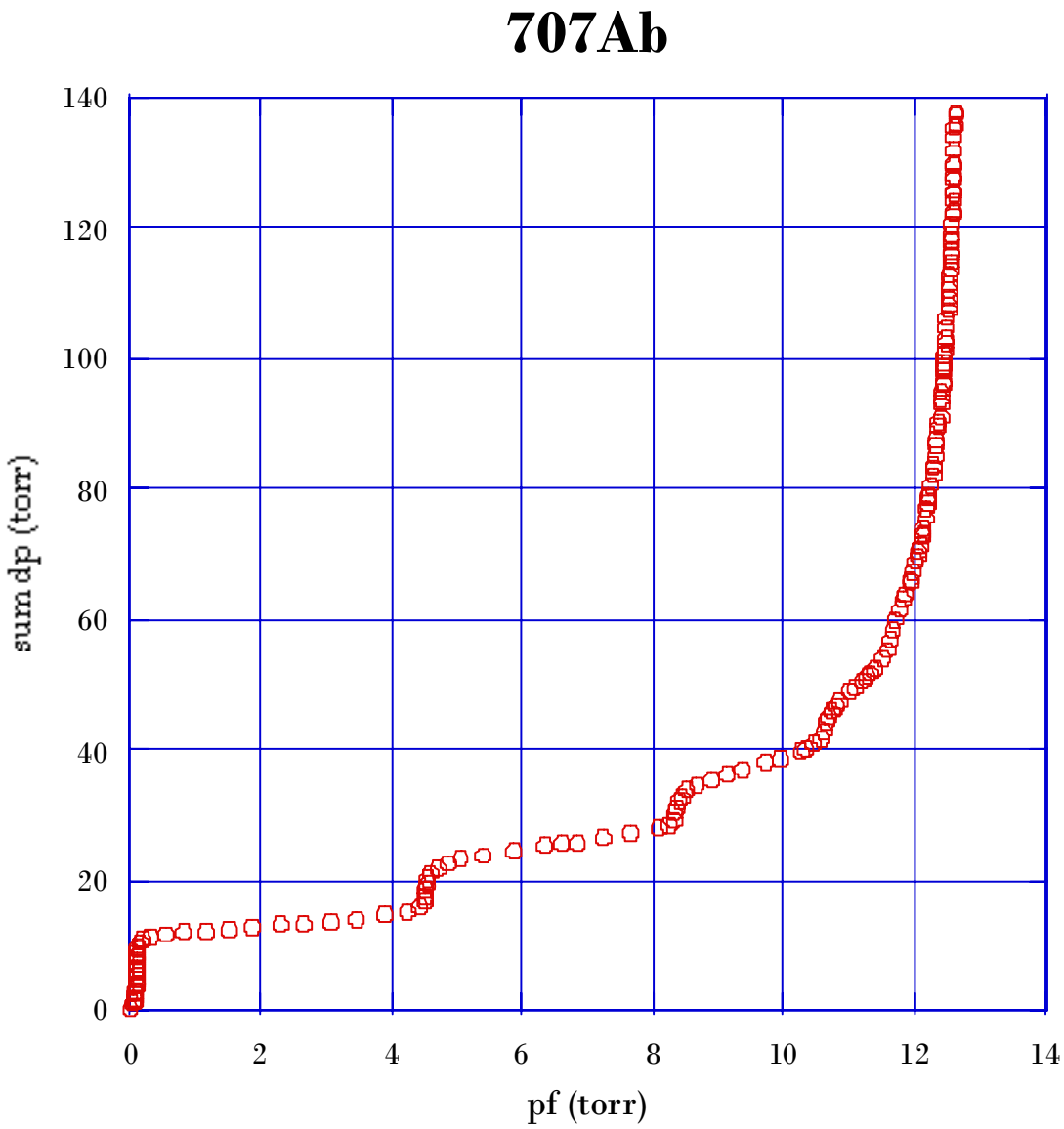


Figure 7.15 – Methane isotherm on sample 707Ab

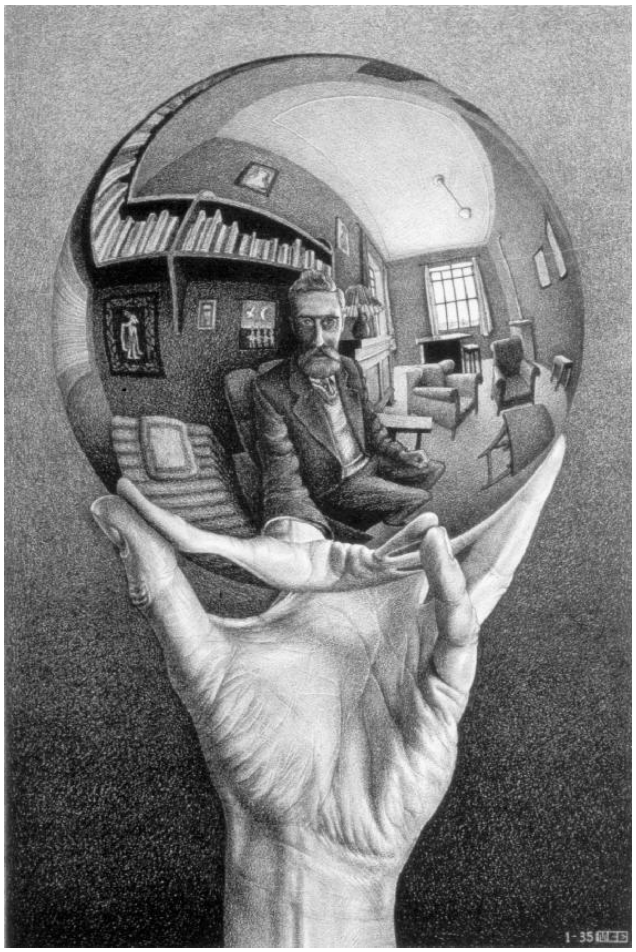
Table A.2 – Monolayer Coverage based on Point B Method

sample	Tset	Tavg	Sum ΔP	mmol	mmol/m^2
606Ia	10.5	11.28467	30.667	0.062756285	0.015692994
606Ia	9.5	10.317	30.833	0.063092714	0.015777123
606Ia	9	9.804367	31.389	0.064232049	0.016062028
606Ia	10	10.75933	31.389	0.064227499	0.01606089
606Ia	8.5	9.3849	32.972	0.067468873	0.016871436
606Ia	6.5	7.672933	32.5	0.066506142	0.016630693
606Ia	6.75	7.906567	32.861	0.067245399	0.016815554
606Ia	7.25	8.237467	32.083	0.065653465	0.016417471
606Ia	7.75	8.622367	32.167	0.065825363	0.016460456
606Ia	8.25	9.077967	31.833	0.065140504	0.016289198
606Ia	8.75	9.5568	32	0.065482695	0.016374767
606Ia	9.25	10.0387	31.111	0.063663028	0.015919737
606Ia	9.75	10.54133	31	0.063437729	0.015863398
606Ia	10	10.77833	30.833	0.063092853	0.015777158
606Ia	6.5	7.660567	30.333	0.062071473	0.015521749
606Ia	10.25	11.038	30.556	0.062525316	0.015635238
606Ib	7	8.104033	31.389	0.064232934	0.016748262
606Ib	6.5	7.804067	25	0.051159345	0.01333942

Table A.2 continued

sample	Tset	Tavg	Sum ΔP	mmol	mmol/m2
606Ib	7.5	8.6004	27.639	0.056558906	0.014747316
606Ic	8	9.172033	21	0.042972838	0.015976221
606Ie	7.75	8.730433	19.5	0.039902051	0.016636252
606If	8.5	9.403367	25.556	0.057356413	0.016127207
606If	7.5	8.516367	26.347	0.059135191	0.016627356
606If	8	8.948533	26.111	0.058605349	0.016478377
606cb	8	9.056433	20.444	0.045881518	0.016679336
606cb	7	8.192867	21	0.047135733	0.017135282
606cb	9	9.958467	20.222	0.045389467	0.016500461
606cb	9.5	10.44333	20.319	0.045602178	0.016577787
606cb	10	10.92667	20.125	0.045167913	0.016419919
707A	7.3	8.9226	24.222	0.054364769	0.017139496
707A	7.66	9.2631	23.667	0.053115983	0.016745794
707A	8	9.553333	23.778	0.053367173	0.016824986
707A	10	11.38833	22.667	0.050849839	0.01603135
1107A	11.5	12.52933	23.778	0.053337701	0.015815009
1107A	12.5	13.475	23.333	0.052347432	0.015521388
1107A	7.5	8.7516	25.444	0.05710816	0.016932978
1107A	8.5	9.660167	24.222	0.054366401	0.016120027

Vita



M. C. Escher: Hand with Reflecting Sphere (1935)

Lillian Frazier was born in Austin, Texas on November 16, 1972. She lived with her family in Rockdale, Texas until she was just under a year of age. At that time The Aluminum Company of America (Alcoa) moved them to Pittsburgh, Pennsylvania when she was just 11 months of age. She lived on a dead end street where almost every home had children. There were 5 kids the same age on the street (All boys). So, Lillian grew up in a rough and tumble manner playing with the boys. She also learned at a very young age how to occupy her own time playing with Tinker Toys, Lego's and Lincoln Logs, or playing board games with her stuffed animals (taking turns for all of them). She grew up loving sports of all kinds, loving all animals, and managing to even like school while she was at it. She also became a fan of the Pittsburgh sports teams remembering to always watch for the Terrible Trolley when it rolled past the school yard during recess which celebrated the Steelers four Super Bowl championships and the Pirates pennant wins.

When she was in the 5th grade, Alcoa called her family to Evansville, Indiana. Science became her favorite subject in the 6th grade. With an electrical engineer for a father, she had some of the coolest science projects including a telegraph and an electric motor. She fell in love with chemistry in high school. Her other high school distractions included playing soccer and taking and teaching gymnastics. Upon graduation from Castle High School in 1991, Alcoa strikes for the final time.

Her family moved to Knoxville, Tennessee, approximately two weeks after graduation. This was a bit of a problem as now Purdue would expect out of state tuition. Determined to study chemical engineering, Lillian chose to attend Virginia Tech, a good engineering school with a soccer program. Lillian spent some time working for Dr. William H. Velander in the Biochemical Engineering Laboratory in the chemical engineering department. She graduated in May of 1995 with a BS in chemical engineering and minors in chemistry and biochemistry, while playing college soccer in her spare time.

She moved back to Knoxville when she did not have a job upon graduation. She decided to get some part time work at a local gymnastics academy. She also wound up waiting tables, and got hired on for seasonal work at Eddie Bauer. With no luck on the job front, she eventually took on the role of head coach of the trampoline and tumbling team at the gym. She kept this job until the end of summer 2000. During this time she coached 3 national champions, 10 runner-up national champions, numerous top 10 national finish tumblers. She married in 1998 and took up a bit of rock climbing.

She helped her tumblers with their homework, and they in turn convinced her she would make a good teacher. In August 2000, she began teaching math at a local high school, where she also coached the girls soccer team. At the end of that year, she transferred to a closer school. Teaching in the high school system was extremely

frustrating and by May 2002, she had had enough. She looked for a job through the summer, and with nothing working out, she decided she needed to update her education.

With school beginning the next day, she went with a friend to the chemistry department at the University of Tennessee and asked to be let in. Conveniently they were in need of another Teaching Assistant, and they allowed me into the 2002 incoming class. She began her graduate research under the tutelage of Dr. John Z. Larese. She has spent the past 6 years learning about adsorption and neutron scattering techniques. With her engineering background, she also became the group fix-it-girl, giving her the opportunity to learn many new techniques in electronics and machine work. Lillian will finally achieve her goal of a Ph.D. in Chemical Physics in August of 2008.